Trinity College Dublin
Coláiste na Tríonóide, Baile Átha Cliath
The University of Dublin

MicroRNA-21 Limits Macrophage Responses to *Mycobacterium tuberculosis*

A Thesis Submitted to the University of Dublin, Trinity College, for the Degree of Doctor of Philosophy in the School of Biochemistry and Immunology

by

Emer Hackett

2019

Supervisor: Dr. Frederick Sheedy, PhD

Macrophage Homeostasis
School of Biochemistry & Immunology
Trinity Biomedical Sciences Institute
Dublin 2

I, Emer Hackett, declare that this thesis has not been submitted as an exercise for a degree at this or any other university and it is entirely my own work.

I agree to deposit this thesis in the University's open access institutional repository or allow the library to do so on my behalf, subject to Irish Copyright Legislation and Trinity College Library conditions of use and acknowledgement.

Signed: Date:

_____ _____

Emer Hackett

Summary

Mycobacterium tuberculosis (Mtb) is an intracellular pathogen that subverts the innate immune response. The Mtb pandemic is of global concern. Emerging strains of antibiotic-resistant Mtb warrant the development of host-directed therapies and improved vaccination strategies. The macrophage is the primary host cell for Mtb and understanding how the bacterium co-opts this immune cell as a survival niche is of vital importance. Increased glycolysis is an essential process driving host defence against Mtb, but little is known about how metabolism is regulated during infection. MicroRNA-21 (miR-21) is a putative negative regulator of TLR signalling induced to promote immunoregulatory responses, but its role during Mtb infection has not been described. This work describes a novel role for miR-21 during Mtb infection in the manipulation of metabolic reprogramming.

The findings of this work illustrate that miR-21 is induced by Mtb infection and upregulation of miR-21 coincides with the switch from a pro-inflammatory to an immunoregulatory macrophage permissive to bacterial replication. This overlaps with negative regulation of metabolic reprogramming. Blocking miR-21 increases bacterial containment via increased pro-inflammatory mediators including IL-1β. This increase in IL-1β is dependent on enhanced glycolysis, demonstrating that miR-21 negatively regulates immune activation by limiting metabolic reprogramming. This work also describes the mechanism by which miR-21 limits glycolysis, describing a new target at the committed step of glycolysis, namely one isoform of the phosphofructokinase 1 enzyme - PFK-M. Unlike other glycolytic genes and PFK isoforms, PFK-M expression is repressed during Mtb infection. This repression limits glycolysis and pro-inflammatory responses, however an immune activating signal from IFN-γ can override this brake on immunometabolic reprogramming. IFN-γ post-transcriptionally limits miR-21

expression, thus relieving the repression of PFK-M and permitting full macrophage activation in response to Mtb. This dual targeting of this pathway by miR-21 and targeting of miR-21 by IFN-γ highlight the central importance of immunometabolism to the immune response.

By describing a novel level of regulation of the glycolytic machinery by miR-21, modulated by both host & pathogen responses, these findings open new avenues for targeting immunity in infection as well as other diverse diseases including metabolic syndrome & cancer.

Acknowledgements

Above anyone else I want to express my sincere gratitude to my supervisor, Dr Frederick Sheedy. Your knowledge of, enthusiasm for, and dedication to science is an inspiration to work with. Thank you for always going above and beyond for me. I have been so lucky to work with you and you have taught me so much in the last 4 years. You're (Kil)worth your weight in gold.

Thank you to all the current and former members of the TB Immunology lab in Trinity College Dublin who nurtured me in my early days and have let me haunt their bug hood ever since. Special thanks to the commander in chief Professor Joseph Keane for his infectious enthusiasm and unwavering support.

Thanks to Professor Cliona O'Farrelly and her lab for welcoming us into their space and being making me feel so at home.

Thank you to Dr Sinead Corr, Dr Daniel Johnston and Michelle Williams for all their help with the miR-21 knockout mice.

Sarah Case: you've been my rock and the best work wife ever. Thanks for being so understanding, a relentless sweetheart and the best craic. Lil coffee?

Paul PJ Kelly: your heart is almost as big as your scientific knowledge. I couldn't have had a better comrade to struggle through this with. Don't be a stranger – definitely want to see that farm and your potatoes asap.

Hannah Prendeville: You've been more excited about PFK-M than even me, glad it panned out. You can touch my hand now.

Mag: I'm staff now. See you at 11 o'clock.

Hugo, Simon, Girl RA/Derb, Dalal, Jamie, Cathal and Lena – you're all sound lads.

Dylan: Gonna rat on you about the Oil Red O all over the chemical room unless you take me to a Pats match.

Ben and Mikaela: My two doctors and role models. You got me out of that basement alive.

Thank you to my Mam and Dad for getting me this far and for being such cool and supportive parents.

Lizzie you're the best partner and have been amazing this whole journey. I'm so excited to not be thesis mouse anymore. I love you. Smithwicks?

Finally, I'd like to dedicate this thesis to the loving memory of Carmel Kerr.

Table of Contents

List of Figures

Chapter 1: Introduction

Chapter 2: Materials and Methods

Chapter 3: Macrophage miR-21 and Anti-Mycobacterial Responses

Chapter 4: Macrophage miR-21 and Metabolism

List of Tables

Glossary of Abbreviations

ADC	Albumin Dextrose Catalase
ADP	Adenosine diphosphate
AIDS	Acquired Immune Deficiency Syndrome
AIM2	Absent in Melanoma 2
AM	Alveolar macrophage
APS	Ammonium persulfate
Arg-1	Arginase-1
ASC	Apoptosis-associated speck-like protein containing a caspase recruitment domain
ATCC	American Type Culture Collection
ATP	Adenosine triphosphate
BCG	Bacillus Calmette-Guerin
BMDM	Bone marrow-derived macrophage
BSA	Bovine serum albumin
BSL	Biosafety level
CARKL	Carbohydrate kinase-like protein
CD	Cluster of differentiation
cDNA	Complementary DNA
CFU	Colony forming units
CO_2	Carbon dioxide
COX	Cyclooxygenase

Ct	Cycle threshold
Ctl	Control
CV	Crystal violet
DAMP	Danger-associated molecular pattern
DCFDA	2',7'-dichlorofluorescin diacetate
DM2	Type 2 diabetes
DMEM	Dulbecco's Modified Eagle's Medium
DMSO	Dimethyl sulfoxide
DNA	Deoxyribonucleic acid
DTT	Dithiothreitol
ECAR	Extracellular acidification rate
EDTA	Ethylenediaminetetraacetic acid
ELISA	Enzyme-linked immunosorbent assay
ETC	Electron transport chain
F2,6B	Fructose 2,6-bisphosphate
$FADH_2$	Flavin adenine dinucleotide
FBS	Foetal bovine serum
FCCP	Carbonyl cyanide-4-(trifluoromethoxy)phenylhydrazone
GLUT	Glucose transporter
GR	Glycolytic reserve
H_2SO_4	Sulfuric acid
HDT	Host-directed therapy

HIF-1α	Hypoxia-inducible Factor alpha
HIV	Human Immunodeficiency Virus
HK	Hexokinase
HRE	Hypoxia Response Element
HRP	Horseradish peroxidase
HPRT	Hypoxanthine-guanine phosphoribosyltransferase
IBTS	Irish Blood Transfusion Service
IFN	Interferon
Ig	Immunoglobulin
IKK	Inhibitor of NFκB kinase
IL	Interleukin
IL-1R1	IL-1 receptor
iNOS	Inducible nitric oxide synthase
iRv	γ-irradiated H37Rv
kDa	Kilodalton
KO	Knock-out
LAM	Lipoarrabinomannan
LDHA	Lactate dehydrogenase A
LXA4	Lipoxin
LPS	Lipopolysaccharide
MAPK	Mitogen-activated protein kinase
M-CSF	Macrophage colony-stimulating factor

MDM	Monocyte-derived macrophage
MDR	Multiple drug resistant
MHC	Major histocompatibility complex
miRNA	microRNA
MMP	Matrix metalloproteinase
MOI	Multiplicity of infection
Mph	Morpholino
mRNA	Messenger RNA
Mtb	*Mycobacterium tuberculosis*
mTOR	Mechanistic target of rapamycin
MyD88	Myeloid differentiation primary response gene 88
NAD	Nicotinamide adenine dinucleotide
NADP	Nicotinamide adenine dinucleotide phosphate
NFκB	Nuclear factor κ-light chain enhancer of activated B cells
NK	Natural killer
NLRP3	NACHT, LRR and PYD domains-containing protein 3
NO	Nitric oxide
NOS2	Nitric oxide synthase 2
NOX	NADPH oxidase
OCR	Oxygen consumption rate
OD	Optical density
PAMP	Pathogen-associated molecular pattern

PBMC	Peripheral blood mononuclear cell
PBS	Phosphate buffered saline
PCR	Polymerase chain reaction
PDCD4	Programmed Cell Death 4
PFA	Paraformaldehyde
PFK	Phosphofructokinase
PFKB3	6-phosphofructo-2-kinase/fructose-2,6-bisphosphatase
PGE2	Prostaglandin E2
PI	Propidium iodide
PI3K	Phosphoinositide 3-kinase
PK	Pyruvate kinase
PKM2	Pyruvate kinase M2
PPP	Pentose phosphate pathway
Pre-miR	Precursor microRNA
Pri-miR	Primary microRNA
PRR	Pattern recognition receptor
PTEN	Phosphatase and tensin homolog
qPCR	Quantitative polymerase chain reaction
RNA	Ribonucleic acid
RNS	Reactive nitrogen species
ROS	Reactive oxygen species

RPMI-1640	Roswell Park Memorial Institute-1640 medium
RT-qPCR	Quantitative reverse transcription PCR
SDS	Sodium dodecyl sulfate
SNP	Single nucleotide polymorphism
SRC	Spare respiratory capacity
TBHP	Tert-butyl hydrogen peroxide
TBST	Tris-buffered saline (TBS) and Tween 20
TCA	Tricarboxylic acid
TEMED	Tetramethylethylenediamine
TGF-β	Transforming growth factor-β
TLR	Toll-like receptor
TNF-α	Tumour necrosis factor-α
TNFR1	TNF-α receptor 1
TRIS	Trisaminomethane
WT	Wild type

Chapter 1:

Introduction

1.1 The Immune Response to *Mycobacterium tuberculosis*

1.1.1 *Mycobacterium tuberculosis*: A global health concern

The World Health Organization's 2017 report on tuberculosis highlights the global *Mycobacterium tuberculosis* (Mtb) pandemic[1]. Mtb infection is currently the ninth leading cause of death globally, and it now outstrips HIV/AIDS as the foremost ranking cause of mortality from a single infectious agent. In 2016, it was estimated that 10.4 million people fell ill with Mtb infection. Furthermore, Mtb caused 1.3 million deaths in the HIV-negative population and a further 374,000 deaths in the HIV-positive population. Costing over a billion deaths in the last two centuries it is likely to be the most deadly pathogen in the history of mankind[2]. Of arguably greater concern is the increasing incidence of drug-resistant Mtb. Between 2009 and 2016, incidence of multidrug-resistant (MDR) tuberculosis infection (i.e. resistance to frontline drugs such as rifampicin and isoniazid) increased over 20% annually[3]. In 2016, almost half a million cases of MDR tuberculosis were reported. Moreover, there has been an emergence of extensively drug-resistant (XDR) tuberculosis (i.e. resistance to fluoroquinolone and a second-line intravenous treatment), with 8,000 cases in 72 countries reported in 2016[1]. The prevalence of MDR and XDR Mtb infections is predicted to continue to rise in the coming decades[4]. Drug-sensitive tuberculosis strains are not a trivial infection either, with current recommendations advising six months treatment with four frontline antibiotics[1]. Current estimates of the global reservoir of latent tuberculosis infection place the figure at approximately 1.7 billion individuals, or roughly one quarter of the world's population[5].

These figures make the case for the urgent need for novel interventions for the prevention and treatment of Mtb. Vaccination has thus far failed to provide sufficient protection from Mtb. The live,

attenuated bacille Calmette-Guérin (BCG) vaccine, based on the bovine homolog to Mtb *Mycobacterium bovis*, is given to approximately 100 million infants annually, and although it reduces the incidence of disseminated tuberculosis infection in childhood[6], its efficacy at preventing adult pulmonary tuberculosis is highly variable[7]. The lack of an efficacious vaccine warrants an effective treatment for Mtb infection. Current treatments fall short however, with long treatment regimes, significant pulmonary damage despite curation, ineffective preventative treatments for latent tuberculosis and the ever-increasing prominence of drug-resistance[8]. This highlights the need for new host-directed therapies (HDT) that can improve the immune response to Mtb infection, resulting in efficient clearance of infection and minimising damage to host tissues. In order to develop new HDT, the interactions between the microbe and the host must be well characterised.

1.1.2 *Mycobacterium tuberculosis*: The bacillus

Mtb is a slow-growing bacterium with a doubling time of approximately 24 hours under optimal conditions[9]. Cryo-electron tomography has shown that mycobacteria have an outer membrane that is functionally similar to gram-negative bacteria composed of an asymmetric lipid bilayer which has an inner layer of fatty acids (mycolic acids) and an outer layer of waxy components and glycolipids. A thin layer of peptidoglycan linked to arabinogalactan and lipoarabinomannan is present between these layers, bound to the mycolic acids. The synthesis of mycolic acids and arabinogalactan is targeted by the anti-Mtb drugs isoniazid and ethambutol[9].

Humans are the sole reservoir for Mtb, no other animal has been confirmed as a legitimate host, though a few isolated cases of human Mtb infecting cattle[10, 11] have been reported. Mtb must

cause pulmonary disease in order to transmit disease between individuals[12]. Disease pathology is largely due to the inflammatory response which causes damage to the lung tissue and thus increases the ability of the bacteria to be transmitted[13]. T cell epitope analysis of Mtb has shown that there is very little Mtb antigenic variation and human T cell epitopes are hyperconserved[14, 15], suggesting that Mtb benefits from T cell recognition or uses mechanisms other than genetic variation to avoid host immune responses.

1.1.3 Murine models of *Mycobacterium tuberculosis* infection

Studying the complex immune interaction of Mtb in vivo is difficult. Animal models can accelerate the understanding of the biology of Mtb infection and the development of better treatments and vaccines. Approximately 61% of in vivo Mtb research on is carried out on mice, with guinea pigs and rabbits compromising 25% and 13% of models respectively and the final 2% split between non-human primate and zebrafish models[16]. Mice are widely used because of technical ease and cost-effectiveness however mice do not naturally contract Mtb and due to a less complex bronchiolar tree and a lack of cavitation in the lung pathology[17]. Furthermore, susceptibility of different mouse strains to Mtb infection and response to vaccination varies greatly[18]. Given that the human is the only natural host for Mtb, future studies may find human-based in-vitro tissue models complementary to the animal models currently in use[19].

1.1.4 Pathogenesis of Mtb infection

Mtb has evolved with its human host for an estimated 70,000 years[10], thus the bacterium has developed many mechanisms to

survive and replicate within the host without being eliminated by the immune system. Tuberculosis is an airborne pathogen spread from person to person by coughed aerosols from individuals with active tuberculosis[20]. There are two main categories of tuberculosis infection – pulmonary tuberculosis and extrapulmonary tuberculosis. Extrapulmonary infection occurs in 10 to 42% of cases of pulmonary tuberculosis, depending on a number of host and microbial factors[21]. Clinical features of pulmonary tuberculosis infection include night sweats, weight loss, loss of appetite, chronic cough and haemoptysis.

In an estimated 90% of primary infections with tuberculosis, Mtb is contained by the immune system as an asymptomatic, latent infection or possibly may even be eliminated[22]. Elimination of Mtb by “early clearance”, i.e. a successful eradication of the bacteria before adaptive immunity is initiated, has been described and suggests an endogenous ability of the host innate immune system to contain and eliminate Mtb infection. Epidemiological evidence of this early clearance phenomenon is found in studies which demonstrate that approximately 50% of individuals in close contact with highly active TB patients remain tuberculin skin test (TST) negative (i.e. do not develop a T cell response) and do not develop disease[23, 24]. This indicates that in a large proportion of individuals the innate immune response is sufficient to eliminate Mtb infection. Risk of reactivation of latent infection is approximately 5%[25]. Latent infection reduces the risk of reinfection upon re-exposure, while active tuberculosis is associated with an increased risk of another active infection upon re-exposure[26]. Understanding the factors that result in different clinical outcomes in individuals exposed to Mtb will be important for developing new host-directed therapies and vaccine strategies.

1.1.5 Initial infection: Resident immune cells of the pulmonary compartment

Infection with Mtb must occur through the pulmonary route, thus the immune cells of the lungs are the primary responders to Mtb. Within the pulmonary compartment the primary innate immune cells are dendritic cells, which are infrequent in homeostatic conditions[27], and macrophages. The lung compartment houses two ontologically distinct populations of tissue resident macrophages - alveolar macrophages (AM) and interstitial macrophages (IM). AM are derived from foetal monocytes during lung development and proliferate locally to maintain the population in the lung[28]. The ontogeny of IM is less defined, though some research suggests that IM are derived from circulating blood monocytes that are recruited to the interstitial space[29]. IM are though to account for only 4% of the monocyte/macrophage population in a healthy murine lung[30]. IMs are grossly understudied in all fields of lung biology, due mostly to the technical difficulty of obtaining IM for research[31]. While AM are easily accessed by bronchoalveolar lavage and have been well-defined, accessing IM requires lung resection and sorting. For these reasons, there is little data on the role of IM in Mtb infection.

When an aerosolised droplet containing viable Mtb bacilli is inhaled, it travels to the lower lung and is phagocytosed by AM, and taken up by recruited neutrophils and dendritic cells[32]. AM internalise Mtb through several phagocytic receptors including the mannose receptor, scavenger receptors and particularly complement receptors [33]. After internalisation, a phagosome is formed around the bacterium[34]. One of the most important reasons for the success of Mtb is its ability to block phagolysosomal maturation. Mtb phagosomes do not acidify[35] and do not have mature lysosomal hydrolases[36]. Through phagolysosomal arrest, Mtb transforms the AM from the primary innate responder to infection into a protective niche where it can survive and replicate. Mtb has been shown to

survive in murine macrophage phagosomes 16 days after infection[37]. Evidence from zebrafish models of tuberculosis infection by Ramakrishnan et al[38] indicates that this early recruitment of phagocytes is advantageous to Mtb, providing an abundance of host cells for replication. Activation of the AM with pro-inflammatory signals can overcome this arrest and induce the process of autophagy to clear Mtb-containing vacuoles. During successful immune responses, adaptive-cell derived IFN-γ promotes macrophage activation and allows phagolysosomal maturation to occur[39]. Mtb also uses many other mechanisms to avoid elimination by the AM including induction of an anti-inflammatory response and blocking the production of anti-microbial oxygen and nitrogen species[40].

1.1.6 TLR activation by Mtb

As well as phagocytosing Mtb, AM recognise Mtb and trigger immune responses. Toll-like receptors (TLRs) can be triggered by Mtb. TLR Mtb responses have been shown to be mediated primarily through TLR2 and to a lesser extent TLR4 [41]. Almost 100 TLR2 mycobacterial agonists have been identified, including lipoglycans and lipids, such as lipoarabinomannan (LAM) and LAM precursors lipomannan (LM) and mannoyslated phosphatidylinositol (PIM), lipoproteins such as LpqH and proteins such as the Mtb virulence factor ESAT-6[42]. A mutation in TLR2 inhibited Mtb-induced TNF-α signalling, indicating a role for TLR2 in Mtb recognition[43]. TLR4 was also found to be responsive to Mtb-derived ligand[44] and has been shown to be important in maintaining the balance between apoptotic and necrotic cell death[45]. TLR1[46] and TLR6[47] have been shown to heterodimerise with TLR2 to promote signal transduction, while TLR9 recognises bacterial DNA in the cytosol[48] and SNPs in this gene have been associated with an increased risk of pulmonary tuberculosis[49]. Deletion of both TLR2 and TLR9 does

not have a large effect on Mtb infection control in murine models, however deletion of the shared TLR adaptor MYD88 results in Mtb lethality[50]. This is likely due to defective IL-1 signalling which also requires MYD88[51].

1.1.7 Reactive oxygen and nitrogen species

Recognition of Mtb by the AM induces activation and the production of antimicrobial effectors. Reactive oxygen species (ROS) including superoxide are produced by the phagosomal NAPDH oxidase NOX2 which assembles on the phagolysosomal membrane and produces superoxide[52]. $P47^{phox}$ knockout mice in which part of the phagosomal oxidase machinery has been knocked out show increased susceptibility to the early stages of Mtb infection[53]. Furthermore, there is some evidence that individuals with chronic granulomatous disease which is caused by an inherited mutation in the gene encoding NADPH oxidase are at increased risk of mycobacterial diseases[54]. Mtb has developed mechanisms to detoxify ROS such as the expression of the superoxide dismutase proteins SodA and SodC which detoxify oxygen free radicals[55] and the KatG protein catalase dismutase which detoxifies hydrogen peroxide.[56] Strains that lack these anti-ROS mechanisms are susceptible to macrophage-mediated killing[56].

Reactive nitrogen intermediates including nitric oxide (NO) also play an important role in Mtb infection. NO is a radical gas that has microbicidal activity[57]. Additionally, NO has recently been found to act as a signalling molecule in Mtb infection, mediating IFN-γ responses by activating HIF-1α and repressing NFκB activation[58]. NO is generated by the action of nitric oxide synthase (NOS). There are three isoforms of NOS, the most immunologically relevant form being the inducible form (NOS2 or iNOS). NOS2 is induced by activating signals in the macrophage including IFN-γ and catalyses

the oxidation of l-arginine to NO and citrulline. Murine macrophages deficient in NOS2 are unable to control Mtb growth[57]. The role of NO in human Mtb infection has in the past been debated, partly due to human monocyte-derived macrophages (MDM) from healthy donors not expressing NOS2, whereas healthy tissue-derived macrophages or MDM from diseased humans do express NOS2[59]. Supportive evidence for the importance of NO in human Mtb infection has been growing in recent years. The expression of NOS2 and production of measurable NO in response to Mtb infection has been detected in human MDM[60]. Human AM infected in vitro with Mtb produce NO which inhibits Mtb growth[61] and patients with active Mtb infection have increased exhaled NO and increased expression of iNOS in AM[62], indicating that NO is relevant in both the experimental murine model of Mtb and in human Mtb patients.

1.1.8 Cell death in Mtb infection

Cell death is also a key process in the interaction between Mtb and the host. Mtb infection can induce necrotic cell death whereby the infected cell lyses and allows further spread of the bacilli, which is favourable for Mtb. The Mtb ESX1 secretion system has been shown to be the molecular driver behind this promotion of necrotic cell death and its absence partly responsible for the attenuation of the strain of *Mycobacterium bovis* used in the BCG vaccine[63]. Alternatively, apoptosis can be instigated, a controlled death program that maintains the integrity of the cell membrane and reduces Mtb survival[64]. Infection with Mtb has been shown not only to induce macrophage apoptosis, but also to induce apoptosis of neighbouring uninfected macrophages[65]. This bystander apoptosis may limit Mtb survival by depriving it of its host cell. More virulent strains of Mtb have developed resistance mechanisms to combat this by blocking apoptosis[66]. Inhibition of apoptosis prolongs the

survival of Mtb infected cells, allowing more time for Mtb to replicate before being released from the cell[13]. Mtb infected macrophages may themselves in turn be taken up by uninfected macrophages through the process of effereocytosis[67] to ultimately bring about bacterial killing.

1.1.9 Neutrophils and dendritic cells in Mtb responses

Neutrophils are also infected with Mtb[68] and are the most common infected phagocytic cell in the lungs of Mtb patients[69] and tuberculosis pathology has a distinct neutrophil signature[70]. Recruitment to the site of infection occurs through IL-1β and lipoxygenase signalling pathways[71]. Neutrophil direct killing activities are not well suited to Mtb because of its slow replication[72], however they carry out activating functions to promote Mtb responses in other cells including macrophages[73], dendritic cells[74] and $CD4^+$ T cells[75]. Similar to macrophages, Mtb can inhibit neutrophil apoptosis, delaying $CD4^+$ T cell activation[13].

Mtb responses requires both effective innate and adaptive responses, and dendritic cells (DC) act as a bridge between the innate and adaptive arms of the immune system. Though initial innate phagocytic responses seem to favour Mtb growth by providing the cellular niche for its replication, they also provide foster the subsequent initiation of adaptive immunity by driving DC recruitment and maturation[40]. DC that take up lung neutrophils infected with Mtb migrate and activate $CD4^+$ T cells more efficiently than DC that take up the bacterium alone as neutrophils protect the DC from Mtb-induced migration inhibition[75]. Though macrophages can also present antigen to $CD4^+$ T cells through MHCII, DC are much more potent antigen presenting cells[76]. Initiation of the adaptive immune response by DC is delayed by Mtb however, which has developed mechanisms to impair DC cytokine

production, maturation, and antigen presentation[77]. Impaired DC responses delays DC from migrating to the lymph node and initiating adaptive responses[78]. Adaptive immunity is not initiated until day 12 in murine models and can be delayed up to 6 weeks after infection in humans[79]. Adoptive transfer of Mtb-antigen-specific $CD4^+$ T cells has no effect on bacterial clearance in the first 7 days of infection, suggesting that in this initial phase Mtb is either not able to be recognised or resistant to adaptive anti-microbial activity[80].

1.1.10 Natural Killer cells

Natural Killer (NK) cells are perhaps underappreciated in the immune response to Mtb. NK cells have been observed in the granulomas of Mtb patients [81] and NK cells can provide a source IFN-γ for the activation of macrophages[82]. The importance of NK cells in human Mtb infection is illustrated the varied responses of donor NK cells to Mtb infection according to KIR haplotype[83, 84]. NK cells have been shown to drive anti-Mtb immune responses in mice lacking the Rag1 gene (i.e. lacking functional B an T cell populations) through production of IFN-γ[85], however in the presence of functional B and T cells they play a negligible role in the immune response[86]. This suggests that perhaps NK cells play a more prominent role in specific immunocompromised individuals such as the HIV-positive population.

1.1.11 The roles of TNF-α in the response to Mtb infection

Tumour necrosis factor alpha (TNF-α) is a potent modulator of early immune responses. Binding of TNF-α to either its receptors TNFR1 or TNFR2 induces pro-inflammatory signals via NFκB or MAPK. Enhanced levels of TNF-α are found in the pulmonary compartment during Mtb infection[87]. TNF-α is potently produced by macrophages

in response to Mtb components and this can be boosted by IFN-γ treatment[88]. Dendritic cells[89], T cells[90] NKT and CD1d-restricted T cells[91] and γδ T cells[92] have also been shown to contribute to TNF-α produced at the site of infection. Infliximab, a monoclonal antibody against TNF-α, was approved in 1998 for the treatment of rheumatoid arthritis and Crohn's Disease[93]. After it came into widespread use, an increased risk for activation of latent Mtb infection was recognised[94, 95], highlighting a key role for TNF-α in controlling Mtb infection.

TNF-α has been shown to be important for the formation and maintenance of Mtb granulomas in mice[96], to induce apoptosis in human alveolar macrophages infected with Mtb[97] and to activate macrophages to perform pro-inflammatory functions[98]. Lin et al[99] studied the effect of neutralising TNF-α in a non-human primate model of tuberculosis disease. Neutralisation of TNF-α prior to Mtb infection resulted in disseminated disease and a high bacterial burden, while neutralisation of TNF-α in latently infected animals resulted in disease reactivation in the majority of the monkeys. TNF-α neutralisation had no significant effect on granuloma structure. Furthermore, studies on the effects of anti-TNF-α therapies on Mtb infection have shown that TNF-α is important for phagolysosomal maturation in macrophages perhaps partly through autophagy-related mechanisms and promoting T cell survival[100]. Excessive TNF-α induced inflammation is however associated with immunopathology[101, 102]. Roca et al [102] have shown that in a zebrafish model of mycobacterial infection, excessive TNF-α induced the production of ROS which initially resulted increased macrophage microbicidal activity before rapidly inducing necrotic cell death, allowing mycobacterial dissemination.

1.1.12 The roles of IL-10 in the response to Mtb infection

Interleukin-10 (IL-10) is an immunomodulatory cytokine. It can be produced by T cells (particularly regulatory T cells), B cells, neutrophils, some subsets of DCs and by macrophages[103]. IL-10 signals through its receptors IL10R1 and IL10R2 to activate the Jak-STAT pathway and activate STAT3 to transduce inhibitory signals[104]. One of its key functions is to deactivate macrophages, resulting in less production of Th1-activating cytokines[105], less TNF-α, reactive oxygen and nitrogen species[106] and reduced expression of MHCII to present antigen[107]. IL-10 is found in the BAL fluid of Mtb patients[108] and human IL-10 polymorphisms have been associated with Mtb susceptibility[109], indicating a role for IL-10 in human Mtb infection.

The role of IL-10 in enhancing susceptibility to Mtb infection is not clear and mouse studies have had varying results depending on the genetic background of the animal[110, 111]. Some reports suggest that IL-10 production leads to decreased production of IL-12p40, TNF-α and IFN-γ[112]. A non-human primate model of Mtb infection showed less IL-12 production in pulmonary granulomas, however there was less inflammation found 3-4 weeks post-infection in animals in which IL-10 had been neutralised[113]. Studies on human PBMCs from individuals with Mtb infection indicated that IL-10 negatively regulates IFN-γ production by limiting IL-12 production[114]. There is evidence of some particularly virulent strains of Mtb inducing production of IL-10 as an immune subversion mechanism[115, 116], which is a strong indicator of a negative regulatory effect of IL-10 in Mtb infection. One key activity of Mtb-induced IL-10 is the arrest of phagosomal maturation. Human Mtb-infected MDM and AM treated with IL-10 were inhibited from maturing this phagosomal compartment and this was partly mediated through STAT3 signalling[117]. Phagosomal arrest is one of

the central mechanisms by which Mtb persists within the macrophage, thus this supports the hypothesis IL-10 induction promotes Mtb persistence.

1.1.13 Immunological equilibrium and granuloma formation

There are several outcomes of early infection with Mtb. There is evidence that a minority of individuals are able to clear Mtb with an acute inflammatory response[22]. An estimated 5-10% of those infected will develop clinically evident infection [118] while the majority of those infected will contain the infection in a state of immunological equilibrium. In this state, adaptive immune responses are sufficient to arrest the growth of Mtb but not to fully eradicate it. This containment occurs through the formation of a granuloma. The granuloma contains Mtb and prevents the spread of infection within the host, but also provides a niche environment for Mtb in which it can survive and establish latent infection. Granulomas are not well characterised. Current opinion leans towards the idea that the centre of the granuloma consists of necrotic core of infected macrophages which are encapsulated by a variety of immune cells including activated macrophages and $CD4^+$ and $CD8^+$ T cells which form a dense wall that contains the Mtb infection[119]. In immunocompetent individuals, the granulomas are compact and contain a high proportion of IFN-γ-producing $CD4^+$ T cells. As adaptive immunity is induced, bacterial killing can occur and possibly even sterilisation of granulomas[120]. However, in individuals that become immunocompromised (for example by contracting HIV infection) the granulomas are much larger and have few surrounding lymphocytes[121]. Over time the core of these ill-contained granulomas will become caseous, liquefy and cavitate, releasing Mtb into the lung[122]. The granuloma is thus a state of equilibrium between host and bacteria, dependent on the competence of the innate and adaptive immune response.

1.1.14 Adaptive immunity in Mtb infection

Compared to other bacterial infections, there is a delay in the initiation of T cell responses to Mtb[79]. Approximately 10 days after infection, activation of $CD4^+$ T cells occurs in the lung-draining mediastinal lymph node where expansion of antigen-specific Th1 cells occurs before being trafficked to the lung[123]. While $CD4^+$ T cells are appreciated as playing an essential role in the control of Mtb infection, the importance of $CD8^+$ T cells is less clear. Depletion of $CD8^+$ T cells in a murine model at the chronic stage of Mtb infection resulted in a higher bacterial burden, indicating that these cells may be important for the long-term control of Mtb infection[124]. Though both $CD4^+$ and $CD8^+$ T cells produce IFN-γ, murine research suggests that $CD4^+$ T cells are required for optimal IFN-γ production by $CD8^+$ T cells[125].

$CD4^+$ T cells are essential for Mtb protective responses. Studies using both $CD4^+$ T cell depletion and knockout of MHCII have demonstrated that direct antigen recognition by $CD4^+$ T cells is required for Mtb containment[126]. $CD4^+$ T cell recognition of Mtb-infected macrophages has been shown to outperform $CD8^+$ T cell recognition, which may in part explain why even though $CD8^+$ T cell responses are induced by Mtb, they contribute minimally to infection outcome[127]. IFN-γ is not the only protective mediator produced by $CD4^+$ T cells[128]. For example, TNF-α produced by $CD4^+$ T cells has also shown to be critical in controlling infection[129], however other unidentified mediators may also be important[128].

$CD4^+$ T cells in the Mtb response have been far better characterised in murine models than in humans. Clinical observations however give some insight into the importance $CD4^+$ T cell function. In a large clinical trial with BCG vaccination, $CD4^+$ and $CD8^+$ T cell secretion of TNF-α, IL-12, IL-17 and IFN-γ in

response to mycobacterial antigen was no different in infants that were immune to Mtb and those that developed Mtb infection[130]. Adults infected with Mtb can elicit antigen-specific $CD4^+$ and $CD8^+$ T cell responses and still progress to active Mtb disease[131]. Furthermore, the large incidence of coinfection with Mtb and HIV, both of which exacerbate the morbidity and mortality of the other in what is termed the "syndemic", has increased the understanding of human immunological responses to Mtb. Many studies have shown that HIV infection impairs control of Mtb infection [132], [133] and that HIV-positive individuals are more likely to develop Mtb shortly after HIV infection[134] and more likely to die from Mtb infection[135]. Observations from HIV/Mtb coinfection underline the importance of $CD4^+$ T cells in the Mtb response. Increasing susceptibility to Mtb infection has been correlated with decreasing peripheral $CD4^+$ T cell counts [136], and Mtb-infected HIV-positive individuals have lower $CD4^+$ T cell frequency[137] and lower amounts of IFN-γ [138] in BAL fluid than Mtb-infected HIV-negative individuals. However, the role of HIV on Mtb susceptibility is not is not solely due to reduced $CD4^+$ T cell activity. HIV patients in the early phase of infection as well as those on antiretroviral therapy (i.e. patients with a normal $CD4^+$ T cell count) have been shown to have an increased risk of active tuberculosis[133, 136]. Kuroda et al have provided one possible explanation for this using an SIV model, showing that SIV infection results in a high level of monocyte and macrophage turnover and this is associated with reactivation[139]. Additionally, though $CD4^+$ T cells and IFN-γ are required for the control of Mtb infection, their role may not be exclusively beneficial to the host. Recent evidence suggests that Th1 responses can have a deleterious effect in Mtb infection by reducing tolerance and thus triggering damage to the host. PD1-deficient animals which are resistant to T cell exhaustion and thus generate better anti-Mtb responses exhibited increased susceptibility and immmunopathology after Mtb infection[140]. Furthermore, when mice which were deficient in the mitochondrial

protein cyclophilin D, a deficiency that enabled better T cell activation through metabolic activation, were infected with Mtb, the bacterial burden remained unchanged while the mice were more susceptible to Mtb mortality indicating a breakdown in tolerance[141]. Additionally vaccine strategies which have targeted $CD4^+$ T cell responses have not been shown to improve protection[142]. Together these results indicate that while T cells are required for containment of Mtb infection, enhancing T cell responses does not equate with enhanced Mtb clearance.

The role of B cells in human Mtb infection is unclear. B cells have been shown to be present in follicle-like structures in human Mtb-infected lungs [143]. As of yet, studies examining Mtb susceptibility or reactivation in individuals receiving rituximab, a monoclonal antibody that depletes B cells, have found no increased incidence of Mtb in this cohort[144, 145, 146] which would suggest that they play a minimal role in Mtb immune responses.

1.1.15 Th1 immunity: IL-12 and IFN-γ

Interferon-gamma (IFN-γ) is thought to be one of the key mediators of macrophage activation in the immune response to intracellular pathogens. Mice deficient in IFN-γ are highly susceptible to Mtb infection, failing to produce reactive nitrogen species and allowing unrestricted growth of Mtb[82]. $CD4^+$ T cells have been shown to be essential producers of IFN-γ in Mtb infection in a murine model[147]. Mice deficient in IL-12[148], and to a lesser degree the Th1 transcription factor Tbet[149], are more susceptible to Mtb infection. Induction of protective IFN-γ T cell responses against Mtb is dependent on IL-12 which is mostly secreted by DCs but can also be provided by macrophages[148, 150]. In mice, the IL-12p40 subunit (but not the IL-12p35 subunit) has been shown to be essential for IFN-γ-mediated protection from Mtb, though both subunits are

required for long-term survival [151]. Humans lacking the IL-12Rβ1 IL-12 receptor fail to maintain a Th1 effector memory population indicating that IL-12 is also required for prolonged IFN-γ cellular responses in humans[152]. The importance of IL-12 and IFN-γ in human mycobacterial infection responses is highlighted by patients suffering from Mendelian susceptibility to mycobacterial disease (MSMD) who have a high susceptibility to clinical mycobacterial infections from weakly virulent mycobacteria including the BCG vaccine and non-tuberculous environmental bacteria as well as Mtb[153, 154, 155, 156, 157]. Furthermore, individuals who raise anti-IFN-γ autoantibodies are highly susceptible to both Mtb and opportunistic mycobacterial infections[158, 159, 160, 161].

Though IFN-γ is essential for anti-Mtb responses, the mechanisms through which it exerts its functions are not completely understood. Recently it was shown that IFN-γ instructs macrophages through the upregulation of the target gene iNOS. NO produced by iNOS downstream of IFN-γ modulates macrophage activation through activating HIF-1α and repressing NFκB to balance microbicidal activity and tissue damage during Mtb infection[58]. IFN-γ has been demonstrated to be important in the production of antimicrobial peptides and inducing phagolysosomal maturation[162, 163]. IFN-γ has also recently been shown to induce a metabolic shift in macrophages through HIF-1α to induce aerobic glycolysis[164]. This enhanced glycolysis was found to be essential for the control of Mtb growth in macrophages and to form a positive feedback loop with HIF-1α to boost macrophage activation.

Clinically, interferon-gamma release assays (IGRA) are used to diagnose latent Mtb infection, stimulating patient T cells ex vivo with Mtb antigens to trigger IFN-γ release[165]. Clinical trials have

indicated that IFN-γ, particularly when administered as an aerosol, may be beneficial as an adjuvant therapy and has been well-tolerated in the small trials that have been carried out[166].

1.2 Metabolism and macrophage responses to Mtb infection

1.2.1 IL-1β: A key cytokine in Mtb responses

While IFN-γ requires aerobic glycolysis to transduce its activity, IL-1β requires aerobic glycolysis for its production. IL-1α is encoded by a separate gene to IL-1β but both bind to the same receptor and have similar effector functions. IL-1α is however constitutively expressed in epithelial cells and is released as an alarmin in the case of necrotic cell death, recruiting neutrophils to the site, triggering sterile inflammation, while IL-1β promotes the recruitment of macrophages[167].

IL-1β is a potent pro-inflammatory cytokine produced by monocytes, macrophages and DCs and to a lesser extent by B cells and natural killer cells[168] and is not constitutively expressed but upregulated in response to TLR signalling, activated complement components, other cytokines such as TNF-α, as well as positively feeding back upon its own induction[169]. In the murine Mtb infected lung, monocytes and DCs were shown to be the key IL-1β producing cells[51].

The precursor to IL-1β, pro-IL-1β, is produced in response to PAMP signalling through PRRs[170]. PRR signalling can induce IL-1β transcription through NFκB[171] in response to inflammatory stimuli and in response to IL-1β signalling itself[172, 173] in an autocrine positive feedback loop. TLR stimulation can also activate PI3K

which has been shown to lead to IL-1β transcription in murine macrophages[174]. Additionally, while NFκB is thought to be responsible for the majority of the early induction of IL-1β, HIF-1α can also induce IL-1β transcription with both human and murine IL-1β genes containing HIF-1α binding sites[175, 176] and is thought to be responsible for the sustained induction of IL-1β later in the course of inflammation.

As a potent pro-inflammatory cytokine, IL-1β release must be tightly regulated. The IL-1β precursor needs to be cleaved into a mature, active form by caspase-1[170]. Caspase-1 must itself by cleaved from procaspase-1 into its active form by the inflammasome. Inflammasomes are cytoplasmic, multi-protein complexes which act as scaffolds for the assembly and cleavage of caspases. The NLRP3 inflammasome has been found to be important in Mtb infection, recognising a wide range of stimuli including mitochondrial ROS[177], extracellular ATP[178], potassium efflux[179], and mycobacterial ligands such as muramyl dipeptide[180]. The AIM2 inflammasome which recognises mycobacterial DNA was also shown to be important in controlling Mtb infection[181]. Full NLRP3 activation requires two signals. A priming signal triggers expression of NLRP3, which is lowly expressed in macrophages under homeostatic conditions, and pro-IL-1β after TLR stimulation. An activation signal triggers the activation of procaspase-1, the formation of inflammasome complexes, caspase-1 activation and the cleavage of pro-IL-1β[182]. AIM2 inflammasomes become activated by binding double-stranded DNA which allows oligomerisation of AIM2 and a conformational change that exposes the pyrin domain[183]. Apoptosis-associated speck-like protein (ASC) is important in inflammasome formation, recruiting procaspase-1 through its C-terminal caspase recruitment domain (CARD) and associating with NLRP3 or AIM2 through their pyrin domain (PYD),

thus bridging the inflammasome machinery and procaspase-1[184]. Humans with gain-of-function mutations in the NLRP3 inflammasome have been shown to have an increased capacity to control Mtb growth[185], while mice deficient in AIM2 are highly susceptible to Mtb infection and have a reduced capacity to produce IL-1β and impaired Th1 response[181]. Nitric oxide induced by IFN-γ has been shown to inhibit the assembly of the NLRP3 inflammasome to limit inflammatory damage to the host caused by IL-1β production and the associated neutrophil recruitment and tissue pathology in persistent infection[186].

Upon successful formation of the inflammasome to activate caspase-1, pro-IL-1β is cleaved into its mature active form. BMDM from caspase-1- or ASC-knockout mice infected in vitro had a significant impairment in the production of mature IL-1β[187], however in the same animals in vivo, IL-1β levels in BAL fluid were not significantly different to the wild type mice and these mice were less susceptible to Mtb infection than IL-1β-deficient mice. These findings indicate that caspase-1 independent pathways exist for Mtb-induced IL-1β production in vivo.

IL-1 signalling is essential for the control of Mtb infection. Mice deficient in both IL-1α and IL-1β developed significantly larger granulomas and produced less NO[188]. IL-1R1-deficient mice have also been shown to have larger granulomas and to have increased susceptibility to Mtb infection[189]. A more recent study has found that the presence of either IL-1α or IL-1β is sufficient to control acute Mtb infection, though long-term IL-1α- and IL-1β-deficient mice had increased disease pathology[190]. More specifically, IL-1β-deficient mice were shown to have a higher bacterial burden and increased mortality despite compensatory upregulation of IL-1α[187].

As already discussed, anti-TNF-α antibodies increase susceptibility to and the severity of Mtb infection[94]. Contrastingly, IL-1β blocking agents such as anakinra and canakinumab have not been associated with any increased risk of reactivation of latent Mtb despite being widely used on patients with inflammatory diseases[191]. Isolated cases of Mtb reactivation have been reported[192], however larger studies have not found any significant risk. Vitamin D deficiency has been associated with a higher risk of active Mtb infection[193] and vitamin D has been shown to boost IL-1β production in response to Mtb infection[194]. Human polymorphisms in IL-1β have been associated with Mtb susceptibility[195, 196], indicating a role for IL-1β in determining Mtb responses. A human polymorphism in the IL-1β promoter region which alters transcription factor binding was identified. Surprisingly, the genotype associated with high induction of IL-1β was associated with the development of active Mtb infection, increased disease severity and poor treatment outcome[197]. These findings indicate that while early expression of IL-1β is important in the initial stages of Mtb infection, controlled expression of IL-1β especially later in infection is also highly important to minimise pathology. Identifying the mechanisms controlling IL-1β over time may be key to specifically boost host defence while avoiding the deleterious effects associated with increased IL-1β activity.

There are several mechanisms through which IL-1β likely elicits its protective effects against Mtb infection. IL-1β has been shown to promote production of IL-12p40[198] and IFN-γ[189] and upregulate cell-surface TNFR1 expression[199]. More recently, IL-1β has been shown to promote anti-Mtb responses through the induction of PGE2 which suppresses type I interferons to promote bacterial containment[200]. PGE2 additionally promotes apoptotic rather than necrotic cell death, limiting bacterial dissemination[201]

The relationship between the induction of IL-1β and cellular metabolism is beginning to be appreciated. Innate immune cells activated with LPS have been shown to switch their predominant form of generating cellular energy from oxidative phosphorylation to aerobic glycolysis[202, 203]. This increased rate of glycolysis has been shown to be required for LPS-induced expression of IL-1β[176]. Enhanced glycolytic activity and reduced oxidative phosphorylation through the tricarboxylic acid cycle (TCA) was shown to lead to the accumulation of TCA intermediate metabolites including succinate. Increased succinate levels impair the activity of prolyl-hydroxylases which target HIF-1α for degradation, thus their inhibition allows the stabilisation of HIF-1α protein. HIF-1α can then bind the hypoxia response element in the promoter of the gene encoding IL-1β and initiate its transcription[176]. Recently Gleeson et al[204] have shown that Mtb infection induces this immunometabolic shift to glycolysis in several macrophage models including human alveolar macrophages and that this glycolytic response was essential for sufficient induction of IL-1β and control of Mtb growth.

1.2.2 Interplay between macrophage phenotype and metabolism

The term macrophage encompasses a range of cells that can have different origins, phenotypes and functions. In recent years, it has begun to be appreciated that macrophages fall into two developmentally distinct populations – recruited and tissue-resident macrophages[205, 206]. Recruited macrophages are of monocytic origin. Monocytes are derived from haematopoietic stem cell progenitors in the bone marrow which circulate in the peripheral blood until they migrate into tissues in response to growth factors, pro-inflammatory cytokines and microbial produts[207, 208]. Tissue-resident macrophages however take up residency in specific tissues during embryonic development and proliferate locally,

maintaining the population throughout the animal's lifespan[28, 207, 209]. Resident macrophages carry out homeostatic functions such as the clearance of cellular debris and processing of iron, as well as performing local immune surveillance[210]. Under homeostatic conditions, the AM population monitors the lung independently of monocyte-derived macrophages[211]. Tissue resident macrophages from different tissues are transcriptionally, and thus likely functionally, divergent[212].

At the same time, macrophages are highly plastic. In response to environmental cues they can be activated into one of two broad classifications – classically-activated pro-inflammatory macrophages, often termed "M1" macrophages, or alternatively-activated "M2" macrophages which are more anti-inflammatory and promote wound-healing and immunoregulation. Control of this phenotypic switch depends on many extrinsic factors (cytokines and environmental pathogens) and intrinsic factors (including epigenetics, metabolism and microRNA)[213]. The M1 phenotype is characterized by the expression of pro-inflammatory cytokines, NOS, ROS and promotion of a Th1 response, and is induced by TLR stimulation and IFN-γ through STAT1. M2 macrophages are typically highly phagocytic, express high levels of scavenger receptors and anti-inflammatory cytokines, and are instructed to develop this phenotype by IL-4 and IL-13 through STAT 6[213, 214]. The M1/M2 classification of macrophages was adopted to mirror the Th1/Th2 classifications in the T cell literature and is now somewhat outdated. The concept of macrophages having a broad range of activation states is now the more widely accepted view, with macrophages existing on a spectrum of classically activated, wound-healing and regulatory phenotypes[215], that are perhaps better defined by their activating signal. It should also be noted that macrophage activation status is distinct from macrophage

developmental origin, and that these factors overlay to define macrophage phenotype.

AM are long-lived[216] tissue resident macrophages with a high phagocytic capability and are believed to be the primary initial immune cell to interact with Mtb[28] and are therefore key in determining of the subsequent immune response to Mtb infection. Alveolar macrophages are unique in comparison to other tissue-resident macrophage populations in that they are in direct contact with the external environment, constantly being exposed to inhaled particulates, commensal bacteria and host-epithelial factors such as surfactant. The homeostatic activation state of AM has been controversial. A small population of IL-13-producing macrophages have been characterised in the lung compartment and this population increases in response to cigarette smoke, hinting that perhaps the normal population is more classically activated[217]. Recent evidence indicates that AM are relatively plastic in homoeostatic conditions. A study which examined the lungs of 6 normal donors used immunohistochemistry to determine the activation states of the AM present and found that healthy lung tissue AM expressed neither classical nor alternative activation markers[218]. Interestingly, smoking and COPD increased the expression of both pro- and anti-inflammatory macrophage markers and the co-expression of these markers, highlighting that activation states do not have to be exclusive.

In the context of Mtb infection, murine AM have been shown to become activated towards a pro-inflammatory phenotype with high expression of iNOS and low expression of arginase, and to progress to an M2 phenotype with high expression of arginase and low expression of iNOS later in the course of infection[219]. Interestingly, in this model only AM became activated in response

to infection - recruited monocytes did not, suggesting functional heterogeneity between these two developmental subsets of macrophages. Macrophages in the core of the granulomas of these mice had a persistent pro-inflammatory phenotype while the surrounding macrophages became more anti-inflammatory over time[219]. Transcriptional analysis of murine Mtb-infected murine macrophages showed an induction of classical activation-associated genes[220]. Human AM from patients with Mtb infection have also been transcriptionally profiled[221]. Patients could be separated into two groups – one with a transcriptional profile that suggested a Th1 response and one that indicated a Th2 response. Profiling of monocyte-derived macrophages infected with Mtb in an in vitro granuloma found a progression of macrophage activation from a pro-inflammatory to an anti-inflammatory state over time[222]. Together these findings suggest that Mtb can induce a range of macrophage activation states which can change over time.

Since excessive inflammation in many disease states is harmful to the host, strategies that reprogram macrophage activation state are of great interest. However, defective inflammation characterises other diseases and can be equally harmful to the host, for example in Mtb infection and in cancer. Therefore, a regulated short boost to macrophage pro-inflammatory responses is also of great interest.

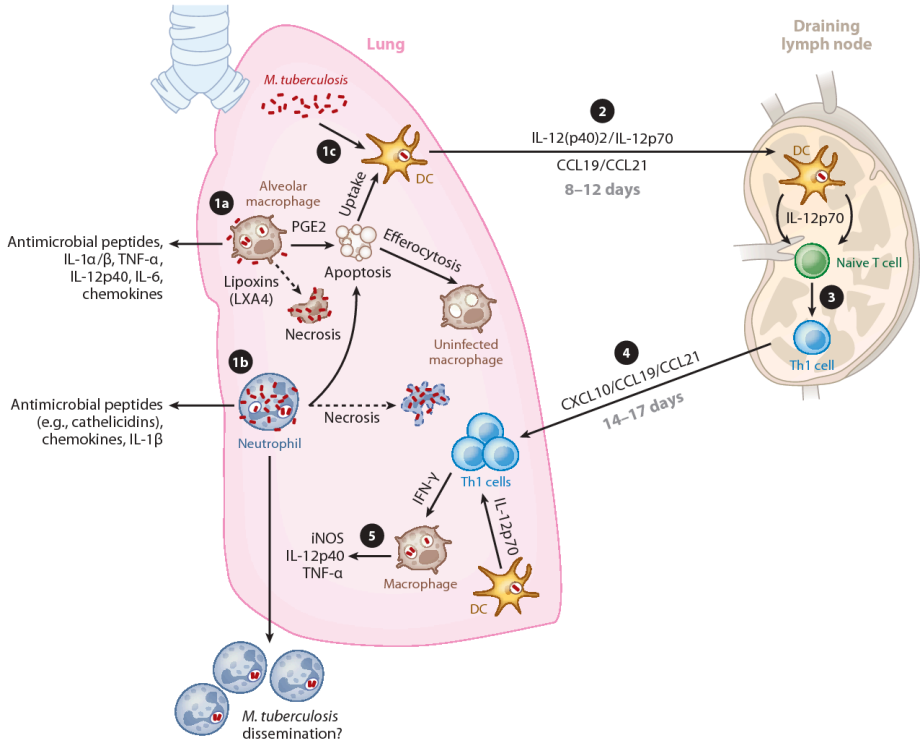

Figure 1.1 The cellular immune response to Mtb. Mtb is inhaled and enters the pulmonary compartment where it can infect resident lung alveolar macrophages (1a), neutrophils (1b) and lung DCs (1c), triggering the production and secretion of antimicrobial peptides, cytokines, and chemokines. The balance of lipid mediators, such as prostaglandin E2 or lipoxin (LX) A4, plays a major role in determining downstream pathways leading to the induction of either apoptosis or necrosis (1a). Infected apoptotic cells can be taken up by resident lung DCs or efferocytosed by uninfected lung macrophages (1c). DCs migrate to the local lung-draining lymph nodes by 8–12 days post infection. DCs migrate to the lymph nodes under the influence of IL-12 and the chemokines CCL19 and CCL21 (2), to drive naive T cell differentiation toward a Th1 phenotype (3). Protective antigen-specific Th1 cells migrate back to the lungs in a chemokine-dependent manner 14–17 days after the point of initial infection/exposure (4) and produce IFN-γ, leading to macrophage activation, cytokine production, the induction of microbicidal factors including iNOS (5), and bacterial control. Reproduced from O'Garra et al[223].

1.2.3 Metabolic reprogramming and macrophage activation

Macrophages of different activation states have different functions to perform, ranging from bacterial killing to wound-healing processes. Cellular energy metabolism in immune cells is receiving much attention of late, in particular how cells utilise the main fuels in their environment - preferentially glucose but also lipids and amino acids – to fuel their various functions. Under homeostatic conditions macrophages utilise mitochondrial oxidative phosphorylation to metabolise glucose and generate ATP. Oxidative phosphorylation forms ATP through the transfer of electrons from NADH or $FADH_2$ to O_2 by a series of electron carriers. This transfer takes place in mitochondria and is the major source of ATP in aerobic organisms. Cytosolic glycolysis generates pyruvate from glucose and while a small amount of that pyruvate is converted to lactate, the majority of pyruvate enters the tricarboxylic acid (TCA) cycle and generates NADH and $FADH_2$ [224]. NADH and $FADH_2$ can then act as electron donors in the mitochondrial electron transport chain located on the inner mitochondrial membrane allowing oxidative phosphorylation to take place and ATP to be generated. Complex I and Complex II accept electrons and transfer them via redox reactions. This electron is used to pump protons into the mitochondrial inter-membrane space through complexes I, III and IV, thus generating an electrochemical proton gradient or mitochondrial membrane potential. This proton gradient is used to drive ATP synthase (Complex V) to generate ATP. In the final reaction of the electron transport chain, oxygen acts as the electron acceptor and is reduced to water, thus oxidative phosphorylation requires and consumes oxygen. If oxygen is not present, pyruvate is not processed via the mitochondria and is instead used to produce lactate in the cytoplasm by glycolysis, generating ATP. This method of ATP production is far less efficient, creating 2 molecules of ATP per

glucose molecule compared with 36-38 molecules of ATP per glucose molecule generated by oxidative phosphorylation.

When macrophages become classically activated a metabolic shift occurs from oxidative phosphorylation towards glycolysis despite the availability of oxygen [225]. Glycolysis converts glucose into pyruvate in the cytoplasm to produce ATP through a pathway made up of 10 catalytic reactions, each catalysed by a specific enzyme. Three of these steps require a large negative Gibbs free energy and are essentially irreversible. Glucose is transported into the cell through a glucose transporter. The primary rate-limiting glucose transporter in pro-inflammatory macrophages is GLUT1[226], encoded by the SLC2A1 gene. GLUT1 is upregulated in response to Mtb infection and the increased requirement for glucose to sustain the induction of glycosis[164]. The first irreversible step of glycolysis is catalysed by hexokinase (HK) and is a rate limiting step, converting glucose to glucose-6-phosphate. This phosphorylation prevents glucose from escaping the cell. Though there are several isoforms of this enzyme, HK2 is the principal regulated form of this enzyme in most cell types[227] and is inhibited by 2-DG and upregulated in response to Mtb infection[164]. Furthermore it has been shown to be downregulated in diabetes patients and associated with increased risk for Mtb infection[228]. Liver cells express HK4 or glucokinase which has a much lower affinity for glucose, and thus only phosphorylates glucose when it is in high abundance, prioritising glucose for use in other tissues over glycogen synthesis when glucose supply is low[229]. Glucose-6-phosphate can at this point continue down the pathway of glycolysis or be converted into glycogen or oxidised by the oxidative branch of the pentose phosphate pathway (PPP)[230]. The PPP is a parallel pathway that occurs alongside glycolysis, converting glucose-6-phosphate into NADPH which can be used in the generation of reactive oxygen and nitrogen species, and ribose-5-phosphate for

the production of nucleotides. Activated macrophages have been shown to have increased PPP activity[231] and TLR stimulation suppresses carbohydrate-kinase like protein (CARKL), an inhibitor of the PPP pathway[232]. Alternatively, glucose-6-phosphate can be converted to generate glycogen. If glucose is to continue down the glycolytic pathway, it must first be converted into fructose-6-phosphate by phosphoglucose isomerase.

The second irreversible step of glycolysis is catalysed by phosphofructokinase (PFK) and is thus the most important rate-limiting enzymatic reaction in glycolysis. It is the first key point of commitment to the glycolytic pathway as it costs a molecule of ATP and is irreversible. PFK-1 converts fructose-6-phosphate and ATP to fructose-1,6-bisphosphate. This step is rate-limiting and therefore a crucial determinant of the rate of glycolytic flux. PFK-1 is allosterically regulated, allowing tight control of glycolysis. PFK-1 is inhibited by ATP and activated by AMP, allowing PFK-1 to be activated only when required by the cell[233], and inhibited by the product of the citric acid cycle citrate[234], but most potently by fructose-2,6-biphosphate (F2,6BP) which can boost PFK-1 activity even in the presence of ATP[235]. F2,6BP uncouples glycolysis from product inhibition. F2,6BP is generated by from fructose-6-phosphate by PFKFB family (6-phosphofructo-2-kinase/fructose-2,6-biphosphatase) and is also degraded by PFKFBs via their phosphatase ability and by TIGAR. PFKFB3 is induced in pro-inflammatory macrophages[202, 236], and in response to Mtb infection[231], and additionally has been shown to be more upregulated in the presence of IFN-γ. It has a high kinase to phosphatase ratio[237], promoting generation of F2,6BP to activate PFK-1 and thus glycolysis.

PFK-1 is a tetrameric enzyme that can be composed of different combinations of the muscle (M), platelet (P) and liver (L) isoforms of the enzyme. Each isoform is encoded by a different gene and isoforms are differentially expressed in different tissues. RNA-seq analysis of murine BMDM showed that PFK-L and PFK-P were upregulated 24 hours post Mtb infection, however PFK-M was not[164].

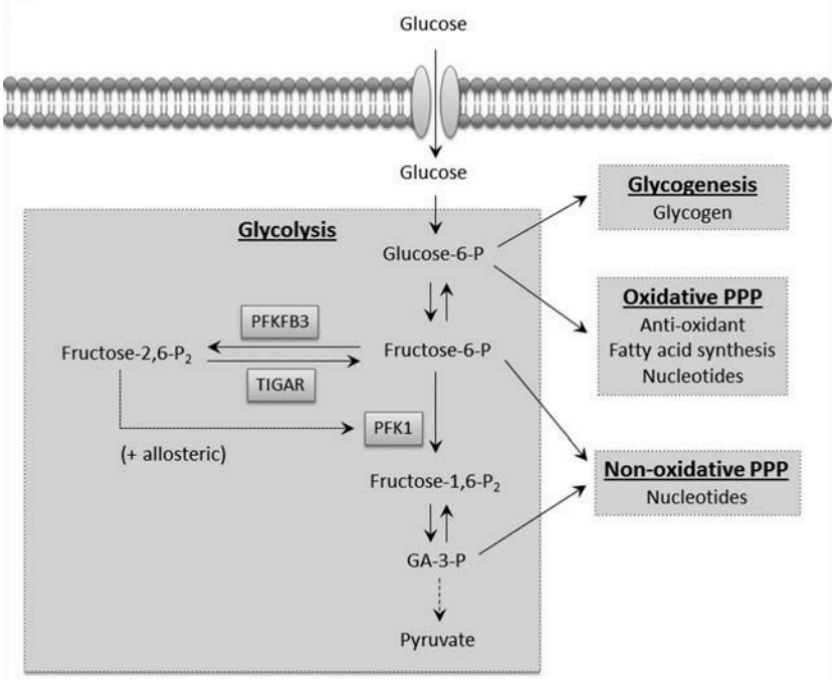

Figure 1.2 Glycolysis and the PPP. Glucose entering the cell is converted to glucose-6-phosphate which can be directed to produce glycogen or to arms of the PPP to generate different metabolites. Phosphofructokinase-1 (PFK-1), which catalyzes the first committed step of glycolysis in an irreversible reaction, is activated by fructose 2,6 bisphosphate (F2,6BP). F2,6BP levels in the cell are determined by the rate of its generation and degradation by 6-phosphofructo-2-kinase/fructose-2,6-bisphosphatases (PFKFB) and TIGAR. Adapted from Mor et al[238].

The third irreversible step in glycolysis is catalysed by pyruvate kinase (PK), generating pyruvate from phosphoenolpyruvate. The PKM2 isoform has been shown to be upregulated in macrophages in response to LPS and to be essential for the glycolytic shift and production of IL-1β[239] and has also been shown to be upregulated in response to Mtb infection[164]. Palsson-McDermott et al have additionally shown that Mtb ligands upregulated expression of PKM2 and HIF-1α, and the targeted blockade of PKM2 with a specific inhibitor resulted in a loss of bacterial containment, similar to blocking glycolysis with 2-DG[239].

Lactate dehydrogenase (LDH) catalyses the interconversion of pyruvate and lactate and accompanying interconversion of NADH and NAD^+. LDHA is upregulated in response to metabolic reprogramming in macrophages and dendritic cells[164, 240]. Accumulation of lactate, the final product of glycolysis, is enhanced in response to increased rates of glycolysis and can be used as a surrogate marker of glycolytic activity[241]. The view of lactate as a waste product of metabolism is beginning to be re-examined. Lactate has been shown to inhibit T cell migration[242], polarise tumour-associated macrophages towards an M2-phenotype[243], inhibit pro-inflammatory macrophage responses and glycolytic programming[244] and drive dendritic cells towards a more tolerogenic phenotype[245]. Lactate has also recently been reported to facilitate Mtb growth by acting as an additional carbon source[246].

Activation-induced switching to aerobic glycolysis, termed "glycolytic reprogramming" is also seen in many other types of immune cells including monocytes[247], neutrophils[248], dendritic cells[203] and lymphocytes[249]. This enhanced glycolytic profile in activated immune cells has been noted in the literature for several decades[250], however only in recent years has metabolic reprogramming has recognised as a key response to stimuli in the cellular environment, and the concept that metabolism may in fact be a major determinant in immune cell phenotype has gained traction. As field of immunometabolism has emerged, the mechanisms behind this metabolic reprogramming are now being explored and the role that aerobic glycolysis plays in immune cell function has begun to be elucidated.

One of the central concepts underpinning the idea that metabolic profiles underpin macrophage function is the clear relationship between macrophage activation state and metabolism.

Macrophages stimulated with pro-inflammatory stimuli such as LPS towards a classically activated phenotype undergo a glycolytic shift, characterised by enhanced lactate production and flux through the pentose phosphate pathway accompanied by decreased TCA cycle activity. On the other hand, macrophages stimulated towards an alternatively activated phenotype with IL-4 or other anti-inflammatory signals primarily utilise oxidative phosphorylation and actively block glycolysis [251].

Glycolytic reprogramming has been reported to be induced via signalling through TLR2[252], TLR3[253], TLR4[239], TLR7/8[253] and TLR9[203]. LPS and other inflammatory stimuli such as hepatitis B virus[254] and *Bordetella pertussis*[176] induce glycolytic reprogramming through diverse signalling pathways. For example, activation of mTOR by TLR stimulation enhances glycolytic and pro-inflammatory gene expression by boosting HIF-1α expression[255, 256]. Pro-inflammatory activation also upregulates inducible nitric oxide synthase (iNOS) expression in macrophages which promotes nitric oxide (NO) production. NO reduces mitochondrial respiration rates by nitrosylating target proteins in the electron transport chain, thus dampening oxidative phosphorylation[257]. AMP-activated protein kinase (AMPK) activity can also be reduced by pro-inflammatory macrophage reprogramming[258], thus decreasing β-oxidation and mitochondrial activity. β-oxidation is the catabolic process by which fatty acids are degraded, generating acetyl-CoA which enters the TCA cycle, and NADH and FADH2 which are co-enzymes in the electron transport chain of oxidative phosphorylation.

The possible benefits of glycolytic reprogramming to an activated macrophage are manifold. The induction of glycolysis may be a way to rapidly ramp up ATP production, as although it is an inefficient process it can be very rapidly induced. Another possible reason pro-inflammatory macrophages have adopted this glycolytic

reprogramming is that the TCA cycle of activated macrophages is downregulated due to decreased delivery of pyruvate and becomes functionally broken in two places leading to an accumulation of citrate[259] and succinate [231] two intermediates which fuel the immune response. Citrate is important for prostaglandin, ROS and NO production, while succinate accumulation leads to HIF-1α activation and IL-1β transcription. Nucleotide biosynthesis is boosted due to the enhanced PPP activity. This could possibly be beneficial for the synthesis of induced mRNA and other non-coding RNA including microRNA. NAPDH production is also boosted due to this PPP activity. NADPH is the substrate through which NADPH oxidase generates reactive oxygen species (ROS) and the substrate for nitric oxide synthase to generate nitric oxide species (NOS). ROS and NOS induction aid bacterial killing.

Conversely, alternatively activated macrophages upregulate oxidative phosphorylation[176] and fatty acid oxidation[260]. A study just published by Herrmann et al [261] has indicated that while glycolysis is essential for pro-inflammatory activation, it is not required for differentiation into an anti-inflammatory phenotype as long as oxidative phosphorylation is unimpeded.

1.2.4 Interplay between macrophage metabolism and Mtb

As Mtb utilises the macrophage as its primary host cell thus serves as a model in which to study the interaction between immunometabolism and infection. Transcriptomic profiling of murine macrophages of Mtb-infected murine lung has shown enhanced expression of glycolysis-associated enzymes, and protein and RNA analysis of Mtb-infected macrophages also show elevated levels of HIF-1α[231], even at 30 days post infection. Higher lactate levels as measured by NMR have also been detected in Mtb-infected murine lungs compared to uninfected[262]. Uptake of

^{18}F-fluorodeoxyglucose (^{18}F-FDG), a glucose analogue, as measured using positron emission tomography coupled with computer tomography (PET/CT) is a method being explored as a means of following tuberculosis disease activity in humans[263, 264]. Type 2 diabetes mellitus (DM2) has been recognised as a risk factor for Mtb. DM2 is characterised by an impairment of glucose utilisation increases the risk of Mtb disease approximately 3-fold[265]. Recent work by Gleeson et al[204] has shown that Mtb induces glycolytic reprogramming in human alveolar macrophages and this is essential for the induction of IL-1β and the control of bacterial growth. Furthermore, the authors went on to show that smokers' alveolar macrophages had an impaired propensity for glycolytic reprogramming, linking macrophage metabolic reserves with the increased susceptibility to Mtb infection observed in smokers[266]. While there is evidence for the interrelatedness of glycolysis and Mtb responses, the field of immunometabolism in the context of Mtb infection is relatively new and underexplored. A greater understanding of how metabolism impacts Mtb immunity and how it is regulated and can be manipulated will open the potential for novel therapeutic interventions and vaccination strategies.

1.3 MicroRNA-21 and the Immune System

1.3.1 Introduction to MicroRNA

In the post-genomic era, with the realisation that non-protein coding RNA can regulate gene expression substantially, microRNA have emerged as key molecules in regulating a range of cellular processes, including innate immunity[267]. microRNAs (miRNA) are small, non-coding RNA molecules which are approximately 22 nucleotides long in animals. MiRNA are estimated to make up about 1% of all genes in mammals[268], found as distinct genetic elements or encoded within host introns, and act as post-transcriptional regulators.

MiRNA biogenesis takes place in several stages. First, miRNA are transcribed by RNA polymerase II and/or III as long primary transcripts known as pri-miRNA which can be 100 to 1,000 nucleotides long[269]. Pri-miRNA transcripts contain sequence complementary regions and form double-stranded stem loops containing a hairpin structure that houses the mature sequence. The pri-miRNA stem loop is processed in the nucleus by a protein complex containing DROSHA and DGCR8 (also known as Pasha) into smaller (60-70 nucleotides long) double-stranded RNA molecules known as pre-miR[270]. Pre-miRNA are exported into the cytoplasm by exportin-5[271] where they are then cleaved to remove the stem loop by the DICER enzyme, creating double-stranded RNA molecules with 2-3 nucleotides overhanging at each end known a miRNA duplexes. The pre-miRNA is loaded onto an Argonaute protein and the strand that is complementary to the target mRNA (guide strand, usually the more stable strand) becomes part of the microRNA-induced silencing complex (RISC), while the other strand (passenger or star strand) is released and degraded. Either strand of the duplex can potentially act as a mature microRNA, but usually just one of the stands is incorporated

into the RISC complex[272]. These steps are illustrated in **Figure 1.3**. miRNA biogenesis can be regulated by different accessory proteins at each of these steps to regulate miRNA homeostasis[273].

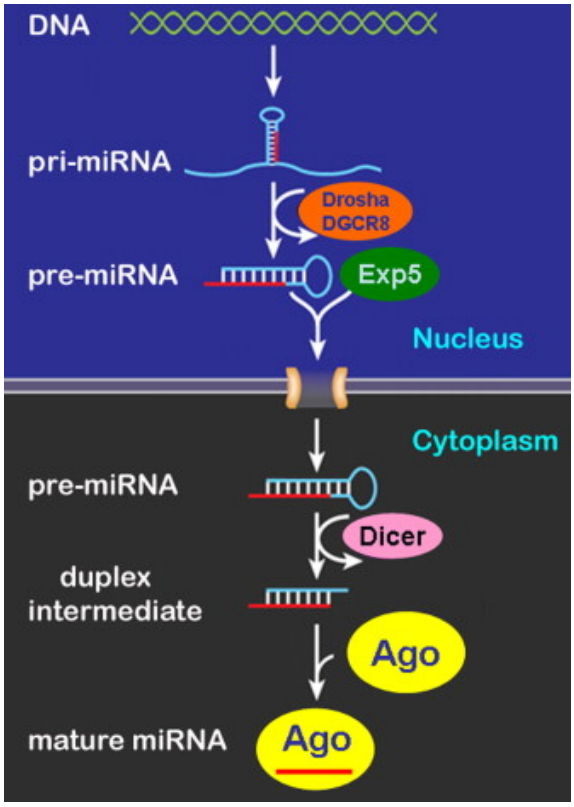

Figure 1.3 microRNA biogenesis. miRNA are transcribed by RNA polymerase II and/or III as long primary transcripts known as pri-miRNA and processed in the nucleus by a protein complex containing DROSHA and DGCR8 to pre-miRNA. Pre-miRNA is exported to the cytoplasm by exportin 5 where it is cleaved by DICER creating an RNA duplex with 2-3 nucleotides overhanging at each end. This is loaded onto an Argonaute (Ago) protein and the strand that is complementary to the target mRNA (guide strand, usually the more stable strand) becomes part of the microRNA-induced silencing complex (RISC), while the other strand (passenger or star strand) is released and degraded. Adapted from Graves et al[274].

miRNA are generally repressive molecules involved in post-transcriptional silencing. Mature, single-stranded miRNA in the RISC bind to complementary regions in the 3' UTR of mRNA. Genes with longer 3'UTR tend to have more miRNA binding sites

and be more susceptible to miRNA regulation, common housekeeping genes tend to have short 3'UTR[275]. Partial complementarity results in repression of mRNA translation while full complementarity leads to degradation of the mRNA transcript[276]. Interactions between miRNA and mRNA is usually confined to a "seed" sequence – nucleotides 2-8 at the 5' terminus of the miRNA. This 6 nucleotide seed sequence is highly evolutionarily conserved[277]. Complementarity at nucleotides 2-7 is generally not sufficient for target repression but an additional base of complementarity at position 8 enhances target repression[278].

Individual miRNA can target many different mRNA. Each miRNA can recognise approximately 100-200 mRNA target sites[279], and conversely at least 50% of human mRNA transcripts have multiple conserved, predicted miRNA binding sites[280]. Thus there is a large number of potential interactions and a huge potential for nuanced regulation of protein expression. Target prediction programs use sequence information, evolutionary conservation and structure-associated free energy to predict miRNA:mRNA interations and often predict a high number of false-positive interactions[281], thus predicted targets must be validated in vitro. MiRNA have been shown to have a long half-life and each miRNA transcript to be able to bind at least 2 target transcripts in vivo, helping to explain how miRNA can regulate many targets at once[282]. miRNA generally do not silence target expression, but rather provide a fine-tuning mechanism for regulating protein expression, with experimental studies showing modest but functional effects at the protein level. Multiple miRNA targeting a single mRNA or targeting multiple mRNA in a single pathway can amplify miRNA effects[283].

Transcription of miRNA genes is similar to that of protein-coding genes[284]. Many transcription factors can positively or negatively

regulate miRNA expression by binding to promoter regions[285]. Genes encoding miRNA are in intra- and inter-genic positions in the genome. More than half of all miRNA are found within the introns of their host genes and co-express with the neighbouring protein-coding sequences[268], though a significant number are encoded far from any protein-coding sequences implying that they are independently transcribed and have their own promoter regions[286]. Many examples of miRNA clusters have been found, with multiple miRNA in polycistronic units, suggesting that they may have shared functionalities[287].

1.3.2 MicroRNA therapeutics

MicroRNAs are emerging targets in the field of drug discovery, and are attractive target molecules because of their small, linear nature allowing easy complementary targeting. MicroRNA dysregulation is a common feature in a wide range of disease states, including cancer, cardiovascular disease and hepatitis[288]. The ability of miRNA to target multiple mRNAs make them interesting candidates to be used as therapeutics (miRNA mimics) or to target (using anti-miRNA). Delivery of miRNA mimics in vivo has several challenges. Chemical modifications that will allow delivery will also reduce the efficiency of loading into RISC and thus reduce the ability of mimics to repress target proteins. Viral vectors may be a future option however the technology is not yet of a suitable safety profile for clinical use[289]. Other delivery systems such as liposomes, and polyethylenimine (PEI) polymers have other drawbacks such as immunostimulatory properties, low efficiency and difficulties in targeting the disease site[290]. Therapeutics targeting miRNA are already in pre-clinical and clinical trials for diseases including heart failure, atherosclerosis, cancer and most notably hepatitis C infection for which positive treatment outcomes with few off-target

effects are being observed with “Miraversin”, which targets hepatic miR-122 implicated in viral persistence, in Phase II clinical trials[289].

1.3.3 microRNA-21

MiR-21 is one of the most highly expressed miRNA with expression in most mammalian cell types[291]. miR-21 is encoded by an intronic gene with its own promoter[292] on chromosome 17q23.2, overlapping with the protein coding gene TMEM49 in humans or VMP1 in mice. Several promoter regions have been identified for miR-21 with conserved enhancer elements including binding sites for AP-1, Ets/PU.1, C/EBPα, NFI, SRF, p53 and STAT3[292, 293, 294, 295]. TLR4 stimulation[296], LPS[297], bacterial[298] and viral[260] infection have all been shown to induce pri-miR-21 transcription. Post-transcriptional regulation of miR-21 expression has also been demonstrated. TGF-β and BMP4 were shown to induce a 4-fold upregulation of pre-miR-21 expression while the expression of pri-miR-21 remained unchanged[299] in vascular smooth muscle cells. Elevated miR-21 levels were shown to be due to enhanced processing of the pri-miR-21 transcript. After activation, signal transducer SMADs (SMAD1/5 and SMAD2/3) were recruited to pri-miR-21 in the Drosha microprocessor complex, enhancing processing of pri-miR-21 to pre-miR-21 thus boosting levels of the mature miR-21 transcript. TGF-β has also been shown to induce miR-21 expression through SMAD3 and contribute to both renal[300] and pulmonary[301] fibrosis and a miR-21-specific anti-miR is being developed as a therapeutic to limit fibrotic damage in kidney disease[302].

MiR-21 has diverse roles. It has been shown to regulate processes in embryonic development, for example in branching morphogenesis where it fine tunes the expression of matrix metalloproteases though targeting of RECK and PDCD4[303]. The

cellular processes that are regulated homeostatically by miR-21, including apoptosis[304], cellular proliferation and invasion[305], make it a prime candidate to act as an onco-miR, a miRNA frequently associated with cancers. It is frequently upregulated in cancers of both solid[306] and leukemic origin[307] and has been proposed as a cancer biomarker for different cancers in different biological materials[308, 309, 310]. A role for miR-21 in the development of organ fibrosis has also be shown[301] and blocking miR-21 activity in vivo in a murine model has a protective effect against fibrosis[311].

It is now also emerging that functionally active miR-21 can be secreted from cells within exosomes and taken up by other cells[312]. For example, the exosomal transfer of miR-21 from tumour-associated macrophages into tumour cells has been shown to suppress cancer cell apoptosis and make cells less receptive to chemotherapy[313]. This suggests that miR-21 could be a key signalling molecule across diverse tissues.

1.3.4 miR-21 in the macrophage

The importance of miRNA in macrophage function is beginning to be recognised. Profiling of classically activated M1 macrophages and alternatively activated M2 macrophages has shown that different microRNA signatures are associated with polarisation states[314]. One of the most highly expressed miRNA in mammalian cells is miR-21[291]. miR-21 target mRNAs include tumour suppressors programmed cell death protein 4 (PDCD4)[296] and phosphatase and tensin homolog (PTEN)[315], STAT3[316] and IL-12p35[317].

Although there has been a lot of interest in miR-21 for its roles in oncogenesis[318], miR-21 is also highly expressed in many cells of

the immune system, including macrophages. It has been proposed as a key regulator of immune processes, with existing literature suggesting that it may act as feedback molecule induced by inflammatory stimuli to limit inflammation-associated host damage[296, 302]. Sheedy et al[296] used a murine model to illustrate that miR-21 negatively regulates TLR4 signalling, promoting IL-10 production through degradation of PDCD4. Johnston et al investigated the role of miR-21 in macrophage responses to infection with *Listeria monocytogenes* using a murine knockout model[298]. Macrophage phagocytic ability and production of TNF-α were found to be significantly higher in response to LPS or *Listeria* infection in miR-21-deficient macrophages, though no difference in IL-10 or NO production was noted. In a model of efferocytosis[319], miR-21 was linked with the induction of an anti-inflammatory phenotype and enhanced levels of IL-10 through the miR-21 target PDCD4. A similar effect was seen in a recently published report examining macrophage responses to peritonitis[109]. Cheadle et al demonstrated that miR-21 is induced in a murine model of LPS peritonitis and this serves a protective effect, limiting inflammation through promoting IL-10 and restricting TNF-α and IL-6 production. However, compared to the efferocytosis model, no effect on levels of the miR-21 target proteins PDCD4 or PTEN thought to control these cytokine changes was observed. Stanley et al[320] show induction of miR-21 by colony stimulating factor 1 (CSF-1) in murine macrophages, and subsequent suppression of M1-associated genes including IL-6, TNF-α and inducible nitric oxide synthase (iNOS) and enhancement of M2-associated genes including arginase 1 and mannose receptor C type 1 (Mrc-1). Together, these studies indicate a role for miR-21 in dampening macrophage inflammatory processes.

While limiting inflammation is important to protect host tissues, in the case of Mtb infection the macrophage response is not

sufficient to totally eradicate the bacteria and does not generate an effective adaptive response[321]. If, as evidence suggests, miR-21 promotes an anti-inflammatory macrophage phenotype, its role in Mtb infection may benefit the bacteria. To date there are few reports on the role of miR-21 induction in macrophage responses to Mtb. A study on the related human pathogen and causative agent of leprosy, *Mycobacterium leprae*, found a significant increase in expression of miR-21 in *M. leprae* infected monocytes[322]. This was associated with a downregulation of IL-1β and induction of IL-10. Li et al[206] have demonstrated that BCG infection induces miR-21 in murine alveolar macrophages in vivo and this suppresses IL-12 production which ultimately leads to reduced anti-mycobacterial T cell responses. More recently, BCG has been shown to induce miR-21 expression in a murine macrophage cell line through TLR4 and this results in higher expression of both TNF-α and IL-10[8]. Another indicator that encourages the hypothesis that reducing miR-21 activity in the context of Mtb infection may result in improved immune responses is the observation that one of the antibiotics currently used to treat Mtb infection disrupts miR-21 induction. Streptomycin was found to bind to pre-miR-21 and inhibit its processing thus reducing the amount of mature miR-21 induced[323].

1.3.5 miR-21 and metabolism

The role of miR-21 cellular metabolism is not well defined. However given that miR-21 is involved in regulating inflammation, a process closely interlinked with metabolism, as well as being associated with many cancers [318] which too are known to display aberrant metabolism, the relationship between metabolic processes and miR-21 warrants investigation. One preliminary study in cancer-associated fibroblasts indicated an association between miR-21 expression and higher rates of glycolytic activity[324], but no work to

date has been published on miR-21 and metabolism in the macrophage.

1.4 Thesis Aims

Mtb is the world's most successful pathogen, subverting the normal host innate immune response to survive within in its primary host cell – the macrophage. This thesis sets out to define how a putative negative regulator of TLR signalling, miR-21, can impact on macrophage responses to Mtb infection. MiR-21 targets the expression of key cytokines in the response to Mtb. This work hypothesises that miR-21 plays an important role in regulating the switch from a pro-inflammatory to an immunoregulatory macrophage phenotype and that Mtb infection exploits this to promote its survival and thus blocking miR-21 activity using anti-miR technology will improve host immunity.

1. To examine the role of miR-21 in the context of macrophage function with an emphasis on responses to Mycobacterium tuberculosis infection by characterising macrophage immune responses when miR-21 activity is blocked

2. To define the targets of miR-21 in the macrophage immune response to Mtb and assess whether these interactions can be therapeutically targeted

3. To investigate the role of immunometabolic reprogramming in Mtb-infected macrophages, the mechanisms regulating its induction and how this reprogramming relates to macrophage activation

Chapter 2:

Materials and Methods

2.1.1 Animals

miR-21 knockout mice were created by Taconic Artemis using a Cre/loxP approach[296, 325]. Two loxP sites were inserted either side of the miR-21 coding region downstream of Tmem49, allowing removal of the floxed miR-21 site by Cre recombinase. After miR-21 deletion, offspring were backcrossed onto a C57BL/6J background. miR-21 knockout homozygotes were identified by PCR and wild-type littermates were used as controls. Mice were bred in specific pathogen-free conditions and were kept according to Irish and European regulations.

2.1.2 Murine bone marrow-derived macrophages

Murine bone marrow-derived macrophages were generated using a protocol adapted from [326]. Mice age 8-12 weeks were sacrificed by CO_2 asphyxiation. Mice were pinned down and sprayed with ethanol. The lower abdomen was opened using scissors, and an incision made down the skin of each leg to expose the hips and legs. Femur and tibia bones were isolated without breaking the bone and the bones placed into DMEM medium. In a tissue culture hood the flesh was removed from the bones using forceps, scissors and rubbing with ethanol-soaked tissue. The extremities of the bones were clipped at each end and bone marrow flushed out into sterile DMEM using a 23G needle and a 5 mL syringe of DMEM. Flushed marrow was pipetted with a P1000 to break up larger clumps and the marrow and medium was then centrifuged at 400 relative centrifugal force (rcf) for 5 minutes. Supernatant was discarded and erythrocytes were lysed in 1 mL of red cell lysis buffer (Sigma-Aldrich) for 1 minute. 9mL DMEM was added to neutralise the lysis buffer and the cells were spun at 400 rcf for 5 minutes. Cell number was calculated using Trypan Blue staining and a haemocytometer. Approximately $10x10^6$ cells plated per 15 cm culture dish in 25 mL of medium (DMEM, 20% L929-conditioned

medium (as generated in **2.1.4**), 10% FBS and 1% penicillin-streptomycin. Cells were gently washed with PBS and fresh medium added every two or three days. On day 7 cells were detached with cold PBS and cell scrapers, counted and seeded at $1x10^6$/mL in DMEM 10% FBS, 5% L929-conditioned medium, one day prior to experiments.

2.1.3 Assessment of BMDM purity by flow cytometry

BMDM purity and yield was assessed in both wild-type and miR-21 knockout cell cultures. When BMDM reached maturity, approximately 1 x 10^6 cells were washed with PBS and scraped using the rubber plunger of a 1 mL syringe and transferred to labelled 5 mL round-bottom polypropylene flow cytometry tubes (Falcon). Tubes had been coated on ice with 500 μL of FBS which was removed before addition of cells to minimise adherence of BMDM to the tubes. Tubes were centrifuged at 300 rcf for 5 minutes and supernatant discarded. Cells were resuspended in 30 μL of PBS containing 2 μL of Fc receptor inhibitor antibody (ThermoFisher) for 5 minutes at room temperature. Sample BMDM were stained with 1 μL of PeCy7 anti-mouse CD11b antibody and 1 μL of APC/Cy7 anti-mouse F4/80 antibody (Biolegend). Samples were also stained with 0.5 μL of Zombie Aqua viability dye (Biolegend). A dead control tube was set up by incubating BMDM with 20% DMSO and viability dye to provide a positive dead population. Fluorescence minus one (FMO) controls were also set up in order to correctly gate upon the stained cell populations. FMO controls contain each dye in the panel bar one and allow the spread of fluorescence into other channels of interest to be identified. The FMO controls are detailed in **Table 2.1**.

	Zombie Aqua	F4/80 APC/Cy7	CD11b Pe-Cy7
Unstained	-	-	-
CD11b FMO	-	+	+
F4/80 FMO	+	-	+
PeCy7 FMO	+	+	-

Table 2.1 FMO controls for BMDM purity assessment.

Sample and FMO tubes were vortexed and incubated in the dark at room temperature for fifteen minutes. 1 mL of PBS was added to each tube and tubes were centrifuged at 300 rcf for 5 minutes. Supernatant was discarded and cells resuspended in 50 μL of PBS.

Compensation beads (Biolegend) were used as single colour controls to set up compensation and minimize the overlapping of emission spectra. One drop of compensation beads was placed in a flow tube and left unstained. A tube of beads was set up for each antibody (0.5 μL of antibody was added per tube).

Samples were analysed using the FACSCANTO II flow cytometer (BD Biosciences). Cells were gated upon according to their size (as determined by forward scatter area) and their granularity (as determined by side scatter area) to exclude debris. Single cells were then gated upon according to forward scatter height and area to exclude doublets of cells as these can skew results. Dead cells (i.e. those positive for the dead cell stain) were excluded from the analysis as they may stain non-specifically with antibodies. Finally, BMDM were defined as CD11b and F4/80 double positive cells, two

surface antigens classically used to define macrophages. A sample gating strategy is shown in **Figure 2.1**. BMDM were found to be of a high purity of Cd11b/F4/80 double positive cells and no significant difference in purity was found between genotypes, **Table 2.2**.

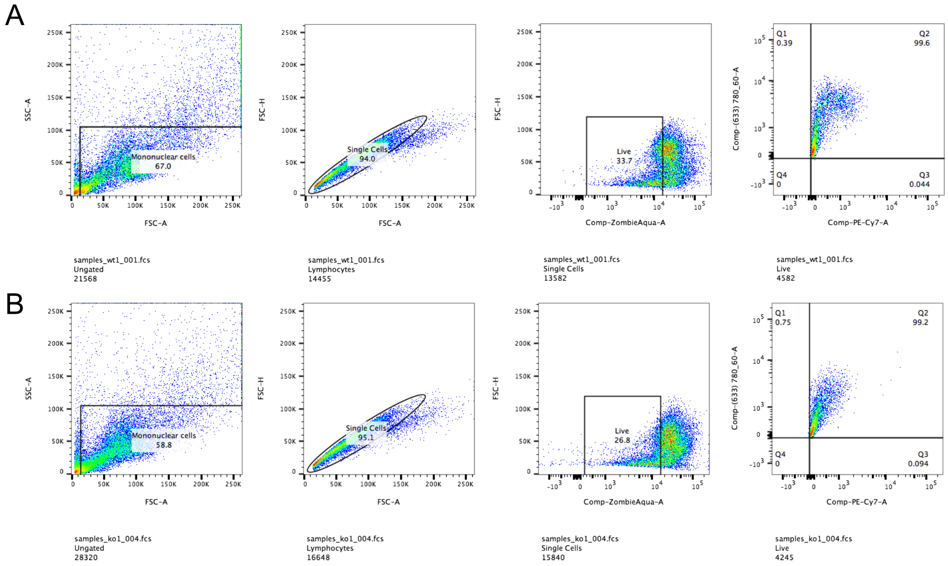

Figure 2.1 Sample gating strategy for BMDM assessing population purity. Wild-type (A) and miR-21 (B) knockout BMDM were matured for 7 days. Cells were washed and scraped to into a single cell suspension. Cells were blocked with an Fc receptor inhibitory antibody and stained with the viability die Zombie Aqua, PeCy7 anti-mouse CD11b antibody and APC/Cy7 anti-mouse F4/80 antibody. Cells were analysed using the FACSCANTO II flow cytometer.

	% CD11b^{+}F4/80^{+}		
WT	99.6	99.4	97.6
miR-21-/-	99.2	98	99.6

Table 2.2 BMDM purity as assessed by CD11b/F4/80 double positivity

2.1.4 Culture of L929 cells and generation of L929-conditioned medium

The L929 cell line is a murine fibroblast cell line. L929 cells produce M-CSF required for macrophage differentiation. L929-conditioned medium was generated by seeding 4.7 x 10^5 L929 cells in a 75 cm^2 culture flask in 55 mL of medium (DMEM GlutaMAX I, 10% foetal bovine serum (FBS), 1% HEPES and 1% penicillin-streptomycin). Cells were left to become over-confluent for 7 days. The supernatant was then collected and sterile-filtered using a 0.45 µM filter. Filtered supernatant was pooled, aliquoted and frozen at -20°C.

2.1.5 Isolation of murine alveolar macrophages and culture ex vivo

Immediately after mice were sacrificed by CO_2 asphyxiation, the trachea was exposed using a scalpel and forceps. A 20G IV catheter (BD) was inserted intratracheally. 0.5 mL of PBS at a time was syringed through the catheter to lavage the lungs. PBS was syringed back out of the lungs and retained. The lavages were repeated approximately 10 times with fresh PBS to obtain maximal cell yield. Lavage fluid was centrifuged at 400 rcf for 5 minutes. The cell pellet was resuspended in 1 mL red cell lysis buffer for 1 minute and then neutralised in 2 mL of DMEM. Cells were centrifuged again at 400 rcf for 5 minutes and then counted and plated in DMEM supplemented with 10% FBS and 1% penicillin streptomycin on plastic at 1x10^6 cell/mL to allow adherence of macrophages. Non-adherent cells were washed and removed after 24 hours.

2.1.6 Isolation of human monocytes and differentiation into macrophages

Primary human monocytes derived macrophages (MDM) were isolated from Buffy packs by density gradient centrifugation and adherence purification. Buffy packs were obtained from the Irish Blood Transfusion Service. Donors were not screened for blood type. Peripheral blood mononuclear cells (PBMC) were isolated by density gradient centrifugation. Buffy packs were cut open using a sterile scalpel and blood was poured into a sterile 100 mL container. The blood was then diluted 1:1 with sterile phosphate-buffered saline (PBS) and mixed using a serological pipette. 25 mL diluted blood was then slowly layered on top of 15 mL Lymphoprep (Stemcell) in a 50 mL tube. The layered mixture was centrifuged at 400 rcf for 25 minutes at room temperature with no brakes. The buffy coat layer of PBMC were transferred to a fresh 50 mL tube using a Pasteur pipette. The volume in the PBMC tube was brought to 50 mL with PBS and the tube spun at 300 rcf for 10 minutes (with brakes). Supernatant was discarded and the PBMC pellet resuspended in 1 mL of red cell lysis buffer (Sigma) for 1 minute to lyse contaminating erythrocytes. The volume of the tube was brought to 50 mL with PBS and the tube spun at 300 rcf for 10 minutes. Supernatant was discarded and cells were resuspended in 5 mL warm medium (RPMI 1640, 10% human serum).

Cells were counted and the volume of the cell stock diluted accordingly. Cells were seeded in non-coated 12-well tissue culture plates (Corning) at 2 x 10^6 cells per well in 2 mL of medium. Non-adherent cells were washed away with PBS and fresh medium was added every two to three days. Monocytes are highly adherent to plastic and thus the purification of monocytes was based on this attribute. On day six media was removed and cells washed three times with PBS to remove contaminating cells, leaving a field of

macrophages for experiments. Cells were either stimulated in these plates or gently scraped and reseeded as necessary.

2.1.7 Human primary alveolar macrophages

Human AM were isolated from bronchoalveolar lavage (BAL) fluid from patients of St James's Hospital. Patients consented for additional BAL fluid to be obtained while undergoing bronchoscopy as approved by the St James's Hospital / AMNCH Research Ethics Committee. BAL fluid was filtered through a 100 μm cell strainer (BD Falcon) and centrifuged at 390 rcf for 15 minutes. Supernatant was discarded and cells were resuspended in RMPI-1640 with 10% human serum, 50μg/mL fungizone and 50μg/mL cefotaxime. Cells were counted and plated onto Nunc 24-well tissue culture-treated plates (Sigma-Aldrich). After 24 hours of incubation, non-adherent cells were washed away and cells used for experiments. The AM used in this thesis were prepared in this manner by members of Professor Joseph Keane's research group and received at this stage of preparation. PCR for miR-21 in human AM was carried out by Dr. Seonadh O'Leary, Trinity College Dublin.

2.1.8 Culture of *Mycobacterium tuberculosis*

All work with live Mtb was carried out in a Biosafety Level 2 facility. Live Mtb H37Ra was obtained from the American Type Culture Collection (ATCC 25177) and was grown to log phase in Middlebrook 7H9 broth (Difco) supplemented with ADC enrichment medium (Becton Dickinson) and 0.05% Tween 80 (Difco) made in sterile water. Mtb was then sub-cultured weekly for four to five weeks. Prior to infection, bacteria were centrifuged at 3800 rpm for 10 minutes. The supernatant was discarded and the pellet was resuspended in 1 mL of warm DMEM. Bacteria were syringed with

a 25G needle several times to ensure at bacteria were dispersed and not clumping. The syringed solution was then centrifuged for 2 minutes at 800 rpm to remove any remaining clumps and the supernatant retained for experiments.

2.1.9 Preparation of irradiated *Mycobacterium tuberculosis*

Irradiated, non-viable H37Rv γ-irradiated whole cells (NR-49098) (BEI Resources, NIAID, NIH) (referred to as iRv, iMtb) were separated into 1 mL aliquots in 15mL tubes and stored at -80°C. Aliquots were thawed, resuspended in 5 mL of sterile PBS and sonicated for 15 minutes. Tubes were then centrifuged at 3800 rcf for 10 minutes. This process was repeated 10 times. The supernatant was discarded and the pellet was then resuspended in 2 mL of DMEM and sonicated for 15 minutes. This was then syringed through a series of needles of decreasing gauge size down to 25G until the solution passed though the needle with little resistance. The solution was then diluted further to a total volume of 10 mL and was stored at -80°C in 2 mL aliquots. Prior to use the aliquots were thawed and sonicated for 15 minutes and syringed through a 25G needle 10 times.

2.1.10 Mycobacterial infections

To control for different phagocytic abilities of different donor macrophages and variation in the final concentration of mycobacterial stock, multiplicity of infection (MOI) was determined for each experimental infection with iH37Rv (iMtb) and H37Ra (Mtb) on the same day as the experiment was carried out. Cells of interest were seeded on Nunc Lab-Tek II 8-well chamber slides (a glass slide treated to allow adherent cell culture with a plastic chamber structure that can be removed to allow microscopic examination of the slide) at the same time and at the same density as cells for experiments were seeded. LabTek chambers were

infected with a range of volumes of the mycobacterial stock. Slides were then incubated and three hours post-infection extracellular mycobacteria were washed off with PBS and cells fixed in 2% paraformaldehyde for 10 minutes. PFA was removed by 3 washes with water. Fixed cells were stained for mycobacteria using the Modified Auramine Stain kit (Becton Dickinson). Cells were covered with Auramine O for 1 minute, washed 3 times with water, covered in Auramine O Decolouriser for 1 minute and washed 3 times with water. Nuclei were stained for 5 minutes in the dark with 10 μg/mL Hoechst 33358 (Sigma-Aldrich) and washed 3 times with water. The plastic chamber on the slide was then removed and cover slips placed gently over the cells with a few drops of Dako fluorescent mounting medium (Agilent). Slides viewed under the 100X oil objective on an inverted fluorescent microscope (Olympus IX51) and MOI determined as the number of mycobacteria phagocytosed per cell and percentage of cells infected, e.g. 0-5 bacteria per cells with approximately 60% of cells infected as in **Figure 2.2**. The volume of Mtb stock required to achieve the desired MOI was calculated and cells were infected for experiments with volume required scaled up for the surface area of the experimental culture wells. Extracellular bacteria were removed 3 hours after infection to maintain the desired MOI. Media was removed and centrifuged to pellet the bacteria and bacteria-free supernatant was returned to the cells after two washes with media. Media was centrifuged rather than replaced to retain any early cytokine produced.

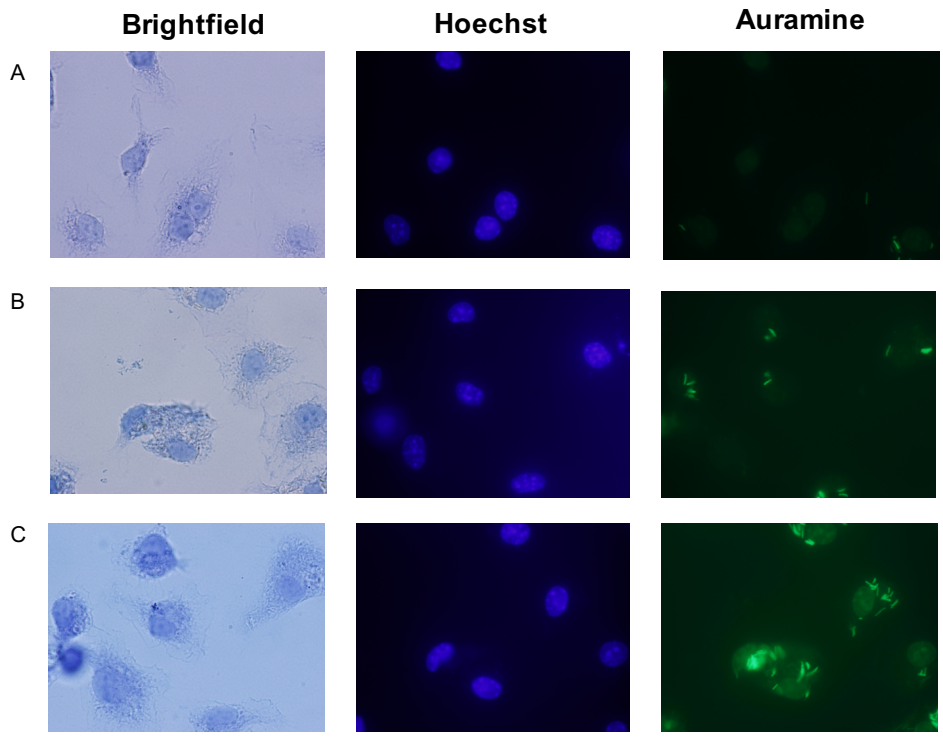

Figure 2.2 Example of fluorescent microscopy to calculate MOI. BMDM were infected for 3 hours with H37Ra and fixed. The cells were then stained with Hoechst 33358 (nuclei, blue) and Auramine O (Mtb, green) and imaged using an inverted fluorescent microscope. Rows A, B and C show an MOI of 2, 5 and 10 respectively.

2.1.11 Preparation of Middlebrook broth

Middlebrook broth was used for the culture of Mtb H37Ra and the dilution of cellular lysates for Mtb growth assays. The components required for 100 mL of broth are detailed in **table 2.3**. These components (except the ADC) were measured and combined in a glass bottle and autoclaved. After cooling to 45°C, the ADC was added. Middlebrook broth was used within 4 weeks of preparation.

Middlebrook 7H9 broth base (Sigma-Aldrich)	0.47 g
Tween 80 (Difco)	50 μL
Deionised water	90 mL
ADC enrichment medium (Becton Dickinson)	10 mL

Table 2.3 Components for 100 mL of Middlebrook broth

2.1.12 Preparation of Middlebrook agar

Agar plates for Mtb growth assays were prepared at least 1 day prior to use. The components required for 100 mL of agar are detailed in **table 2.4**. These components (except the OADC and cyclohexamide) were measured and combined in a glass bottle and autoclaved. After cooling to 55°C the solution was incubated at 55°C in a water bath for 45 minutes. Following this the OADC and cycloheximide were added. Cycloheximide is a eukaryotic protein synthesis inhibitor which prevents the growth of contaminating yeasts and moulds. Aliquots of 15 mL of agar were then immediately distributed into petri dishes using a serological pipette under sterile conditions. After allowing the plates 10 minutes to cool and solidify they were stored inverted at 4°C. The day before use the plates were incubated at 37°C with no CO_2.

Middlebrook 7H10 agar base (Sigma-Aldrich)	1.9 g
L-asparagine (Sigma-Aldrich)	0.1 g
Glycerol (Difco)	0.5 mL
Deionised water	90 mL
OADC enrichment medium (Becton Dickinson)	10 mL
Cycloheximide (Sigma-Aldrich)	50 μg/mL

Table 2.4 Components for 100 mL of Middlebrook agar

2.1.13 Mtb bacterial growth assay

Macrophages were infected with at an MOI of 5 bacteria per cell for 3 hours after which extracellular bacteria were removed by collecting the supernatant which was then centrifuged at 10,000 rcf for 10 minutes to pellet extracellular bacteria. Centrifuged media was replaced on the macrophages after 2 washes with fresh media. Cells were lysed in 0.1% Triton-X for 10 minutes at the desired time points. For the 3 hour time point, representative of bacterial uptake, 50 μL of this lysate was serially diluted into 450 μL of Middlebrook broth supplemented with ADC to create 10^{-1}, 10^{-2} and 10^{-3} dilutions. These were plated on 7H10 Middlebrook Agar in triplicate and colony-forming units counted after incubation at 37°C without CO_2 for 14 – 21 days. For later time points, the supernatants from the cells were centrifuged to pellet any extracellular bacteria and this bacterial pellet was combined with the cellular lysate.

2.1.14 Isolation and purification of total RNA using PureLink RNA Mini Kit

RNA was isolated from cells using the PureLink Mini RNA Kit (ThermoFisher) using a modified protocol. To minimise RNA degradation RNA isolation was performed on ice, the centrifuge was pre-cooled to 4°C and RNase-free tubes and pipette tips were used. Cell culture plates were placed on ice. Medium was removed from the cells and cells were lysed in 350 µL of RNA lysis buffer. Cells were scraped for a few seconds using a cell scraper and the samples were then pipetted into an Eppendorf tube and immediately placed on ice. Samples were frozen at -80°C until purification. Manufacturer's instructions were adapted to extract small RNA as follows. Harvested samples were thawed and immediately resuspended in 1.5 volumes of 100% molecular grade ethanol, added to the column and centrifuged for 30 seconds at 10,000 rcf. Flow-through was discarded and the columns washed twice with 500 µL of wash buffer II for 30 seconds at 10,000 rcf. Columns were placed onto fresh spin column and spun at full speed for 5 minutes to remove any remaining ethanol. Columns were then placed onto a fresh eppendorf and 30 µL of RNase-free water was added to elute the RNA bound to the filter. The column was centrifuged at 10,000 rcf for 1 minute. Flow-through was then returned to the column and centrifuged at 10,000 rcf for 1 minute again to maximise RNA yield. Samples were stored at -80°C.

2.1.15 Quantification of RNA and quality assessment

RNA concentration and quality was determined using the Nanodrop 2000 UV spectrophotometer (Thermo Fisher Scientific). The Nanodrop was cleaned and blanked with RNase-free water and 2 µL samples were run in duplicate. The yield and 260/280 ratio were recorded. A 260/280 value of approximately 2 was regarded as indicative of pure RNA yield. A low 260/280 ratio can indicate the

presence of protein contamination contaminants from the extraction protocol while a high ratio can be due to a contaminated blank.

2.1.16 Reverse transcription of mRNA

For transcription of mRNA into cDNA, the Taqman MicroRNA reverse transcription kit (Applied Biosystems) was used. The samples in each experiment were normalised to a selected amount of total RNA (typically 1 µg, less for samples of lower yield) to a total final volume of 13.2 µl in RNase-free water. Then 6.8 µL of reverse transcription mix (see **table 2.5** below) was added to give a final volume of 20 µL in a 0.2 mL RNase-free Eppendorf tube.

Component	Volume per reaction (µL)
10X Reverse Transcription Buffer	2
25X 100 mM dNTP	0.8
10X Random Primers	2
RNase Inhibitor	1
Reverse Transcriptase	1
Total	6.8

Table 2.5 Reverse transcription mix for mRNA

Samples were centrifuged at 500 rcf for 20 seconds and placed into a thermocycler and run according to the program in table 2.6.

	Step 1	Step 2	Step 3	Step 4
Temperature (°C)	25	37	85	4
Time (minutes)	10	120	5	∞

Table 2.6 Thermocycle program for reverse transcription of mRNA

Samples were stored at -20°C (short term) or at -80°C (long-term) until real-time PCR was performed.

2.1.17 Reverse transcription of microRNA

MicroRNA reverse transcription was carried out by first diluting the RNA with RNase-free water to make a 2 ng/μL stock of each sample. 5 μl of this stock was added to 10 μL of the reverse transcription mix (again using the Taqman MicroRNA reverse transcription kit) detailed in **table 2.7** in a 0.2 mL Eppendorf tube.

Component	Volume per reaction (µL)
10X Reverse Transcription Buffer	1.5
25X 100 mM dNTP	0.15
RNase-free water	6.41
RNase Inhibitor	0.19
Reverse Transcriptase	1
20X miR primer (specific to microRNA being targeted)	0.75
Total	10

Table 2.7 Reverse transcription mix for microRNA

Samples were centrifuged at 500 rcf for 20 seconds and placed into a thermocycler and run according to the program in **table 2.8** below.

	Step 1	Step 2	Step 3	Step 4
Temperature (°C)	16	42	85	4
Time (minutes)	30	30	5	∞

Table 2.8 Thermocycle program for reverse transcription of microRNA

Samples were stored at -20°C (short term) or at -80°C (long-term) until real-time PCR was performed.

2.1.18 Relative quantification of gene expression by Real-Time PCR

Relative mRNA and microRNA quantities were determined using FAM-labelled, pre-designed Taqman real-time PCR gene expression assays (Applied Biosystems, **table 2.9**). 2 µL of the cDNA was pipetted into a MicroAmp optical 384-Well reaction plate (Applied Biosystems). cDNA was diluted 1:10 with RNase-free water for mRNA samples made using 1 µg of total RNA and the dilution factor adjusted accordingly for samples of lower concentration. cDNA was used neat for the microRNA samples. 8 µl of RT-PCR mix (described in **table 2.10**) was added to each well. All samples were run in triplicate for each probe. HPRT and 18S were used as housekeeping genes for mRNA normalisation and RNU6B as the housekeeping gene for miRNA normalisation. The plates were sealed with MicroAmp optical adhesive film (Applied Biosystems) and centrifuged at 400 rcf for 1 minute. The plates were run on Applied Biosystems 7900HT Fast Real-Time PCR System according to protocol in **table 2.11**.

Gene	Taqman Assay ID
18S (mouse)	Mm04277571_s1
18S (human)	Hs03003631_g1
Arg-1 (mouse)	Mm00475988_m1
Hexokinase 2 (mouse)	Mm00443385_m1
Hexokinase 2 (human)	Hs00606086_m1
HPRT (mouse)	Mm01545399_m1
HPRT (human)	Hs02800695_m1
IL-1β (mouse)	Mm00434228_m1
IL-1β (human)	Hs01555410_m1
IL-10 (mouse)	Mm00439614_m1
IL-10 (human)	Hs00961622_m1
LDHA (mouse)	Mm01612132_g1
LDHA (human)	Hs01378790_g1
miR-21 (conserved)	Hs04231424_s1
NOS2 (mouse)	Mm00440502_m1
PDCD4 (mouse)	Mm01266062_m1
PDCD4 (human)	Hs00377253_m1
PFKL (mouse)	Mm00435587_m1
PFKL (human)	Hs01036347_m1

PFKM (mouse)	Mm01309576_m1
PFKM (human)	Hs01075411_m1
PFKP (mouse)	Mm00444792_m1
PFKP (human)	Hs00737347_m1
PTEN (mouse)	Mm00477208_m1
PTEN (human)	Hs02621230_s1
Pri-miR-21 (mouse)	Mm03306822_pri
Pri-miR-21 (human)	Hs03302625_pri
RNU6B (conserved)	001093
Slc2a1 (mouse)	Mm00441480_m1
Slc2a1(human)	Hs00892681_m1
TNF-α (mouse)	Mm00443258_m1
TNF-α (human)	Hs00174128_m1

Table 2.9 List of pre-designed Taqman real-time PCR gene expression assays

Component	Volume per reaction (µL)
2 X Taqman FAST advanced master mix	5
RNase-free water	2.5
20 X Taqman gene expression assay probe	0.5
Total	8

Table 2.10 Real-time PCR assay mix

Step	1 – Hold	2 – Hold	3 – Cycle	4 - Cycle
Temperature (°C)	50	95	95	60
Time	2 minutes	10 minutes	15 seconds	1 minute

Table 2.11 Real-time PCR program

RT-PCR data was analysed using the ΔΔ Cycle Threshold (ΔΔCt) value method. SDS software was used to calculate the Ct values of the endogenous controls and target genes. The Ct values for the target genes were normalised to the corresponding endogenous control, yielding the ΔCt value. The ΔCt value of the control sample was then subtracted from the ΔCt value of the samples under investigation, giving the ΔΔCt value. This value was normalised by the formula $2^{(-\Delta\Delta Ct)}$ to generate the fold change in expression of the target gene relative to the control sample.

2.1.19 Transfection of MDM with miRIDIAN microRNA Hairpin Inhibitors

The activity of miR-21 was specifically blocked in MDM using the miRIDIAN hairpin inhibitor of hsa-miR-21 (Dharmacon). These oligonucleotides are single-stranded RNA molecules that can be transfected into cells where they bind target mature microRNA species, preventing the microRNAs from binding their mRNA targets. RNase-free pipette tips and Eppendorfs were used for the transfection procedure.

The lyophilised inhibitors were resuspended in RNase-free water to generate a 20μM stock solution which was aliquoted and stored at -20°C. A non-targeting oligonucleotide (miRIDIAN microRNA hairpin inhibitor negative control #1) was incorporated into all transfection experiments. Cells were transfected with oligonucleotides using a 2% Lipofectamine-2000/Opti-MEM reduced serum medium solution, the volume of which being one tenth of the volume of medium on the cells. Opti-MEM was pre-warmed to 37°C before being pipetted onto the required volume of Lipofectamine in a cell culture hood. This mixture was mixed and allowed to sit at room temperature for 5 minutes. The volume of hairpin inhibitor required for a final concentration of 50 nM per well was pipetted into a fresh Eppendorf and the Lipofectamine/Opti-MEM mixture was pipetted drop-wise onto the inhibitor. This was then mixed and incubated at room temperature for 20 minutes. Cells were washed with PBS and given fresh medium during this wait. The transfection mixture was then pipetted drop-wise onto the cells. Cells were allowed to rest for 24 hours prior to experiments and medium changed before any treatments. Cell viability was assessed after transfection.

2.1.20 Propidium iodide viability assay

Cell viability after transfection was determined using the propidium iodide (PI) exclusion method adapted from the method developed by collaborators in the Keane group [327]. Staurosporine (1 μM) was used as a positive control to induce apoptosis. MDM were transfected with anti-miR control or anti-miR-21 as described in **2.1.17**. MDM were transferred into media containing 10% FBS instead of 10% human serum before staining as the human serum caused imaging issues. Cells were treated with 10 μg/mL PI, 10 μg/mL Hoechst 33342 and 10 μg/mL Hoechst 33358 (Sigma) for 10 minutes at room temperature. The number of PI-positive cells relative to total nuclei was determined using the Cytell Cell Imaging System. No significant toxicity was associated with transfection (**Figure 2.3**).

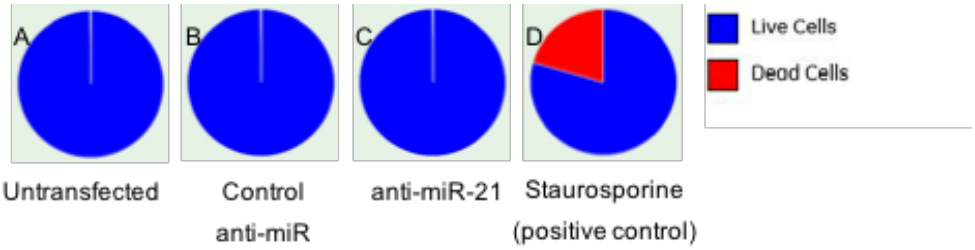

Figure 2.3 Propidum iodide viability assay to assess toxicity of transfection. Human MDM were transfected with 50 nM negative control anti-miR or anti-miR-21 using a 2% Lipofectamine/Opti-MEM transfection solution. 24 hours after transfection, cells were treated with 10 μg/mL PI, 10 μg/mL Hoechst 33342 and 10 μg/mL Hoechst 33358 for 10 minutes at room temperature. The number of PI-positive cells relative to total nuclei was determined using the Cytell Cell Imaging System.

2.1.21 Detection of secreted cytokine by ELISA

Enzyme Linked Immunosorbent Assay (ELISA) quantification of supernatant cytokine content was carried out using ELISA Ready-

SET-Go! from eBioscience. High-binding flat-bottom 96 well plates were coated with 50 µL per well of capture antibody diluted in coating buffer and incubated overnight at 4°C. Plates were washed three times the following day in ELISA wash buffer (0.05% Tween 20 in PBS). After each wash step plates were dried by banging them upside down on tissue. 150 µL of ELISA diluent was added to each well to block any remaining binding sites and the plate incubated for 1 hour at room temperature.

Standards were made using a serial dilution method in ELISA diluent. Frozen supernatant samples were thawed and vortexed. The plate was washed three times and the standards and samples added in triplicate, including ELISA diluent as a blank. For some cytokines (e.g. TNF-α) the samples were diluted to ensure they were within the range of the standard curve. The plates were incubated at 4°C overnight.

Plates were washed three times and 50 µL of detection antibody diluted in ELISA diluent added to each well. Plates were then incubated at room temperature for one hour. Plates were washed three times. 50 µL of streptavidin-horseradish peroxidase conjugate diluted in ELISA diluent was added to each well. Plates were incubated in the dark for 30 minutes at room temperature. Plates were then washed seven times. 50 µL of TMB substrate reagent was added to each well. The colorimetric reaction was allowed to develop until the lowest standards of the standard curve turned light blue. The reaction was stopped with 25 µL of “stop solution” (1 M H_2SO_4). The plate was read using a microplate reader set to a wavelength of 450 nm. Microsoft Excel software was used to generate a standard curve from which the cytokine concentration of the samples was determined.

2.1.22 Lactate quantification

Extracellular L(+)-lactate secreted from cells was measured in supernatants using the Lactate Assay Kit (MAK064) (Sigma Aldrich). The assay is enzymatic and results in a colorimetric product which is proportional to the lactate concentration present in the sample. Supernatants were preferably used fresh, or frozen at -80°C and thawed and vortexed before use. The kit was used as per manufacturer's instructions. Briefly, a standard curve was freshly prepared with a top concentration of 100 picomole/well. Master mix containing the assay enzyme mix, probe and assay buffer was prepared and added to the standard curve on a 96-well plate. A range of dilutions of the supernatants were tested to find a dilution which fell within the range of the assay. MDM and BMDM supernatants from 12-well plates were generally diluted 1:50 in assay buffer. The absorbance of the plate was read at 570 nm. Microsoft Excel software was used to generate a standard curve from which the lactate concentration of the samples was determined.

2.1.23 Glucose concentration assay

Glucose concentration in supernatants was determined using the Glucose Assay Kit (ab65333) (Abcam). Assay buffer was warmed to room temperature before use. Glucose probe was warmed for 5 minutes at 37°C to thaw DMSO solution. Fresh standards were prepared for each assay with a top concentration of 10 nmol/well. Master mix containing the assay enzyme mix, probe and assay buffer was prepared and added to the standard curve on a 96-well plate. A range of dilutions of the supernatants were tested to find a dilution which fell within the range of the assay. Supernatants from 12-well plates were generally diluted 1:100 in assay buffer. The plate was incubated in the dark at 37°C for 30 minutes. The absorbance of the plate was read at 570 nm. Microsoft Excel

software was used to generate a standard curve from which the glucose concentration of the samples was determined.

2.1.24 Measurement of phosphofructokinase enzyme activity

Cellular phosphofructokinase (PFK) activity was analysed using the Phosphofructokinase Activity Colorimetric Assay Kit (MAK093) (Sigma-Aldrich). The assay uses a coupled enzyme reaction to measure PFK activity. The fructose-6-phospate and ATP in the reaction mix is converted to fructose-1,6-diphosphate and ADP by the PFK enzyme present in the sample lysates. The ADP is then converted by the enzyme mix to NADH and AMP. NADH reduces the probe in the reaction mix to a coloured product which is proportional to the PFK activity.

A standard curve was prepared with a top standard of 10 nmole/well in 25 μL of assay buffer in a 96-well plate. $2x10^6$ cells per condition were lysed in 200 μL of ice cold assay buffer. Lysates were centrifuged at 13,000 g for 10 minutes to remove insoluble material. The supernatants were then diluted to within the range of the standard curve (generally 1:50) in assay buffer and 25 μL of the diluted lysates added to the 96-well plate. Samples were also plated for blank reactions that omit the PFK substrate to account for background signal from NADH and ADP. 25 μL of reaction buffer containing enzyme mix, ATP and developer was added as per manufacturer's instructions, as was the blank buffer lacking the substrate. The buffers were added to the samples and standards, the plate protected from light with foil and placed on a shaker to mix briefly. The plate was then incubated for 5 minutes at 37 °C and then read on a plate reader at 450 nm. The 5-minute incubation and absorbance readings were repeated every 5 minutes until the most active sample was out of the range of the standard curve.

Activity of each sample was calculated by first subtracting the final blank reading from the final sample reading. The adjusted readings and the following formula were then used:

$$Activity = \frac{(NADH_{calc})x\ Dilution\ Factor}{\left(T_{final} - T_{initial}\right) x\ V}$$

where NADHcalc is the amount of NADH generated between the initial and final readings calculated from the standard curve (nmole), Tfinal – Tinitial is the time in minutes between the initial and final readings and V is the sample volume in mL added per well. Activity is thus nmole/min/mL which is equal to one milliunit/mL, i.e. the amount of PFK enzyme that generates 1 mmole of NADH per minute at pH 7.4 at 37 °C.

2.1.25 Measurement of Hexokinase enzyme activity

Cellular hexokinase (HK) activity was analysed using the Hexokinase Activity Colorimetric Assay Kit (MAK091) (Sigma-Aldrich). The assay uses a coupled enzyme reaction to measure HK activity. Glucose in the reaction mix is converted to glucose-6-phosphate by the HK enzyme present in the sample lysates. The glucose-6-phosphate is then converted by glucose-6-phosphate dehydrogenase in the enzyme mix to NADH. NADH reduces the probe in the reaction mix to a coloured product which is proportional to the HK activity.

A standard curve was prepared with a top standard of 12.5 nmole/well in 25 μL of assay buffer in a 96-well plate. $2x10^6$ cells per condition were lysed in 200 μL of ice cold assay buffer. Lysates were centrifuged at 13,000 g for 10 minutes to remove insoluble material. The supernatants were then diluted to within the range of

the standard curve (generally 1:50) in assay buffer and 25 μL of the diluted lysates added to the 96-well plate. Samples were also plated for blank reactions that omit the HK substrate to account for background signal from NADH. 25 μL of reaction buffer containing enzyme mix, ATP and developer was added as per manufacturer's instructions, as was the blank buffer lacking the substrate. The buffers were added to the samples and standards, the plate protected from light with foil and placed on a shaker to mix briefly. The plate was then incubated for 5 minutes at room temperature and then read on a plate reader at 450 nm. The 5-minute incubation and absorbance readings were repeated every 5 minutes until the most active sample was out of the range of the standard curve.

Activity of each sample was calculated by first subtracting the final blank reading from the final sample reading. The adjusted readings and the following formula were then used:

$$Activity = \frac{(NADH_{calc}) x\ Dilution\ Factor}{\left(T_{final} - T_{initial}\right) x\ V}$$

where NADHcalc is the amount of NADH generated between the initial and final readings calculated from the standard curve (nmole), Tfinal – Tinitial is the time in minutes between the initial and final readings and V is the sample volume in mL added per well. Activity is thus nmole/min/mL which is equal to one milliunit/mL, i.e. the amount of HK enzyme that generates 1 mmole of NADH per minute at pH 8 at room temperature.

2.1.26 Seahorse extracellular flux analysis of macrophages

Metabolic characteristics of cells were measured using the XF^e24 Seahorse Analyser (Agilent). The Seahorse machine can measure the extracellular acidification rate (ECAR) and oxygen consumption rate (OCR) of cells in real time. ECAR serves as an indicator of the level of glycolytic metabolism. Cells are seeded onto a Seahorse cell culture plate and a Seahorse cartridge is placed over this. The cartridge has extruding sensors that sit 200 μm over the cells, creating a micro-chamber of about 2 μL volume that allows changes in metabolism to be detected instantaneously. The sensors contain two fluorophores, one of which is quenched by oxygen and can thus give a readout of mitochondrial respiration. The second fluorophore is quenched by protons and is used to monitor glycolysis. Ports in the Seahorse cartridge can be loaded with inhibitors and other substances and injected into the wells on command allowing readouts of the effects of the injected substances in real time. Probes lift and allow mixing of the medium in the well between repeated readings.

The Seahorse Assay cartridge was hydrated in 1 mL of Seahorse calibrant per well for 24 hours at 37 °C in a carbon dioxide-free incubator. BMDM were cultured as usual and then seeded in the Seahorse plates at an optimised density of $1x10^5$ cells in 500 μL of medium per well. MDM were cultured as usual and then lifted with gentle scraping and recounted and seeded at an optimised density of $2x10^5$ cells in 500 μL of medium per well. 4 wells spread at random over the plate were left empty to account for any background noise. Cells were treated or transfected for experiments in the Seahorse cell culture plates the following day. Supplemented Seahorse medium was made up on the day of the Seahorse run. Bicarbonate-free Seahorse medium was warmed to 37°C, and glucose (10 mM) and glutamine (2 mM) added. The

supplemented medium sterile was filtered through a 0.2 μm filter. 450 μL of medium was removed from each well of the Seahorse plate, 450 μL of supplemented medium added. This was then repeated to remove all the original buffered medium from the cells without letting them dry.

The Seahorse cartridge ports were loaded with the mitochondrial inhibitors oligomycin, carbonyl cyanide-4-(trifluoromethoxy)phenylhydrazone (FCCP), and rotenone and antimycin A. These inhibitors target different components of the electron transport chain to elucidate mitochondrial functions in the target cells. Oligomycin targets ATP synthase/complex V, FCCP uncouples oxygen consumption from ATP production, and rotenone and antimycin A target complex I and III. The inhibitors were made fresh on the day of each experiment in fresh supplemented Seahorse medium. Oligomycin and FCCP were used at a final concentration of 1 μM, and FCCP was used at a final concentration of 0.5 μM.

When the assay was ready to be run, the cartridge was inserted and the machine was equilibrated. The microplate containing the cells was then inserted and 3 measurements of basal respiration was performed before each of the inhibitors of the Mito Stress test kit were sequentially injected with 3 measurements of ECAR and OCR in between. Results were exported to Microsoft Excel for analysis and normalised for cell number using the crystal violet assay detailed in **2.1.24**. Oligomycin inhibits ATP synthase and thus blocks ATP synthesis through oxidative phosphorylation forcing cells to increase glycolysis. The difference between ECAR after oligomycin treatment and baseline ECAR thus represents the glycolytic reserve (GR) of the cell. FCCP uncouples the passage of protons across the mitochondrial membrane from ATP synthase

which forces the electron transport chain complexes to increase their activity to maintain the potential of the mitochondrial membrane resulting in an increase in OCR. The difference in maximal OCR (OCR after the addition of FCCP) and basal OCR represents the spare respiratory capacity (SRC) of the cell. Rotenone and antimycin A completely block the activity of the electron transport chain thus eliminating all mitochondrial oxygen consumption. Remaining OCR after rotenone and antimycin A treatment therefore represents non-mitochondrial oxygen consumption. These parameters are indicated on a representative Seahorse analysis in **Figure 2.4**.

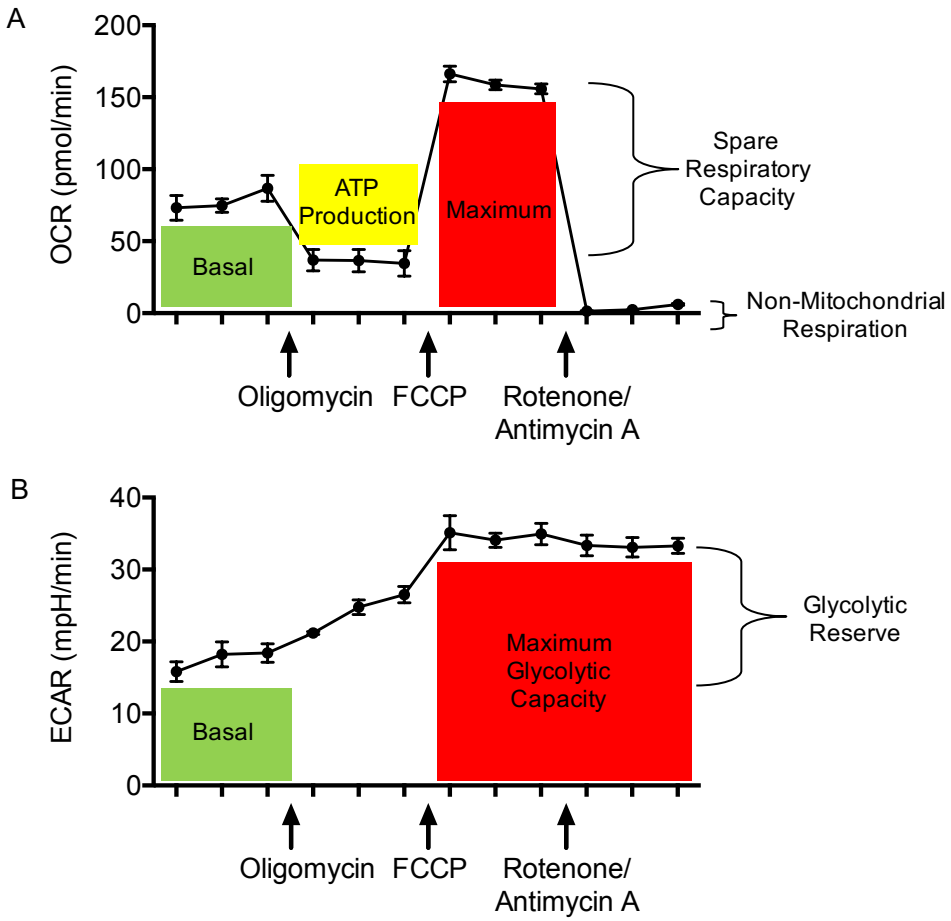

Figure 2.4 Metabolic parameters determined using the mitochondrial inhibitor assay. Extracellular flux analysis was performed on BMDM using the XFe24 extracellular flux analyser. Oxygen consumption rate (A) and extracellular acidification rate (B) were measured basally and after the addition of each inhibitor. Metabolic parameters are illustrated on these traces. Data shown as the standard deviation of 2 technical replicates in one representative experiment.

2.1.27 Intracellular ROS Measurement

Intracellular ROS were quantified using the DCFDA/H2DCFDA Cellular Reactive Oxygen Species Detection Assay Kit (ab113851) (Abcam). Cells were treated with 20 μM dichlorofluorescin diacetate (DCFDA) and incubated for 30 minutes at 37°C in the dark. DCFDA is a dye that can diffuse into the cell where it is

deacetylated by cellular esterases to a non-fluorescent compound which is then oxidized by ROS species into 2', 7'-dichlorofluorescein (DCF). DCF is highly fluorescent and thus can be measured by flow cytometry. Cells were scraped into a single cell suspension after staining and read at Ex/Em 485/535 nm on the BD Accuri C6 flow cytometer.

2.1.28 In silico analysis of miR-21 target genes and PFK-M

Candidate target mRNA for miR-21 were identified using the TargetScanHuman website (version 7.2 http://www.targetscan.org/vert_72/). The species was selected as "Human" and the microRNA name entered as "miR-21-5p". 319 predicted targets with conserved sites were identified. These were evaluated for relevance to the glycolytic pathway and phosphofructokinase, muscle-type (PFK-M) was selected as a potential candidate. PFK-M was predicted to had a 7mer-m8 site at position 289-295 in its 3'UTR; i.e. an exact match to position 2-8 of miR-21 or the seed sequence and position 8 (**Figure 2.5**). The low (-0.40) weighted context ++ score (a score that takes 14 different prediction parameters into account) and high level of conservation of the site across mammalian species (**Figure 2.6**) indicated that it may be a true target of miR-21.

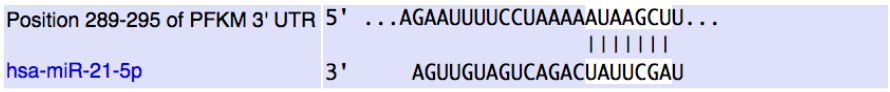

Figure 2.5 Predicted pairing of the target region of the PFK-M 3'UTR (top) and miR-21-5p (bottom). Generated by Targetscan.

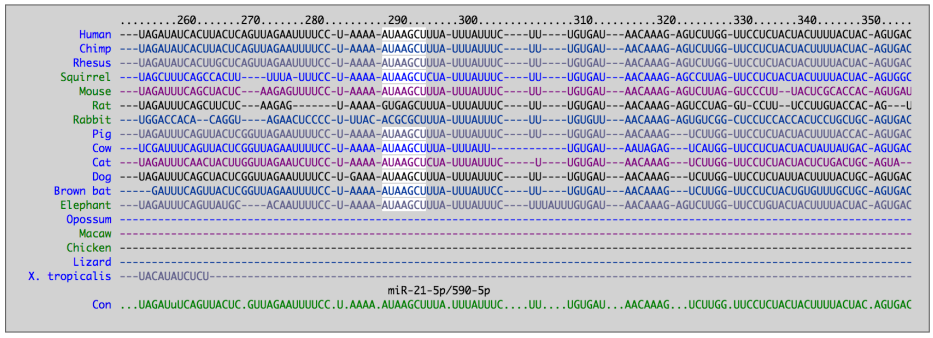

Figure 2.6 Conserved vertebrate miR-21 sites in the 3'UTR of PFK-M. (Generated by Targetscan)

2.1.29 PFK-M 3'UTR luciferase assay

The ability of miR-21 to bind to the predicted target site in the 3'UTR of Human PFKM (NM_000289.5) was determined using a luciferase assay. The 3'UTR of PFK-M or a control mutated sequence was cloned into a luciferase reporter plasmid (Genecopoeia). The plasmid design is shown in **figure 2.7**. Sequences are listed in **table 2.12** with the binding site highlighted.

PFK-M	acctctctggagtgaggggaatagattacctgatcatggtcagctcacaccctaataagt ccacatcttctcagtgttttagctgtttttttcattaggtttccttttattctgtaccttgcagccatg accagttctggccaggagctggaggagcaggcagtgggtgggagctccttttaggtag aatttaacatgacttctgccccagctttatctgtcacacaaggctgggcacctctagtgcta ctgctagatatcacttactcagttagaattttcctaaaATAAGCTttatttatttctttgtgat aacaaagagtcttggttcctctactacttttactacagtgacaaattgtaactacactaata aatgccaactggtcactgtgcttttgcttctcctgttatcatcttcctaagtggaatgtaatact gtcagccccatgtatcagacacttgtctgatgaagcagtaaagacgttaagggtatcac agggggtggaggaagggattatctctagtacactacttgctggctgtctgaaaaattgtc actgccaaactctaaaaacagttctaaatagtgactgagaaggtttgttgctggagtcag ggaataaggcagccaaatactctttgcacagttctttagtgggaagagaaattaacaat aaatatcaagcactgtgaaaaaaaaaa
Control mutated sequence	acctctctggagtgaggggaatagattacctgatcatggtcagctcacaccctaataagt ccacatcttctcagtgttttagctgtttttttcattaggtttccttttattctgtaccttgcagccatg accagttctggccaggagctggaggagcaggcagtgggtgggagctccttttaggtag aatttaacatgacttctgccccagctttatctgtcacacaaggctgggcacctctagtgcta ctgctagatatcacttactcagttagaattttcctaaaaTTTATGGttatttatttctttgtg ataacaaagagtcttggttcctctactacttttactacagtgacaaattgtaactacactaat aaatgccaactggtcactgtgcttttgcttctcctgttatcatcttcctaagtggaatgtaata ctgtcagccccatgtatcagacacttgtctgatgaagcagtaaagacgttaagggtatca caggggtggaggaagggattatctctagtacactacttgctggctgtctgaaaaattgt cactgccaaactctaaaaacagttctaaatagtgactgagaaggtttgttgctggagtca gggaataaggcagccaaatactctttgcacagttctttagtgggaagagaaattaacaa taaatatcaagcactgtgaaaaaaaaaa

Table 2.12 PFK-M and mutated control insert sequences for 3'UTR luciferase reporter plasmids

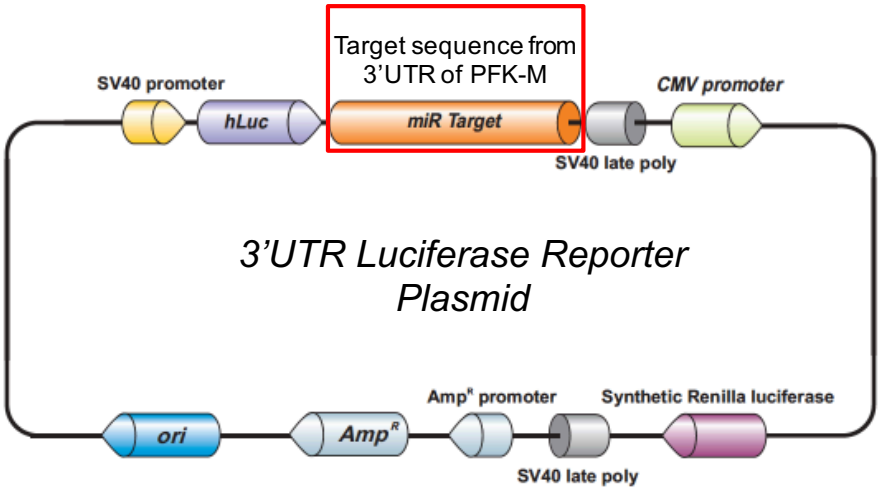

Figure 2.7 PFK-M 3'UTR luciferase reporter plasmid design, adapted from Genecopoeia

The 3'UTR luciferase assay was designed to elucidate whether miR-21 directly binds to the predicted target site in the 3'UTR of PFK-M. The plasmid contains the 3'UTR of PFK-M downstream of the luciferase gene which is expressed under the control of the SV40 promoter. The luciferase is transcribed with the 3'UTR mRNA site attached. A miR-21 mimic can be transfected into the cell and if it binds the site in the PFK-M 3'UTR, some of the mRNA will be degraded by the RISC complex. Cells are lysed and luciferins provided which are processed by luciferase and emit luminescence. This luminescence can be measured and used to determine the amount of luciferase present and thus deduce whether any microRNA-mediated degradation is occurring. This is summarised in **Figure 2.8**.

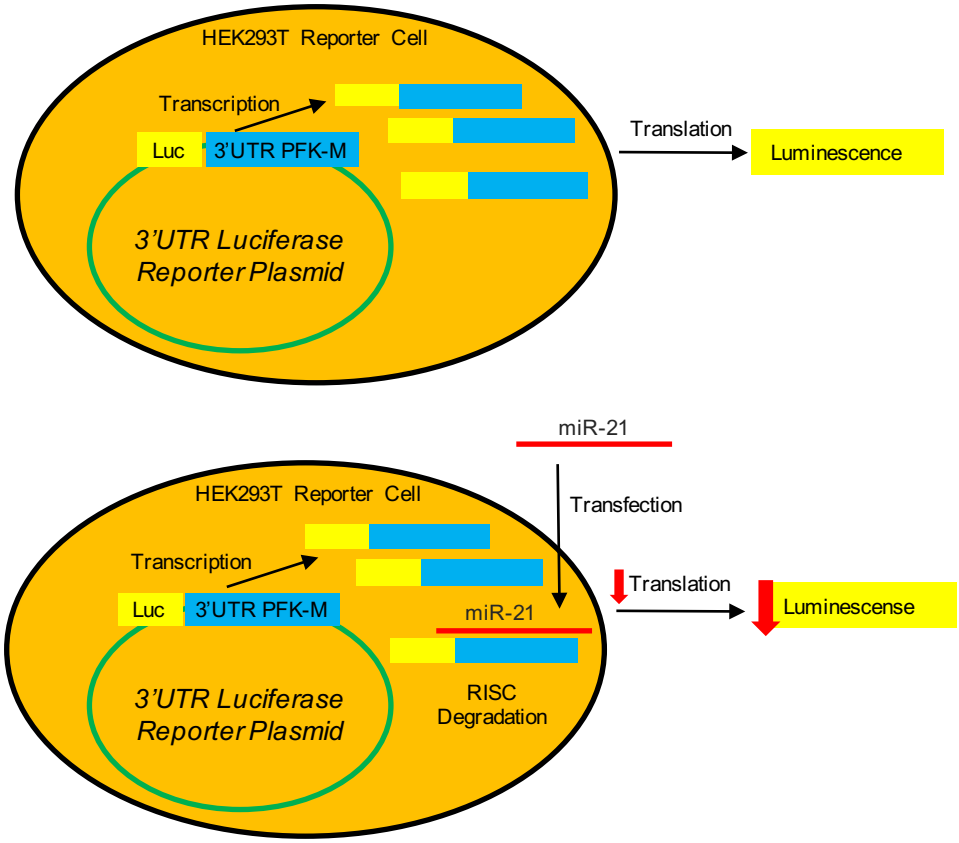

Figure 2.8 Rationale for the 3'UTR microRNA target luciferase assay

Plasmids were transformed into MAX Efficiency DH5α competent E. coli cells (ThermoFisher) upon receipt. A 30 μL aliquot of cells were thawed on ice for 30 minutes and 2 μL or approximately 100 ng of DNA added to the tube and gently mixed. The cells were incubated on ice for 30 minutes and then heat-shocked by placing the tube into a 42°C water bath for 45 seconds. The tubes were then replaced on ice for 30 minutes. 250 μL of SOC media was added to the bacteria which were grown in a shaking incubator at 37°C for 1 hour. An LB agar plate containing 100 μg/mL ampicillin was warmed to room temperature and 50 μL of the broth was plated. The agar plate was inverted and incubated at 37°C overnight. As the plasmid contains an ampicillin resistance gene, only cells that have been transformed will grow. The following day 50 mL of LB broth containing 100 μg/mL ampicillin was added to a

250 mL flash. A sterile pipette tip was used to select one colony from the agar plate and was submerged in the broth. The mouth of the flask was loosely covered with sterile aluminium foil and incubating at 37°C in a shaking incubator for 18 hours.

The bacteria were then centrifuged at 4000 rcf for 30 minutes. DNA was then extracted using the Plasmid Plus Maxi Kit (Qiagen) as per the manufacturer's instructions. Briefly, the pellet was resuspended in 4 mL of buffer P1 by vortexing. The bacteria were then lysed in 4 mL of buffer P2 and mixed thoroughly. 4 mL of chilled buffer P3 was then added and the mixture inverted 6 times and placed on ice for 15 minutes. This was then centrifuged at 20,000 rcf for 10 minutes at 4°C. The supernatant containing the plasmid DNA was then removed and centrifuged again at 20,000 rcf for 15 minutes at 4°C. A QIAGEN-tip was equilibrated with 4 mL of buffer QBT and the column allowed to drain. Supernatant was then added to the QIAGEN-tip. The QIAGEN-tip was then washed twice with 10 mL of buffer QC. DNA was then eluted with 5 mL of buffer QF. DNA was precipitated by adding 3.5 mL of room temperature isopropanol. This was mixed and centrifuged at 15,000 rcf for 30 minutes at 4°C. The supernatant was carefully discarded and the pellet washed with 2 mL of room temperature 70% ethanol and centrifuged at 15,000 rcf for 10 minutes to remove salt. The pellet was then air-dried for 10 minutes and dissolved in TE buffer. The plasmid concentration was determined using the Nanodrop 2000 (which was blanked with TE buffer).

HEK293T cells were grown in DMEM supplemented with 10% FBS and 1% penicillin and streptomycin. Cells were seeded in 96-well plates at $2x10^5$ cells/mL in 100 µL per well. When cells were 80% confluent, they were transfected with the plasmids using a 6% GeneJuice (Merck)/Opti-MEM solution, the volume of which being

one tenth of the volume of medium on the cells. Opti-MEM was pre-warmed to 37°C before being pipetted onto the required volume of GeneJuice in a cell culture hood. This mixture was mixed and allowed to sit at room temperature for 10 minutes. 100 ng of plasmid DNA was aliquoted into an Eppendorf and the GeneJuice/Opti-mem mixture was slowly pipetted on top. This was incubated for 15 minutes at room temperature and then added to the cells.

Cells were allowed 24 hours to recover and then subsequently transfected with 50 nM miRIDIAN microRNA human hsa-miR-21-5p mimic (Dharmacon) or 50 nM miRIDIAN microRNA mimic negative control #1 (Dharmacon) as described in **2.1.17**.

After 24 hours, cells were washed with 100 μL of PBS and lysed in 50 μL of 1X Passive Lysis Buffer (ThermoFisher) for 15 minutes at room temperature on a shaker. 20 μL of lysate was placed into a Corning 96-well white polystyrene microplate (Fisher) to assay for Firefly luciferase activity, and 20 μL of lysate placed into a second white microplate to assay for Renilla luciferase activity. 40 μL of 1X luciferase assay buffer (Sigma-Aldrich) was added to each well of the Firefly plate and 40 μL of 20 μM coelenterazine (Sigma-Aldrich) diluted in PBS was added to the Renilla plate. Luminescence was read on a luminometer. Firefly luciferase activity was normalised to Renilla luciferase activity to account for any differences in transfection efficiency.

2.1.30 Target protection using morpholino technology

To block miR-21 from binding to the predicted target site in PFK-M while preserving its interactions with other targets, morpholino technology was employed. Morpholinos are stable and highly

specific oligomers that bind to their target and prevent it from carrying out its function. A target-protecting morpholino specific to the miR-21 target site in the 3'UTR of PFK-M was ordered from GeneTools, as well control morpholino which would not bind this site. The sequences for these morpholinos are detailed in **table 2.13**. Morpholinos were received lyophilised and were reconstituted to a 1 mM stock solution in molecular grade water and stored at room temperature. Morpholinos were delivered into cells using Lipofectamine 2000 as described in **2.1.17**.

PFK-M Target Protector	5'-AGCTTATTTTTAGGAAAACTCTTGAGTAGC-3'
Control Morpholino	5'-ACCTTTTTTTTACGAAAACTGTTGAGTACC-3'

Table 2.13 Target protecting and control morpholino sequences

2.1.31 Crystal Violet assay for cell viability

After extracellular flux analysis was performed, a crystal violet (CV) assay was performed to measure cell viability in each well. Media was removed and 50 μL 1% glutaraldehyde (Sigma-Aldrich) was added to each well for 15 minutes. Wells were then washed twice with 200 μL of PBS and 50 μL of 0.1% CV (Sigma-Aldrich) was added to each well for 30 minutes. CV was aspirated and the plate was inverted and dried overnight. 40 μL of 1% Triton X solution was added to each well and the plate was placed on a shaker for 15 minutes. The solution was pipetted into a fresh 96-well microplate and the absorbance was read at 595 nm on a plate reader. The absorbances were used to normalise the readings from the extracellular flux analysis and thus took into account donor variations in viability.

2.1.32 Western Blot analysis of protein in cellular lysates

2.1.32.1 Sample preparation

Media was removed from cells (at least 2 x 10^6 cells per condition) and 50 μL of 5X SDS lysis buffer (as prepared in **table 2.14**) was added to each well. Lysates were scraped to ensure full lysis, pipetted into 1.5 mL Eppendorf tubes and stored at -80°C. Samples were heated at 95°C for 10 minutes to denature the proteins before use.

Glycerol (Sigma)	10% (v/v)
Sodium dodecyl sulphate (SDS) (Sigma)	2% (w/v)
Bromophenol blue (Sigma)	200 μg/mL
Tris pH 6.8	215 mM
Dithiothreitol (DTT) (1M)	50 μL per mL

Table 2.14 Composition of 5X SDS Lysis buffer

2.1.32.2 SDS polyacrylamide gel electrophoresis (SDS-PAGE)

SDS-PAGE was used to separate proteins in the samples based on molecular weight. The gels were placed into an SDS-Page apparatus and the base filled with 1X running buffer (100 mL of 10X running buffer **table 2.15** and 900 mL of water). 40 μL of sample was pipetted into a 12-well 5% stacking gel on a 10% resolving gel, prepared as in **table 2.16**. 5 μL of PageRuler Prestained protein ladder 10-180 kDa (ThermoFisher) was also run to reference protein band sizes.

MOPS (Sigma)	104.6 g
TRIS base (Sigma)	60.6 g
Ethylenediaminetetraacetic acid (EDTA)	3 g
SDS	10 g
Deionised water	Make to final volume of 1 L

Table 2.15 Composition of 10X running buffer

Component	Resolving Gel (10%) (mL)	Stacking Gel (5%) (mL)
Deionised water	5.9	3.4
30% acrylamide mix (Sigma)	5	0.83
1.5M Tris pH 8.8 (Sigma)	3.8	-
1M Tris pH 6.8 (Sigma)	-	0.63
10% SDS (Sigma)	0.15	0.05
10% ammonium persulfate (APS) (w/v) (Sigma)	0.15	0.05
Tetramethylethylenediamine (TEMED) (Sigma)	0.006	0.005

Table 2.16 Composition of 10% resolving gel and 5% stacking gel (recipe sufficient for two gels)

2.1.32.3 Transfer of proteins to PVDF membrane by electrophoresis

Following the running of the gel, the stacking layer was cut off using a sharp blade. PVDF membrane and two pieces of filter paper were cut to the size of the gel. The membrane was activated in 100% methanol for 1 minute and the filter was soaked in 1X transfer buffer (100 mL 10X transfer buffer as in **table 2.17,** 200 mL of methanol and 700 mL of deionised water). One piece of filter paper was placed on the black, cathode side of a transfer cassette, and the gel was carefully placed on top. The activated membrane was placed on top of this, followed by a piece of filter paper. Any bubbles were rolled away with a tube and the cassette was closed and placed into a tank filled with transfer buffer. The apparatus was

attached to a power box and run at 60 volts for 1 hour and then at 80 volts for approximately an additional hour until the protein ladder reach the end of the gel. An ice pack was placed in the tank and the tank placed in a box of ice to prevent overheating. The tank was connected to a power pack and run at 70 amps overnight to transfer the proteins to the membrane.

250 mM TRIS (Sigma)	30.3 g
1.9 M Glycine (Sigma)	140.28 g
Deionised water	Make to final volume of 1 L

Table 2.17 Composition of 10X transfer buffer

2.1.32.4 Blocking the membrane and incubation with antibodies

After the proteins had been transferred, the membrane was blocked in 5% (w/v) milk powder in TBST for 1 hour on a shaker at room temperature to prevent non-specific binding of antibodies. The membrane was then washed in TBST (**table 2.18**) for 15 minutes. 5 mL of 1:1000 primary antibody was prepared in 5% (w/v) milk powder in TBST and the membrane was incubated in this solution at 4°C overnight. PFK-M was detected using Human/Mouse/Rat Muscle Phosphofructokinase/PFKM Antibody (MAB7687) (R&D systems) and β-actin was detected using β-actin (4267) (Cell Signaling). The membrane was then washed 3 times for 5 minutes in TBST and incubated in 5 mL of 1:2000 secondary antibody specific for the species in which the primary antibody was raised (Jackson Laboritories) in 5% (w/v) milk powder in TBST for 1 hour at room temperature. The membrane was again washed 3 times for 5 minutes in TBST. 1X LumiGLO chemiluminescent substrate and 1X peroxide (Cell Signaling) were mixed and added to the

membrane immediately before visualising the protein using the ChemiDoc MP gel imaging system (Biorad).

TRIS (Sigma)	12.11 g
1.9 M Glycine (Sigma)	87.6 g
Tween-20 (Sigma)	10 mL
Deionised water	Make to final volume of 1 L

Table 2.18 Composition of 10X TBST

2.1.33 Reagents

Recombinant mouse IL-10 protein, recombinant human and mouse IFN-γ protein and Ultrapure LPS (E. coli 0111:B4) were obtained from Invitrogen and stored at -20°C. Murine IL-1β-neutralising antibody (MAB4012), control mouse anti-hamster IgG antibody (MAB011), mouse TNF-α antibody (AF410) and goat IgG control (AB108) were obtained from R&D systems.

Chapter 3: Macrophage miR-21 and Anti-Mycobacterial Responses

3.1 Introduction

Mtb is an intracellular pathogen that can subvert the normal innate immune response and survive within the primary host cell for Mtb, the alveolar macrophage. The macrophage can be viewed as a pivotal immune cell in Mtb infection, responsible for bacterial killing and the instruction of other immune cells.

Macrophages are highly plastic, capable of taking on a spectrum of phenotypes when activated depending on their microenvironment[328]. Classically activated macrophages are induced by a pro-inflammatory stimulus such as LPS or IFN-γ and take on a pro-inflammatory phenotype, producing cytokines such as TNF-α and IL-1β and bactericidal mediators such as ROS and NOS. Alternatively activated macrophages are induced by IL-4 or IL-13 and are anti-inflammatory, producing cytokines such as IL-10 and promoting tissue repair[329]. In the context of Mtb infection, a spectrum of macrophage activation states is induced[330], and this changes over time. It has been shown that macrophages can induce a pro-inflammatory phenotype capable of bacterial killing and forming granulomas in the initial stages of infection, however over time Mtb infection alters this phenotype, generating a macrophage more permissible to Mtb growth[222]. Understanding the processes that mediate this transition from a predominantly pro-inflammatory macrophage population to a permissive one may provide new therapeutic targets to manipulate to promote bacterial clearance.

The mechanisms by which the macrophage is co-opted by Mtb to promote an environment amenable to its growth are not clearly understood. Uptake of the Mtb bacilli activates the macrophage to produce pro-inflammatory cytokines including TNF-α and IL-1β and antimicrobial mediators[331], leading to a local inflammatory

response and the recruitment of additional macrophages and lymphocytes and ultimately granuloma formation[332]. TNF-α activates macrophages to kill bacteria and promotes apoptotic cell death which reduces cell-to-cell spread of Mtb[97]. IL-1β promotes the production of IL-12p40[198] and IFN-γ[189] which can drive a Th1 immune response and thus promote bacterial killing and clearance. IL-1β also enhances macrophage sensitivity to TNF-α by inducing upregulation of the TNFR1 receptor[199]. Suppression of type I interferons by IL-1β-induced PGE2 has also recently been shown to promote containment of Mtb infection[200], and PGE2 additionally promotes apoptotic rather than necrotic cell death, limiting bacterial dissemination[201]. Inducible nitric oxide synthase (iNOS) is a key marker for pro-inflammatory macrophages, and has been shown to be essential for containment of Mtb infection in murine models[57], and evidence for a role in human Mtb infection is emerging[60].

Despite these initial pro-inflammatory responses, Mtb persists within the macrophage and is not completely eradicated. Macrophages infected with Mtb have been shown to induce a process known as phagolysosomal arrest, blocking phagosome maturation, allowing the bacilli to survive in unacidified vacuoles[333]. IL-10 production is also induced by Mtb which can downregulate Th1 responses[108], reduce TNF-α-mediated apoptosis[334, 335], and crucially has been shown to contribute to phagolysosomal arrest[117]. Expression of arginase 1 characterises the alternatively activated macrophage[336]. Arginase competes with iNOS for its substrate, arginine, converting it to proline which has roles in wound healing[337], and is associated with a reduced propensity for bacterial clearance[338]. The iNOS/arginase 1 macrophage activation state paradigm is more clearly defined in the murine model, while signals in the human model that drive macrophage activation remain much more elusive, suggesting that macrophages in human Mtb infection fall on a spectrum of activation and skewing the population towards

either end of this spectrum is what determines infection outcome. Non-human primates infected with Mtb have been shown to have both iNOS- and arginase 1-expressing macrophages in granulomas, with pro-inflammatory macrophages organised at the centre of the granuloma surrounded by alternatively activated macrophages, and this distribution is mirrored in human granulomas[339].

Regulation of macrophage activation is complex and involves many signalling pathways. MicroRNAs have emerged as key modulators of gene expression, capable of fine-tuning signalling pathways through nuanced modulation of many targets simultaneously to effect cellular changes[340], and thus represent excellent candidates to regulate the process of macrophage activation.

An in silico study associated aberrant microRNA expression profiles induced by Mtb with macrophage polarisation to a permissive anti-inflammatory phenotype[341]. MicroRNA-21 is one of the most highly expressed microRNAs in macrophages and has been shown to regulate TLR signalling and act as a feedback mechanism that promotes resolution of the inflammatory response[302]. LPS signalling through TLR4 has been shown to induce miR-21, and this induction of miR-21 boosted early IL-10 production[296]. Enhanced expression of IL-10 was found to be mediated by the degradation of the negative regulator of IL-10, PDCD4. The miR-21/PDCD4 interaction has been shown to have functional importance in autoimmune disease models including a protective role in type 1 diabetes[342] and SLE[343]. Macrophage miR-21 has also been shown to be upregulated following efferocytosis of apoptotic cells, and this boost in miR-21 levels leads to enhanced IL-10 production through PDCD4. Early induction of IL-10 has been linked to negative outcomes in a murine model of mycobacterial

infection[344]. Furthermore, IL-10 has been shown to be a key cytokine facilitating Mtb by phagolysosomal arrest[117] and IL-10-deficient mice have been shown to induce earlier and more potent Th1 responses in the pulmonary compartment, facilitating bacterial containment[345].

MiR-21 has also been shown to negatively regulate several pro-inflammatory macrophage functions, including the induction of TNF-α following efferocytosis via targeting of PTEN[319] and the induction of IL-1β in the context of *Mycobacterium leprae* infection[322].

Given this evidence that miR-21 negatively feeds back on inflammatory activation to promote an anti-inflammatory macrophage phenotype characterised by increased IL-10 expression, and IL-10 is highly important in determining the immune response to Mtb, this chapter will investigate miR-21 as a candidate molecule regulating this process in the context of Mtb infection. Although miR-21 is known to be induced by pathogenic stimuli, its role in regulating Mtb responses has been poorly studied to date. This work aims to characterise the interplay between miR-21 and Mtb in the macrophage, summarised **in figure 3.0**.

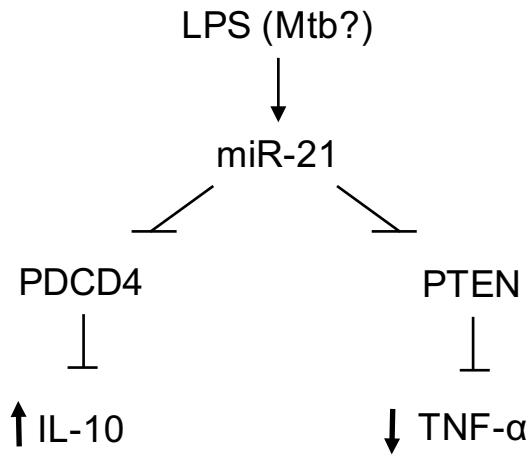

Figure 3.0 Chapter 3 Hypothesis. LPS has been shown to induce microRNA-21 to boost the induction of IL-10 through targeting of PDCD4 and to limit TNF-α induction through targeting of PTEN. As IL-10 and TNF-α are also key cytokines in Mtb infection, it is hypothesised that miR-21 is also induced by Mtb infection to promote IL-10 and limit TNF-α production.

3.2 Results

3.2.1 Induction of macrophage miR-21 by Mycobacterium tuberculosis

Given the importance of miR-21 in modulating TLR signalling and that TLR signalling is activated by Mtb, the expression of miR-21 in macrophages infected with Mtb was examined. Bone-marrow derived macrophages were harvested and cultured as per the protocol described in **2.1.2**. Mature BMDM were infected with irradiated H37Rv prepared as described in **2.1.9** at a multiplicity of infection (MOI) of 5 bacteria per cell as determined in **2.1.10** or with LPS at 100 ng/mL. After 24 hours, qPCR for miR-21 was performed. iMtb significantly enhanced miR-21 expression relative to the untreated control, inducing a mean fold induction of 3.6 (**Figure 3.1A**). As already reported in the literature, LPS also significantly induced miR-21 expression in BMDM (approximately a 3-fold induction in this model).

The induction of miR-21 by iMtb was then confirmed in a human macrophage model. Human MDM were prepared as in (**2.1.6**). Upon maturation, they were infected with iH37Rv at an MOI of 5 bacteria per cell or LPS at 100 ng/mL and after 24 hours relative expression of miR-21 was examined as described above. As in the murine model, iMtb induced significant miR-21 expression in human MDM (3-fold induction) and LPS also induced miR-21 (2.4-fold induction) (**Figure 3.1B**).

As alveolar macrophages are the primary host cell for Mtb, it was important to confirm that the observed effects of Mtb on BMDM and MDM were also observed in this cell type. Murine AM were isolated by bronchoalveolar lavage as described in (**2.1.4**) and after 24 hours rest were infected with iH37Rv at an MOI of 5 bacteria per

cell. After 24 hours miR-21 was measured by qPCR as before. Mtb caused a 2-fold, significant induction of miR-21 (**Figure 3.2**).

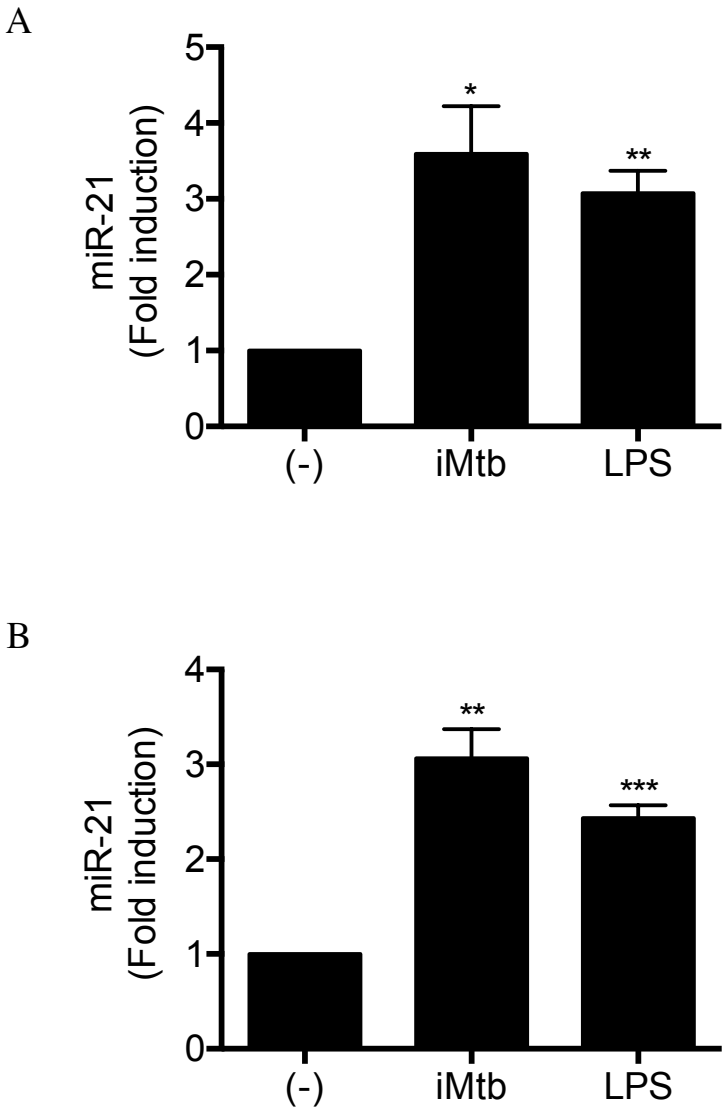

Figure 3.1 Irradiated Mtb and LPS induce miR-21 expression in macrophages. Murine BMDM (A) or human MDM (B) were infected with irradiated Mtb (H37Rv strain) (iMtb) at an MOI of 5 bacteria per cell or stimulated with 100ng/mL of LPS for 24 hours. qPCR was performed and expression of miR-21 relative to the untreated control was calculated. Data were normalised to RNU6B. Statistical analysis was performed using a paired one-way ANOVA with each mean compared to the control mean. *, ** and *** represent $p<0.05$, 0.01 and 0.001 respectively. Data shown as mean ± SEM, n = 3 independent experiments.

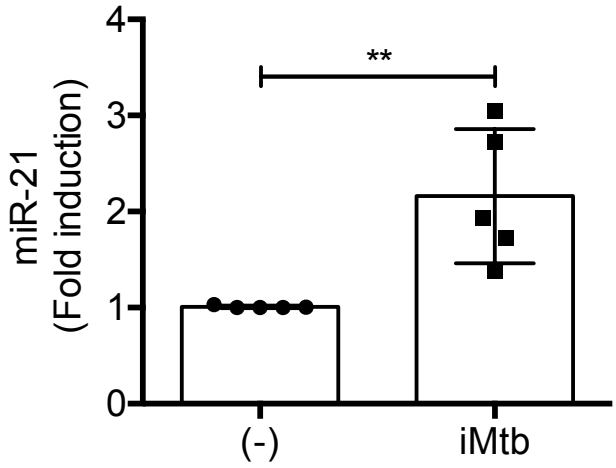

Figure 3.2 Mtb induces expression of miR-21 in alveolar macrophages. Murine AM were infected with irradiated Mtb (H37Rv strain) (iMtb) at an MOI of 5 bacteria per cell for 24 hours. qPCR was performed and expression of miR-21 relative to the untreated control was calculated. Data were normalised to RNU6B. Statistical analysis was performed using a paired, two-tailed Student's t-test. *, ** and *** represent $p<0.05$, 0.01 and 0.001 respectively. Data shown as mean ± SEM, n = 5 independent experiments.

Having confirmed that miR-21 is induced in macrophages by mycobacterial infection, this induction was then characterised in more detail. Murine BMDM (**Figure 3.3A**) or human MDM (**Figure 3.3B**) were infected with a range of doses of iMtb (0, 2, 5 and 10 bacteria per cell) and a 100 ng/mL LPS positive control was included alongside. After 24 hours miR-21 was measured. miR-21 was found to be dose-dependently induced by iMtb in murine macrophages, continuing to increase at the top dose of 10 bacteria per cell. miR-21 induction peaked at an MOI of 5 bacteria per cell in the human MDM model, possibly due to cell death at higher levels of infection. An MOI of 5 was chosen as the optimal dose of Mtb for this work as this induced approximately 3-fold induction of miR-21 in both species of macrophages.

The kinetics of miR-21 induction were then interrogated using this optimal dose of iMtb. BMDM were infected with iMtb at an MOI of 5 bacteria per cell for 3, 24 and 72 hours. Peak significant induction of miR-21 was observed at 24 hours (**Figure 3.4A**). No early induction above baseline levels was observed, fitting with the view of miR-21 being enhanced later in the course of infection as a negative regulator of pro-inflammatory signalling. At 72 hours miR-21 levels return to baseline, in line with the idea of the resolution phase of inflammation coming into effect. The primary transcript, pri-miR-21, from which miR-21 is derived via nuclear and cytosolic processing, was also measured by qPCR at these time points. The appearance of mature miR-21 at 24 hours post-infection is preceded by an induction of the primary microRNA transcript 3 hours following Mtb infection (**Figure 3.4B**). An approximate 3-fold induction of the primary transcript is maintained throughout the infection time course. TMEM49, the gene that overlaps miR-21, was measured as a negative control and was found to be differentially induced to pri-miR-21, providing confirmation that it is transcribed via its own promoter. Furthermore, when the induction of TNF-α and IL-10 protein was measured alongside miR-21, miR-

21 induction at 24 hours was found to coincide with the high induction of both TNF-α- and IL-10 protein expression (**Figure 3.5**).

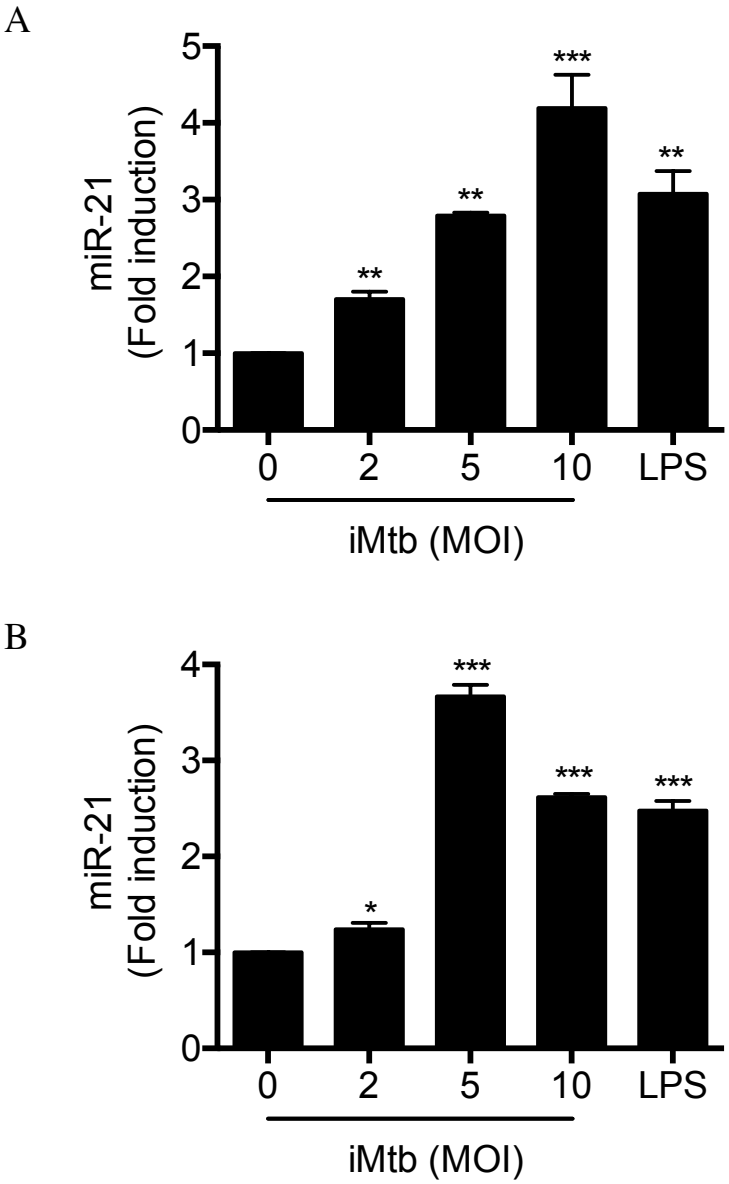

Figure 3.3 Mtb induced miR-21 expression in macrophages is dose-dependent. Murine BMDM (A) or human MDM (B) were infected with irradiated Mtb (H37Rv strain) (iMtb) at an MOI of 0, 2, 5 or 10 bacteria per cell or stimulated with 100ng/mL of LPS for 24 hours. qPCR was performed and expression of miR-21 relative to the untreated control was calculated. Data were normalised to RNU6B. Statistical analysis was performed using a paired, two-tailed Student's t-test, *, ** and *** represent $p<0.05$, 0.01 and 0.001 respectively. Data shown as mean ± SEM, n = 3 independent experiments.

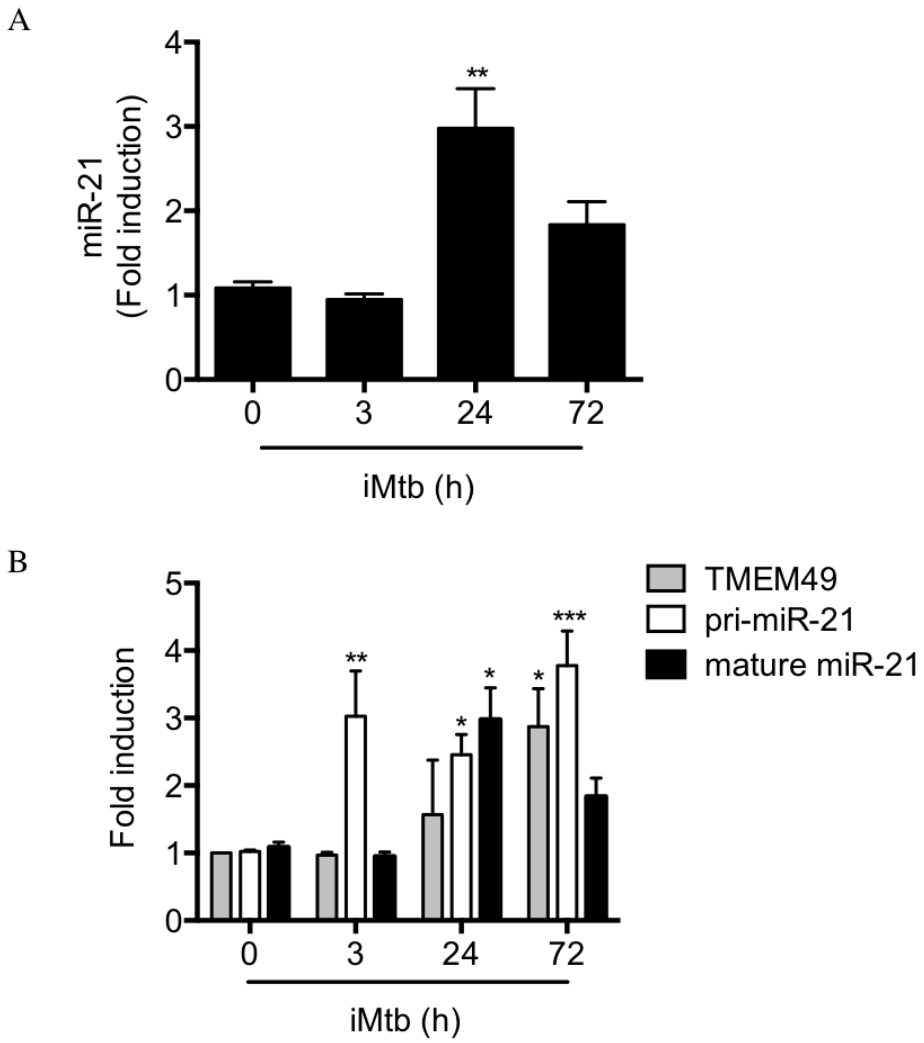

Figure 3.4 miR-21 induction is temporally regulated. Murine BMDM were infected with irradiated Mtb (H37Rv strain) (iMtb) at an MOI of 5 bacteria per cell for 3, 24 and 72 hours. qPCR was performed and expression of TMEM49, pri-miR-21 and mature miR-21 relative to the untreated control was calculated. Data were normalised to 18S and RNU6B respectively. Statistical analysis was performed using two-way ANOVA with Sidak's multiple comparisons test. *, ** and *** represent $p<0.05$, 0.01 and 0.001 respectively. Data shown as mean ± SEM, n = 3 independent experiments.

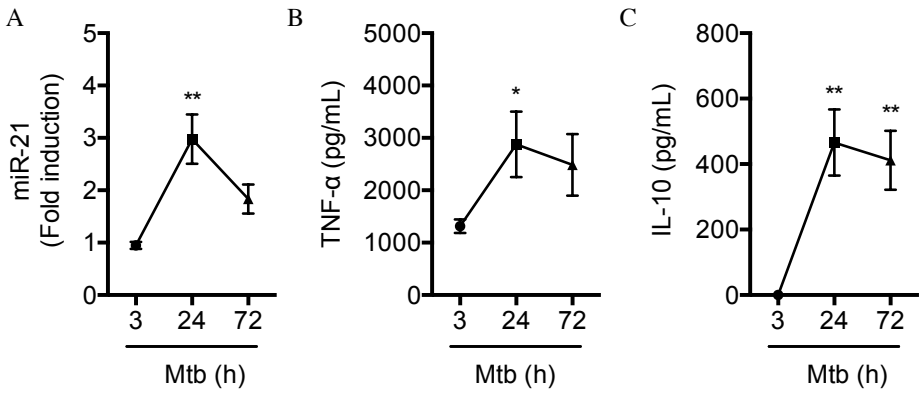

Figure 3.5 miR-21, TNF-α and IL-10 induction by Mtb. Murine BMDM were infected with irradiated Mtb (H37Rv strain) (iMtb) at an MOI of 5 bacteria per cell for 3, 24 and 72 hours. qPCR was performed and expression of mature miR-21 relative to the untreated control was calculated (A). Data were normalised to RNU6B. Supernatants were collected and ELISA was used to measure TNF-α (B) and IL-10 (C) protein. Statistical analysis was performed using one-way ANOVA with Fisher's LSD test. *, ** and *** represent $p<0.05$, 0.01 and 0.001 respectively. Data shown as mean ± SEM, n = 3 independent experiments.

3.2.2 Induction of miR-21 is sustained in macrophages by live Mtb

Initial investigation into the temporal induction of miR-21 by Mtb showed resolution of induction towards later time points. However in vivo studies have shown sustained induction of miR-21 in whole lung tissue[346]. To more closely study the in vivo role of miR-21 in Mtb infection, live Mtb infection in the BMDM model was investigated. BMDM were infected for 24 hours with a live, attenuated strain of Mtb (H37Ra) alongside a heat-killed version of the same strain (**Figure 3.6A**). miR-21 induction showed similar dose-dependency between live and dead bacteria, however the level of induction differed. At a low MOI, there was no observed disparity, however a significant difference between the dead and live infection was observed at an MOI of 5 and 10 bacteria per cell. Live Mtb at these doses induced significantly more miR-21 than its dead counterpart, induction being approximately double that seen with dead bacteria.

The difference between the induction of miR-21 by live Mtb and dead Mtb was also examined over a longer course of infection. BMDM were infected with heat-killed, attenuated Mtb (H37Ra) and live, attenuated Mtb (H37Ra) at an MOI of 5 bacteria per cell for 24 and 72 hours. RNA was isolated and qPCR for miR-21 was performed at each time point. Live Mtb induced significantly more miR-21 at both time points, and this enhancement was particularly evident at 72 hours (**Figure 3.6B**). Heat-killed Mtb showed no significant differences in the level of miR-21 induced between 24 and 72 hours, however live Mtb showed a significant enhancement in induction at 72 hours, indicating that live Mtb induces more miR-21 and importantly sustains this induction at later time points.

Additionally, the induction of miR-21 in response both non-viable and live Mtb was investigated in primary human alveolar

macrophages. Primary human AM were isolated as described in **2.1.7** and infected with non-viable, irradiated Mtb (H37Rv strain) (iMtb) or live Mtb (H37Rv strain) (Mtb) at the same MOI for 24 and 48 hours. Similar to what had been seen in the murine AM with attenuated Mtb strains, live infection with this virulent strain of Mtb induced significantly more miR-21 expression at later time-points than the irradiated version of the same strain (**Figure 3.7**).

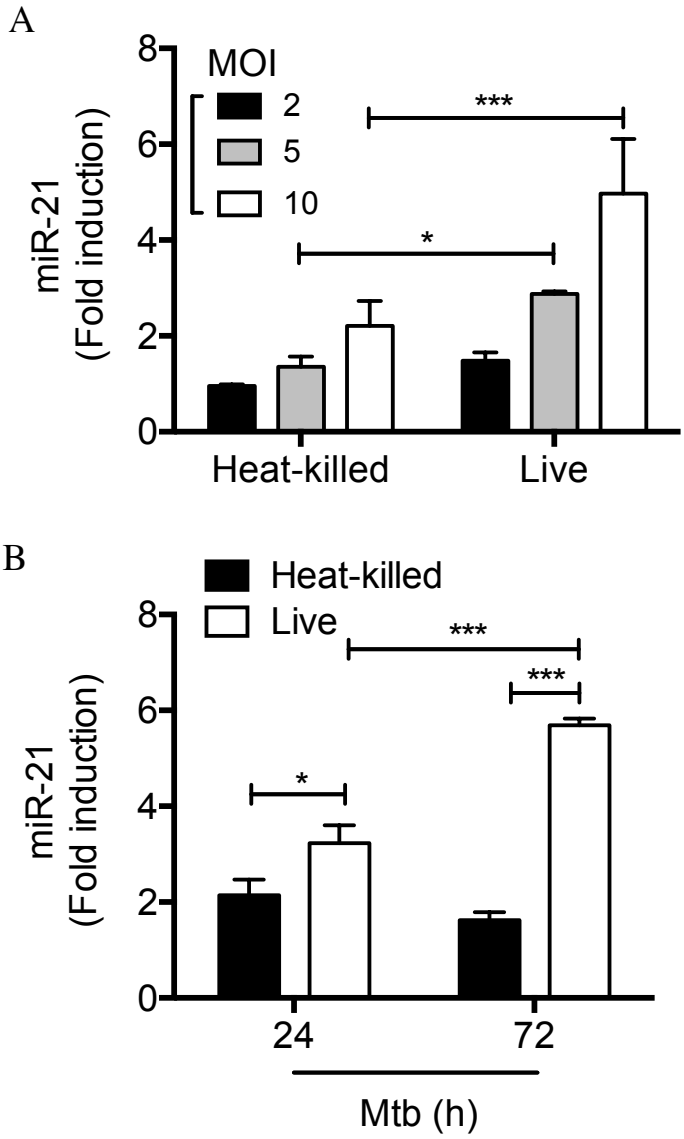

Figure 3.6 Heat-killed Mtb induces lower expression of miR-21 than live Mtb. A) Murine BMDM were infected with heat-killed Mtb (H37Ra strain) (Heat-killed) or live Mtb (H37Ra strain) (live) at an MOI of 0, 2, 5 or 10 bacteria per cell for 24 hours, and B) Murine BMDM were infected with heat-killed Mtb (H37Ra strain) (Heat-killed) or live Mtb (H37Ra strain) (live) at an MOI of 5 bacteria per cell for 24 and 72 hours. qPCR was performed and expression of miR-21 relative to the untreated control was calculated. Data were normalised to RNU6B. Statistical analysis was performed using two-way ANOVA with Sidak's multiple comparisons test. *, ** and *** represent $p<0.05$, 0.01 and 0.001 respectively. Data shown as mean ± SEM, n = 3 independent experiments.

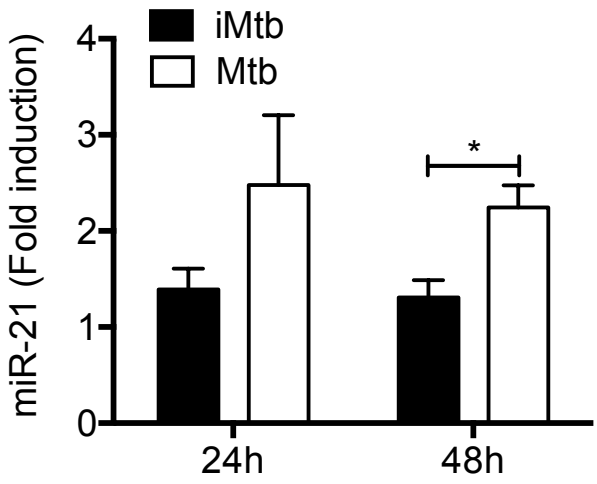

Figure 3.7 Live Mtb sustains miR-21 expression in human alveolar macrophages. Human AM were infected with non-viable, irradiated Mtb (H37Rv strain) (iMtb) or live Mtb (H37Rv strain) (Mtb) at an MOI of 2 bacteria per cell for 24 and 48 hours. qPCR was performed and expression of miR-21 relative to the uninfected control at each time point was calculated. Data were normalised to RNU6B. Due to the virulent nature of this live strain of Mtb, this data was generated by Dr Seonadh O'Leary in a Containment Level 3 unit. Statistical analysis was performed using two-way ANOVA with Sidak's multiple comparisons test. *, ** and *** represent $p<0.05$, 0.01 and 0.001 respectively. Data shown as mean ± SEM, n = 5 independent experiments.

3.2.3 Developing a model of macrophage miR-21 deficiency

Having confirmed that miR-21 is induced by Mtb infection and performed rudimentary investigation into the temporal, dose-dependent and strain-specific characteristics of miR-21 induction, the consequence of this miR-21 expression was next explored. To further understand the role of miR-21 in Mtb infection, models of miR-21 deficiency were employed. A miR-21 knockout mouse had previously been generated using Cre-Lox recombination[296, 298] (**2.1.1**) and BMDM from this murine model were obtained. To confirm the functional deficiency of miR-21 even after Mtb infection, wild-type and miR-21 knockout BMDM were infected with irradiated H37Rv for 24 hours at an MOI of 5 bacteria per cell for 24 hours and miR-21 measured by qPCR. miR-21 was detected and induced by Mtb infection in the wild-type macrophages and, as expected, no miR-21 was detected in the miR-21 knockout macrophages even after infection (**Figure 3.8A**).

TMEM49, the gene overlapping with miR-21, and two known direct mRNA targets of miR-21, PTEN[319] and PDCD4[296] were also measured by qPCR to further confirm a knockout phenotype. TMEM49 expression remained unchanged by the knockout (**Figure 3.8B**), confirming the specificity of the knockout. PTEN, which is known to be directly targeted by miR-21 during the wound-healing, efferocytosis response[319] to negatively regulate the NFκB pathway[347], was significantly enhanced in miR-21 knockout compared to wild-type BMDM after infection with Mtb (**Figure 3.8C**). PDCD4, which is targeted by miR-21 resulting in enhanced production of IL-10[296], was significantly higher in uninfected miR-21 knockout macrophages compared to wild-type controls **Figure 3.8D**). This difference was not as pronounced after infection but still trended towards enhanced levels of PDCD4 mRNA compared to the wild-type BMDM.

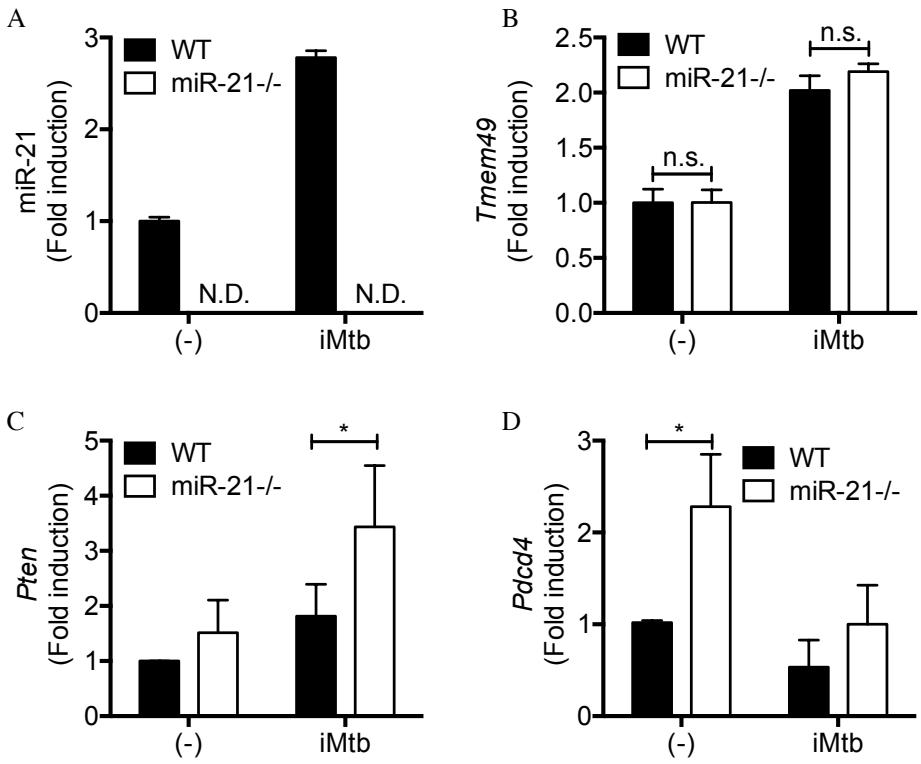

Figure 3.8 BMDM from miR-21 deficient mice do not express miR-21. Murine BMDM were infected with irradiated Mtb (H37Rv strain) (iMtb) at an MOI of 5 bacteria per cell for 24 hours. qPCR was performed and expression of miR-21 (A), *Tmem49* (B), *Pten* (C) and *Pdcd4* (D) relative to the untreated control were calculated. Data were normalised to RNU6B (A) and 18S (B-D). Statistical analysis was performed using a paired, two-tailed Student's t-test. *, ** and *** represent $p<0.05$, 0.01 and 0.001 respectively. Data shown as mean ± SEM, n = 3 independent experiments.

Though miR-21 knockout BMDM are a valuable resource for studying miR-21 and Mtb interactions, Mtb is a disease that infects humans and does not naturally infect mice. Thus, an additional model of human macrophage miR-21 deficiency was desired as an additional supportive model with therapeutic relevance. A microRNA hairpin inhibitor specific to miR-21 was employed. The inhibitor is complementary to the mature miR-21 sequence and is designed to bind tightly to the microRNA preventing it from binding to its targets. The inhibitor was delivered to the cytosol using a liposomal transfection protocol detailed in (**2.1.17**). Cells were transfected with 50 nM of anti-miR-21 or negative, non-targeting control anti-miR and allowed to recover 24 hours prior to infection. Cells were then infected with irradiated H37Rv at an MOI of 5 bacteria per cell for 24 hours and miR-21, PDCD4 and PTEN expression measured by qPCR. miR-21 induction was not affected by the negative control non-targeting anti-miR, with similar levels of upregulation observed as in untransfected cells. (**Figure 3.9A**). Transfection with anti-miR-21 rendered miR-21 undetectable by qPCR. PTEN expression was significantly enhanced after infection with Mtb, though not basally, as was observed in the BMDM model (**Figure 3.9B**). PDCD4 mRNA was significantly higher in both uninfected and infected treated with anti-miR-21 (**Figure 3.9C**).

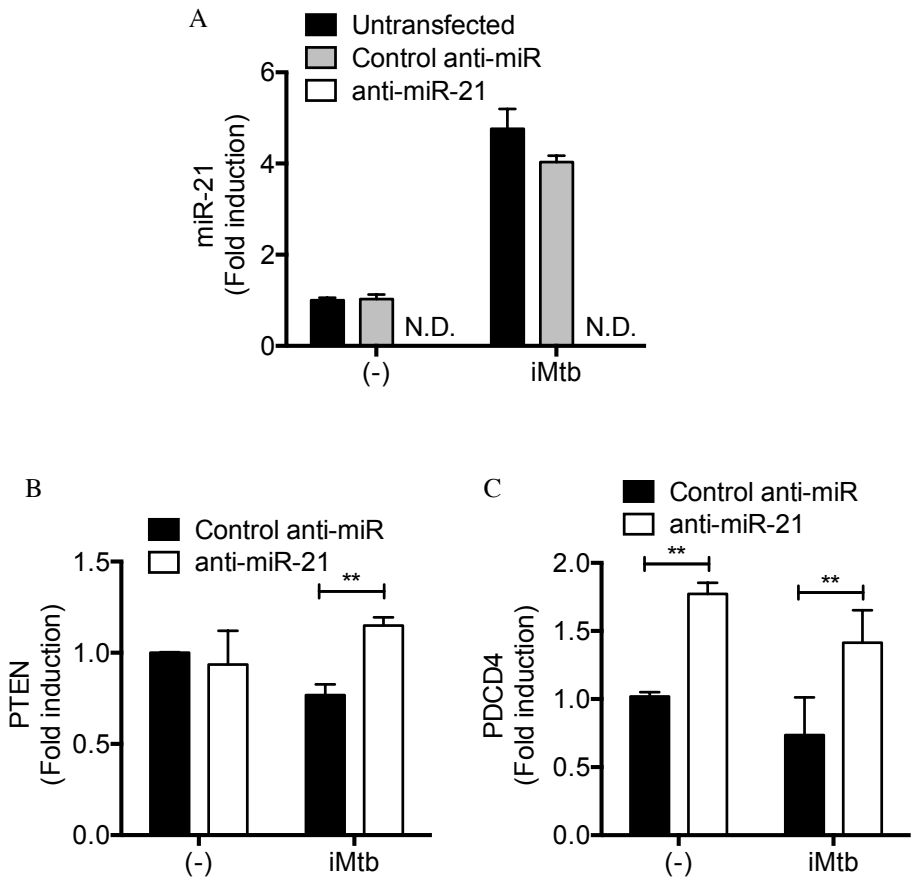

Figure 3.9 Transfection of MDM with a microRNA hairpin inhibitor effectively knocks down miR-21. Human MDM were transfected with 50 nM of miRIDIAN microRNA hairpin inhibitor specific to a negative control sequence (Control anti-miR) or specific to miR-21 (anti-miR-21) using a 2% Lipofectamine/Optimem solution. MDM were allowed 24 hours to recover and were infected with irradiated Mtb (strain H37Rv) (iMtb) at an MOI of 5 bacteria per cell for 24 hours. qPCR was performed and expression of miR-21 (A), PTEN (B) and PDCD4 (C) relative to the untreated control was calculated. Data were normalised to RNU6B (A) and 18S (B and C). Statistical analysis was performed using a paired, two-tailed Student's t-test, *, ** and *** represent $p<0.05$, 0.01 and 0.001 respectively. Data shown as mean ± SEM, n = 3 independent experiments.

3.2.4 miR-21 does not influence mycobacterial uptake

Having established both mouse and human macrophage models of miR-21 deficiency, bacterial uptake by both genotypes was assessed. Wild-type and miR-21 knockout BMDM and human MDM transfected with control anti-miR or anti-miR were grown on glass slides and infected with a range of volumes of live H37Ra for 3 hours. Cells were fixed and stained with the nuclear dye Hoechst 33342 (blue) and mycobacteria were stained for with the Modified Auramine Stain kit (green). Stained cells were viewed under a fluorescent microscope (as in the representative field of view in the merged image (**Figure 3.10A**). The number of bacteria per cell was counted in several fields of view and the mean uptake calculated. No significant difference in uptake of Mtb at 3 hours between wild-type and miR-21 knockout BMDM was noted (**Figure 3.10B**). Similarly, no difference in bacterial uptake was observed between untransfected, control anti-miR and anti-miR-21 transfected MDM (**Figure 3.10c**). Data for bacterial uptake at an MOI of 5 bacteria per cell is shown here however this same finding was consistent over a range of different MOI.

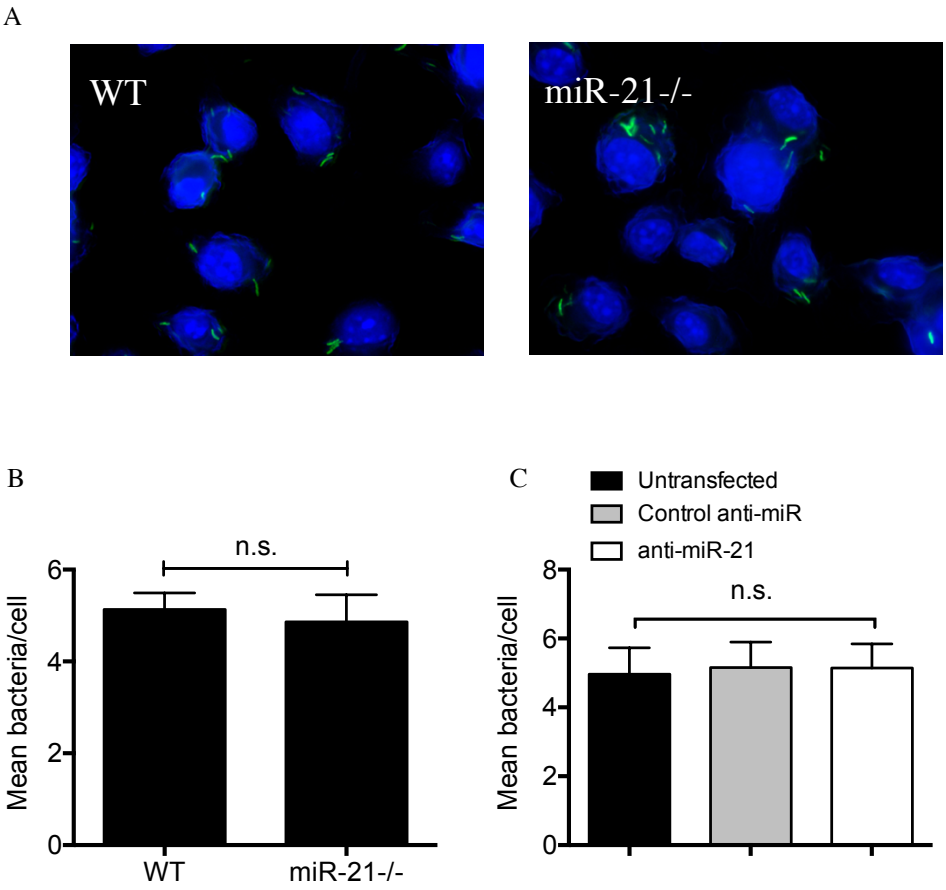

Figure 3.10 miR-21 deficiency does not alter bacterial uptake. Wild-type and miR-21 deficient murine BMDM (A and B) and human MDM transfected with a control anti-miR or anti-miR-21 (C) were grown on Nunc Lab-Tek II 8-well chamber slides and infected with live Mtb (strain H37Ra) for 3 hours. Cells were fixed and stained with the nuclear dye Hoechst 33342 (blue) and mycobacteria were stained for with the Modified Auramine Stain kit (green). Stained cells were viewed under a fluorescent microscope (as in the merged image in A) and the number of bacteria per cell counted in several fields of view and the mean uptake calculated (B and C). Statistical analysis was performed using a paired, two-tailed Student's t-test, *, ** and *** represent $p<0.05$, 0.01 and 0.001 respectively. Data shown as mean ± SEM, n = 5 independent experiments.

3.2.5 miR-21 induction promotes Mtb growth

Though it was found that miR-21 deficiency did not affect uptake of Mtb at 3 hours, the role of miR-21 in a longer course of infection remained unexplored. To assess whether miR-21 played a role throughout the course of Mtb infection, wild-type and miR-21 knockout BMDM were infected with live H37Ra at an MOI of 5 bacteria per cell for 3, 24 and 72 hours. Supernatants were removed 3 hours post infection and centrifuged to remove any extracellular bacteria. At each time-point cells were lysed and diluted lysates were streaked on Middlebrook agar. Colony forming units were counted and the number of colonies relative to the 3-hour time point calculated (**2.1.11**).

There was no significant difference in CFU count 3 hours post-infection, as was expected from the fluorescent microscopy examining bacterial uptake (**Figure 3.11A**). Both wild-type and miR-21 knockout macrophages were able to contain Mtb growth at 24 hours post-infection, trending towards a reduction in the number of CFU relative to 3 hours. As the time course was extended however, a marked difference between the genotypes became apparent. Wild-type macrophages were unable to contain Mtb growth at this later stage of infection and the CFU count rose approximately 4-fold relative to the 3-hour time point. In comparison, bacterial growth in miR-21 knockout BMDM was significantly lower and the macrophages contained growth to similar levels as the 3-hour time point.

A similar experiment was performed in the human model. Untransfected MDM and MDM transfected with control-anti-miR and anti-miR-21 infected were with H37Ra at an MOI of 5 bacteria per cell for 3, 24, 72 and 120 hours. Untransfected MDM were initially able to contain Mtb growth but this was significantly impaired at later time-points (**Figure 3.11B**). No significant

difference in bacterial growth between untransfected MDM and MDM transfected with anti-miR control was noted at any time point. Similar to the results for BMDM, there was no difference in bacterial containment between control anti-miR and anti-miR-21 transfected cells at 3- or 24-hours post-infection. At 72 hours however, there was significantly improved containment of growth in the anti-miR-21 treated MDM, and this difference became even more significant 120 hours post-infection.

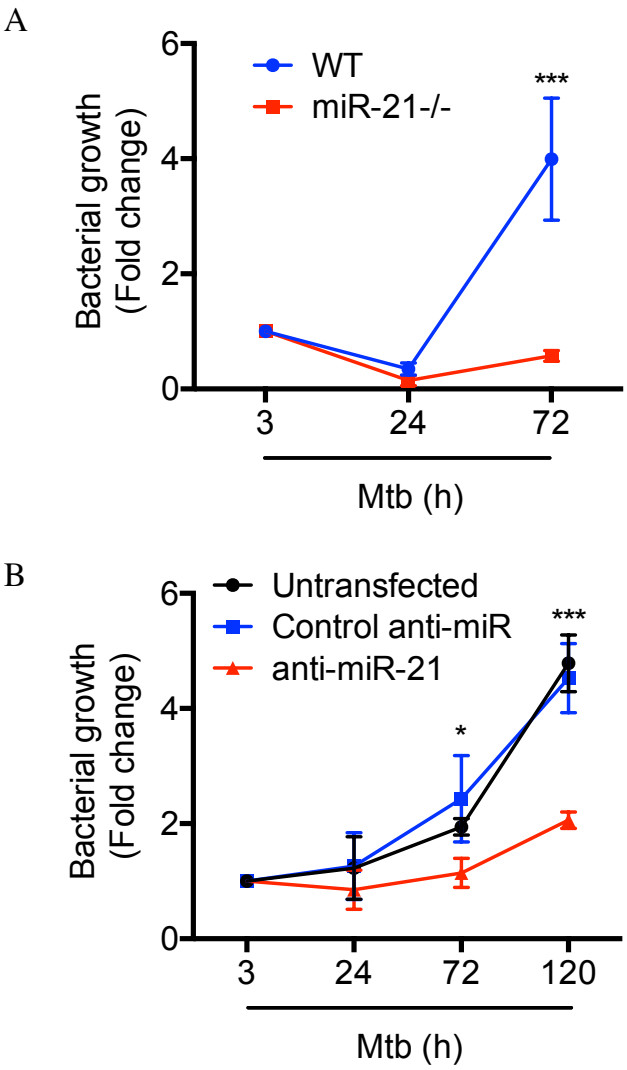

Figure 3.11 miR-21 depletion significantly improves containment of Mtb growth. Murine wild-type and miR-21-deficient BMDM (A) and human MDM untransfected or transfected with a control anti-miR or anti-miR-21 (B) were infected with live Mtb (strain H37Ra) at an MOI of 5 bacteria per cell. Cells were lysed in 0.1% Triton X-100 at the indicated time-points and diluted lysates were streaked in triplicate on Middlebrook agar plates and incubated at 37°C for approximately 14 days. Colony forming units were counted and the number of colonies relative to the 3-hour time point calculated. Statistical analysis was performed using a paired, two-tailed Student's t-test. * and *** represent $p<0.05$ and 0.001 respectively. Data shown as mean ± SEM, n = 3 independent experiments.

3.2.6 miR-21 negatively regulates anti-microbial oxidative species

Having shown that miR-21 can promote bacterial survival, the mechanisms through which it makes the macrophage more permissible to bacterial growth were of interest. Reactive oxygen species[56, 177] and particularly reactive nitrogen species are potent anti-microbial effectors and signalling molecules[58] and were interrogated in the absence of miR-21. Arginine can be metabolised by macrophage nitric oxide synthase (NOS) to produce citrulline and nitric oxide. Nitric oxide can be further metabolised into reactive nitrogen species, including nitrite, which can act as antimicrobial effectors against Mtb. Inducible nitric oxide synthase (iNOS) is encoded by the NOS2 gene and is the isoform of this enzyme that can be upregulated upon inflammatory activation and can function independently of calcium, unlike the constitutive isoforms. Conversely, arginase 1, the cytoplasmic isoform of arginase which Mtb is known to specifically drive in infection, inhibits nitric oxide synthesis through several proposed mechanisms including competing with NOS for arginine as a substrate. Arginase 1 converts arginine into ornithine from which hydroxyproline and polyamines can be generated for wound-healing[348]. Polyamines themselves can also inhibit iNOS activity[349]. Arginase 1 is upregulated downstream of TLR- and cytokine-signalling and can reduce iNOS activity and impair the production of nitrite species[338]. The balance between these enzymes is important in determining the fate of arginine in the macrophage and thus its potential to produce anti-microbial nitrogen species.

Wild-type and miR-21-deficient murine BMDM were infected with iH37Rv at an MOI of 5 bacteria per cell or 100 ng/mL of LPS for 24 hours. RNA was extracted and qPCR was performed. Expression of iNOS and arginase 1 mRNA relative to the untreated control was calculated. iNOS was induced by LPS and to a lesser extent by Mtb

in both genotypes (**Figure 3.12A**). LPS induced significantly more iNOS (2.3-fold) in miR-21-deficient BMDM than in wildtype, however there was no significant difference in iNOS mRNA expression basally or when induced by Mtb.

Arginase 1 mRNA was induced by both LPS and Mtb, though to a far greater extent by Mtb (**Figure 3.12B**). miR-21-deficient BMDM induced less arginase 1 mRNA than wild-type BMDM, most significantly in the Mtb infected cells (1000-fold induction in wild-type versus 500-fold induction in miR-21 knockout macrophages). The enhanced induction of iNOS and lower induction of Arginase 1 by miR-21 deficient macrophages in response to LPS and Mtb indicates that miR-21 limits the induction of a pro-inflammatory phenotype.

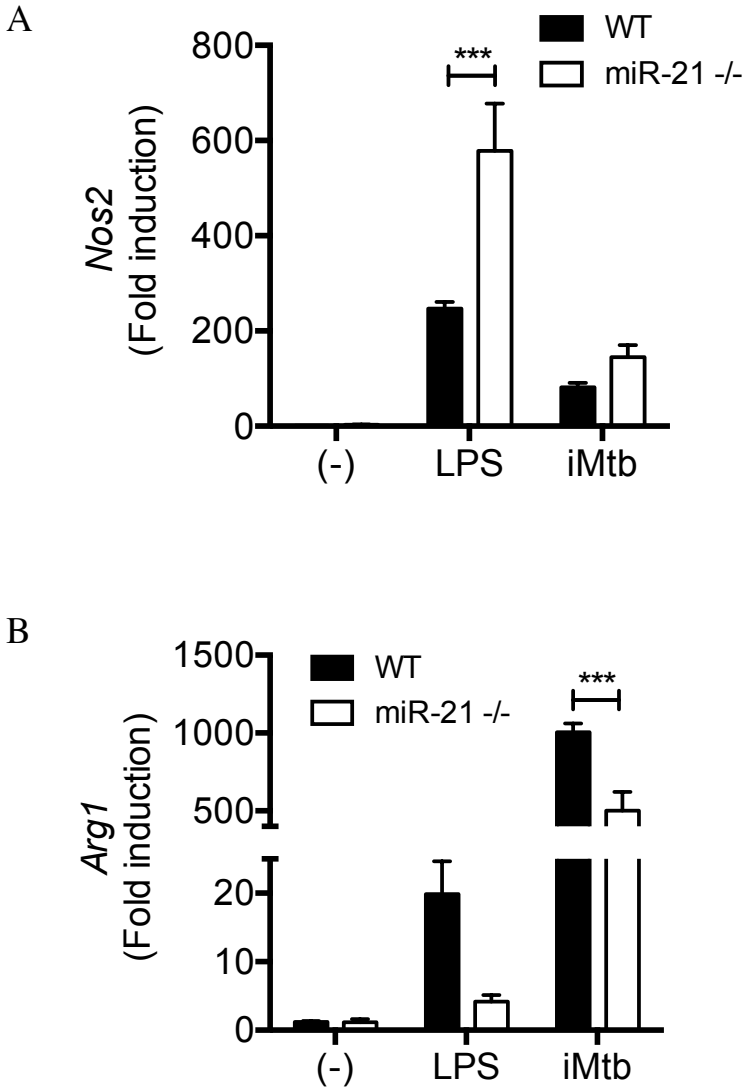

Figure 3.12 miR-21 deficiency alters *Nos2* and *Arg1* expression in response to LPS and Mtb. Wild-type and miR-21-deficient murine BMDM were infected with irradiated Mtb (strain H37Rv) (iMtb) at an MOI of 5 bacteria per cell or 100 ng/mL of LPS for 24 hours. RNA was harvested and qPCR was performed. Expression of *Nos2* (A) and *Arg1* (B) mRNA relative to the untreated control was calculated. Data were normalised to 18S. Statistical analysis was performed using a paired, two-tailed Student's t-test. *, ** and *** represent $p<0.05$, 0.01 and 0.001 respectively. Data shown as mean ± SEM, n = 3 independent experiments.

To assess the functional outcome of this altered iNOS and arginase 1 mRNA expression between wild-type and miR-21-deficient BMDM, nitrite in the supernatant from this experiment was measured by Griess assay. Nitrite was detected and there was no difference in uninfected macrophages between genotypes (**Figure 3.13A**). LPS stimulation enhanced nitrite induction but this was not significant and was not significantly different between genotypes. Significantly induction of nitrite was measured in sample treated with Mtb, and this induction was significantly higher in miR-21 knockout macrophages (1.6-fold higher).

The effect of miR-21 activity on nitrite production in response to Mtb infection was then confirmed in murine alveolar macrophages. Alveolar macrophages isolated from murine lungs by bronchoalveolar lavage and allowed 24 hours to recover. The cells were then infected with iH37Rv at an MOI of 5 bacteria per cell for 24 hours. Supernatants were collected and nitrite was measured using a colorimetric Griess assay. In contrast to the BMDM, nitrite levels detected from the alveolar macrophages were much lower. Mtb infection enhanced nitrite levels but this was only significant in the miR-21-deficient macrophages (**Figure 3.13B**). miR-21-deficient macrophages produced significantly more nitrite than wild-type macrophages after infection but to a more modest degree than in BMDM (1.3-fold).

Finally, the ability of miR-21-deficient macrophages to produce more nitrite in response to live Mtb infection was assessed. Wild-type and miR-21-deficient BMDM were infected with live H37Ra at an MOI of 5 bacteria per cell for 3, 24 and 72 hours and nitrite measured in supernatants using the Griess assay. Nitrite accumulated in both genotypes over the course of infection (**Figure 3.14**) and nitrite measured was significantly higher in miR-21

knockout BMDM 72 hours post-infection, reaching 20 μM higher concentration.

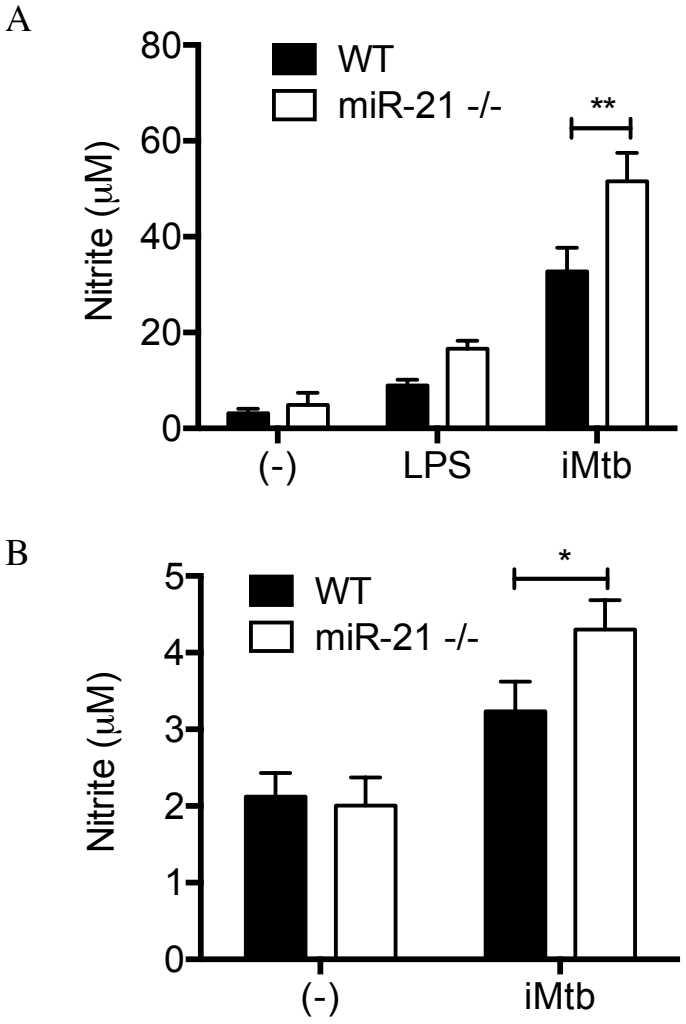

Figure 3.13 miR-21 deficiency enhances nitrite production in response to Mtb infection. (A) Murine BMDM were infected with irradiated Mtb (strain H37Rv) (iMtb) at an MOI of 5 bacteria per cell or 100 ng/mL of LPS for 24 hours. (B) murine AM isolated from lungs by bronchoalveolar lavage and allowed 24 hours to recover. The cells were then infected with irradiated Mtb (strain H37Rv) (iMtb) at an MOI of 5 bacteria per cell for 24 hours. Supernatants were collected and nitrite species measured using a colorimetric Griess assay Statistical analysis was performed using a paired, two-tailed Student's t-test. *, ** and *** represent $p<0.05$, 0.01 and 0.001 respectively. Data shown as mean ± SEM, n = 3 and 5 independent experiments respectively.

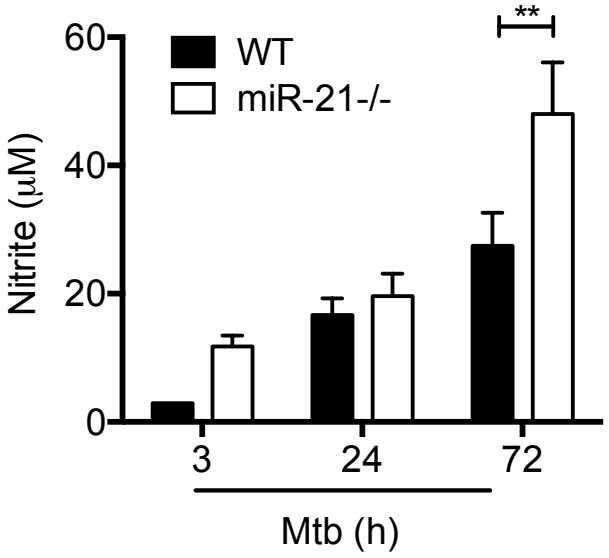

Figure 3.14 miR-21 deficiency enhances nitrite production in response to live Mtb infection. Wild type and miR-21-deficient murine BMDM were infected with live Mtb (strain H37Ra) at an MOI of 5 bacteria per cell for 3, 24 and 72 hours. Supernatants were collected and nitrite species measured using a colorimetric Griess assay Statistical analysis was performed using a paired, two-tailed Student's t-test. *, ** and *** represent $p<0.05$, 0.01 and 0.001 respectively. Data shown as mean ± SEM, n = 3 independent experiments.

Nitrite is far less potently produced by human macrophages and was out of range of the sensitivity of the Griess assay. Furthermore, iNOS and arginase are highly variable in human MDM and are not recommended as markers of macrophage activation. Thus, a different intracellular antimicrobial oxidant was studied in the human MDM knockdown model. Reactive oxygen species or ROS are recognised as important effectors against Mtb infection.

Wild-type and miR-21-deficient BMDM and human MDM transfected with a control anti-miR or anti-miR-21 were then infected with iH37Rv at an MOI of 5 bacteria per cell for 24 hours. Cells were then stained with 20 μM DCFDA, a membrane permeable compound that is oxidised by ROS into a fluorescent product and fluorescence was measured by flow cytometry (**2.1.25**). Staining positivity relative to the untreated control was calculated.

Mtb infection resulted in significant induction of ROS in both genotypes of BMDM, though this was significantly higher in miR-21-deficient macrophages (1.6-fold greater) (**Figure 3.15A**). Significant induction of ROS after infection with Mtb was detected in both negative-control transfected and anti-miR-21 transfected MDM (**Figure 3.15B**). The generation of ROS was significantly higher in the miR-21-depleted macrophages (1.6-fold greater).

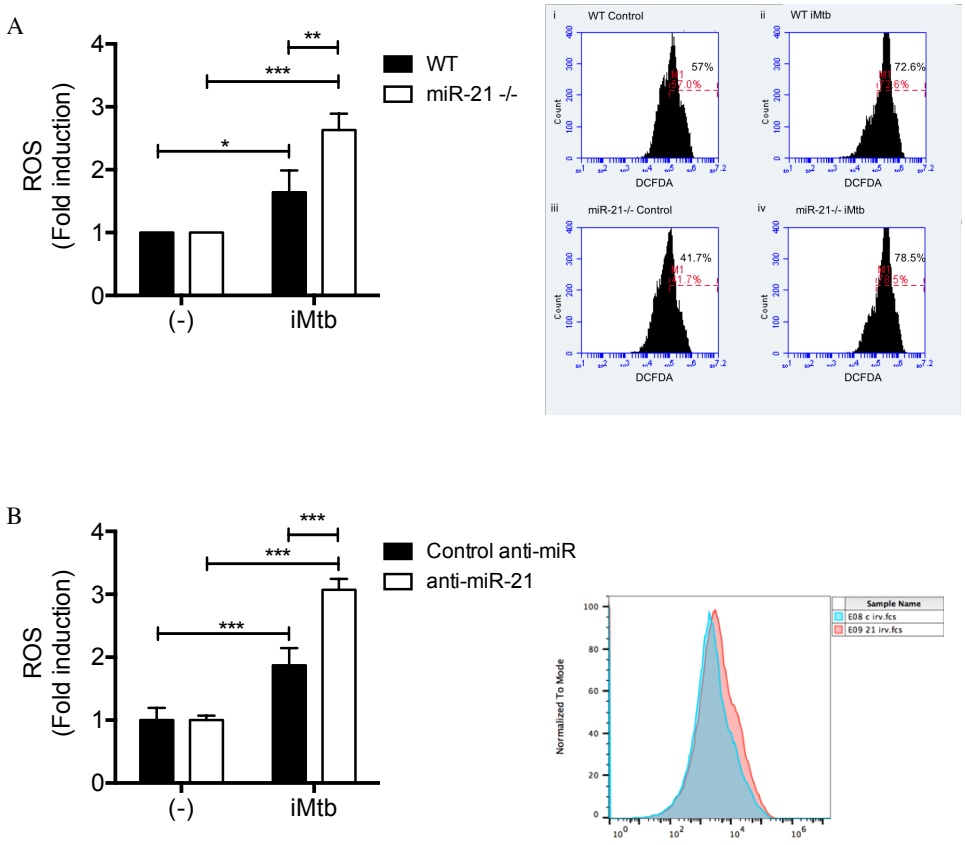

Figure 3.15 miR-21 depletion enhances reactive oxygen species in response to Mtb infection. (A) Wild-type and miR-21-deficient murine BMDM and (B) human monocyte-derived macrophages transfected with a control anti-miR or anti-miR-21 were infected with irradiated Mtb (strain H37Rv) (iMtb) at an MOI of 5 bacteria per cell for 24 hours. Cells stained with 20 μM DCFDA and fluorescence was measured by flow cytometry. Representative flow plots shown alongside mean data. Brightness relative to the untreated control calculated. Statistical analysis was performed using a paired, two-tailed Student's t-test. *, ** and *** represent $p<0.05$, 0.01 and 0.001 respectively. Data shown as mean ± SEM, n = 3 independent experiments.

3.2.7 miR-21 expression promotes IL-10 production in response to Mtb infection

Having found significant differences in the production of antimicrobial mediators ROS and NOS in the absence of miR-21, the cytokines controlling these effectors were examined. IL-10 is a key cytokine involved in the immune response to Mtb infection, and LPS-driven IL-10[350] has been shown to be enhanced by miR-21 through its targeting of PDCD4[296]. IL-10 is known to be induced during Mtb infection and has also been shown to downregulate ROS and NOS in other models[351, 352]. This shared relevance of IL-10[102, 117] to both Mtb infection and miR-21 activity made it an ideal starting candidate for investigating the mechanism behind the enhanced bacterial containment observed in miR-21-deficient macrophages.

IL-10 induction during the course of Mtb infection was examined. Wild-type and miR-21-deficient macrophages were infected with live H37Ra at an MOI of 5 bacteria per cell for 3, 24 and 72 hours. Supernatants were collected at each time point and IL-10 protein was quantified by ELISA. IL-10 protein was induced by Mtb, with peak induction at 24 hours post-infection (**Figure 3.16A**). No significant difference between genotypes was found 3 post infection, however miR-21-deficient macrophages produced significantly less IL-10 24 hours and particularly 72 hours post-infection (1.7-fold and 3.3-fold lower respectively).

These findings were also confirmed in the human MDM knockdown model. Again, IL-10 was induced by Mtb infection and was significantly lower at 24 and 72 hours post-infection when miR-21 activity was blocked (**Figure 3.16B**) (1.8-fold and 1.7-fold lower respectively). IL-10 was not significantly affected by the transfection. No difference between the negative control anti-miR and anti-miR-21 was observed at 3 or 120 hours post infection.

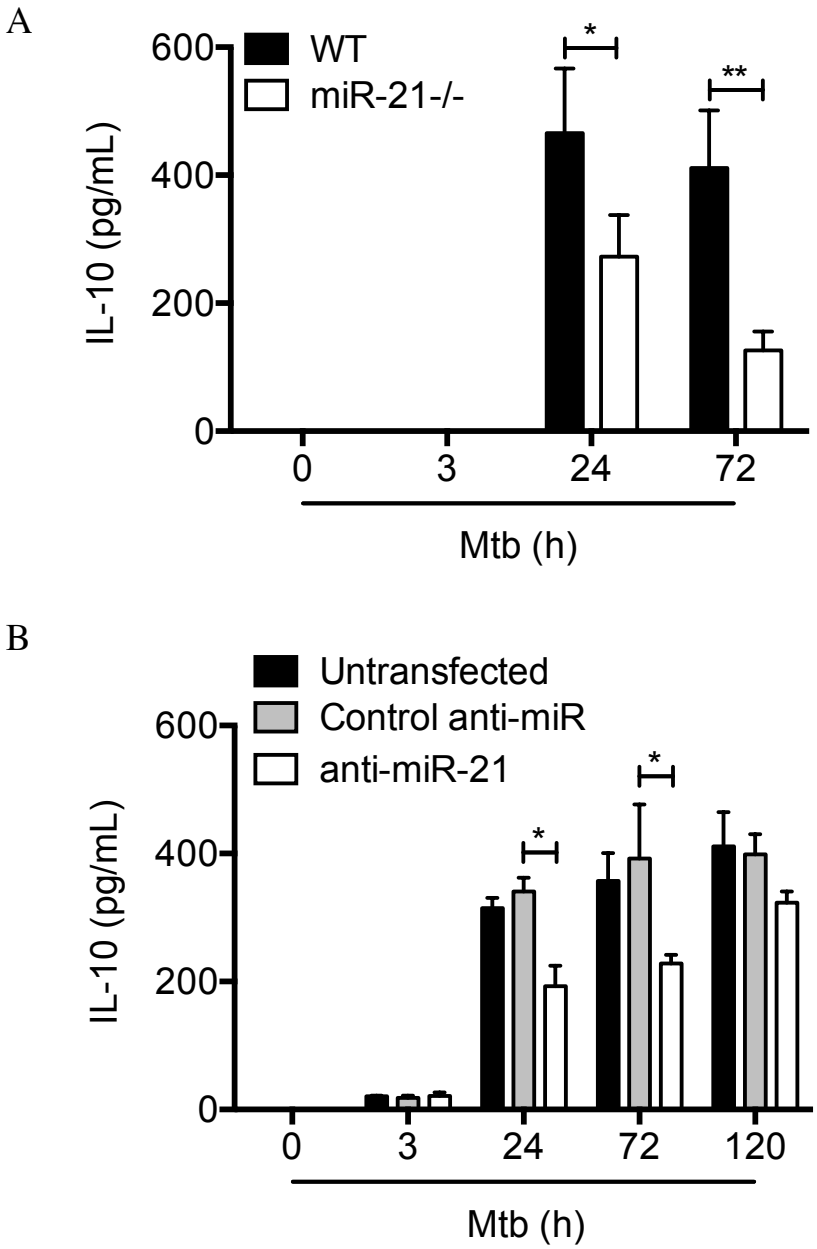

Figure 3.16 miR-21 deficiency restricts IL-10 production in response to Mtb infection. (A) Murine BMDM and (B) human MDM transfected with anti-miR control or anti-miR-21 were infected with live Mtb (strain H37Ra) at an MOI of 5 bacteria per cell for 3, 24 and 72 hours. Supernatants were collected at these time-points and IL-10 protein quantified using an ELISA. Statistical analysis was performed using a paired, two-tailed Student's t-test. *, ** and *** represent $p<0.05$, 0.01 and 0.001 respectively. Data shown as mean ± SEM, n = 3 independent experiments.

The induction of IL-10 protein by infection of macrophages with live Mtb was found to be significantly downregulated in the absence of miR-21. This repression of IL-10 activity in miR-21-deficient BMDM seen with live bacteria was next confirmed with the TLR agonists irradiated H37Rv and LPS and the effect on IL-10 at the mRNA level was also investigated. Wild-type and miR-21-deficient BMDM were infected with irradiated Mtb at an MOI of 5 bacteria per cell or with 100 ng/mL LPS as a positive control for 24 hours. qPCR for IL-10 mRNA was performed and IL-10 protein was measured in supernatants by ELISA.

No significant difference in IL-10 mRNA expression in response to LPS or irradiated Mtb was detected (**Figure 3.17A**). LPS did not significantly induce IL-10 mRNA, irradiated Mtb induced roughly 30-fold induction of IL-10 mRNA in both genotypes. At the protein level, there was significantly less IL-10 protein produced by miR-21-deficient BMDM in response to LPS (approximately 1.7-fold less) however no difference in IL-10 protein produced in response to irradiated Mtb (**Figure 3.17B**). Conversely to the mRNA profile, IL-10 protein expression was induced by both LPS and irradiated Mtb.

These results were also confirmed in the human MDM knockdown model. Similarly to the findings in the murine model, no significant difference in IL-10 mRNA expression in response to LPS or irradiated Mtb was detected (**Figure 3.18A**). LPS did not induce IL-10 mRNA expression, while irradiated Mtb induced roughly 12-fold induction in both genotypes (**Figure 3.18A**). Again, as was noted in the murine macrophages, IL-10 protein was secreted both in response to LPS and irradiated Mtb. Levels of IL-10 protein were significantly lower in the miR-21-deficient macrophages in response to LPS (approximately 1.7-fold less as in the BMDM), while no difference in IL-10 protein was seen in response to irradiated Mtb. Together these results indicate that while the

induction of IL-10 is limited by miR-21 by live Mtb, this does not occur in response to irradiated Mtb.

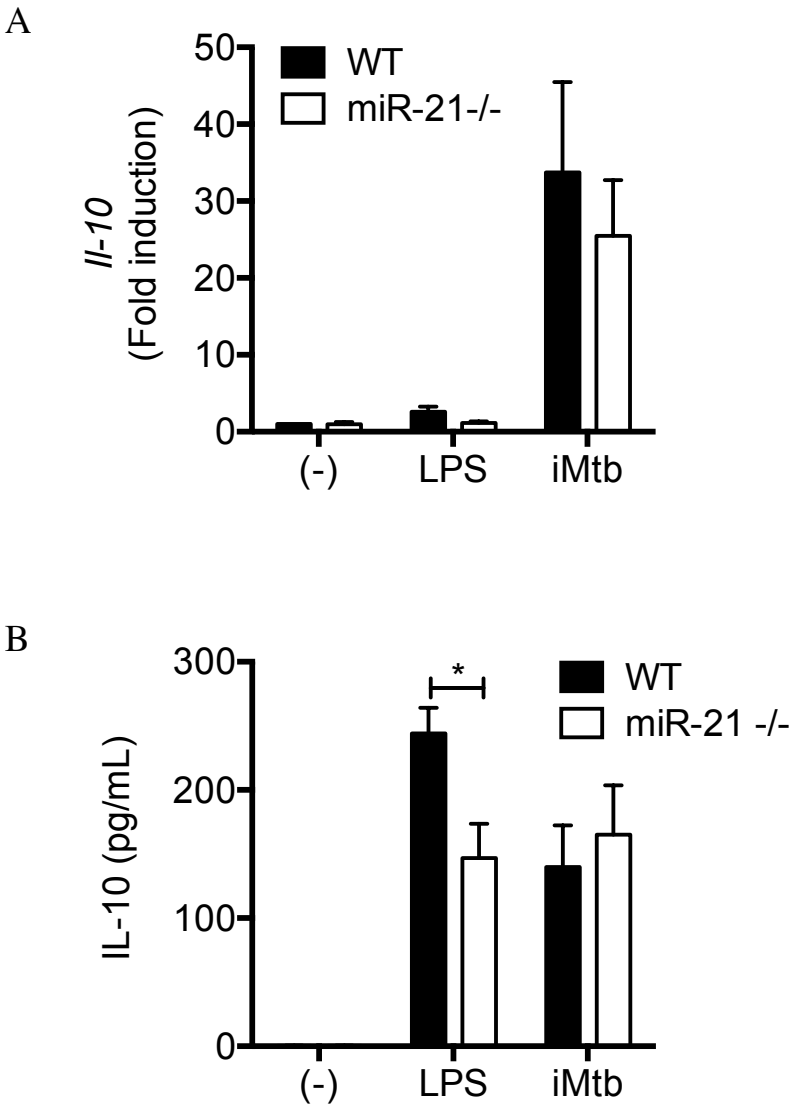

Figure 3.17 miR-21 deficiency restricts IL-10 production in response to LPS and Mtb in BMDM. Murine BMDM were infected with irradiated Mtb (strain H37Rv) (iMtb) at an MOI of 5 bacteria per cell or 100 ng/mL of LPS for 24 hours. RNA and supernatants were collected. qPCR was performed and expression of IL-10 mRNA relative to the untreated control was calculated. Data were normalised to 18S (A). IL-10 protein was quantified using an ELISA (B). Statistical analysis was performed using a paired, two-tailed Student's t-test. *, ** and *** represent $p<0.05$, 0.01 and 0.001 respectively. Data shown as mean ± SEM, n = 3 independent experiments.

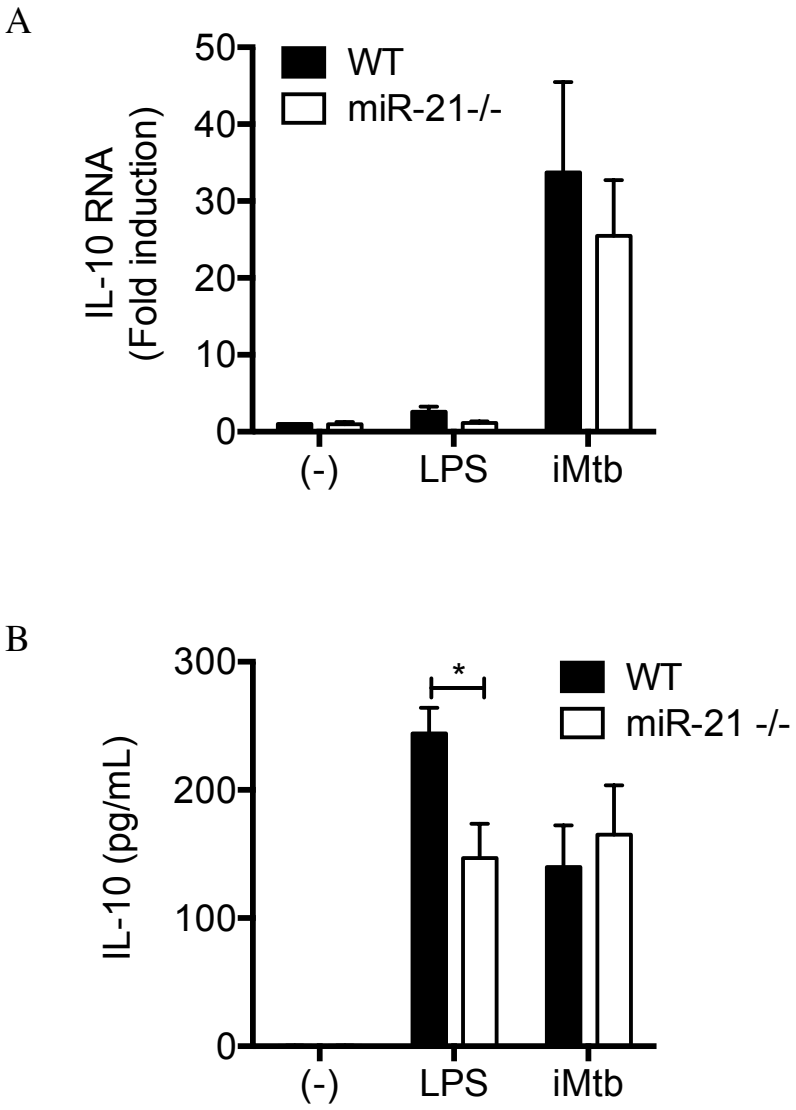

Figure 3.18 miR-21 depletion restricts IL-10 production in response to LPS and Mtb in MDM. Human MDM were transfected with a control anti-miR or anti-miR-21 and allowed 24 hours to recover. The cells were then infected with irradiated Mtb (strain H37Rv) (iMtb) at an MOI of 5 bacteria per cell or 100 ng/mL of LPS for 24 hours. RNA and supernatants were collected. qPCR was performed and expression of IL-10 mRNA relative to the untreated control was calculated. Data were normalised to 18S (A). IL-10 protein was quantified using an ELISA (B). Statistical analysis was performed using a paired, two-tailed Student's t-test. *, ** and *** represent $p<0.05$, 0.01 and 0.001 respectively. Data shown as mean ± SEM, n = 3 independent experiments.

3.2.8 Exogenous IL-10 does not fully restore a complete phenocopy of infection outcome in miR-21 knockout macrophages

IL-10 protein was found to be significantly reduced in response to live Mtb in the absence of miR-21. The contribution of this IL-10 suppression by miR-21 to Mtb infection outcome was assessed.

Wild-type and miR-21-deficient BMDM were infected with live Mtb for 72 hours. 3 hours post-infection BMDM were treated with 10 ng/mL recombinant IL-10. Cells lysates were streaked on Middlebrook agar plates and incubated at 37°C for approximately 14 days. Colony forming units were counted and the number of colonies relative to the 3-hour time point calculated.

In wild type macrophages, addition of exogenous IL-10 significantly enhanced bacterial growth, as would be expected, confirming that the model was working (**Figure 3.19**). miR-21-deficient macrophages were also significantly more permissible to Mtb growth when treated with recombinant IL-10, however miR-21-deficient macrophages were still significantly (though to a slightly lesser degree) better at containing Mtb even in the presence of exogenous IL-10.

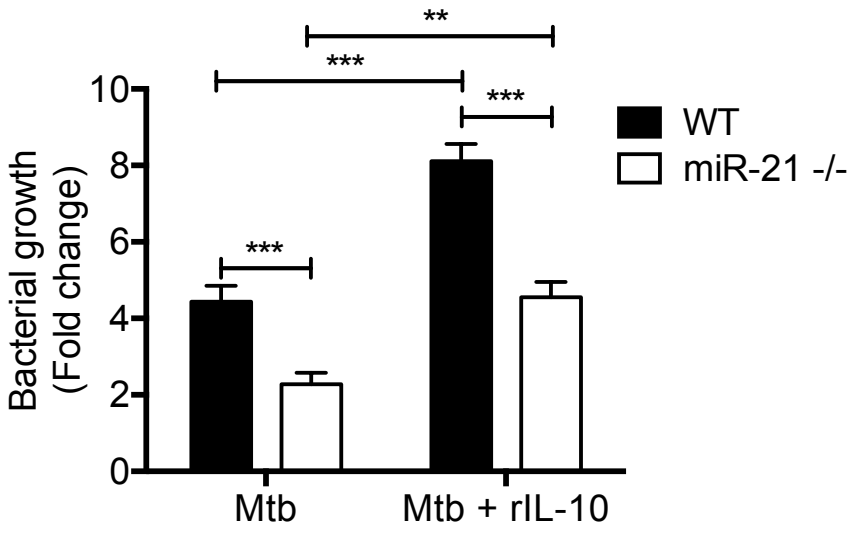

Figure 3.19 Exogenous IL-10 does not restore miR-21 deficiency phenotype. Murine BMDM infected with live Mtb (H37Ra) at an MOI of 5 bacteria per cell for 72 hours. Cells were treated with 10 ng/mL recombinant IL-10 3 hours post-infection. Cells were lysed in 0.1% Triton X-100 at the indicated time points and the lysates diluted in Middlebrook broth supplemented with ADC. Aliquots of the lysates were then streaked in triplicate on warm Middlebrook agar plates and incubated at 37°C for approximately 14 days. Colony forming units were counted and the number of colonies relative to the 3-hour time point calculated. Statistical analysis was performed using a paired, two-tailed Student's t-test. *, ** and *** represent $p<0.05$, 0.01 and 0.001 respectively. Data shown as mean ± SEM, n = 3 mice in one experiment.

3.2.9 TNF-α is negatively regulated by miR-21 during Mtb infection

While boosting production of IL-10 may contribute to miR-21 facilitating Mtb growth within the macrophage, addition of recombinant IL-10 to miR-21-deficient macrophages did not result in a full phenocopy of wild-type infection outcome, implying that other factors also contribute to the observed protection in miR-21-deficient macrophages. TNF-α is another key cytokine involved in the immune response to Mtb infection. TNF-α production is known to be suppressed by miR-21 through targeting of PTEN to dampen NFκB signalling in response to LPS[319, 347] and was therefore investigated as another mediator linking miR-21 and mycobacterial growth.

Wild-type and miR-21 knockout BMDM were infected with live Mtb (strain H37Ra) at an MOI of 5 bacteria per cell for 3, 24 and 72 hours. Supernatants were collected at each time point and TNF-α protein present was quantified by ELISA. TNF-α protein was induced by Mtb, with peak induction at 24 hours post-infection (**Figure 3.20A**). No significant difference between genotypes was found at 3 or 72 hours post infection. Induction of TNF-α by miR-21-defiicent BMDM was significantly higher at 24 hours. At this time-point there roughly 1.6-fold increase in the amount of TNF-α present, equating roughly an additional 2000 pg/mL of protein. This would be consistent with miR-21 limiting TNF-α production during infection.

These findings were also confirmed in the human MDM knockdown model. The kinetics of TNF-α induction were found to be different in MDM, with TNF-α production peaking at 72 hours post-infection (**Figure 3.20B**). TNF-α was found to be significantly enhanced by anti-miR-21 compared to the negative control anti-miR at 24, 72

and 120 hours post-infection in human macrophages. This enhancement was most pronounced at 72 hours. At this time-point miR-21-deficient macrophages produced approximately 3-fold or 1000 pg/mL more TNF-α.

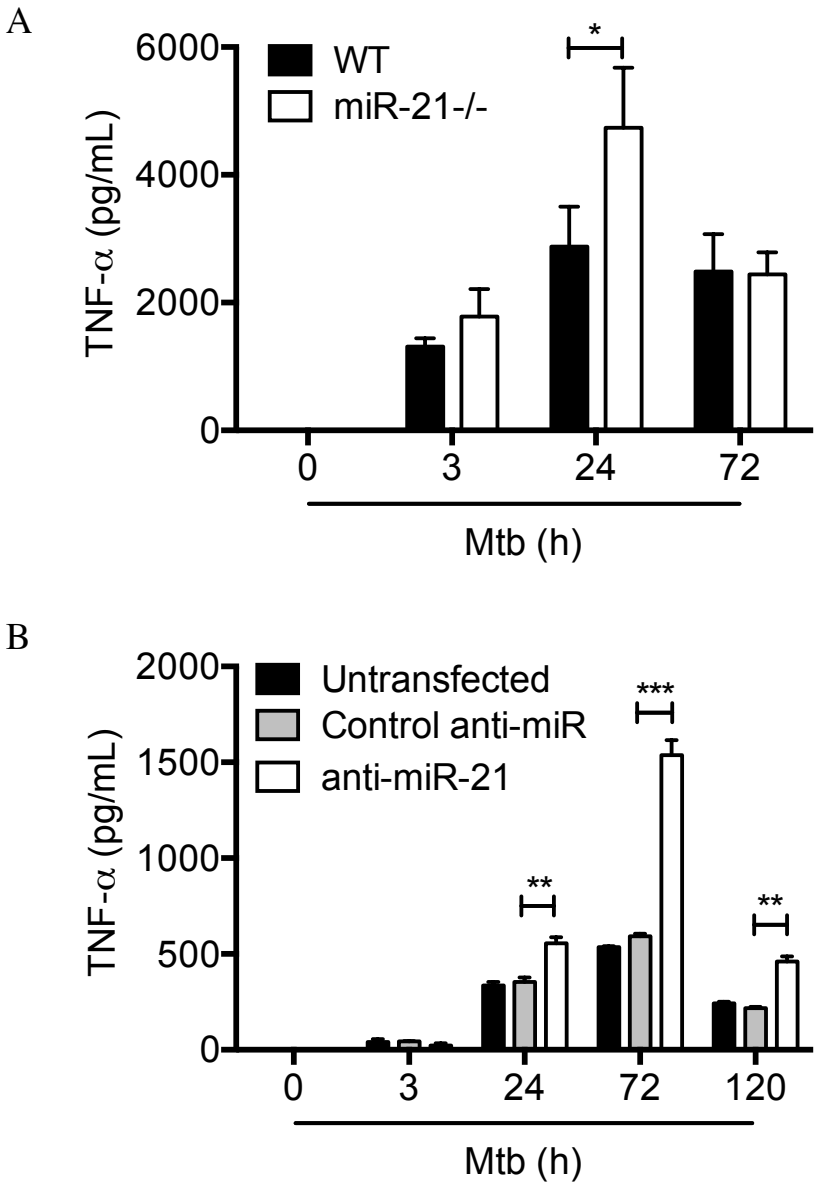

Figure 3.20 miR-21 deficiency enhances TNF-α production in response to Mtb infection in BMDM. Murine BMDM (A) and human MDM either untransfected or transfected with control anti-miR or anti-miR-21 (B) were infected with live Mtb (strain H37Ra) at an MOI of 5 bacteria per cell for 3, 24 and 72 hours. Supernatants were collected at these time-points and TNF-α protein quantified using an ELISA. Statistical analysis was performed using a paired, two-tailed Student's t-test. *, ** and *** represent $p<0.05$, 0.01 and 0.001 respectively. Data shown as mean ± SEM, n = 3 independent experiments.

TNF-α protein induction by live Mtb was found to be significantly enhanced by blockade of miR-21. TNF-α mRNA was next investigated using irradiated H37Rv to induce TNF-α expression. The effect on TNF-α at the protein level was also investigated. Wild-type and miR-21-deficient BMDM were infected with irradiated Mtb at an MOI of 5 bacteria per cell or with 100 ng/mL LPS as a positive control for 24 hours. RNA was isolated and qPCR for TNF-α mRNA was performed. TNF-α protein was measured in supernatants by ELISA. The enhanced TNF-α protein induction seen in miR-21-deficient BMDM with live Mtb infection was also observed in response to iMtb and LPS. Basal levels of TNF-α mRNA were similar across genotypes (**Figure 3.21A**). After stimulation with irradiated Mtb or LPS significantly more TNF-α was detected in miR-21-deficient BMDM (approximately 1.8- and 2.5-fold higher respectively).

As had been observed with live Mtb, miR-21-deficient BMDM produced significantly more TNF-α protein (approximately 2.5-fold higher) than wild-type BMDM when infected with irradiated Mtb (**Figure 3.21B**). Consistent with the literature, TNF-α protein was significantly higher in miR-21 knockout macrophages after stimulation with LPS (2.75-fold higher).

A similar experiment was performed in human MDM transfected with control anti-miR or anti-miR-21. Results were comparable to those determined in the murine model. Transfection with anti-miR-21 did not result in any basal differences in TNF-α at the mRNA or protein level (**Figure 3.22A**). TNF-α mRNA was significantly more induced following stimulation with LPS and irradiated Mtb in miR-21-deficient MDM (approximately 1.8- and 2.5-fold higher respectively) (**Figure 3.22A**). TNF-α protein was also significantly higher after LPS or iMtb stimulation (2.5- and 2.75-fold respectively) in the absence of miR-21 activity (**Figure 3.22B**).

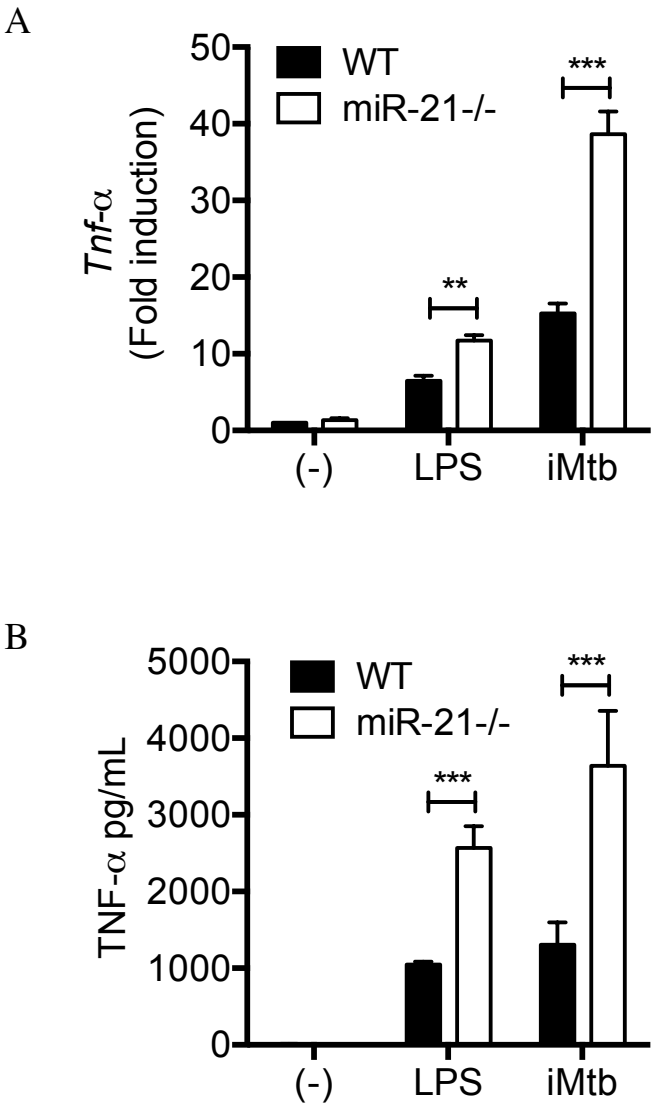

Figure 3.21 miR-21 deficiency in murine BMDM enhances TNF-α production in response to LPS and Mtb. Murine BMDM were infected with irradiated Mtb (strain H37Rv) (iMtb) at an MOI of 5 bacteria per cell or 100 ng/mL of LPS for 24 hours. RNA and supernatants were collected. qPCR was performed and expression of TNF-α mRNA relative to the untreated control was calculated. Data were normalised to 18S (A). TNF-α protein was quantified using an ELISA (B). Statistical analysis was performed using a paired, two-tailed Student's t-test. *, ** and *** represent $p<0.05$, 0.01 and 0.001 respectively. Data shown as mean ± SEM, n = 3 independent experiments.

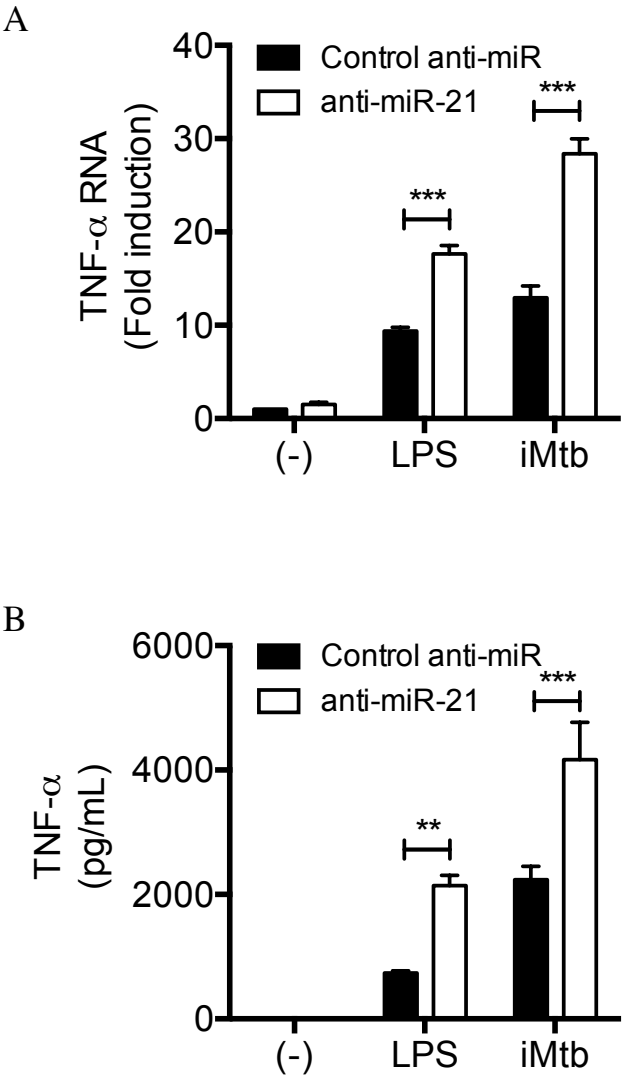

Figure 3.22 miR-21 deficiency in human monocyte-derived macrophages enhances TNF-α production in response to LPS and Mtb infection. Human MDM were transfected with a control anti-miR or anti-miR-21 and allowed 24 hours to recover. The cells were then infected with irradiated Mtb (strain H37Rv) (iMtb) at an MOI of 5 bacteria per cell or 100 ng/mL of LPS for 24 hours. RNA and supernatants were collected. qPCR was performed and expression of TNF-α mRNA relative to the untreated control was calculated. Data were normalised to 18S (A). TNF-α protein was quantified using an ELISA (B). Statistical analysis was performed using a paired, two-tailed Student's t-test. *, ** and *** represent $p<0.05$, 0.01 and 0.001 respectively. Data shown as mean ± SEM, n = 3 independent experiments.

Finally, the relevance of enhanced TNF-α production in response to Mtb by macrophages lacking miR-21 was confirmed in alveolar macrophages, the primary host cell of Mtb. Alveolar macrophages were isolated from wild-type and miR-21-deificient mice by bronchoalveolar lavage as described in **(2.1.4)**. Alveolar macrophages were cultured for 24 hours and then infected with irradiated Mtb at an MOI of 5 bacteria per cell for 24 hours. TNF-α mRNA was measured by qPCR and TNF-α protein was measured by ELISA.

TNF-α mRNA and protein were not induced as potently in alveolar macrophages by Mtb as they were in BMDM and MDM. There was no significant difference in TNF-α mRNA or protein basally or after Mtb infection (**Figure 3.23A**). miR-21 knockout alveolar macrophages produced significantly higher TNF-α protein in response to Mtb infection, generating 1.6-fold more TNF-α than their wild-type counterparts (**Figure 3.23B**).

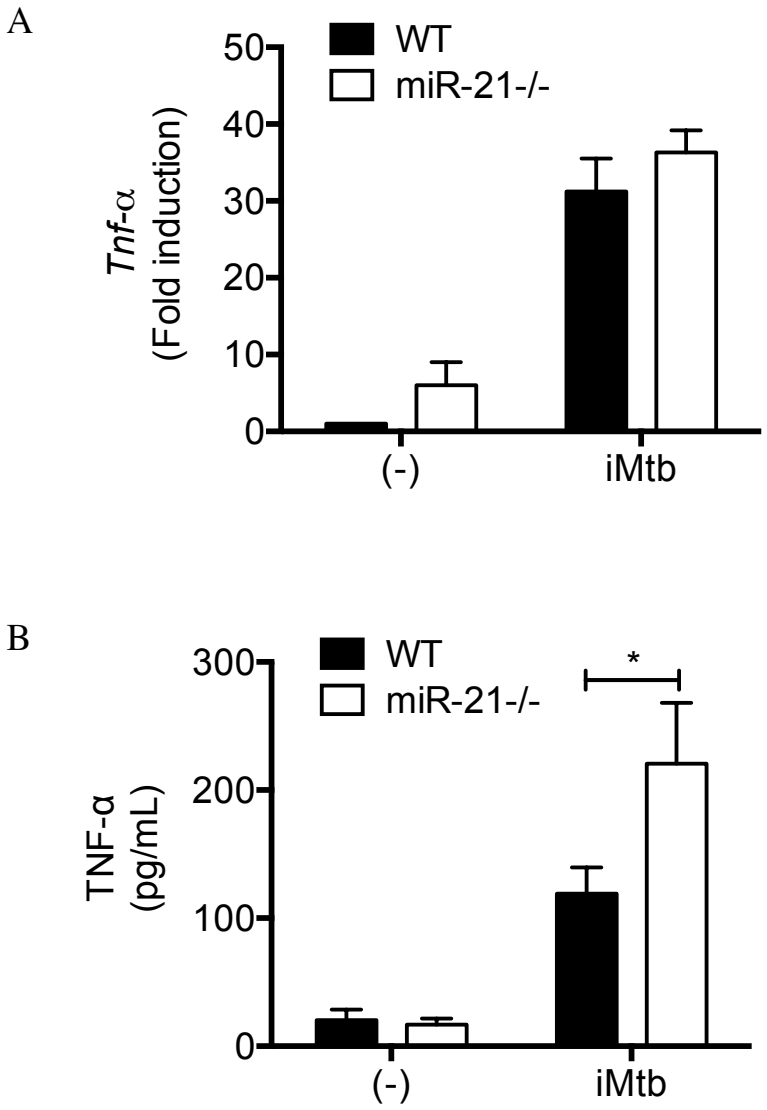

Figure 3.23 miR-21 deficiency in murine alveolar macrophages enhances TNF-α production in response to Mtb. Murine AM were isolated from lungs by bronchoalveolar lavage and allowed 24 hours to recover. The cells were then infected with irradiated Mtb (strain H37Rv) (iMtb) at an MOI of 5 bacteria per cell for 24 hours. RNA and supernatants were collected. qPCR was performed and expression of TNF-α mRNA relative to the untreated control was calculated. Data were normalised to 18S (A). TNF-α protein was quantified using an ELISA (B). Statistical analysis was performed using a paired, two-tailed Student's t-test. *, ** and *** represent $p<0.05$, 0.01 and 0.001 respectively. Data shown as mean ± SEM, n = 4 mice per genotype in one experiment.

3.2.10 Blocking TNF-α in wild-type and miR-21 knockout BMDM does not create an identical phenotype

Having determined that miR-21 suppresses the early induction of TNF-α in Mtb infection, the contribution of this to infection outcome was investigated. Wild-type and miR-21-deficient BMDM were infected with live Mtb for 3, 24 and 72 hours. 3 hours post-infection BMDM were treated with an anti-TNF-α antibody or control IgG at the same concentration and growth was measured using CFU assays as before.

Wild-type and miR-21-deficient macrophages treated with control IgG behaved normally, controlling growth of Mtb to a similar extent up to 24 hours post-infection, after which wild-type BMDM cannot contain Mtb growth and miR-21-deficient BMDM permit significantly less CFU to grow (**Figure 3.24**).

As expected given the evidence in the literature, blocking TNF-α with a specific IgG increased growth in wild-type BMDM, demonstrating the functionality of the experimental approach. However, although BMDM of both genotypes had significantly more bacterial growth at 72 hours when treated with anti-TNF-α antibody compared to the IgG control, growth in miR-21-deficient BMDM was not restored to a similar level as the wild type BMDM treated with anti-TNF-α. This implies the existence of a TNF-α-independent mechanism through which miR-21 regulates bacterial growth.

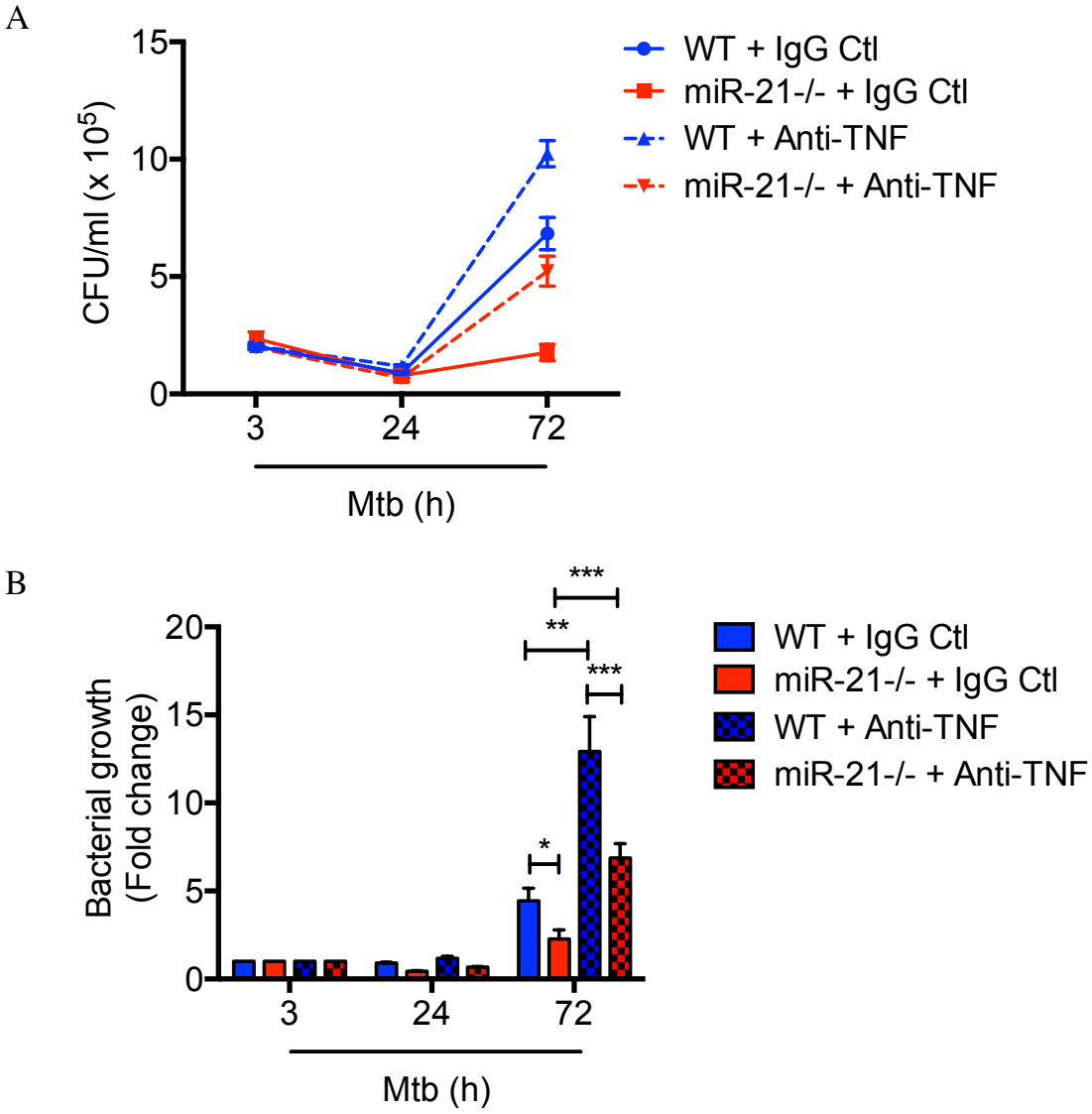

Figure 3.24 Blocking TNF-α does not restore miR-21-deficiency bacterial growth phenotype. Murine BMDM infected with H37Ra at an MOI of 5 bacteria per cell for 3, 24 and 72 hours. Cells were treated with 1 μg/mL anti-TNF-α antibody or the same concentration of control IgG 3 hours post-infection. Cells were lysed at the indicated time points and the lysates streaked on Middlebrook agar plates and incubated at 37°C for approximately 14 days. Colony forming units were counted (A) and the number of colonies relative to the 3-hour time point calculated (B). Statistical analysis was performed using a paired, two-tailed Student's t-test. *, ** and *** represent $p<0.05$, 0.01 and 0.001 respectively. Data shown as mean ± SEM, n = 3 independent experiments.

3.2.11 miR-21 negatively regulates IL-1β production

Having found that miR-21 can suppress anti-Mtb responses, the mechanisms behind this remained elusive. miR-21 was found to negatively regulate TNF-α production and promote induction of IL-10. Although these cytokines are likely of some consequence in determining outcome in the initial stages of infection, miR-21-deficient macrophages still retained significant advantage in containing Mtb growth over wild-type macrophages when TNF-α was blocked or recombinant IL-10 was supplemented. This indicated that other factors regulated by miR-21 were important in modulating later events in the anti-Mtb response.

Recent work has shown that IL-1β is essential for containing Mtb growth in macrophages. Additionally, elevated IL-1β production by miR-21-deficient macrophages has been reported in the context of Mycobacterium leprae infection. For these reasons, IL-1β was chosen as a candidate cytokine to investigate in the miR-21 deficiency model. Having identified IL-1β as a potential factor targeted by Mtb-induced miR-21 to control infection outcome, its expression was characterised throughout an Mtb infection time course in miR-21-deficient macrophages.

Wild-type and miR-21-deficient BMDM were infected with live Mtb for 3, 24 and 72 hours at an MOI of 5 bacteria per cell. As expected from the literature, Mtb infection induced a significant amount of IL-1β mRNA and protein in a time-dependent manner. IL-1β mRNA trended non-significantly higher in knockout macrophages at 24 hours and was significantly and dramatically increased 72 hours after infection (**Figure 3.25A**). 72 hours post-infection miR-21-deficient BMDM produced approximately double the level of IL-1β mRNA as their wild-type counterparts. This was reflected at the protein level, with miR-21-deficient BMDM producing 2- and 2.5-

fold more IL-1β protein 24 and 72 hours post-infection respectively (**Figure 3.25B**). This significant enhancement in IL-1β production was particularly evident 72 hours post-infection, with knockout macrophages producing roughly 400 pg/mL more cytokine.

These findings were then confirmed in the human model of miR-21 deficiency. Human MDM were transfected with control anti-miR and anti-miR-21 and infected with live Mtb for 3, 24 and 72 hours. As found in the murine model, loss of miR-21 lead to significant enhancement of IL-1β. Both mRNA and protein levels of IL-1β were significantly higher 24 and 72 hours post-infection when miR-21 activity was blocked (**Figure 3.26**).

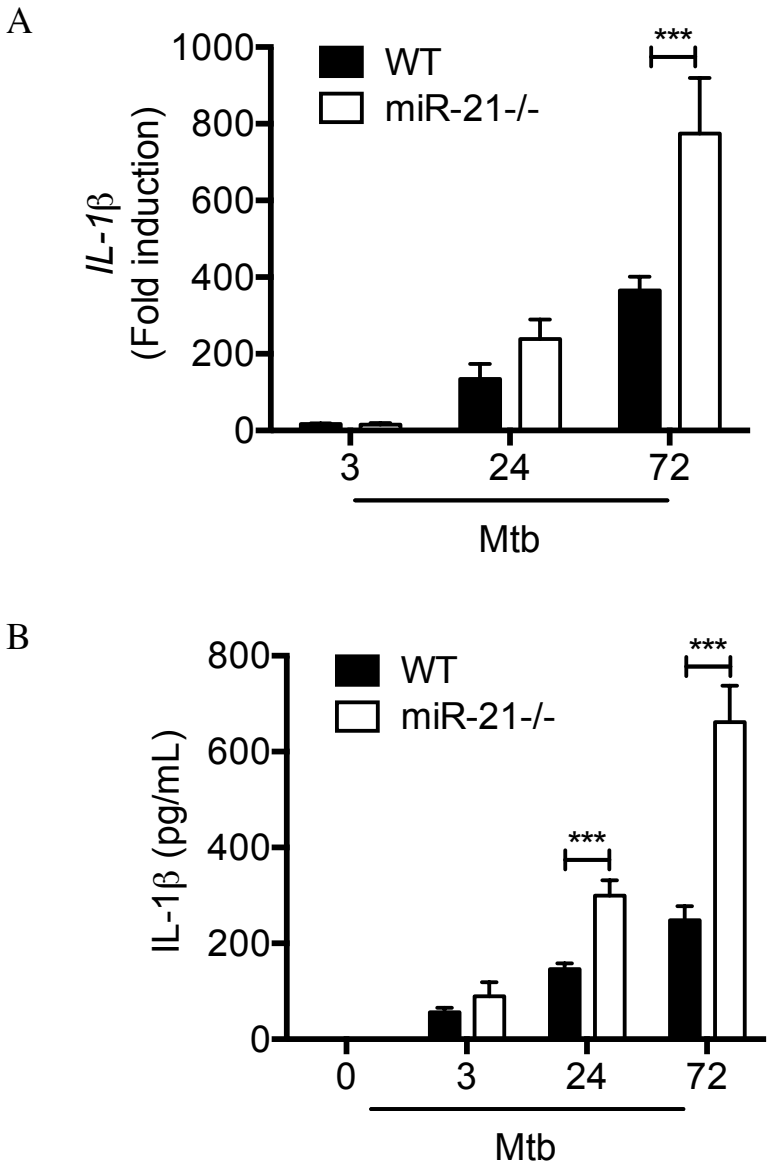

Figure 3.25 miR-21 deficiency enhances IL-1β production in response to Mtb infection in BMDM. Murine BMDM were infected with live Mtb (strain H37Ra) at an MOI of 5 bacteria per cell for 3, 24 and 72 hours. RNA and supernatants were collected. qPCR was performed and expression of IL-1β mRNA relative to the untreated control was calculated. Data were normalised to 18S (A). IL-1β protein was quantified using an ELISA (B). Statistical analysis was performed using a paired, two-tailed Student's t-test. *, ** and *** represent $p<0.05$, 0.01 and 0.001 respectively. Data shown as mean ± SEM, n = 3 independent experiments.

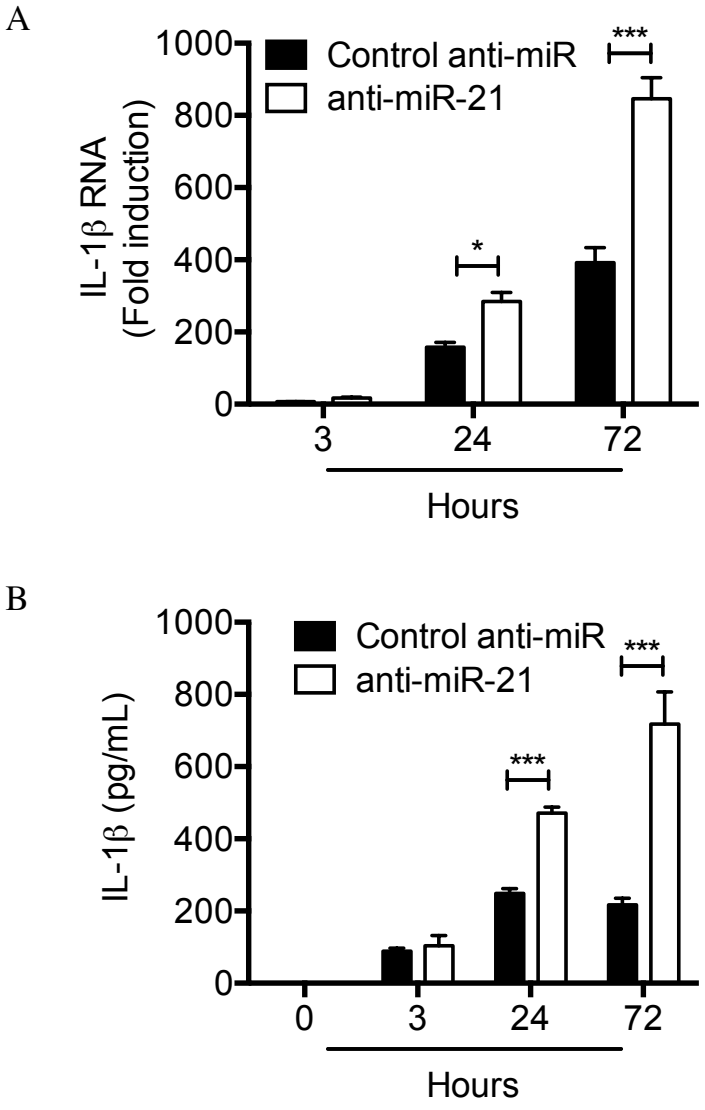

Figure 3.26 Knockdown of miR-21 enhances IL-1β production in response to Mtb infection in MDM Human MDM were transfected with a control anti-miR or anti-miR-21 and allowed 24 hours to recover. The cells were then infected with live Mtb (strain H37Ra) at an MOI of 5 bacteria per cell for 3, 24 and 72 hours. RNA and supernatants were collected at these time points. qPCR was performed and expression of IL-1β mRNA relative to the untreated control was calculated (A). Data were normalised to 18S. IL-1β protein quantified using an ELISA (B). Statistical analysis was performed using a paired, two-tailed Student's t-test. *, ** and *** represent $p<0.05$, 0.01 and 0.001 respectively. Data shown as mean ± SEM, n = 3 independent experiments.

IL-1β produced in response to live Mtb infection was found to be significantly higher in the absence of miR-21 activity. This boost in IL-1β was next confirmed with non-viable Mtb which is known to induce inflammatory signalling and, to extend this to other inducers of IL-1β apart from Mtb, with the TLR4 activator LPS.

Wild-type and miR-21-deficient BMDM were infected with iH37Rv at an MOI of 5 bacteria or 100 ng/mL of LPS per cell for 24 hours. Non-viable Mtb induced IL-1β though not with the same potency as live Mtb due to less efficient inflammasome activation[353]. As had been observed with live Mtb, IL-1β induction in miR-21-deficient BMDM was significantly higher response to iMtb (**Figure 3.27**). At the both the mRNA and protein level, the genotypes were basally similar, however after infection with irradiated Mtb significantly more IL-1β was detected in miR-21-deficient BMDM (approximately double the amount expressed by wild-type BMDM). LPS induced IL-1β mRNA expression, though no IL-1β protein secretion because of the absence of a inflammasome activating signal. LPS-induced IL-1β mRNA trended higher in miR-21-deficient BMDM though it did not reach significance.

A similar experiment in human MDM transfected with control anti-miR or anti-miR-21. Results were similar to those determined in the murine model. Transfection with anti-miR-21 did not result in any basal differences in IL-1β at the mRNA or protein level (**Figure 3.28**). IL-1β mRNA and protein were significantly more induced following infection with irradiated Mtb in miR-21-deficient MDM (approximately 2- and 1.3-fold higher respectively). Again, LPS induced IL-1β mRNA expression, though no IL-1β protein secretion and induced IL-1β mRNA trended higher in anti-miR-21 treated macrophages but it did not reach significance.

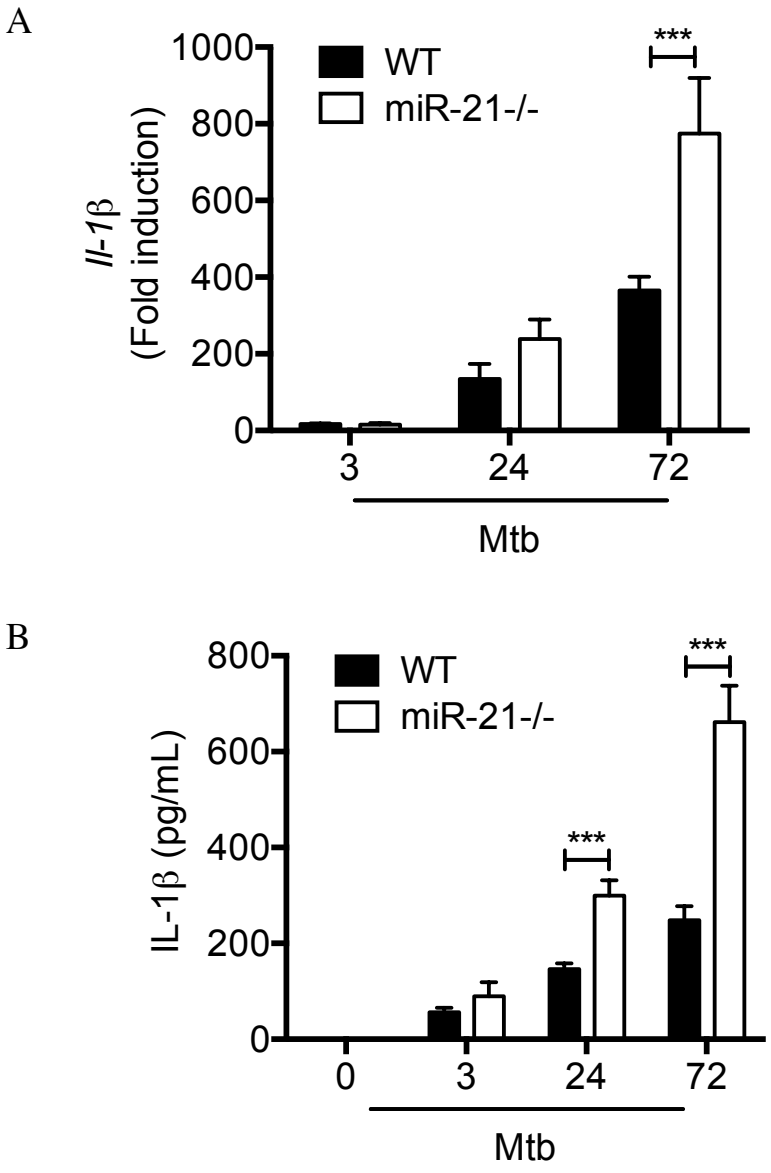

Figure 3.27 miR-21 deficiency in murine BMDM enhances IL-1β production in response to iMtb infection. Murine BMDM were infected with irradiated Mtb (strain H37Rv) (iMtb) at an MOI of 5 bacteria per cell for 24 hours. RNA and supernatants were collected. qPCR was performed and expression of IL-1β mRNA relative to the untreated control was calculated (A). Data were normalised to 18S. IL-1β protein was quantified using an ELISA (B). Statistical analysis was performed using a paired, two-tailed Student's t-test. *, ** and *** represent $p<0.05$, 0.01 and 0.001 respectively. Data shown as mean ± SEM, n = 3 independent experiments.

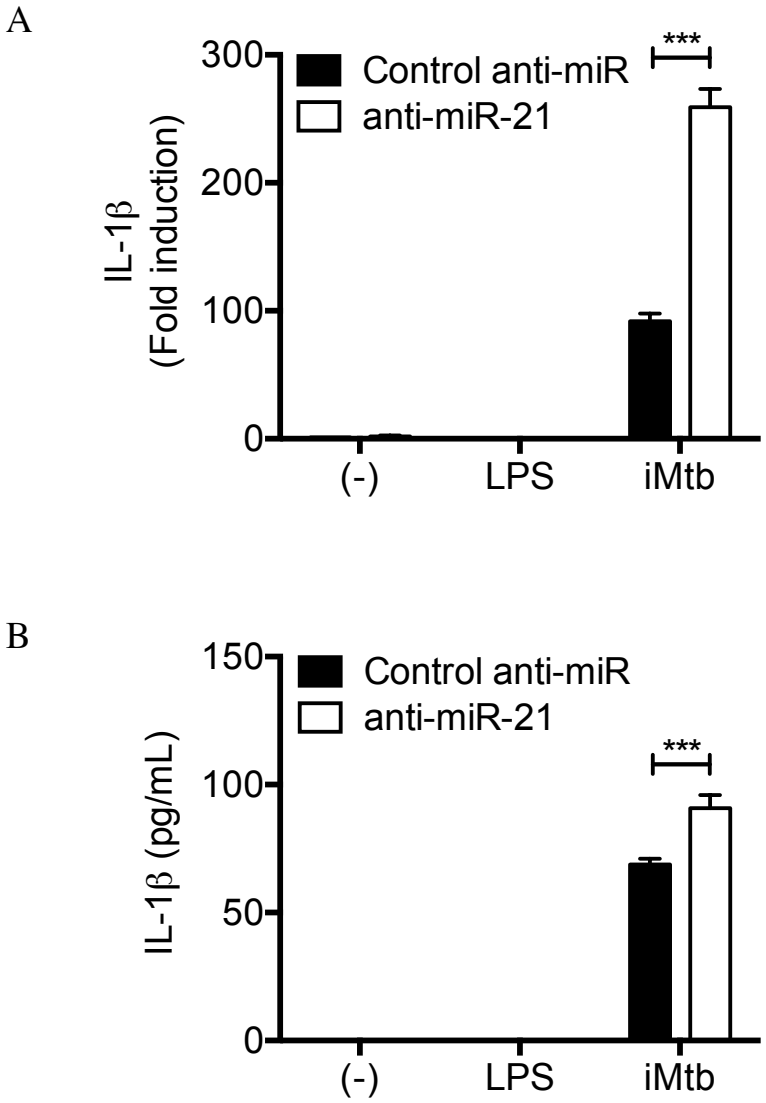

Figure 3.28 Knockdown of miR-21 enhances IL-1β production in response to iMtb infection in human MDM. Human MDM were transfected with a control anti-miR or anti-miR-21 and allowed 24 hours to recover. Cells were infected with irradiated Mtb (strain H37Rv) (iMtb) at an MOI of 5 bacteria per cell for 24 hours. RNA and supernatants were collected. qPCR was performed and expression of IL-1β mRNA relative to the untreated control was calculated (A). Data were normalised to HPRT. IL-1β protein was quantified using an ELISA (B). Statistical analysis was performed using a paired, two-tailed Student's t-test. *, ** and *** represent $p<0.05$, 0.01 and 0.001 respectively. Data shown as mean ± SEM, n = 3 independent experiments.

Enhanced IL-1β production in the absence of miR-21 activity was then confirmed in the primary host cell of Mtb, the alveolar macrophage. Human alveolar macrophages were isolated from BAL fluid, transfected with control anti-miR or anti-miR-21, and polarised towards a pro-inflammatory phenotype with LPS and IFN-γ or towards an anti-inflammatory phenotype with IL-4 for 24 hours. AM that had been polarised towards a pro-inflammatory phenotype significantly induced IL-1β mRNA and this induction was significantly higher in the absence of miR-21 (**Figure 3.29**).

Murine alveolar macrophages were isolated by bronchoalveolar lavage from wild-type and miR-21-deficient mice and infected with irradiated Mtb at an MOI of 5 bacteria per cell for 24 hours. IL-1β was significantly induced by both genotypes by Mtb infection. IL-1β mRNA was basally comparable but was significantly higher in miR-21-deficient AM after Mtb infection (**Figure 3.30A**). The amount of IL-1β protein produced by miR-21 knockout AM was also significantly higher than wild-type AM, though overall induction was not as high as in the other macrophage models of Mtb infection (**Figure 3.30B**).

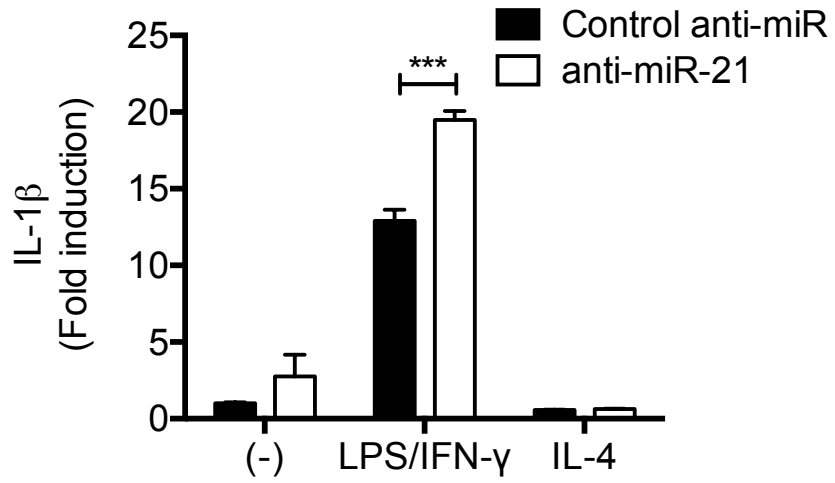

Figure 3.29 Knockdown of miR-21 enhances IL-1β mRNA in primary human alveolar macrophages. Human AM were isolated from BAL fluid and transfected with a control anti-miR or anti-miR-21 and allowed 24 hours to recover. Cells were stimulated with 100 ng/mL of LPS and 5 ng/mL of IFN-γ for 24 hours. RNA and supernatants were collected. qPCR was performed and expression of IL-1β mRNA relative to the untreated control was calculated. Data were normalised to 18S. IL-1β protein was quantified using an ELISA. Statistical analysis was performed using a paired, two-tailed Student's t-test. *, ** and *** represent $p<0.05$, 0.01 and 0.001 respectively. Data shown as mean ± SEM, n = 2 donors in one experiment.

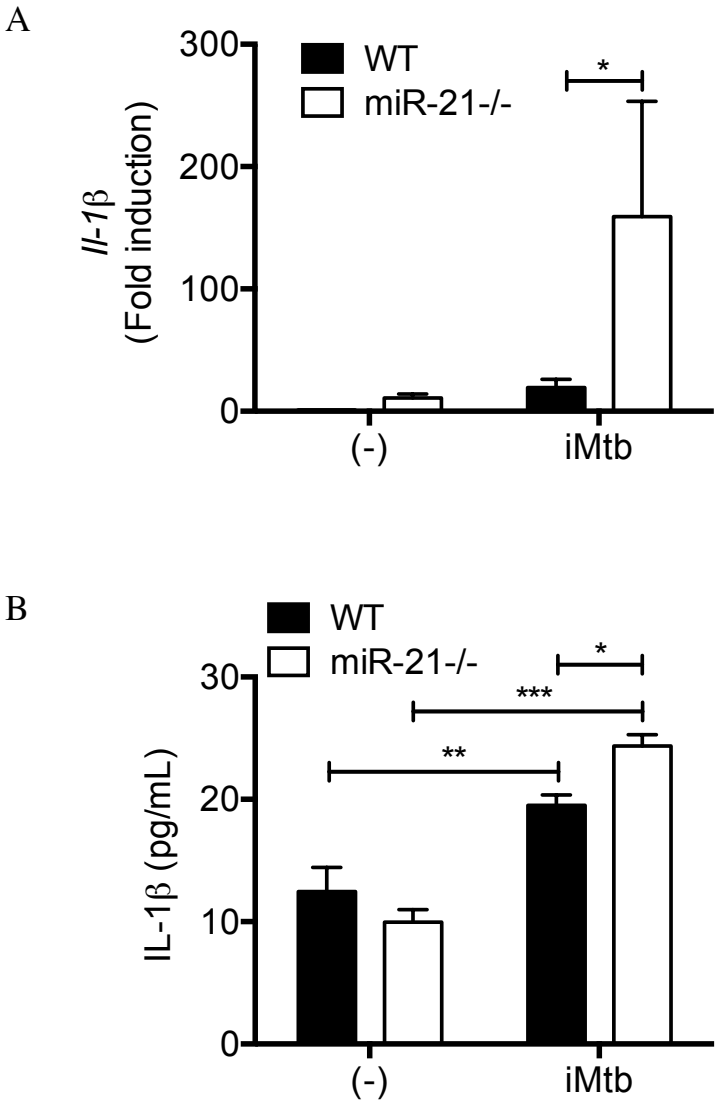

Figure 3.30 miR-21 deficiency in murine alveolar macrophages enhances IL-1β production in response to Mtb. Murine AM were isolated from lungs by bronchoalveolar lavage and allowed 24 hours to recover. The cells were then infected with irradiated Mtb (strain H37Rv) (iMtb) at an MOI of 5 bacteria per cell for 24 hours. RNA and supernatants were collected. qPCR was performed and expression of IL-1β mRNA relative to the untreated control was calculated (A). Data were normalised to 18S. IL-1β protein was quantified using an ELISA (B). Statistical analysis was performed using a paired, two-tailed Student's t-test. *, ** and *** represent $p<0.05$, 0.01 and 0.001 respectively. Data shown as mean ± SEM, n = 5 different mice per genotype in one experiment.

3.2.12 MiR-21 controls bacterial growth by negatively regulating IL-1β

IL-1β induction in response to Mtb infection was found to be supressed by miR-21. Mayer-Barber et al have shown that IL-1β boosts anti-Mtb responses through the induction of eicosanoids to limit excessive type I interferon production, and boosting eicosanoids prevented lethality in acute Mtb infection[200], highlighting the importance of IL-1β in macrophage responses to Mtb. To look at the effect of the interplay between miR-21 and IL-1β on the containment of Mtb growth, IL-1β activity was blocked using a monoclonal antibody. Wild-type and miR-21 knockout macrophages were infected with live Mtb and 3 hours after infection a monoclonal antibody specific for IL-1β was administered.

Macrophages were capable of containing the early growth of Mtb in the absence of IL-1β activity (**Figure 3.31A**). However, as infection progressed neither genotype could control Mtb growth. Bacterial CFU were significantly higher in both wild-type and miR-21 knockout BMDM treated with anti-IL1β antibody at 72 hours and no significant difference was observed between genotypes in the absence of IL-1β activity (**Figure 3.31B**).

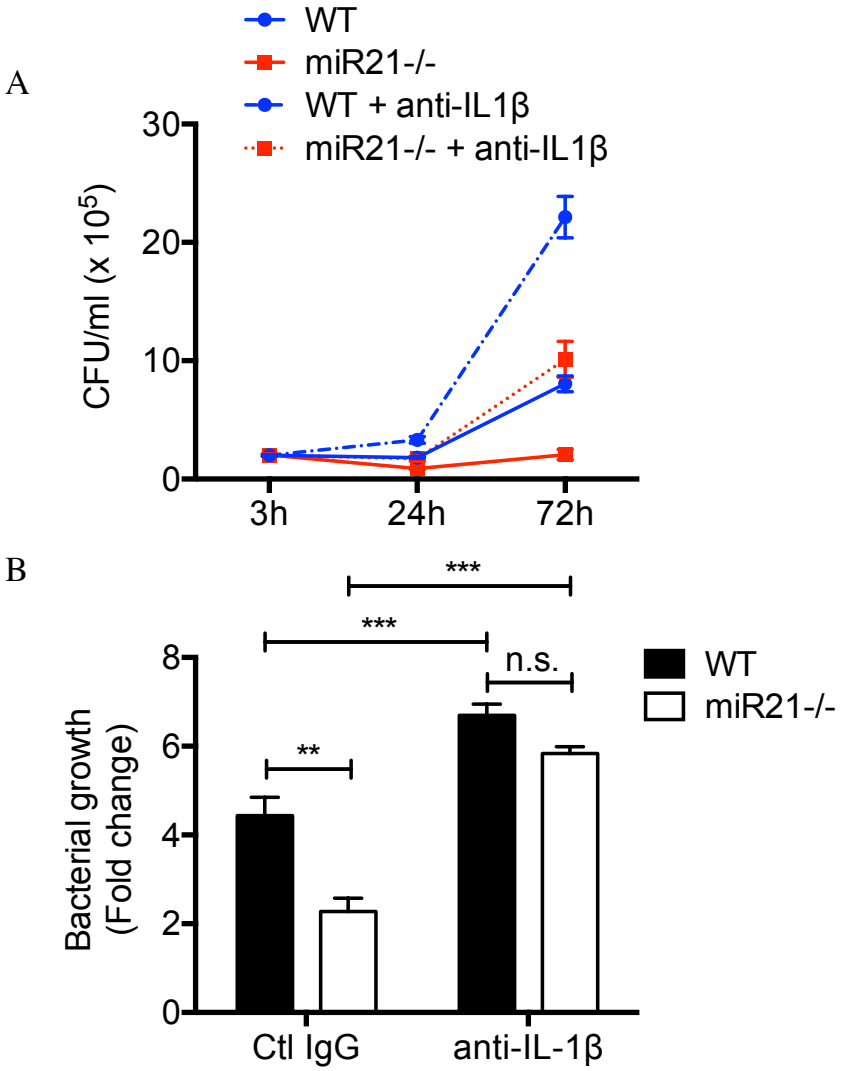

Figure 3.31 Blocking IL-1β eliminates miR-21-deficiency advantage for mycobacterial containment. Murine BMDM were infected with live Mtb (strain H37Ra) at an MOI of 5 bacteria per cell for 3, 24 and 72 hours. Cells were treated with control IgG or anti-IL-1β antibody (1 μg/mL) 3 hours post-infection. Cells were lysed in 0.1% Triton X-100 at the indicated time points and diluted in lysates were streaked in triplicate on warm Middlebrook agar plates and incubated at 37°C for approximately 14 days. Colony forming units were counted (A) and the number of colonies relative to the 3-hour time point calculated (B). Statistical analysis was performed using a paired, two-tailed Student's t-test. *, ** and *** represent $p<0.05$, 0.01 and 0.001 respectively. Data shown as mean ± SEM, n = 3 independent experiments.

3.3 Discussion

Macrophage immune responses against Mtb are essential in the response against infection. They are the first immune cell to encounter invading mycobacteria and provide cytokines which drive bacterial elimination and immunological memory responses. However, Mtb drives an anti-inflammatory phenotype in macrophages which limits the antimicrobial responses and aids bacterial persistence. While limiting inflammation is important to protect host tissues, in the case of Mtb infection the macrophage response is not sufficient to totally eradicate the bacteria. If, as evidence suggests, miR-21 is a feedback mechanism in the inflammatory response that promotes a pro-resolution macrophage phenotype, its role in Mtb infection may benefit the bacteria. To date there are few reports on the role of miR-21 in macrophage responses to Mtb, thus this chapter examined the induction of miR-21 by Mtb, the functional consequences of this induction, and assessed whether depletion of miR-21 can boost defective inflammation.

TLR signalling is a known inducer of miR-21 expression. As TLR signalling is activated by Mtb, the expression of miR-21 in response to inactive, non-viable Mtb was investigated. These initial experiments demonstrated that miR-21 is induced in macrophages by iMtb infection. This is in line with evidence for *Mycobacterium leprae*- and BCG-driven expression of miR-21[8, 322]. Irradiated Mtb was found to induce a significant amount of miR-21 peaking 24 hours after infection, both in murine BMDM and human MDM (**Figure 3.1**). The level of miR-21 induction was similar in both species and was comparable to the level of expression induced by a standard 100 ng/mL dose of LPS (approximately 3-fold induction).

Mtb primarily infects alveolar macrophages thus confirming the induction of miR-21 by Mtb in this cell type was of importance. miR-21 was found to be induced by iMtb in murine alveolar macrophages, though induction (2-fold) was to a lesser degree than in murine BMDM and human MDM (**Figure 3.2**). One possible reason for this difference in degree of induction could be that the baseline level of miR-21 are lower in the murine and human macrophage in vitro models are naïve, previously unpolarised macrophages that have been derived in a relatively sterile environment in culture. In comparison, murine alveolar macrophages are tissue-resident cells that have already been modulated by factors in the lung and may have a higher baseline expression of miR-21 because of this or perhaps because of the extraction procedure.

Mtb-induced miR-21 expression was found to be dose-dependent in murine BMDM (**Figure 3.3A**). Human MDM also showed some dose-dependency in miR-21 induction however maximal induction was found at an MOI of 5 bacteria per cell rather than at an MOI of 10 bacteria per cell as seen in the BMDM (**Figure 3.3B**). The reason for this bell curve in induction in MDM may be due to MDM being more susceptible to cell death induced by Mtb. Mtb has evolved mechanisms to induce necrotic cell death to facilitate dissemination. As Mtb has evolved in humans, not mice, these mechanisms may be more potent in human MDM and high levels of infection may prevent the macrophage from being able to transcribe and process miR-21 as efficiently. An MOI of 5 bacteria per cell in both human MDM and mouse BMDM resulted in approximately 3-fold induction of miR-21 with both cell types looking reasonably viable 24 hours after infection, thus this was chosen as the MOI for future experiments.

The kinetics of miR-21 expression after Mtb infection were investigated. No significant induction above baseline was found 3 hours after infection (**Figure 3.4**). Peak induction of miR-21 was found at 24 hours in BMDM, with expression returning to baseline levels at 72 hours. These observations fit with the concept of miR-21 being induced as a negative regulator of inflammation later in the course of infection to bring about resolution and limit damage to host tissues. The expression of the primary transcript from which miR-21 is derived, i.e. the first product of miR-21 transcription, was found to precede the appearance of the mature, active form of miR-21. This induction was independent of the overlapping gene *Tmem49*, indicating specific activation of the miR-21 locus. Pri-miR-21 was induced 3-fold after 3 hours of Mtb infection. This suggests the induction of mature miR-21 is due to de novo miR-21 gene transcription induced by Mtb rather than increased processing of its precursors. This level of pri-miR-21 expression was maintained throughout the infection time course, still being found at levels approximately 3-fold over baseline 72 hours post-infection despite the mature form being back to baseline levels. This may imply that the molecular mechanism to terminate miR-21 activity in the macrophage is, at least initially, independent of transcription. Not much is known about the regulation of miRNA processing and turnover in general, though some studies are beginning to address this and miR-21 itself can be regulated by inflammatory stimuli post-transcriptionally[299].

To ensure that the infection with iMtb was inducing the expected macrophage responses, TNF-α and IL-10 protein were measured alongside miR-21. While TNF-α was induced early in infection, peaking at 24 hours and then declining, IL-10 secretion was delayed, appearing at 24 hours and sustaining this induction at 72 hours (**Figure 3.5**). Peak induction of miR-21 coincides with this switch from an initial TNF-α dominated pro-inflammatory response

to an IL-10 dominated anti-inflammatory response. This fits with the notion of miR-21 as a central hub in the macrophage, regulating the balance between pro- and anti-inflammatory immune responses, and is consistent with the hypothesis that a danger signal is needed to induce miR-21 which then negatively feeds back on the system.

These preliminary studies with iMtb indicated that there is temporal resolution of miR-21 induction. However, unpublished data from a long-term in vivo infection study from a collaborator shows that miR-21 is sustained weeks after infection. For this reason, the induction of miR-21 by live Mtb was explored in vitro.

Both live and dead avirulent H37Ra induced dose-dependent expression of miR-21. miR-21 expression induced by heat-killed H37Ra was comparable to that induced by iMtb. However, at higher MOI, miR-21 induction was significantly higher with live Mtb - approximately double the expression measured after infection with non-viable Mtb (**Figure 3.6A**). Additionally, when this time course was extended, miR-21 induced by live Mtb was significantly higher 72 hours post-infection compared to 24 hours, whereas no significant upregulation at this later stage of infection was found with heat-killed Mtb (**Figure 3.6B**). Importantly, this effect was also seen with a virulent strain of Mtb in primary human alveolar macrophages (**Figure 3.7**). Live Mtb not only induces more miR-21 but also sustains this high level of expression. This could be because dead forms of Mtb cannot replicate and trigger macrophage necrosis and subsequent infection of other macrophages and thus trigger more TLR-driven miR-21 expression. Live bacteria may also have some inherent characteristics that are conducive to miR-21 expression. For example, though live and dead Mtb may induce miR-21 expression through TLR4 signalling, live Mtb may also induce miR-21 through

another means such as so-called vita-PAMPS (e.g. bacterial mRNA) which would not be present in dead Mtb and would also continue to be detected during infection with live Mtb resulting in sustained induction.

Having confirmed that miR-21 is induced by Mtb, the consequence of this induction on Mtb infection outcome was not understood. Though limiting inflammation is indeed important, in the case of persistent Mtb infection where macrophage responses are insufficient to clear the bacteria, miR-21 may be beneficial to Mtb survival. The sustained upregulation of miR-21 by live bacterial infection may represent a novel immune evasion strategy. To test this hypothesis and explore the role of miR-21 in anti-Mtb responses, a model of miR-21 deficiency in both human and murine macrophages was developed.

The murine knockout model has no detectable miR-21 expression and thus this has an effect on the expression of target mRNA (**Figure 3.8**). PTEN, a negative regulator of the PI3K/Akt pathway and target of miR-21, is reported to be induced by LPS[319]. In this knockout model, levels trend towards a higher level of PTEN mRNA expression basally but this does not reach significance. After infection, however, there is significantly greater induction of PTEN in the miR-21-deficient macrophages, suggesting that PTEN induction is not being constrained by miR-21 targeting in these cells. PDCD4, another target of miR-21, has been shown to be negatively regulated by miR-21 to promote IL-10 expression[296]. In this model, PDCD4 is significantly higher basally, providing further evidence for an effective knockout of miR-21 in these BMDM. After infection with Mtb, expression was reduced in both wild-type and miR-21 knockout BMDM though levels trended non-significantly higher in knockout macrophages. From the literature, this negative

regulation of PDCD4 after a TLR4 stimulus was expected[354]. Knockout of miR-21 did not fully protect from this negative regulation after Mtb infection however, suggesting that Mtb infection differs from LPS stimulation and other molecular processes are engaged.

A model of miR-21 deficiency in human macrophages was successfully developed. Transfection with a miR-21 hairpin inhibitor effectively ablated detectable miR-21 expression in human MDM (**Figure 3.9**). No basal difference in PTEN expression was noted but after infection with Mtb there is significantly greater induction in miR-21 knockdown macrophages. PDCD4 was higher in knockdown MDM basally and after Mtb infection.

These data indicate that both the murine and human miR-21 deficiency strategies are effective models to explore miR-21 function. It is desirable to use both the murine and human model for several reasons. The murine knockout model is a complete knockout of the miR-21 gene and negates the need for any confounding complications from transfection. Murine BMDM are also inherently less variable than MDM from human donors. Mtb is a disease of human macrophages however so confirmation of key findings in this model is important. The MDM knockdown model also blocks miR-21 induction only at maturity, thus does not have any potential effects on macrophage development. The human model also provides additional supportive data with therapeutic relevance.

Though miR-21 has been shown to limit uptake of *Listeria monocytogenes*[298], no difference in uptake of Mtb was evidenced by microscopy in either murine BMDM or human MDM (**Figure 3.10**). This equal uptake was further confirmed when bacterial

growth 3 hours after infection was examined (**Figure 3.11**). Mtb bacilli are approximately ten times longer than Listeria, permitting less phagocytosis and total bacterial burden, thus perhaps the differences in uptake in miR-21 knockout macrophages due to phagocytic regulation reported in Listeria infection are not applicable here.

Containment of bacterial growth was identical between genotypes in the early stages of Mtb infection. However, both murine BMDM and human MDM deficient in miR-21 were significantly better at containing Mtb growth beyond 24 hours. Wild-type macrophages are initially able to contain Mtb growth but as infection progresses this control is lost. When miR-21 activity is blocked, this containment is sustained significantly later in the infection time-course. These findings suggest that miR-21 plays a key role in the later stages of mycobacterial infection. This again fits with the idea that miR-21 is an anti-inflammatory feedback mechanism that is induced by Mtb, and this prematurely curbs the inflammatory response, allowing Mtb to survive and replicate within the macrophage. The viability of macrophages of both genotypes after infection should be measured in order to address any differences in cell death in response to Mtb in the absence of miR-21.

Having found that miR-21 is essential for containment Mtb growth, a number of mechanisms which may contribute to this difference were explored. Reactive oxygen species and reactive nitrogen species are microbicidal effectors and were investigated. iNOS mRNA was found to be significantly higher in miR-21 knockout BMDM 24 hours after stimulation with LPS, however iNOS was not induced to the same extent by irradiated Mtb and no difference between genotypes was noted (**Figure 3.12A**). This may be due to the kinetics of iNOS induction by Mtb and perhaps significant differences may be apparent at different time points. Arginase 1 by

contrast was induced to a much greater extent by iMtb than by LPS and this was significantly lower in miR-21 knockout macrophages (500-fold induction in knockout macrophages compared to 1000-fold increase in wild-type) (**Figure 3.12B**). This may be of key functional relevance to Mtb infection. El Kasmi et al[338] have previously reported that arginase 1 is induced by Mtb through TLR signalling, and its induction is associated with a higher bacterial burden in a murine in vivo model of Mtb infection.

Consequently, when the product of the balance between these two enzymes, nitrite, was measured, there was a modest trend towards more nitrite in miR-21 knockout macrophages stimulated with LPS while iMtb drove a significantly higher nitrite induction in miR-21 deficient macrophages. These results indicate that it is the promotion of arginase 1 activity by miR-21 that is limiting nitrite production in response to Mtb. This is in line with the concept of miR-21 promoting an anti-inflammatory macrophage phenotype. These findings were confirmed in the murine alveolar macrophage, where miR-21 deficiency allowed a significantly higher induction of nitrite (**Figure 3.13**). Nitrite was enhanced by Mtb infection but not to significance in wild-type AM, emphasising the potential importance of this finding. Nitrite production was also significantly higher in response to live Mtb infection in miR-21 knockout BMDM 72 hours after infection (**Figure 3.14**). These observations that miR-21 is upregulated later in infection and negatively regulates anti-microbial oxidant species are consistent with the finding that miR-21 promotes bacterial growth. The cytokines through which these anti-microbial responses were being controlled were thus examined in the absence of miR-21.

IL-10 was investigated as a potential cytokine targeted by miR-21 to downregulate Mtb responses as miR-21 is known to promote IL-

10 in response to LPS stimulation by targeting PDCD4 and to suppress anti-microbial mediators in macrophages[351, 352]. IL-10 induced by live Mtb was significantly lower 24 an 72 hours after infection in both murine and human miR-21 deficient macrophages (**Figure 3.16**), corresponding with time points of significant miR-21 induction. LPS did not induce IL-10 mRNA induction in either species, but protein was significantly lower in miR-21 deficient macrophages (**Figure 3.17 and 3.18**). Conversely, irradiated Mtb induced equal amounts of mRNA in both genotypes and there was no difference in the amount of IL-10 protein measured. This is unexpected and may be a phenomenon specific to Mtb infection, which has evolved many mechanisms to escape host immunity. IL-10 may be being induced by live Mtb by way of a pathway independent of PDCD4 since significant downregulation of PDCD4 mRNA by irradiated Mtb was not observed. MiR-21 targeting of PDCD4 has been shown to inhibit IL-10 post-transcriptionally, inhibiting translation through interactions with the eukaryotic translation-initiation factors eIF4a and eIF4G[355]. However more recent findings have shown that PDCD4 degradation releases Twist2, an IL-10 transcription factor, and that PDCD4 degradation occurs mainly through mTOR signalling[239], so perhaps both these processes are at play here.

Though IL-10 protein induced by live Mtb infection was found to be significantly lower in miR-21-deficient macrophages, this did not transpire to be the major mechanism through which miR-21-deficient macrophages contain Mtb growth. Restoring IL-10 with recombinant IL-10 increased Mtb growth in wild-type BMDM, but did not restore growth in miR-21-deficient BMDM to wild-type levels (**Figure 3.19**). This finding indicated that another cytokine was being targeted by miR-21 to alter macrophage containment of Mtb growth.

TNF-α is known to be negatively regulated by miR-21 in response to LPS through the targeting of PTEN. PTEN is a phosphatase that limits PI3K/Akt signaling, thus its downregulaion by miR-21 favours activated Akt. Activated Akt usually inhibits GSK3β, which in turn usually inhibits NFκB. Thus miR-21 blunts NFκB signaling via targeting of PTEN and GSK3β[319]. As TNF-α is vital in anti-Mtb responses, it was next investigated as a factor targeted by Mtb-induced miR-21 to promote bacterial survival.

MiR-21 was found to control TNF-α in Mtb infection, however this was only obvious at 24 hours post-infection (**Figure 3.20A**). This difference was not evident at 3 or 72 hours after infection, fitting with the peak level of miR-21 expression at 24 hours seen in this model. By comparison, TNF-α secretion in knockdown human MDM was significantly higher 24, 72 and 120 hours after infection (**Figure 3.20B**), matching with the sustained induction miR-21. TNF-α secretion peaked at 72 hours in human MDM and this is where the difference between control anti-miR and anti-miR-21 macrophages was most apparent.

TNF-α suppression was not unique to live Mtb. Irradiated Mtb and LPS induced significantly more TNF-α mRNA and protein in both human and mouse miR-21-depleted macrophages (**Figure 3.21 and 3.22**). This TNF-α repression was also confirmed in the primary host cell of Mtb, the alveolar macrophage. TNF-α production by these cells is of key clinical relevance. Therapeutics which neutralise TNF-α activity for the treatment of diseases such as rheumatoid arthritis have been associated with an increased risk of Mtb activation[94]. TNF-α was not induced as potently in murine AM as in the other models (**Figure 3.23**) but this is not surprising given that AM are tissue-resident macrophages that need to be more tightly regulated to avoid tissue damage and may be basally activated from the in vivo setting or the extraction process. TNF-α

mRNA trended non-significantly higher in miR-21 knockout AM basally and after Mtb infection and TNF-α protein was significantly higher in miR-21 knockout AM after Mtb infection, giving weight to the argument that repression of TNF-α through miR-21 is important in determining infection outcome.

To test the contribution of TNF-α to containment of Mtb growth in the context of miR-21 deficiency, TNF-α activity was blocked with an antibody. TNF-α blockade significantly enhanced bacterial growth (**Figure 3.24**), as would be expected from the literature which has shown a clear increased risk of the reactivation of latent Mtb infection in patients being treated with TNF-α neutralising antibodies[94]. However, bacterial growth at 72 hours was still significantly lower in the absence of both TNF-α and miR-21, i.e. blocking TNF-α activity does not make miR-21 BMDM phenocopy wild-type BMDM in their ability to contain Mtb growth. This observation indicates that other factors are also being targeted by miR-21 to promote Mtb survival.

Although TNF-α and IL-10 were both found to be regulated by miR-21 in Mtb infection, cytokine induction profiles and bacterial growth studies indicated that miR-21 may be regulating events later in the response to Mtb infection. IL-1β has recently been shown to be essential in controlling Mtb growth in the macrophage and was thus investigated as a potential candidate through which miR-21 could be suppressing Mtb responses[164, 204].

IL-1β mRNA and protein induction in response to live Mtb was found to be significantly higher in miR-21 deficient BMDM, particularly at later time-points (**Figure 3.25**), knockout macrophages producing at least double the quantity of IL-1β as

wild-type BMDM. This enhanced induction of IL-1β in the absence of miR-21 was also found in human MDM (**Figure 3.26**). Enhanced IL-1β production was also observed in response to non-viable Mtb in both human and murine macrophages (**Figure 3.27 and 3.28**). Importantly enhanced IL-1β in the absence of miR-21 was also seen in primary human alveolar macrophages in response to pro-inflammatory polarisation with LPS and IFN-γ and in primary murine alveolar macrophages after iMtb infection (**Figure 3.29 and 3.30**). Blocking IL-1β activity with a monoclonal antibody significantly impaired wild-type containment of Mtb, and critically it restored growth in miR-21 deficient macrophages to wild-type levels 72 hours after infection (**Figure 3.31**), thus negative regulation of IL-1β induction was found to be a key determinant of miR-21 facilitating Mtb growth.

These findings are in line with the recent literature that has shown that Mtb infection induces metabolic reprogramming in macrophages and this induction of enhanced glycolysis is essential for bacterial containment because it promotes production of IL-1β. IL-1β has key roles in Mtb infection – promoting the production of IL-12p40[198] and IFN-γ[189] and upregulating cell-surface TNFR1 expression making cells more receptive to TNF-α signalling[199]. More recently, IL-1β has been shown to promote anti-Mtb responses through the induction of PGE2 which suppresses type I interferons to promote bacterial containment[200] and promotes apoptotic rather than necrotic cell death, limiting bacterial dissemination[201]. The finding that IL-1β is dramatically and significantly higher in miR-21-deficient macrophages at later time-points in the course of Mtb infection, along with the finding that blocking IL-1β restores a wild type phenotype in miR-21-deficient macrophages in the context of bacterial containment, suggests that

suppression of IL-1β is a crucial aspect of miR-21 activity to limit macrophage pro-inflammatory activation.

3.4 Conclusion

The results of Chapter 3 strongly suggest an important role for miR-21 in macrophage responses to Mtb. The results confirm that miR-21 expression is induced by Mtb infection in murine BMDM and AM and human MDM. This induction is both dose-dependent and temporal. The finding that live Mtb is a potent inducer of miR-21 and can sustain this miR-21 induction may represent a novel immune evasion strategy by Mtb. The mechanism by which live Mtb differentially effects miR-21 expression warrants further investigation.

Importantly, the induction of miR-21 by Mtb is of functional consequence. This work has shown for the first time that miR-21 promotes Mtb survival in vitro. miR-21 negatively regulates TNF-α production and promotes induction of IL-10 by Mtb. Though these cytokines both contribute to the control of macrophage function to promote Mtb survival, perhaps they are more important in the first days of infection and other factors are more important as infection progresses. MiR-21 was shown to supress IL-1β transcription in response to Mtb infection, in line with previous findings in *M. leprae* infection[322]. Crucially, this suppression of IL-1β was found to be the key factor through which miR-21 induction renders macrophages more permissible to mycobacterial growth in the later stages of infection.

Chapter 4: Macrophage miR-21 and Metabolism

4.1 Introduction

MiR-21 was found to promote Mtb growth in the macrophage and a key element in this process was determined to be the repression of IL-1β production. Given that recent studies have shown the importance of macrophage metabolism for the induction of IL-1β and control of Mtb growth[204], investigation into the role of miR-21 in macrophage metabolism was warranted.

Metabolic reprogramming has become recognised as a key cellular process that controls the responses of immune cells[356]. Immune cells in different activation states preferentially induce different forms of metabolism to suit their energy requirements (bursts of activity in pro-inflammatory macrophages and sustained regulatory functions in alternatively macrophages) and to generate metabolic intermediates that act as signalling molecules. Pro-inflammatory macrophages have been shown rely on glycolysis to promote antimicrobial responses[176], including the induction of IL-1β. Enhanced glycolytic activity leads to the accumulation of TCA intermediate metabolites including succinate. Higher levels of cellular succinate results in the stabilisation of HIF-1α which can the bind the hypoxia response element in the promoter of the gene encoding IL-1β and initiate its transcription[176]. NFκB is believed to be responsible for the majority of the immediate early induction of IL-1β, while HIF-1α is thought to be responsible for the sustained induction of IL-1β later in the course of inflammation. Recently Gleeson et al[204] have shown that Mtb infection induces this immunometabolic shift to glycolysis in several macrophage models including human alveolar macrophages and that this glycolytic response was essential for sufficient induction of IL-1β and control of Mtb growth.

While there is substantial evidence for the link between macrophage activation, metabolism and IL-1β, the mechanisms regulating these pathways are poorly understood. Negative regulatory roles for miR-21 in macrophage polarisation have been established, however little exploration of the relationship between miR-21, metabolism and IL-1β has been carried out. One study on human monocytes showed that miR-21 downregulates IL-1β in the context of *Mycobacterium leprae* infection[322]. miR-21 has been shown to be induced by HIF-1α and in turn to upregulate HIF-1α expression, however HIF-1α is not a direct predicted target of miR-21 and regulation is mediated through the PTEN/Akt pathway[357].Targets for miR-21 to bring about this downregulation however remain unidentified. Furthermore, no targets for miR-21 in the glycolytic pathway have been verified.

There are three steps in the glycolytic pathway which require a large Gibbs free energy and are essentially irreversible. The second irreversible step of glycolysis is catalysed by phosphofructokinase (PFK), known as the gatekeeper reaction in glycolysis, representing a key point for regulation, however it has been largely unexplored in the context of infection. PFK-1 converts fructose-6-phosphate and ATP to fructose-1,6-bisphosphate and is a tetrameric enzyme that can be composed of different combinations of the muscle (M), platelet (P) and liver (L) isoforms of the enzyme. Each isoform is encoded by a different gene and isoforms are differentially expressed in different tissues.

PFK isoforms and their enzymatic characteristics have not been well characterised, though examination of clinical evidence indicates that they are not redundant and that different isoforms possess different biochemical properties. Mutations in PFKM cause Type VII glycogen storage disease (GSDVII), also known as Tarui

disease, characterised by glycogen accumulation in skeletal muscle. Loss of PFKM activity causes a build-up of fructose-6-phosphate which is shuttled into glycogen synthesis and accumulation. The effects of the disease can range in severity from exercise intolerance to childhood death. A GWAS study of SNPs associated with breast cancer identified PFK-M as a breast cancer gene[120]. The tumour suppressor protein p53 has been shown to suppress PFK-M expression[358], while tumorigenic cell lines have been shown to produce truncated forms of PFK-M which are resistant to citrate inhibition and promote glycolysis[359]. This association of PFKM with cancer tissues indicates a strong role for PFK-M in promoting glycolytic metabolism.

PFK-1 has not been a focus of Mtb research, however Cooper & Gennaro et al[231] profiled the transcriptome of lung tissue from Mtb-infected mice. While PFK-L and PFK-P were upregulated over the course of Mtb infection by approximately 1.5-fold, PFK-M was down-regulated 2-fold. At time zero, PFK-L and PFK-P compromised approximately 40% of the PFK-1 mRNA each, PFK-M making up the other 10%. The differential regulation of PFK-M in comparison to the other isoforms in Mtb infection and in silico predictions of a miR-21 binding site in PFK-M 3'UTR provides evidence that it may be a miR-21 target. Furthermore, miR-302a has been shown to target PFKM in adenocarcinoma and diaphragm muscle to negatively regulate glycolytic activity[360].

PFKM knockout mice were developed and while severe effects in glucose metabolism were seen in skeletal muscle tissues which exclusively express the PFKM isoform, erythrocytes which normally express both the PFKM and PFKL isoforms had 50% reduced PFK activity in knockout animals[361]. This is consistent with reports that patients with GSDVII suffer from haemolytic anemia[362]. Cardiac muscle, which expresses all three PFK isoforms[363], showed a 20% reduction in PFK activity in PFKM knockout mice compared to wild-

type mice. These murine observations again indicate a non-redundant role for PFK-M in determining the activity PFK-1 tetramers.

Taken together, these findings warranted the investigation of miR-21 as a regulator of IL-β production through unknown targets in the glycolytic pathway. PFK-M presents itself as a potential target through which glycolytic activity can be fine-tuned through microRNA targeting, summarised in **figure 4.0**.

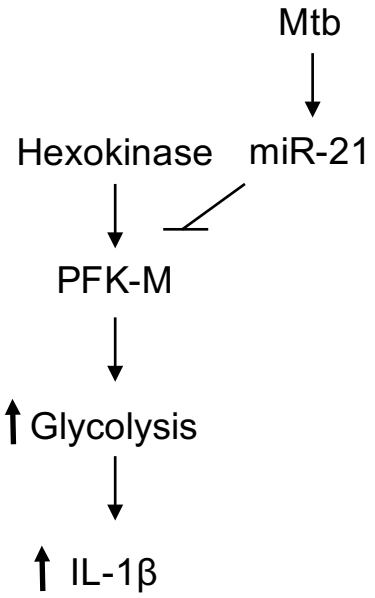

Figure 4.0 Chapter 4 Hypothesis. Mtb induces microRNA-21 and this limits the induction of IL-1β. PFK-M, a subunit of the glycolytic enzyme PFK-1, is a predicted target of miR-21. As the induction of glycolysis in response to Mtb is necessary for sufficient IL-1β production, it is hypothesised that PFK-M is target of miR-21 and this targeting of PFK-M limits macrophage glycolytic activity and thus the induction of IL-1β.

4.2 Results

4.2.1 IL-1β targeting by miR-21

IL-1β is a key factor controlled by miR-21 to impact the outcome of Mtb infection. There is some evidence for IL-1β as a direct target of miR-21, Fabri et al found some reduced 3'UTR luciferase activity in a vector reporter system when miR-21 was present, however this targeting was not confirmed by blocking the interaction between miR-21 and the IL-1β 3'UTR target site[163]. To investigate if this was the way in which miR-21 was affecting IL-1β production in response to Mtb infection, an experiment with actinomycin D was performed. Actinomycin D blocks the transcription of RNA, allowing inferences about RNA stability to be made. 18S was used as a control housekeeping gene as it is highly stable with a long half-life and thus will not be affected by actinomycin D treatment.

Wild-type and miR-21 knockout BMDM were infected with Mtb for 24 hours and then treated with actinomycin D for 30 minutes. Decay appeared slower in uninfected miR-21 knockout BMDM, suggesting the presence of miR-21 could impact IL-1β mRNA stability. However, after infection IL-1β mRNA is more stable across both genotypes, not consistent with it being a direct target of miR-21.

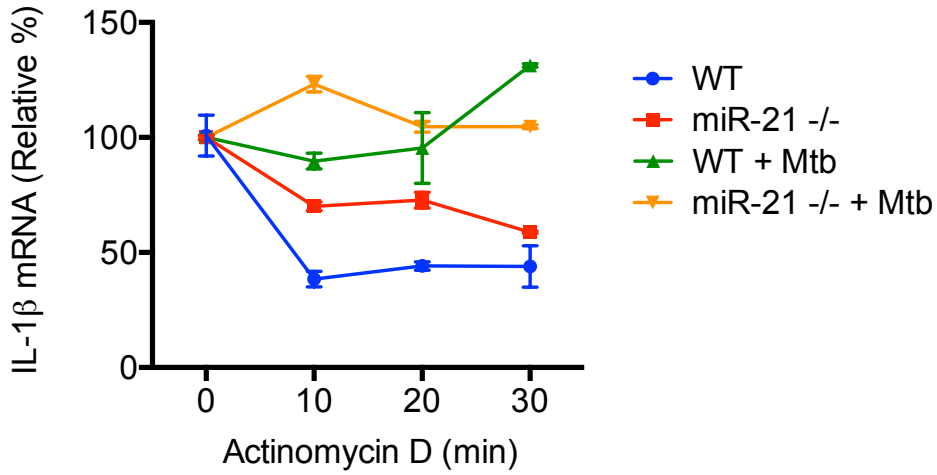

Figure 4.1 miR-21 destabilises resting but not induced IL-1β mRNA. Murine BMDM were infected with live Mtb (strain H37Ra) at an MOI of 5 bacteria per cell for 24 and then treated with 1 μg/mL actinomycin for 30 minutes. RNA was collected and IL-1β mRNA was measured by qPCR. Data were normalised to 18S. Statistical analysis was performed using a paired, two-tailed Student's t-test. *, ** and *** represent $p<0.05$, 0.01 and 0.001 respectively. Data shown as mean ± SD of experimental replicates, n = 1 representative plot, representative of 2 other experiments.

4.2.2 Macrophage lactate production in response to Mtb infection is significantly higher in the absence of miR-21

It was observed that miR-21-deficient macrophages induce significantly more IL-1β mRNA in response to Mtb infection, however actinomycin experiments indicated that this was not as a result of direct targeting by miR-21 and that another process was being targeted to promote higher levels of IL-1β in the context of Mtb infection. Recent studies have shown that macrophages undergo a metabolic shift towards aerobic glycolysis when infected with Mtb. This glycolytic switch was shown to be essential for the production of IL-1β and containment of Mtb growth. Furthermore, enhanced glycolysis positively feeds back on late IL-1β transcription through HIF-1α. The significant enhancement in IL-1β production particularly at later time-points observed in miR-21 knockout and knockdown macrophages suggested that miR-21 may play a role in regulating this metabolic switch in Mtb-infected macrophages. Thus, it was investigated whether enhanced glycolysis was the driving force behind enhanced anti-Mtb responses in macrophages deficient in miR-21.

Lactate is the final product of the glycolytic pathway and is exported from cells by monocarboxylate transporters. Extracellular lactate can be measured in cell supernatant as a surrogate marker of glycolytic activity. Lactate was measured in wild-type and miR-21 knockout BMDM after infection with live Mtb (**Figure 4.2A**). Lactate was significantly induced over the course of infection, as expected from the literature. As predicted by the high levels of IL-1β, miR-21-deficient macrophages produced significantly more lactate than wild-type BMDM 24 and 72 hours post-infection.

2-deoxyglucose (2-DG) is a glycolytic inhibitor which competitively inhibits hexokinase, effectively shutting down the glycolysis pathway. Lactate induction was blocked in both wild-type and miR-21-deficient BMDM in the presence of 2-DG (**Figure 4.2B**), indicating that the lactate induction measured in response to Mtb infection was as a result of upregulated glycolytic metabolism.

Lactate induction during Mtb infection was also measured in human MDM treated with control anti-miR or anti-miR-21 (**Figure 4.3**). As in the murine model, lactate was significantly enhanced over the course of infection and this lactate production was significantly higher in miR-21 knockdown macrophages.

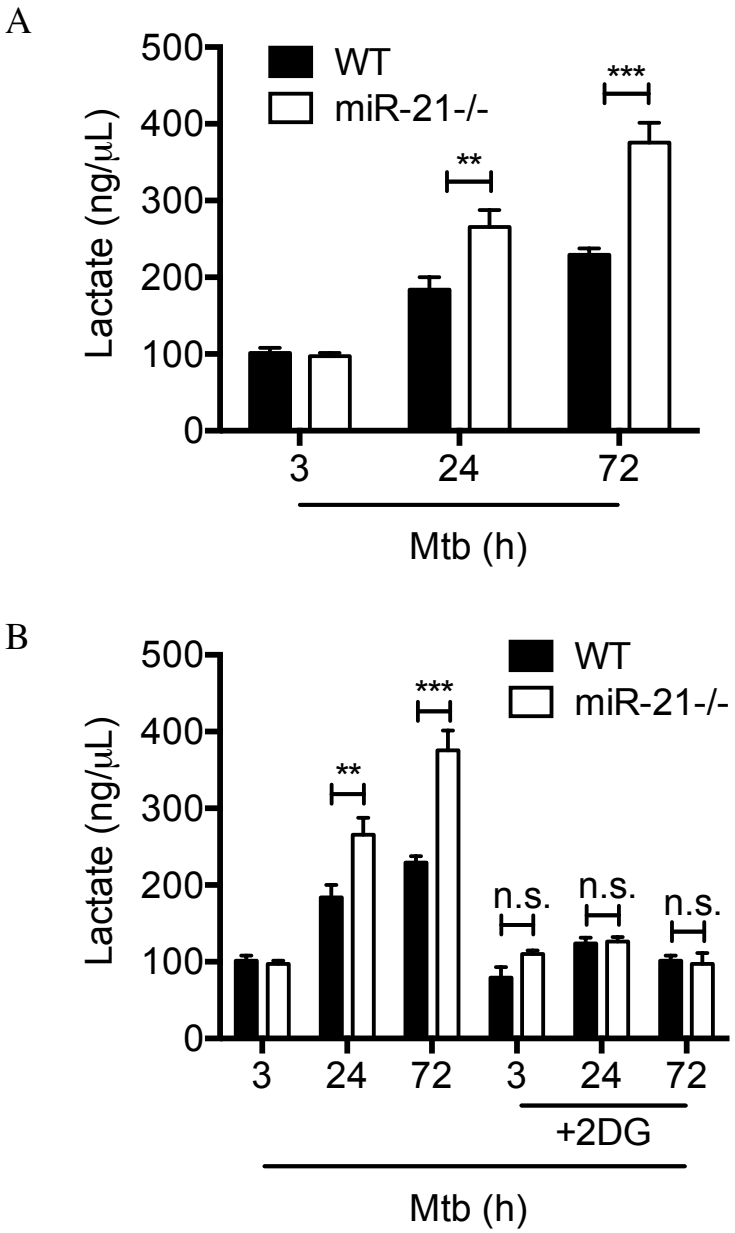

Figure 4.2 miR-21 deficiency in murine BMDM enhances lactate production in response to Mtb. A) Murine BMDM and B) murine BMDM pre-treated with 10 mM 2-DG for 30 minutes were infected with live Mtb (strain H37Ra) at an MOI of 5 bacteria per cell for 3, 24 and 72 hours. Supernatants were collected and lactate concentration was measured using a colorimetric assay. Statistical analysis was performed using a paired, two-tailed Student's t-test. *, ** and *** represent $p<0.05$, 0.01 and 0.001 respectively. Data shown as mean ± SEM, n = 3 independent experiments.

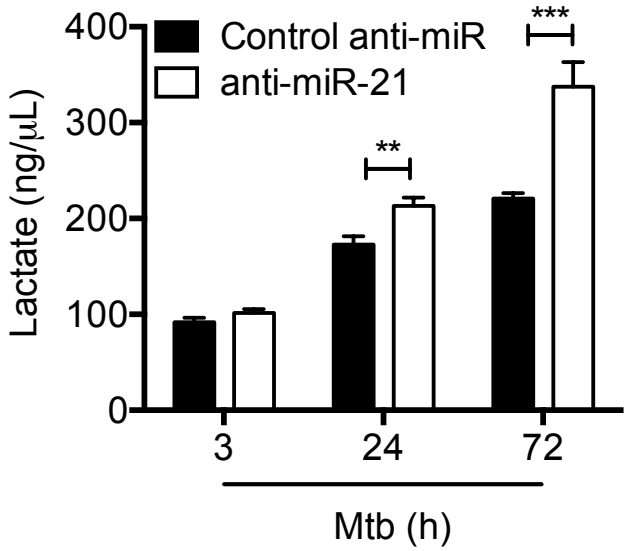

Figure 4.3 Loss of miR-21 enhances lactate production in response to Mtb in MDM. Human MDM were infected with live Mtb (strain H37Ra) at an MOI of 5 bacteria per cell for 3, 24 and 72 hours. Supernatants were collected and lactate concentration was measured using a colorimetric assay. Statistical analysis was performed using a paired, two-tailed Student's t-test. *, ** and *** represent $p<0.05$, 0.01 and 0.001 respectively. Data shown as mean ± SEM, n = 3 independent experiments.

Differences in the induction of glycolysis were confirmed with LPS and non-viable Mtb. Murine wild-type and miR-21 knockout BMDM were infected with irradiated Mtb (strain H37Rv) at an MOI of 5 bacteria per cell or 100 ng/mL of LPS for 24 hours. LPS and irradiated Mtb significantly induced lactate production in both genotypes and significantly more lactate was produced by miR-21 knockout macrophages (**Figure 4.4A**). Similarly, human MDM transfected with a negative control anti-miR or anti-miR-21 were infected with iH37Rv at an MOI of 5 bacteria per cell or 100 ng/mL of LPS for 24 hours significantly upregulated lactate production and this was significantly enhanced in the miR-21 knockdown macrophages (**Figure 4.4B**).

Having found in the previous chapter that live Mtb induces more miR-21 and better sustains this induction compared to heat-killed Mtb, the effect of this enhanced miR-21 induction on glycolysis was examined. Heat-killed Mtb induced greater induction of lactate than live Mtb, however this level of induction was not well sustained over time by heat-killed or live Mtb (**Figure 4.5**). Additionally, though the absence of miR-21 significantly boosted lactate production by both heat-killed and live Mtb, there was still a significant difference in lactate induction in miR-21-deficient macrophages dependent on viability, indicating that increased induction of miR-21 by Mtb is not the only factor suppressing glycolysis in this instance.

Enhanced lactate production in the absence of miR-21 was confirmed in primary murine alveolar macrophages. AM were isolated from murine lungs by bronchoalveolar lavage and infected with irradiated Mtb for 24 hours. Lactate was significantly induced in both genotypes (**Figure 4.6**). In contrast to the other macrophage models, lactate was significantly higher in miR-21 knockout AM both basally and after Mtb infection, perhaps indicative of in vivo

activation. Despite this, more lactate is produced by miR-21-deficient murine AM.

Finally, as there is some evidence in other models that IL-1β promotes glycolysis in a positive feedback loop[364], lactate produced by Mtb-infected BMDM in the presence of an anti-IL-1β antibody was measured. No significant difference in lactate production in response to Mtb-infection in BMDM treated with anti-IL-1β antibody compared to an IgG control antibody was detected, indicating that increased glycolysis is promoting IL-1β expression in miR-21-deficient background and is not a consequence of IL-1β feedback (**Figure 4.7**).

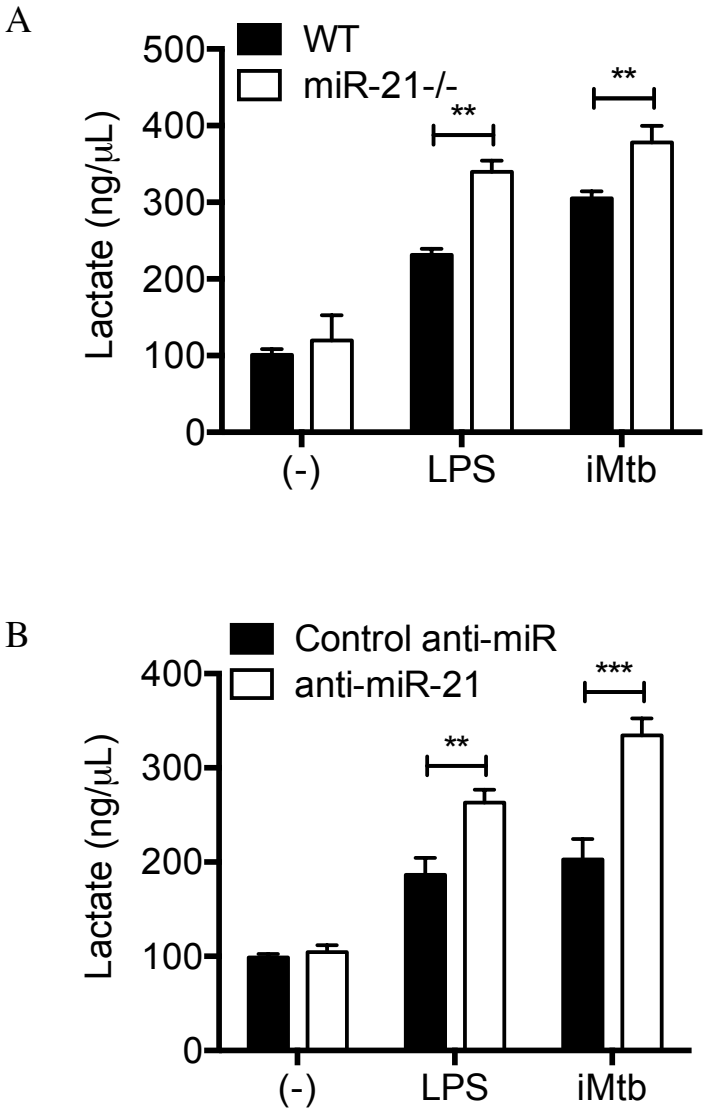

Figure 4.4 Loss of miR-21 enhances lactate production in response to LPS and irradiated Mtb. Wild type and miR-21-deficient murine BMDM (A) and human MDM transfected with a control anti-miR or anti-miR-21 (B) were infected with irradiated Mtb (strain H37Rv) (iMtb) at an MOI of 5 bacteria per cell or 100 ng/mL of LPS for 24 hours. Supernatants were collected and lactate concentration was measured using a colorimetric assay. Statistical analysis was performed using a paired, two-tailed Student's t-test. *, ** and *** represent $p<0.05$, 0.01 and 0.001 respectively. Data shown as mean ± SEM, n = 3 independent experiments.

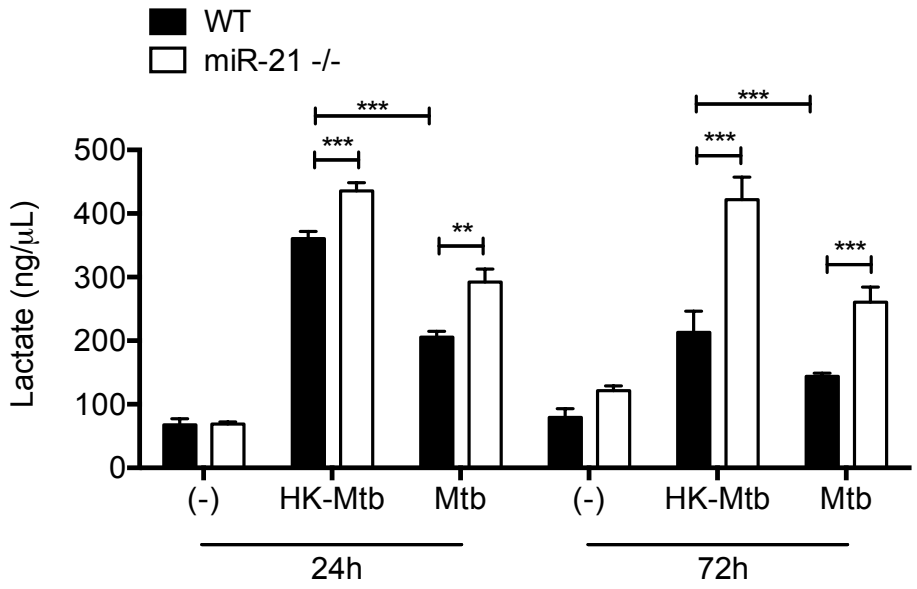

Figure 4.5 Live Mtb drives less lactate production than heat-killed Mtb. Wild type and miR-21-deficient murine BMDM were infected with heat-killed Mtb (strain H37Ra) (HK-Mtb) or live Mtb (strain H37Ra) (Mtb) at an MOI of 5 bacteria per cell or 100 ng/mL of LPS for 24 hours. Supernatants were collected and lactate concentration was measured using a colorimetric assay. Statistical analysis was performed using a paired, two-tailed Student's t-test. *, ** and *** represent $p<0.05$, 0.01 and 0.001 respectively. Data shown as mean ± SEM, n = 3 independent experiments.

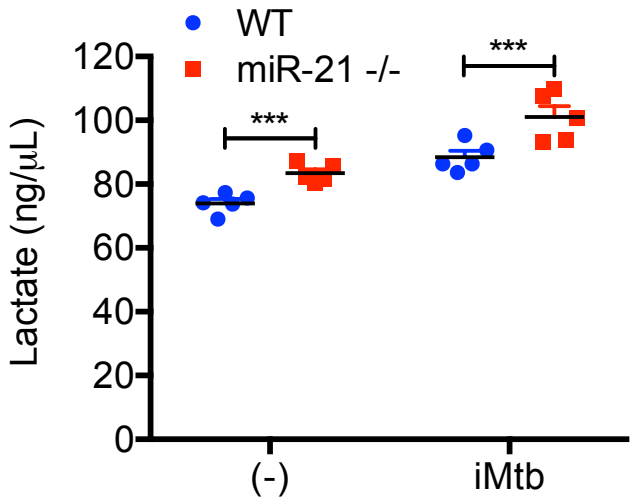

Figure 4.6 miR-21 deficiency enhances lactate production in response to Mtb in murine alveolar macrophages. Murine AM were infected with irradiated Mtb (strain H37Rv) (iMtb) at an MOI of 5 bacteria per cell for 24 hours. Supernatants were collected and lactate concentration was measured using a colorimetric assay. Statistical analysis was performed using a paired, two-tailed Student's t-test. *, ** and *** represent $p<0.05$, 0.01 and 0.001 respectively. Data shown as mean ± SEM, n = 5 mice per genotype in one experiment.

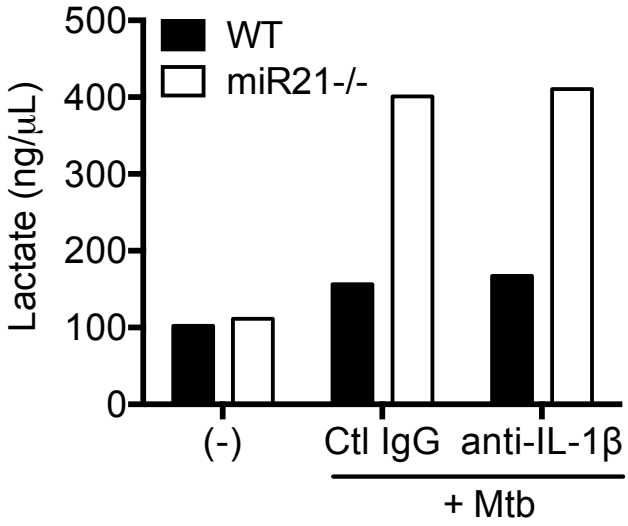

Figure 4.7 Blocking IL-1β does not alter lactate production. Murine BMDM infected with live Mtb (strain H37Ra) at an MOI of 5 bacteria per for 72 hours. Cells were treated with control IgG (Ctl IgG) or an IL-1β-neutralising antibody (anti-IL-1β) (1 μg/mL) 3 hours post-infection. Supernatants were collected and lactate measured by colorimetric assay. n = 1.

4.2.3 Blocking glycolysis inhibits containment of Mtb

To better understand the functional consequences of enhanced glycolysis in macrophages lacking miR-21, glycolysis was blocked. While 2-DG was used for blockade of glycolysis in murine BMDM, a different method was used in human MDM which are more sensitive to the toxic effects of 2-DG. For human MDM, medium was changed to a glucose-free media supplemented with 10 mM glucose or 10 mM galactose. Galactose supplementation is a less toxic method by which to inhibit the glycolytic pathway. In order to be used for glycolysis, galactose must be catabolised to glucose via the Leloir pathway which costs ATP. Cells preferentially therefore use oxidative phosphorylation and do not undergo glycolytic switching as cells cultured in glucose would[204]. Newly published research has shown that 2-DG also blocks other metabolic processes including oxidative phosphorylation[261] so this method of blocking glycolysis by galactose supplementation rather than with the 2-DG inhibitor supports findings from 2-DG inhibition experiments in the BMDM model.

Firstly, the effect of blocking glycolysis on the induction of miR-21 was examined. Murine BMDM were pre-treated with 10 mM 2-DG for 30 minutes and then infected with iH37Rv at an MOI of 5 bacteria per cell or 100 ng/ml of LPS for 24 hours. No significant difference in miR-21 basally or in response to these stimuli was observed in cells treated with 2-DG (**Figure 4.8A**). Similarly, human MDM were cultured in glucose- or galactose-supplemented media and infected with iH37Rv at an MOI of 5 bacteria per cell or 100 ng/ml of LPS for 24 hours. No basal difference in miR-21 expression or difference in the induction of miR-21 in response to infection was recorded (**Figure 4.8B**).

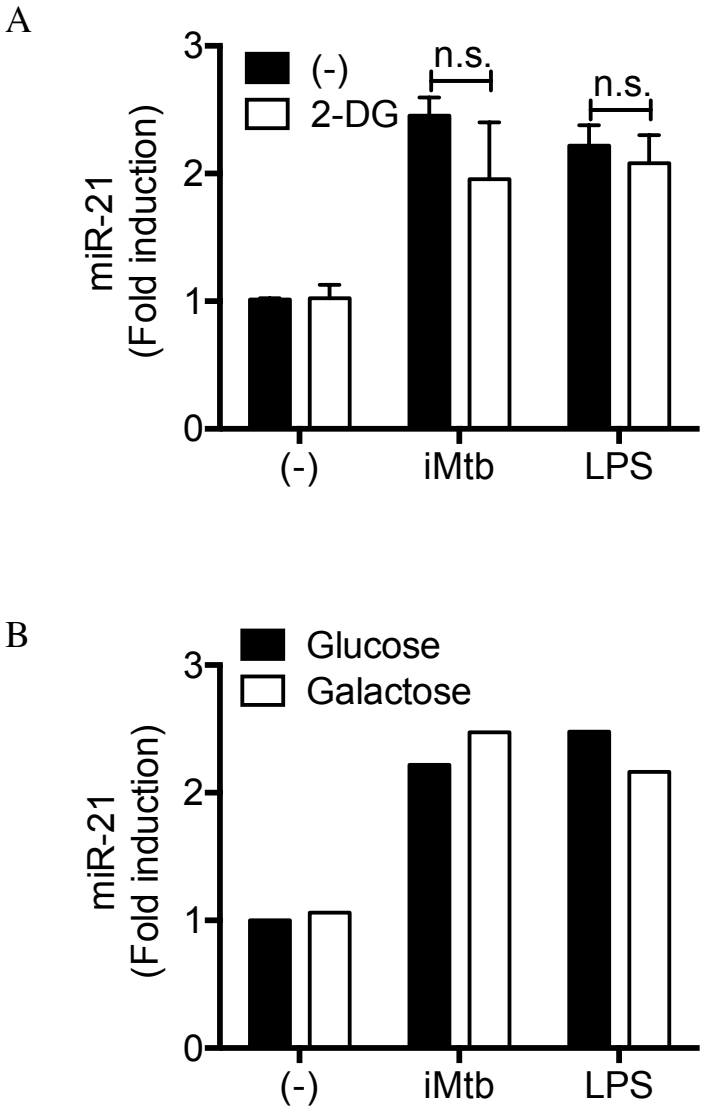

Figure 4.8 Blocking glycolysis does not affect miR-21 expression. A) Murine BMDM were pre-treated with 10 mM 2-DG for 30 minutes and B) human MDM were cultured for 24 hours in media supplemented with 10 mM glucose or 10 mM galactose. Cells were then infected with irradiated Mtb (strain H37Rv) (iMtb) at an MOI of 5 bacteria per cell or 100 ng/mL of LPS for 24 hours. RNA was isolated and qPCR was performed. Expression of miR-21 relative to the untreated control was calculated. Data were normalised to RNU6B. Statistical analysis was performed using a paired, two-tailed Student's t-test. *, ** and *** represent $p<0.05$, 0.01 and 0.001 respectively. Data shown as mean ± SEM, n = 3 independent experiments and n = 1.

Having confirmed that glycolysis was not directly affecting miR-21 expression, the effect of blocking the induction of glycolysis on the outcome of Mtb infection was then investigated. Wild-type and miR-21 knockout BMDM were pre-treated with 10 mM 2-DG for 30 minutes and then infected with live H37Ra at an MOI of 5 bacteria per cell. In comparison to untreated BMDM which could contain Mtb growth until 24 hours, BMDM that had been treated with 2-DG were unable to contain Mtb growth even in the initial stages of infection (**Figure 4.9A**). At 72 hours post-infection, growth in both wild-type and miR-21 knockout BMDM that had been treated with 2-DG was significantly higher than in untreated cells (**Figure 4.9B**). In BMDM in which glycolysis was allowed to proceed, miR-21-deficient macrophages were significantly better at containing Mtb growth. In the presence of 2-DG however, there was no significant difference between wild-type and miR-21 knockout cells.

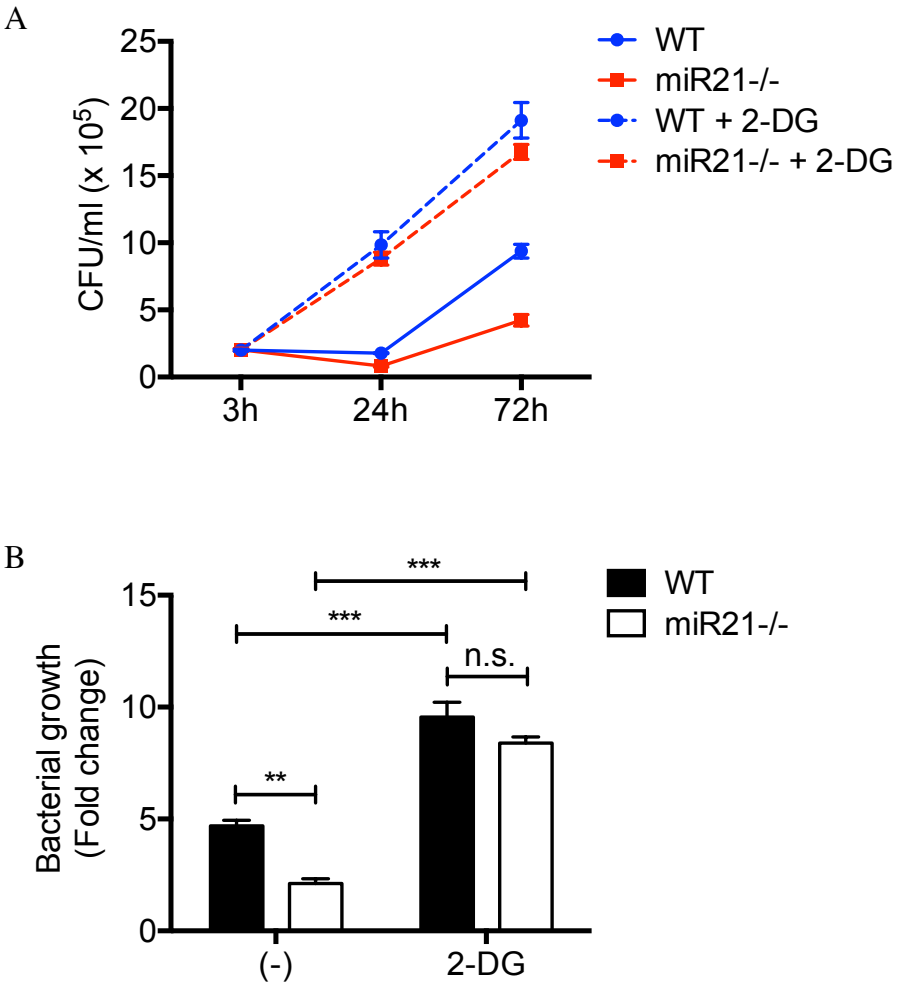

Figure 4.9 Blocking glycolysis inhibits bacterial containment. Murine BMDM were pre-treated with 10 mM 2-DG for 30 minutes and infected with live H37Ra at an MOI of 5 bacteria per cell for 3, 24 and 72 hours. Cells were lysed in 0.1% Triton X-100 at the indicated time points and the lysates diluted in Middlebrook broth supplemented with ADC. Aliquots of the lysates were then streaked in triplicate on warm Middlebrook agar plates and incubated at 37°C for approximately 14 days. Colony forming units were counted (A) and the number of colonies at 72 hours post-infection relative to the 3-hour time point calculated (B). Statistical analysis was performed using a paired, two-tailed Student's t-test. *, ** and *** represent $p<0.05$, 0.01 and 0.001 respectively. Data shown as mean ± SEM, n = 3 independent experiments.

4.2.4 Blocking the induction of glycolysis by Mtb inhibits anti-microbial responses

miR-21 deficient macrophages cannot contain Mtb infection when glycolysis is impaired. In order to further understand how this occurs, glycolysis was blocked and anti-microbial responses measured. Wild-type and miR-21 deficient BMDM were pre-treated with 2-DG and infected with live Mtb for 24 hours. TNF-α production was significantly stunted in the presence of 2-DG in both genotypes (**Figure 4.10A**). miR-21 knockout macrophages still produced significantly more TNF-α than wild-type macrophages even with glycolytic switching blocked. IL-1β production was significantly blocked with 2-DG treatment and, in comparison to TNF-α production, there was no significant difference in the amount of IL-1β produced in response to live Mtb infection between genotypes when glycolysis was blocked (**Figure 4.10B**). These observations with live Mtb were then confirmed with irradiated Mtb. Blocking glycolysis had no effect on TNF-α production in response to infection with irradiated Mtb or LPS (**Figure 4.11A**). LPS alone does not result in IL-1β protein secretion so only irradiated Mtb was used in this instance. 2-DG fully blocked any IL-1β production in response to irradiated Mtb (**Figure 4.11B and C**), indicating that iMtb-induced IL-1β production is dependent on glycolysis.

Nitrite production was also significantly repressed by blocking glycolysis. BMDM treated with 2-DG produced significantly less nitrite in response to irradiated Mtb and LPS (**Figure 4.12A**). miR-21-deficient BMDM also produced significantly less nitrite when treated with 2-DG, retaining a trend towards higher production when stimulated with LPS and producing significantly more when infected with irradiated Mtb (**Figure 4.12B**) though levels were still very much stunted compared to macrophages in which glycolysis could proceed unimpeded.

Human MDM were transfected with negative control anti-miR or anti-miR-21 and prevented from switching to glycolytic metabolism by culturing in galactose supplemented media. TNF-α and IL-1β production was significantly stunted by galactose supplementation in control transfected cells, but importantly the enhanced production in miR-21 silenced cells was abrogated. (**Figure 4.13**).

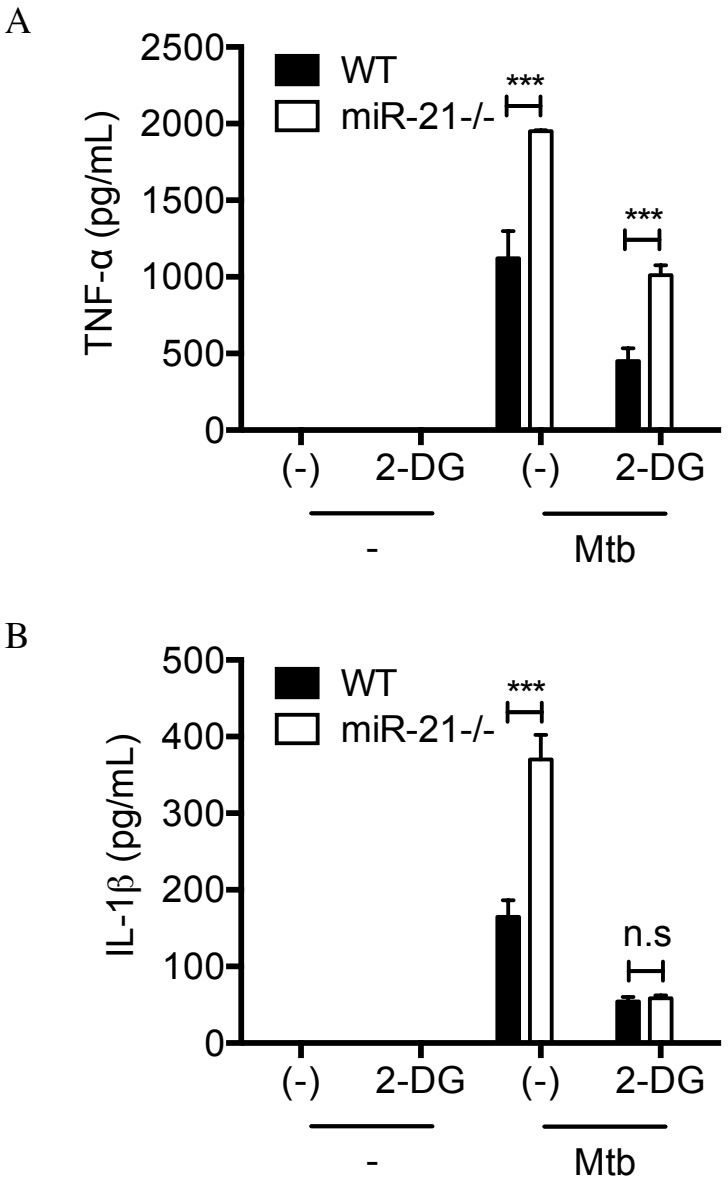

Figure 4.10 Blocking glycolysis blocks enhanced production of IL-1β in miR-21 knockout BMDM. Murine BMDM were pre-treated with 10 mM 2-DG for 30 minutes and infected with live Mtb (strain H37Ra) at an MOI of 5 bacteria per cell for 24 hours. Supernatants were collected. TNF-α (A) and IL-1β (B) protein were quantified using an ELISA. Statistical analysis was performed using a paired, two-tailed Student's t-test. *, ** and *** represent $p<0.05$, 0.01 and 0.001 respectively. Data shown as mean ± SEM, n = 3 independent experiments.

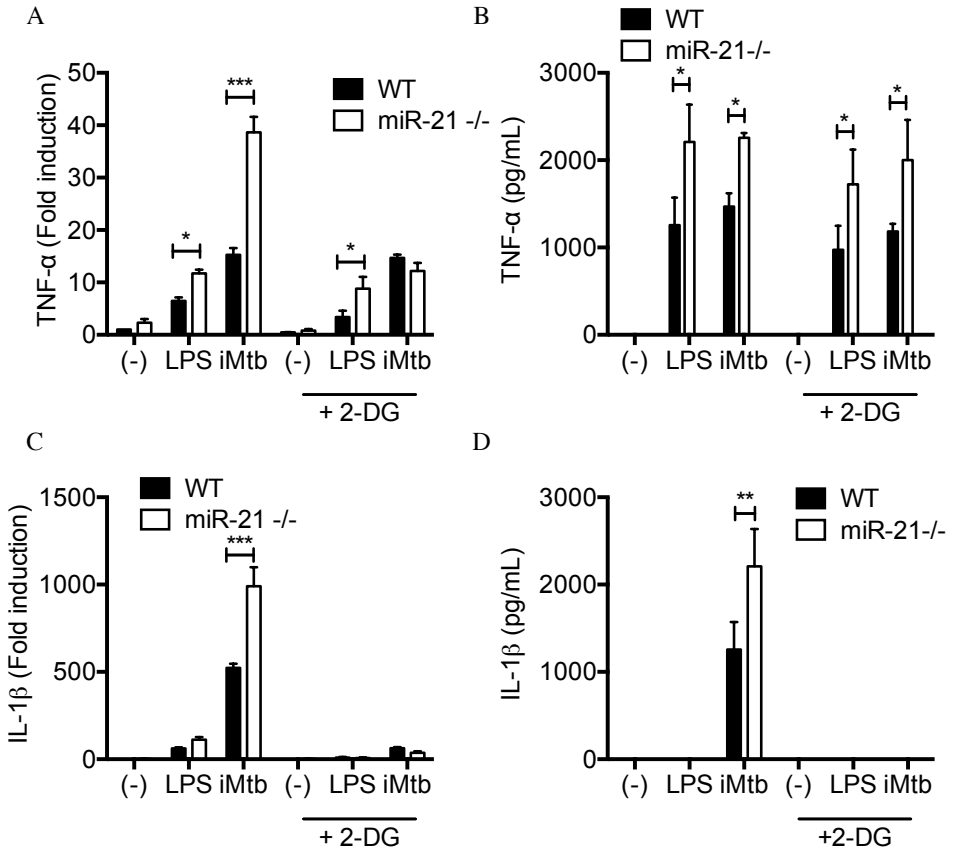

Figure 4.11 Blocking glycolysis blocks enhanced production IL-1β in miR-21 knockout BMDM. Murine BMDM were pre-treated with 10 mM 2-DG for 30 minutes and infected with live Mtb (Strain H37Ra) at an MOI of 5 bacteria per cell for 24 hours. Supernatants were collected. TNF-α mRNA (A) and protein (B) and IL-1β mRNA (C) and protein (D) were quantified using qPCR and ELISA. Statistical analysis was performed using a paired, two-tailed Student's t-test. *, ** and *** represent $p<0.05$, 0.01 and 0.001 respectively. Data shown as mean ± SEM, n = 3 independent experiments.

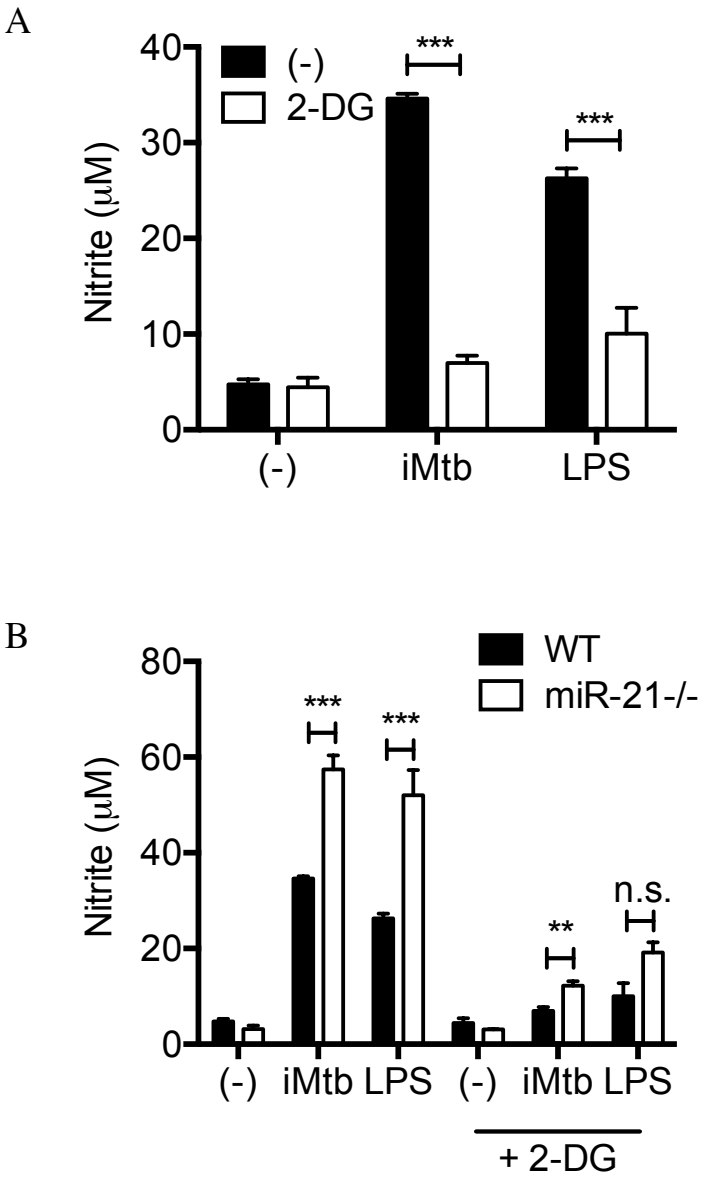

Figure 4.12 Blocking glycolysis limits nitrite production. Wild type murine BMDM (A) and wild type and miR-21-deficient BMDM (B) were pre-treated with 10 mM 2-DG for 30 minutes and infected with irradiated Mtb (strain H37Rv) (iMtb) at an MOI of 5 bacteria per cell or stimulated with 100 ng/mL of LPS for 24 hours. Supernatants were collected and nitrite production was measured using a colorimetric Griess assay. Statistical analysis was performed using a paired, two-tailed Student's t-test. *, ** and *** represent $p<0.05$, 0.01 and 0.001 respectively. Data shown as mean ± SEM, n = 3 independent experiments.

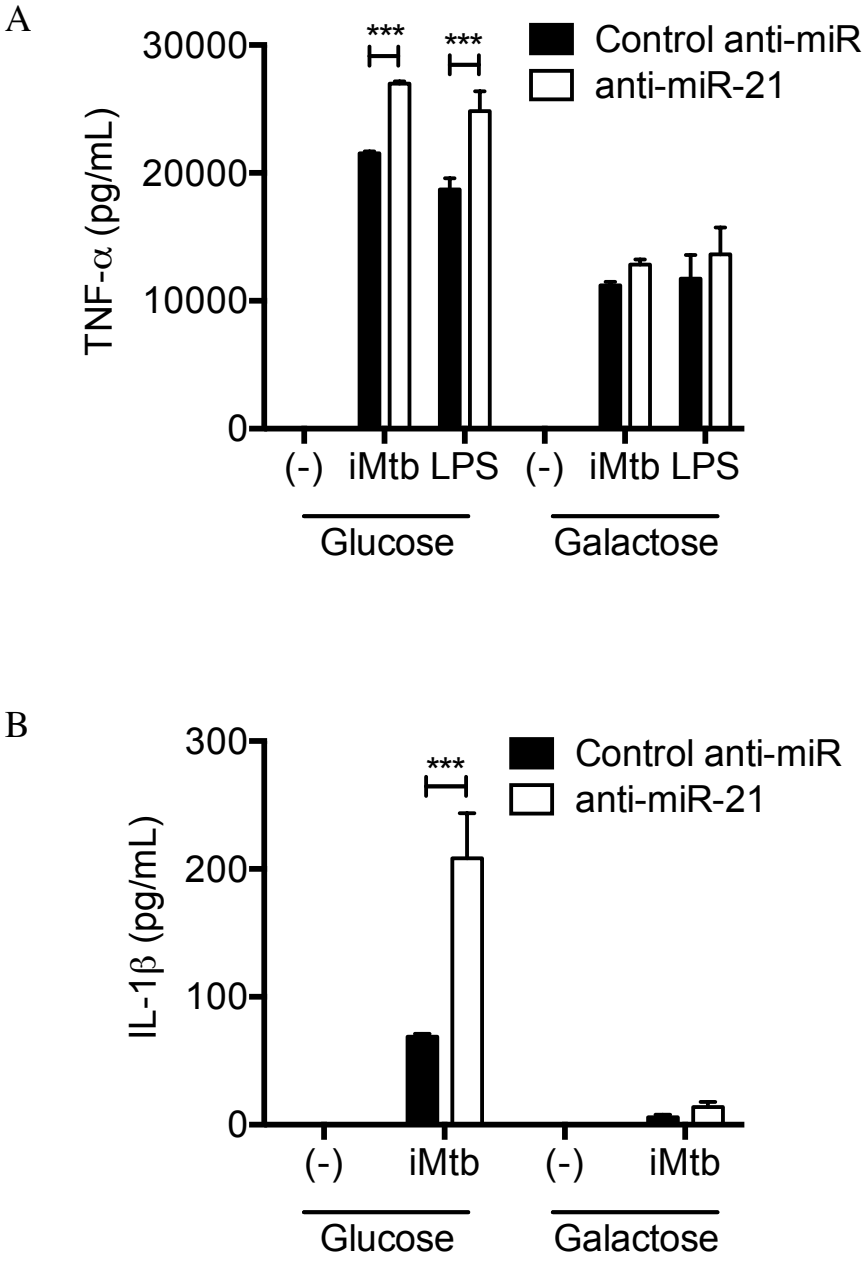

Figure 4.13 Blocking glycolysis blocks enhanced production IL-1β in miR-21 silenced MDM. Mature human MDM were cultured in 10 mM glucose or 10mM galactose for 24 hours and infected with irradiated Mtb (strain H37Rv) (iMtb) at an MOI of 5 bacteria per cell for 24 hours. Supernatants were collected. TNF-α (A) and IL-1β (B) protein were quantified using an ELISA. Statistical analysis was performed using a paired, two-tailed Student's t-test. *, ** and *** represent $p<0.05$, 0.01 and 0.001 respectively. Data shown as mean ± SEM, n = 3 donors in one experiment.

4.2.5 Loss of miR-21 promotes a glycolytic phenotype after Mtb infection

Lactate production is a crude surrogate marker of glycolytic activity. Extracellular flux analysis can provide a more informative view of the metabolic profile of a cell population. The Seahorse XF analyser can measure in real-time the oxygen consumption rate (OCR), an indicator of the level of oxidative phosphorylation, and the extracellular acidification rate (ECAR), an indicator of glycolysis, of a monolayer of cells (described in detail in **2.1.24**). Measuring both of these parameters in tandem provides a more accurate view of the metabolic state of the cell. Profound changes in metabolism have been observed in activated macrophages using this technology recently, therefore this technology was employed to characterise macrophage metabolism in the context of miR-21 deficiency.

Metabolic changes in response to treatment with irradiated Mtb were characterised in wild-type BMDM. Irradiated Mtb rather than live Mtb had to be used as the Seahorse analyser did not accommodate biosafety level 2 bacteria. Cells were seeded in Seahorse cell culture plates and infected with iH37Rv or 100 ng/mL LPS for 24 hours before extracellular flux analysis was performed. OCR was unchanged by infection with Mtb or LPS (**Figure 4.14A**), however ECAR was significantly higher after stimulation with LPS and trended towards higher after infection with iMtb, though this was not significant (**Figure 4.14B**). To obtain a better representation of the overall metabolic state of the cell, the ratio of ECAR to OCR was calculated. When this relative ratio was considered, iMtb and LPS both induced a significant shift towards glycolytic metabolism (**Figure 4.14C**).

miR-21 knockout macrophages were also metabolically profiled. Like wild-type BMDM, iMtb and LPS induced no significant

difference in OCR, and rates were not significantly different between genotypes (**Figure 4.15A**). Basal ECAR was identical in both genotypes, however ECAR was significantly upregulated following stimulation with iMtb and LPS and this upregulation was significantly higher in miR-21 knockout macrophages (**Figure 4.15B**). Consequently, the ratio of ECAR to OCR was no different basally but was significantly higher following iMtb and LPS stimulation (1.6-fold higher in both cases) (**Figure 4.15C**). Representative extracellular flux traces of uninfected (**Figure 4.16**) and infected BMDM (**Figure 4.17**) are shown.

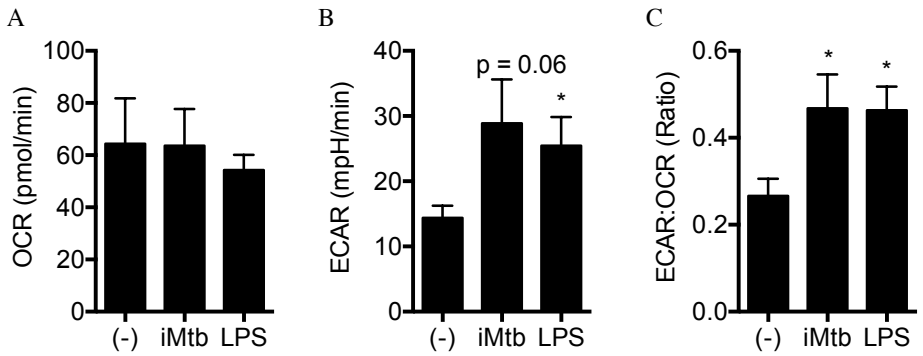

Figure 4.14 Mtb infection drives glycolysis. BMDM were infected with iH37Rv at an MOI of 5 bacteria per cell or 100 ng/mL LPS for 24 hours. Extracellular flux analysis was performed and data normalised for cell number using a crystal violet assay. Statistical analysis was performed using a paired, two-tailed Student's t-test. *, ** and *** represent $p<0.05$, 0.01 and 0.001 respectively. Data shown as mean ± SEM, n = 6 independent experiments.

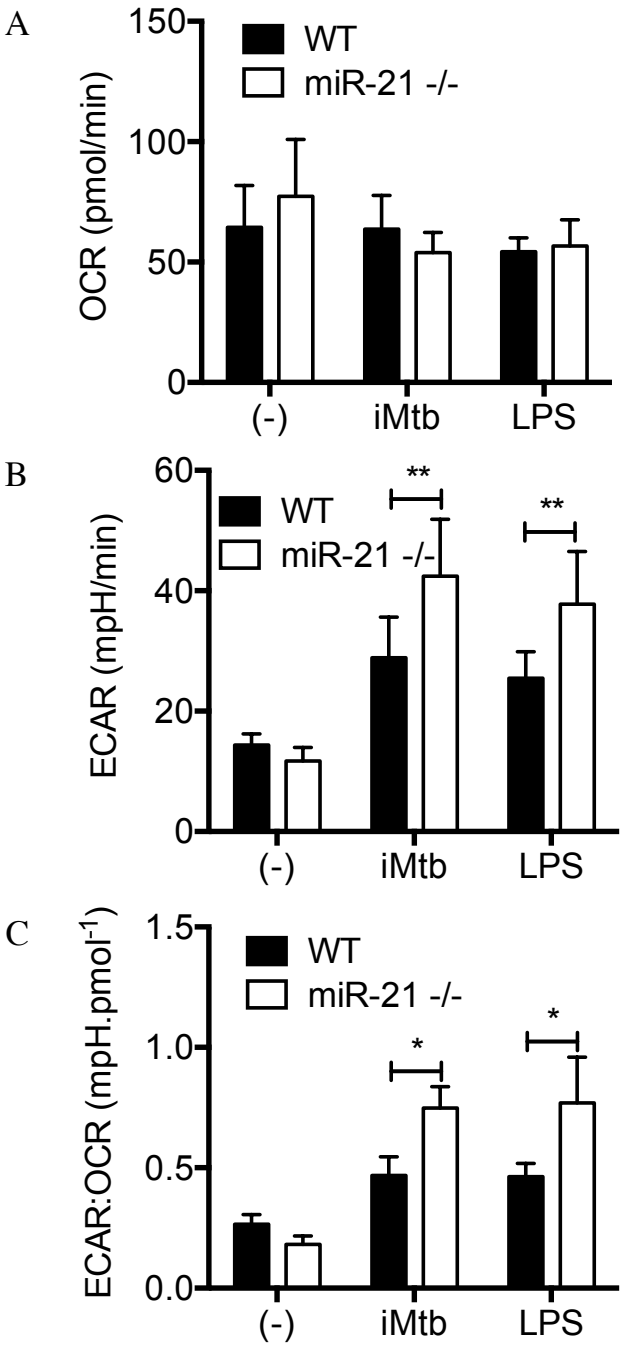

Figure 4.15 miR-21 deficient macrophages are more glycolytic after Mtb infection. BMDM were infected with iH37Rv at an MOI of 5 bacteria per cell or 100 ng/mL LPS for 24 hours. Extracellular flux analysis was performed and data normalised for cell number. Statistical analysis was performed using a paired, two-tailed Student's t-test. *, ** and *** represent $p<0.05$, 0.01 and 0.001 respectively. Data shown as mean ± SEM, n = 6 independent experiments.

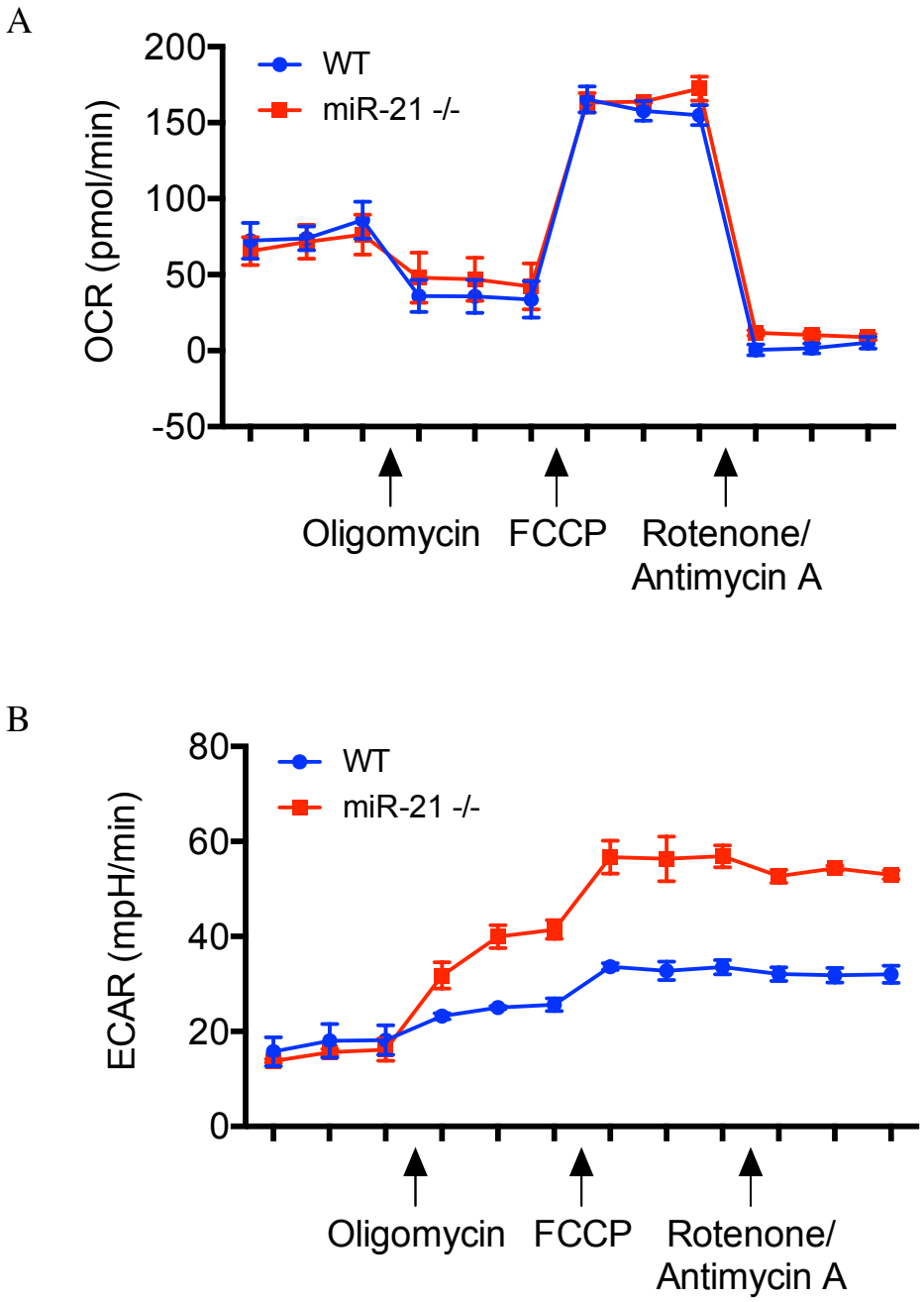

Figure 4.16 Extracellular flux analysis of basal wild-type and miR-21 deficient macrophages. Extracellular flux analysis was performed on wild-type and miR-21 knockout BMDM with sequential addition of mitochondrial inhibitors. Data were normalised for cell number using a crystal violet assay and oxygen consumption rate (A) and extracellular acidification rate (B) charted. Representative trace shown.

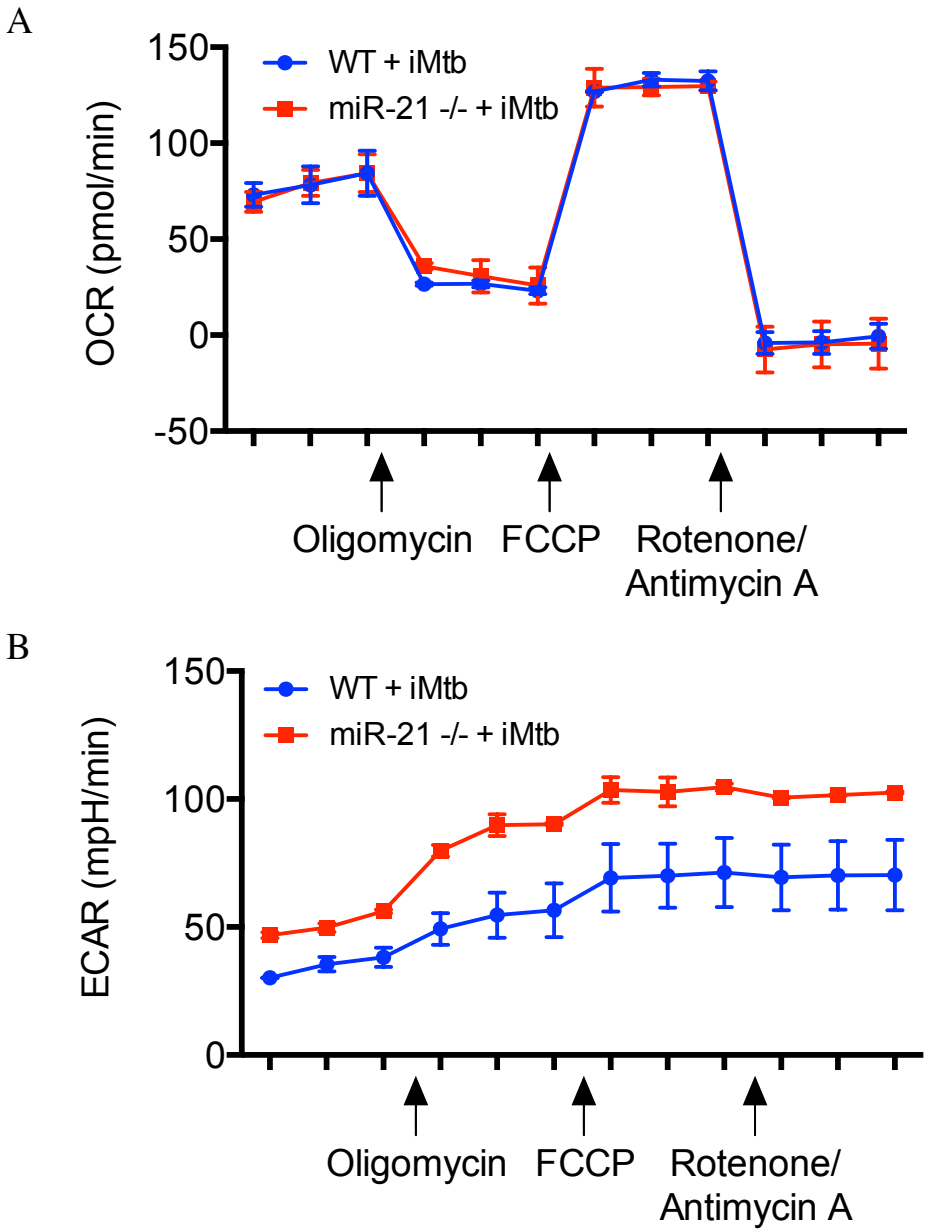

Figure 4.17 Extracellular flux analysis of Mtb-infected wild-type and miR-21 deficient macrophages. Wild-type and miR-21 knockout BMDM were infected with iH37Rv at an MOI of 5 bacteria per cell for 24 hours. Extracellular flux analysis was performed with sequential addition of mitochondrial inhibitors. Data were normalised for cell number using a crystal violet assay and oxygen consumption rate (A) and extracellular acidification rate (B) charted. Representative trace shown.

4.2.6 miR-21 knockout macrophages have a higher glycolytic reserve

To further assess the metabolic capacity of wild-type and miR-21-deficient macrophages, mitochondrial inhibitors were added sequentially to the cells and the resulting changes in metabolic parameters monitored in real-time.

Spare Respiratory Capacity (SRC) is defined as the ability of a cell to enhance mitochondrial respiration when stressed. FCCP is a mitochondrial uncoupler which allows protons to pass freely through the inner mitochondrial membrane without passing through ATP synthase. This results in maximal oxygen consumption at complex IV to maintain the mitochondrial membrane potential, reflected in an elevated OCR. The difference between the baseline OCR and OCR following treatment with FCCP (i.e. maximal OCR) thus indicates the SRC of the cells. SRC was measured in this manner in wild-type and knockout BMDM. SRC was no different basally between genotypes and did not change significantly with infection with iMtb or stimulation with LPS (**Figure 4.18A**).

Another important parameter of metabolic function is glycolytic reserve (GR). Glycolytic reserve is the potential of a cell to enhance glycolytic rate when needed, i.e. the difference between the rate of glycolysis and the total glycolytic capacity of a cell. Oligomycin is an ATP synthase inhibitor which blocks oxidative phosphorylation, reducing the ADP/ATP ratio and thus driving glycolysis to capacity. The difference between ECAR after the addition of oligomycin (maximal ECAR) and basal ECAR gives an indication of the glycolytic reserve.

Wild-type and miR-21 deficient macrophages were treated with oligomycin and the glycolytic reserve calculated. Basally, GR

trended higher in miR-21 knockout BMDM though this did not reach significance (**Figure 4.18B**). GR trended slightly (non-significantly) lower in wild-type macrophages after infection with iMtb and LPS since their basal glycolysis rates are enhanced. Thus despite having a higher glycolytic rate after iMtb stimulation, miR-21 knockout BMDM retained a significantly higher glycolytic capacity than wild-type BMDM (approximately 2.6-fold more GR).

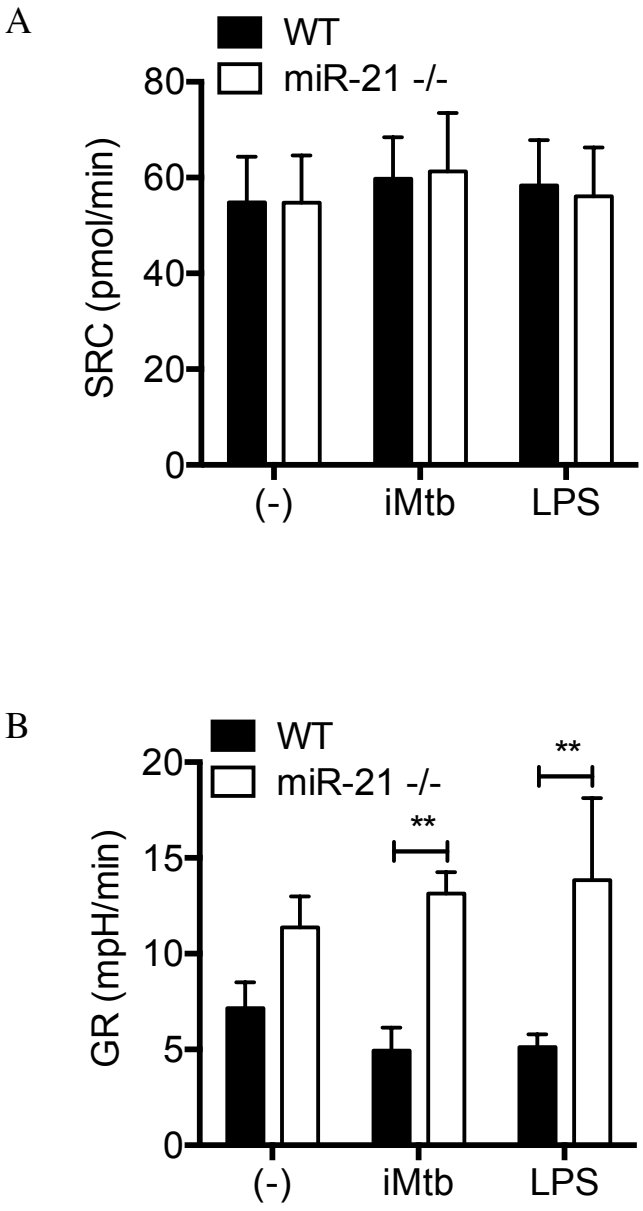

Figure 4.18 miR-21 deficient macrophages have more glycolytic reserve. BMDM were infected with iH37Rv at an MOI of 5 bacteria per cell or 100 ng/mL LPS for 24 hours. Extracellular flux analysis was performed with sequential addition of mitochondrial inhibitors. Data were normalised for cell number using a crystal violet assay and spare respiratory capacity (A) and glycolytic reserve (B) calculated. Statistical analysis was performed using a paired, two-tailed Student's t-test. *, ** and *** represent $p<0.05$, 0.01 and 0.001 respectively. Data shown as mean ± SEM, n = 6 independent experiments.

These findings were then confirmed in human macrophages. Human MDM were transfected with a negative control anti-miR or anti-miR-21 and extracellular flux analyses performed. As human donors were much more metabolically variable, to interpret the data one representative analysis is shown in **Figure 4.19**, and six donors in **Figure 4.20**. Firstly, there was no significant difference in metabolic activity between untransfected MDM and MDM transfected with a negative control anti-miR. As in the murine macrophages, MDM in which miR-21 activity had been blocked had significantly higher ECAR following stimulation with iMtb and LPS. The ratio of ECAR to OCR was also significantly higher following Mtb infection in the miR-21 knockdown macrophages. LPS induced higher ECAR:OCR in some donors but this did not reach significance when all donors were averaged.

Spare respiratory capacity was again found to be unchanged by miR-21 status (**Figure 4.21A**). Glycolytic reserve was significantly higher basally in miR-21 knockdown macrophages and trended towards higher glycolytic reserve than anti-miR control treated macrophages after iMtb and LPS stimulation (**Figure 4.21B**).

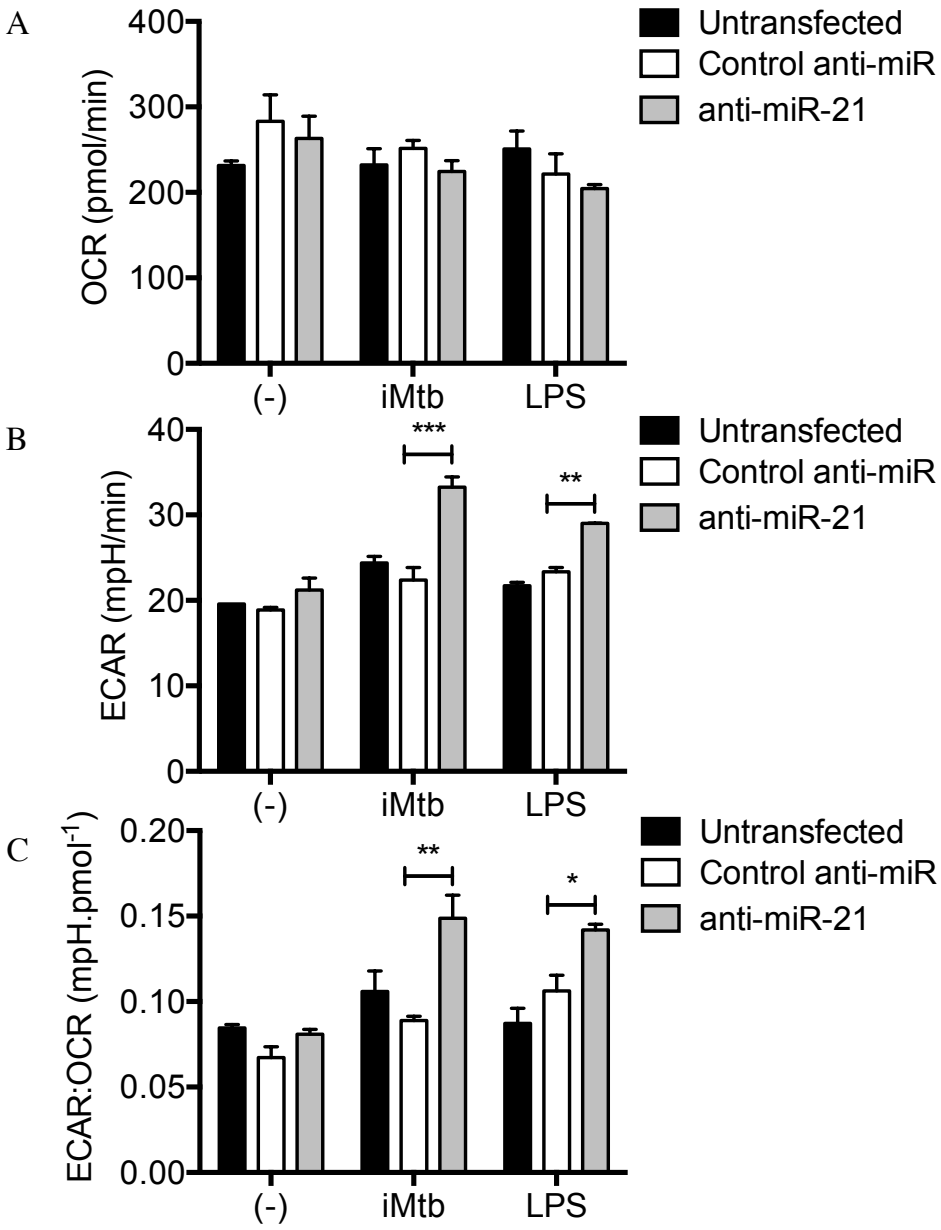

Figure 4.19 Loss of miR-21 makes MDM more glycolytic after Mtb infection. MDM were infected with iH37Rv at an MOI of 5 bacteria per cell or 100 ng/mL LPS for 24 hours. Extracellular flux analysis was performed and data normalised for cell number using a crystal violet assay. Data shown as mean ± SEM of experimental replicates, n = 1 representative experiment.

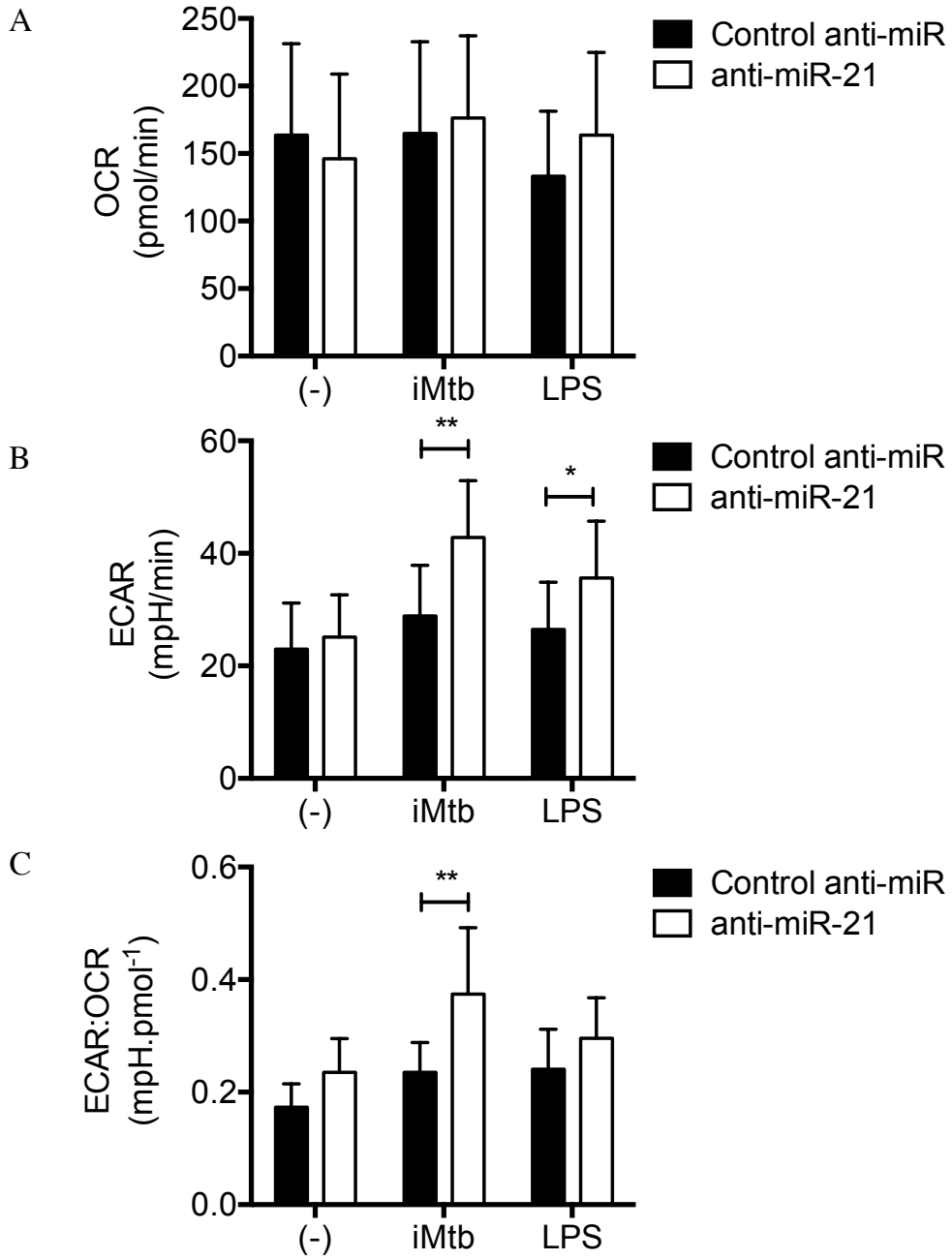

Figure 4.20 Loss of miR-21 makes MDM more glycolytic after Mtb infection. MDM were infected with iH37Rv at an MOI of 5 bacteria per cell or 100 ng/mL LPS for 24 hours. Extracellular flux analysis was performed and data normalised for cell number. Statistical analysis was performed using two-way ANOVA. *, ** and *** represent $p<0.05$, 0.01 and 0.001 respectively. Data shown as mean ± SEM, n = 6 independent experiments.

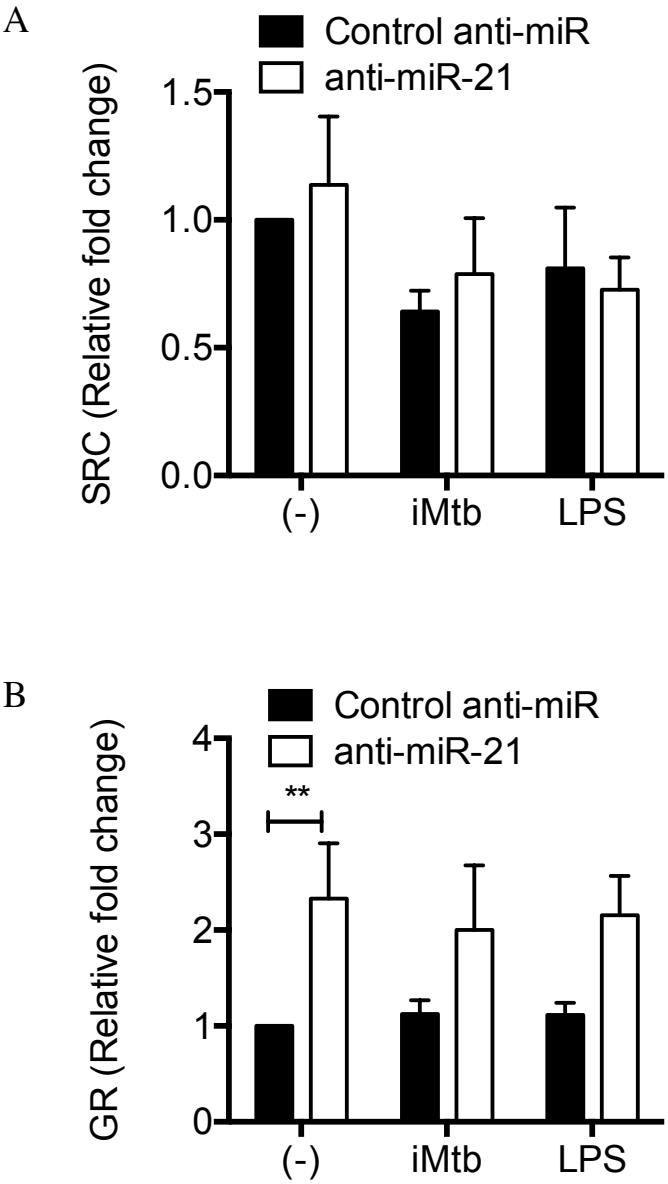

Figure 4.21 Loss of miR-21 gives human MDM higher glycolytic reserve. MDM were infected with iH37Rv at an MOI of 5 bacteria per cell or 100 ng/mL LPS for 24 hours. Extracellular flux analysis was performed with sequential addition of mitochondrial inhibitors. Data were normalised for cell number using a crystal violet assay and spare respiratory capacity (A) and glycolytic reserve (B) calculated. Data were normalised to the unstimulated control anti-miR for each donor. Statistical analysis was performed using a paired, two-tailed Student's t-test. *, ** and *** represent $p<0.05$, 0.01 and 0.001 respectively. Data shown as mean ± SEM, n = 6 independent experiments.

4.2.7 Pro-glycolytic genes are more highly expressed in macrophages lacking miR-21

Macrophages lacking miR-21 activity were found to be more glycolytic after a pro-inflammatory stimulus at a cellular level. Looking for more molecular confirmation of these findings, the expression of several pro-glycolytic genes known to be upregulated to promote metabolic reprogramming was examined. The upregulation of genes involved in the glycolytic pathway is a key mechanism by which the cell switches to and maintains a glycolytic phenotype. Many of these genes are potentiated by HIF-1α, thus HIF-1α activators such as PKM2 and succinate which are enhanced in glycolysis drive a glycolytic transcription program to sustain this metabolic phenotype.

Live Mtb, irradiated Mtb and LPS were all found to induce the expression of Slc2a1 (encoding the glucose transporter Glut1), LdhA (lactate dehydrogenase A which is required for continued glycolysis) and Hk2 (hexokinase 2 which is essential for increased glycolysis). Though no basal differences were present, all three genes were all significantly higher in miR-21 knockout BMDM after infection with live Mtb, irradiated Mtb and LPS (**Figure 4.22**). The enhanced expression of these pro-glycolytic genes in miR-21 deficient BMDM was ablated by treatment with 2-DG (**Figure 4.23**), consistent with the notion that enhanced gene expression in a miR-21-deficient context is driven by increased positive feedback from glycolysis-driven HIF-1α activation, and implies that none of these genes are direct miR-21 targets which would be maintained regardless of the glycolytic status of the cell.

Furthermore, primary human alveolar macrophages were infected with live and irradiated Mtb and infection with live Mtb was found to have a reduced propensity for the induction of glycolytic gene

expression (**Figure 4.24**). This correlates with the increased and sustained induction of miR-21 in response to live Mtb infection which was described in the previous chapter.

Enhanced pro-glycolytic gene expression was also confirmed in primary murine alveolar macrophages. miR-21 knockout AM had higher basal expression of Slc2a1 and LdhA, possibly due to in vivo activation as AM are not in a completely sterile environment or the extraction process. Regardless, when challenged with iMtb, Slc2a1, LdhA and Hk2 all enhanced expression and this was augmented in miR-21-deficient cells (**Figure 4.25**).

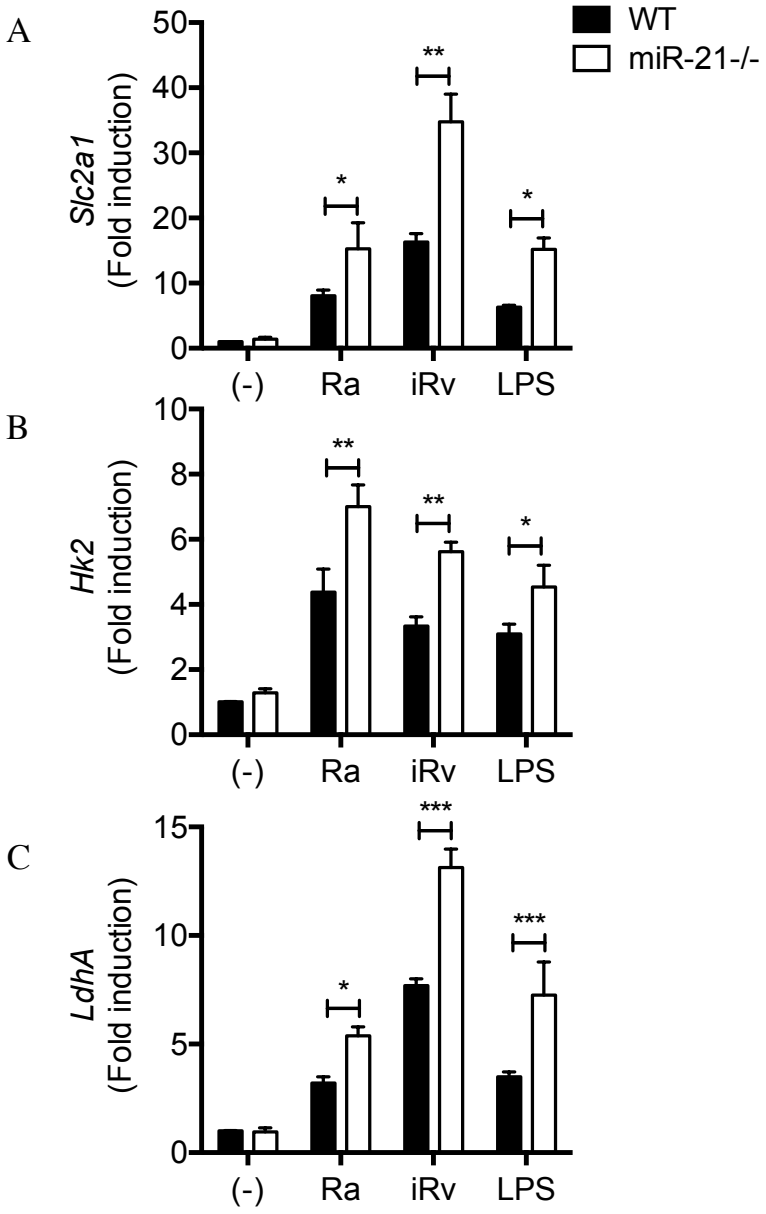

Figure 4.22 miR-21 deficient BMDM express higher levels of genes on the glycolytic pathway after Mtb infection. BMDM were infected with live Mtb H37Ra (Ra) or irradiated H37Rv (iRv) at an MOI of 5 bacteria per cell or 100 ng/mL LPS for 24 hours. qPCR was performed and expression of *Slc2a1* (A), *Hk2* (B) and *LdhA* (C) mRNA relative to the untreated control was calculated. Data were normalised to 18S. Statistical analysis was performed using a paired, two-tailed Student's t-test. *, ** and *** represent $p<0.05$, 0.01 and 0.001 respectively. Data shown as mean ± SEM, n = 3 independent experiments.

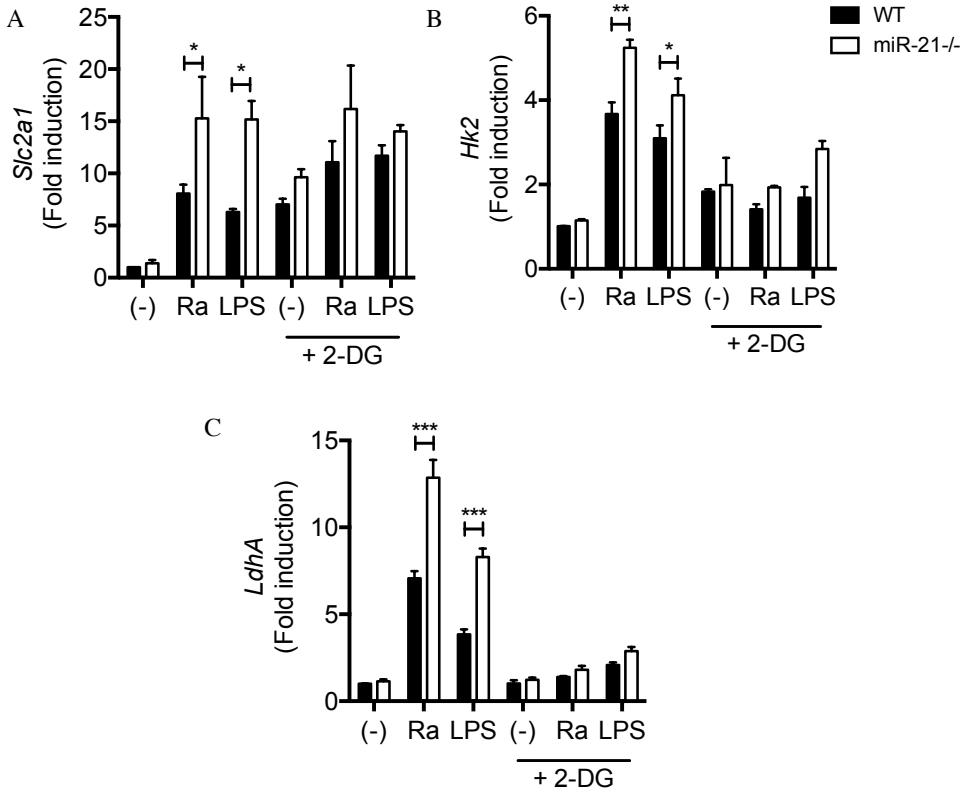

Figure 4.23 miR-21 deficient BMDM express higher levels of genes on the glycolytic pathway after Mtb infection. BMDM were pre-treated for 30 minutes with 10 mM 2-DG and infected with live Mtb (strain H37Ra) (Ra) at an MOI of 5 bacteria per cell or 100 ng/mL LPS for 24 hours. qPCR was performed and expression of *Slc2a1* (A), *Hk2* (B) and *LdhA* (C) mRNA relative to the untreated control was calculated (A). Data were normalised to 18S. Statistical analysis was performed using a paired, two-tailed Student's t-test. *, ** and *** represent $p<0.05$, 0.01 and 0.001 respectively. Data shown as mean ± SEM, n = 3 independent experiments.

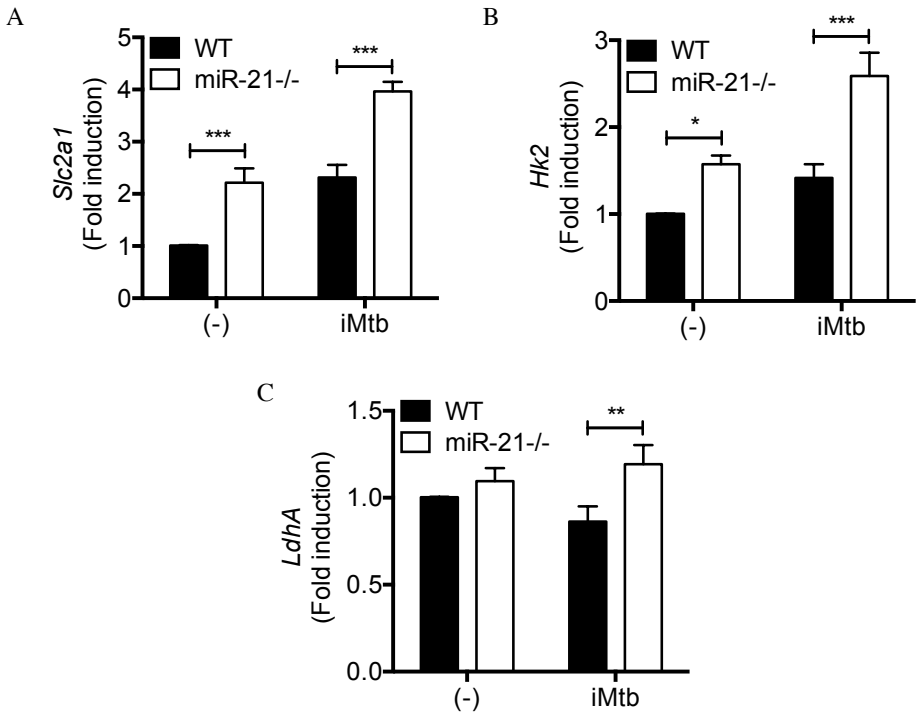

Figure 4.24 miR-21 deficiency in murine alveolar macrophages enhances expression of genes on the glycolytic pathway in response to Mtb infection. Murine AM were isolated by bronchoalveolar lavage and allowed 24 hours to recover. The cells were then infected with irradiated Mtb (H37Rv) (iRv) at an MOI of 5 bacteria per cell for 24 hours. RNA was isolated and qPCR was performed. Expression of *Slc2a1* (A), *Hk2* (B) and *LdhA* (C) mRNA relative to the untreated control was calculated. Data were normalised to 18S. Statistical analysis was performed using a paired, two-tailed Student's t-test. *, ** and *** represent $p<0.05$, 0.01 and 0.001 respectively. Data shown as mean ± SEM, n = 5 mice per genotype in one experiment.

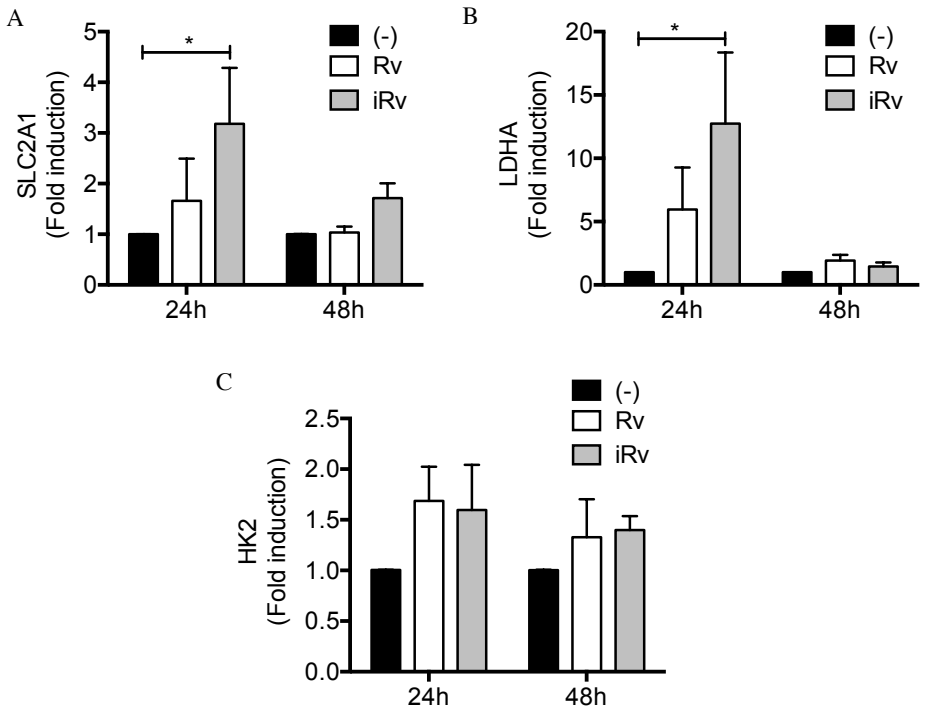

Figure 4.25 Irradiated Mtb induces a stronger glycolytic transcriptional signature than live Mtb in human alveolar macrophages. Human AM were isolated from bronchoalveolar lavage fluid and allowed 24 hours to recover. The cells were then infected with live Mtb (strain H37Rv) (Rv) or irradiated Mtb (strain H37Rv) (iRv) at an MOI of 5 bacteria per cell for 24 hours. RNA was isolated and qPCR was performed. Expression of *Slc2a1* (A), *Hk2* (B) and *LdhA* (C) mRNA relative to the untreated control was calculated. Data were normalised to 18S. Statistical analysis was performed using a paired, two-tailed Student's t-test. *, ** and *** represent $p<0.05$, 0.01 and 0.001 respectively. Data shown as mean ± SEM, n = 3 individual experiments.

4.2.8 miR-21 knockout macrophages do not use more glucose than wild-type macrophages

miR-21 deficient macrophages were found to be more glycolytic following pro-inflammatory stimulation, producing more lactate, having a higher ECAR:OCR ratio and inducing higher levels of pro-glycolytic genes.

As further confirmation of this more glycolytic metabolic profile, glucose consumption was measured. Glucose depletion from media was measured at the 72 hour time point as this was reflective of the end-point of bacterial growth experiments. Unexpectedly, there was no difference in the consumption of glucose between genotypes either basal or after Mtb infection (**Figure 4.26**). This suggests that it is not glucose uptake but rather the kinetics of glycolysis and the metabolic utilisation of glucose altered in miR-21 silenced macrophages.

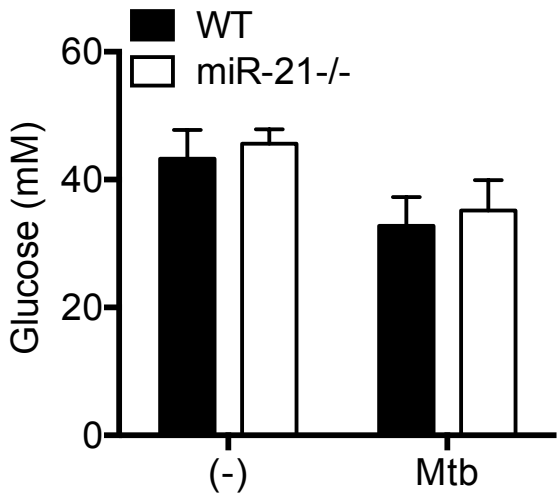

Figure 4.26 Wild-type and miR-21 deficient macrophages consume the similar amounts of glucose. BMDM were infected with H37Ra at an MOI of 5 bacteria per cell for 72 hours. Supernatant was collected and glucose concentration measured by a colorimetric enzyme assay. Statistical analysis was performed using a paired, two-tailed Student's t-test. *, ** and *** represent $p<0.05$, 0.01 and 0.001 respectively. Data shown as mean ± SEM, n = 6 independent experiments.

4.2.9 PFK-M is a novel target of miR-21

miR-21 deficient macrophages were found to be more glycolytically active but not to consume more glucose after Mtb infection. This indicated that miR-21 could target a key process in the glycolytic pathway and thus limit glycolytic activity.

In silico analysis for potential mRNA targets of miR-21 was carried out. An isoform of the enzyme in the first committed step in glycolysis, phosphofructokinase muscle-type (PFK-M), was found to have a target site for miR-21 that was highly conserved across species in its 3'UTR near the open reading frame. In contrast, the other two isoforms of this enzyme (platelet- and liver-type) have much shorter 3'UTR indicating they are less subject to transcriptional regulation (306 and 519 nucleotides compared to 2440) (**Figure 4.27A-C**). Additionally, there are no predicted binding sites for miR-21 in the PFK-P or PFK-L 3'UTR, and PFK-L has no highly conserved predicted microRNA binding sites. A schematic of the PFK-1 isoform mRNAs showing the presence of the miR-21 site and the mutant construct used in the luciferase assay is shown in **Figure 4.27D**.

To assess whether this predicted targeting of PFK-M by miR-21 can occur, the 3'UTR was cloned into a luciferase reporter plasmid. HEK293T cells were transfected with the PFK-M 3'UTR reporter or a control reporter which had the predicted miR-21 binding site mutated. Cells were then transfected with a miR-21 mimic or a negative control mimic and luciferase expression was assayed. Transfection with miR-21 mimic resulted in a significant dose-dependent decrease in luciferase activity (**Figure 4.28**). This decrease in expression was not observed when a similar construct in which the miR-21 site was mutated was used.

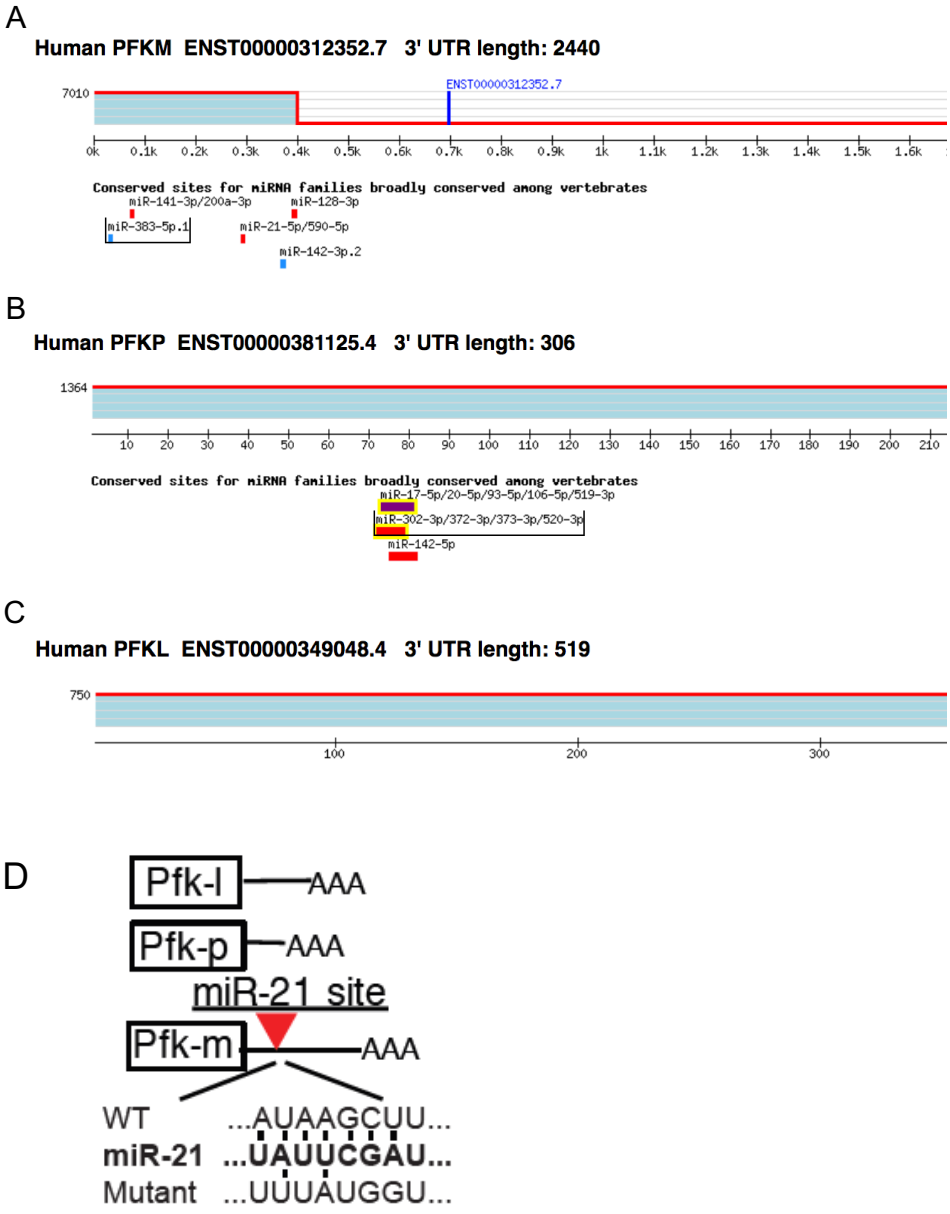

Figure 4.27 The 3'UTR of PFK-M, -P and -L. Predicted microRNA binding sites in the 3'UTR of all three PFK isoforms were examined using TargetScan, version 7 (A-C). The 3'-UTR profiles represent the prevalence of tandem 3' UTR isoforms of differing lengths, all of which share the same stop codon[365]. Schematic of the PFK-1 isoform mRNAs showing the presence of the miR-21 site and the mutant construct used in the luciferase assay.

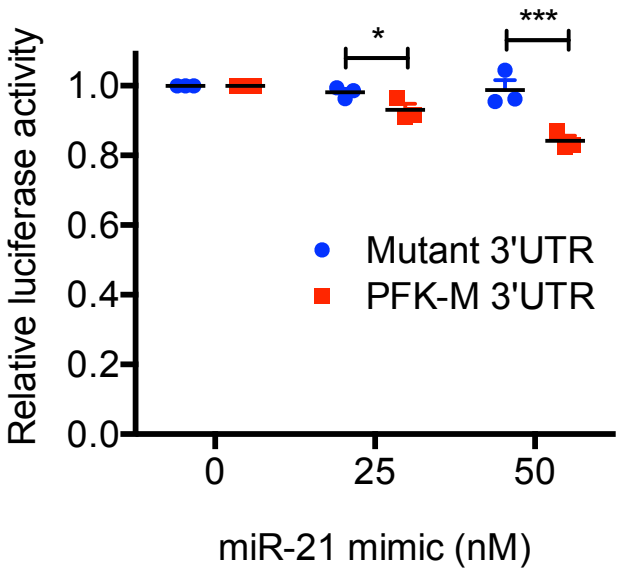

Figure 4.28 The 3'UTR of PFK-M is directly targeted by miR-21. HEK293T cells were transfected with a luciferase reporter plasmid linked to the 3'UTR of PFK-M or a scrambled control plasmid. Cells were then transfected with a miR-21 mimic for 24 hours and firefly luciferase activity assayed. Data were normalised to linked Renilla control luciferase activity. Statistical analysis was performed using a paired, two-tailed Student's t-test. *, ** and *** represent $p<0.05$, 0.01 and 0.001 respectively. Data shown as mean ± SEM, n = 3 independent experiments.

4.2.10 PFK-M mRNA is elevated in the absence of miR-21

The results from the luciferase assay indicated that miR-21 had the potential to target PFK-M, thus further characterisation of the PFK isoforms in the context of infection was warranted. The delta Ct values of all three isoforms in resting murine BMDM and AM were obtained by qPCR in order to determine the relative expression of each isoform. Delta Ct (cycle threshold) is the number of cycles required for the fluorescent signal to cross the threshold (i.e. exceed background levels), taking into account the expression of a housekeeping gene measured in the same sample. dCt levels are inversely proportional to the amount of target nucleic acid in the sample, i.e. the lower the Ct level the greater the amount of target nucleic acid in the sample. PFK-P and PFK-L had comparable expression levels in resting macrophages in both macrophage populations, while PFK-M had lower relative expression compared to the other two isoforms (**Figure 4.29**). There was no significant difference in PFK isoform expression between genotypes. PFK-M represented a lower proportion of the isoform present in AM than in BMDM.

Expression of PFK-P and PFK-L was induced by Mtb infection and LPS in both genotypes (**Figure 4.30A and B**). There were no significant differences basally but PFK-L expression was significantly higher after infection. By contrast, PFK-M was slightly enhanced by LPS but was not by Mtb infection in wild-type cells (**Figure 4.30C**). miR-21-deficient cells however significantly induced PFK-M following Mtb infection. Importantly, unlike the other two isoforms, PFK-M trended towards higher basal expression in miR-21-deficient cells.

PFK isoform expression was also examined in murine alveolar macrophages. Interestingly there was no induction of PFK-P or PFK-L after infection with Mtb and no difference in expression of

PFK-P or PFK-L between genotypes (**Figure 4.31A and B**). PFK-M was not induced by Mtb infection in wild-type AM, however a significant 3-fold induction of observed in miR-21 knockout AM (**Figure 4.31C**).

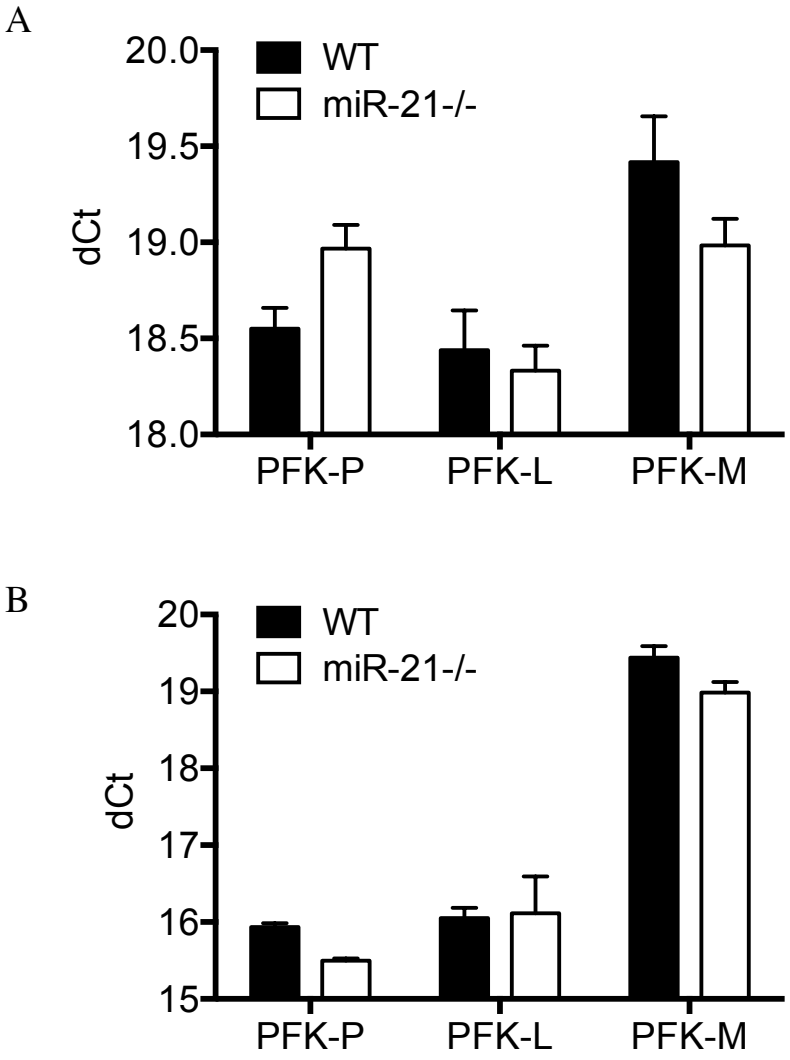

Figure 4.29 Relative expression of PFK isoforms in resting murine BMDM and AM. RNA was isolated from wild-type and miR-21 knockout BMDM (A) and AM (B) and qPCR was performed. Delta Ct values of *Pfk-p*, *Pfk-l* and *Pfk-m* mRNA were obtained. Data were normalised to 18S. Statistical analysis was performed using a paired, two-tailed Student's t-test. *, ** and *** represent $p<0.05$, 0.01 and 0.001 respectively. Data shown as mean ± SEM, n = 3 independent experiments.

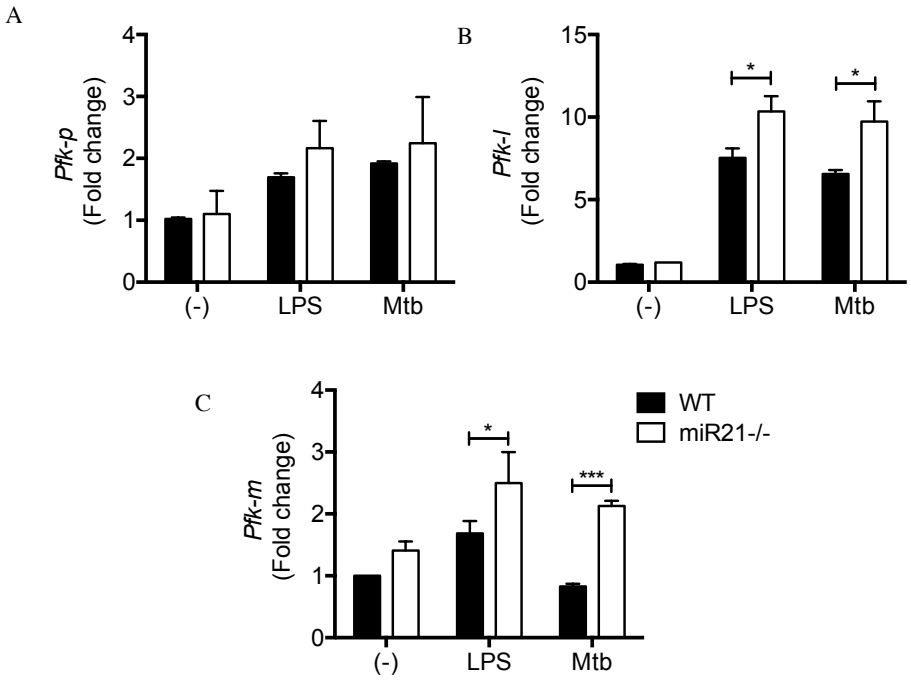

Figure 4.30 Expression of PFK isoforms in wild-type and miR-21 knockout BMDM. Wild-type and miR-21 knockout BMDM were infected with live Mtb (strain H37Ra) at an MOI of 5 bacteria per cell or 100 ng/mL LPS for 24 hours. RNA was isolated and qPCR was performed. Expression of *Pfk-p* (A), *Pfk-l* (B) and *Pfk-m* (C) mRNA relative to the untreated control was calculated. Data were normalised to 18S. Statistical analysis was performed using a paired, two-tailed Student's t-test. *, ** and *** represent $p<0.05$, 0.01 and 0.001 respectively. Data shown as mean ± SEM, n = 3 independent experiments.

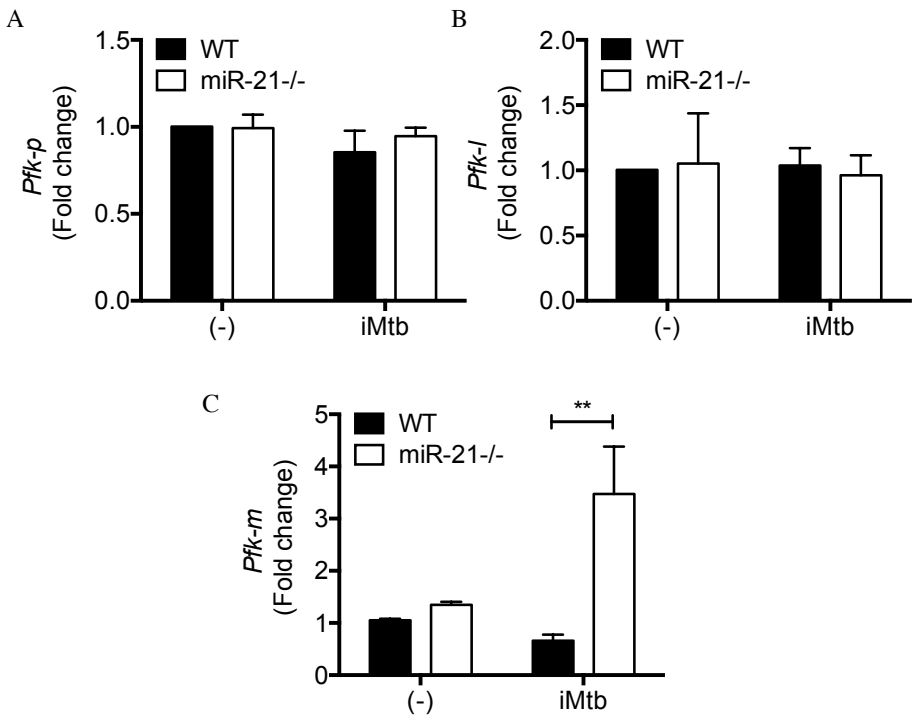

Figure 4.31 Expression of PFK isoforms in wild-type and miR-21 knockout murine AM. Wild-type and miR-21 knockout AM were infected with irradiated Mtb (strain H37Rv) at an MOI of 5 bacteria per cell for 24 hours. RNA was isolated and qPCR was performed. Expression of *Pfk-p* (A), *Pfk-l* (B) and *Pfk-m* (C) mRNA relative to the untreated control was calculated. Data were normalised to 18S. Statistical analysis was performed using a paired, two-tailed Student's t-test. *, ** and *** represent $p<0.05$, 0.01 and 0.001 respectively. Data shown as mean ± SEM, n = 3 mice per genotype in one experiment.

4.2.11 PFK-M protein is higher in the absence of miR-21

The enhanced PFK-M mRNA expression detected basally and in response to Mtb infection in miR-21 knockout macrophages, alongside the luciferase data which showed decreased activity with increasing dose of miR-21 mimic, indicated that PFK-M is a direct target of miR-21. For microRNA targeting of a specific gene to have a functional consequence, it must ultimately affect protein expression. PFK-M protein was therefore measured by Western blot in wild-type and miR-21 knockout macrophages basally and after infection with Mtb. Unexpectedly given the PCR data in which Mtb did not increase PFK-M mRNA in wild-type macrophages (**Figure 4.30C**), PFK-M protein was boosted by infection in both genotypes, but crucially was higher in miR-21 knockout BMDM both basally and after Mtb infection (**Figure 4.32**).

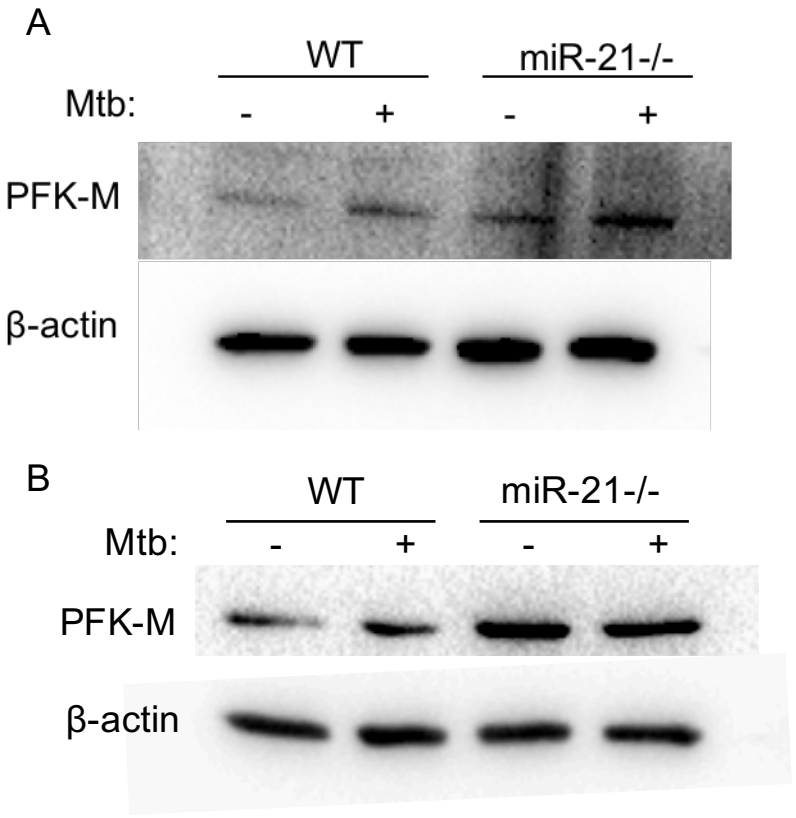

Figure 4.32 miR-21 knockout BMDM express more PFK-M protein. Wild-type and miR-21 knockout BMDM were infected with H37Ra at an MOI of 5 bacteria per cell for 24 hours. Protein was isolated and western blot was performed. PFK-M and β-actin were detected with monoclonal antibodies. Two blots (A and B) were generated.

4.2.12 PFK activity is higher when miR-21 activity is blocked

Studies into the nature of the different PFK isoforms have indicated that PFK-M has an increased affinity for its substrate (fructose-6-phosphate) which permits higher activity[238, 366]. To assess whether this enhanced presence of PFK-M protein in miR-21 deficient macrophages was of functional consequence to total PFK enzyme activity, the activity of the total PFK-1 tetrameric enzyme was measured using a coupled enzyme assay. The assay provides an excess of substrate and ATP which are converted by PFK present in the cell lysates being tested to fructose-1,6-diphosphate and ADP. An enzyme mix converts the ADP to AMP and NADH. The NADH then reduces a probe to produce a coloured product which can be detected by spectrophotometry.

PFK activity was found to be basally significantly higher in miR-21 knockout macrophages (**Figure 4.33A**). Crucially, this activity was significantly reduced in wild-type BMDM following infection with Mtb, however infected miR-21 knockout BMDM maintained the same level of PFK activity as when uninfected. Furthermore, there was no difference found in hexokinase kinase activity basally between genotypes (**Figure 4.33B**). This earlier step in the glycolytic pathway showed significantly enhanced activity in miR-21 knockout BMDM only after Mtb infection consistent with enhanced glycolysis and upregulation of HK2.

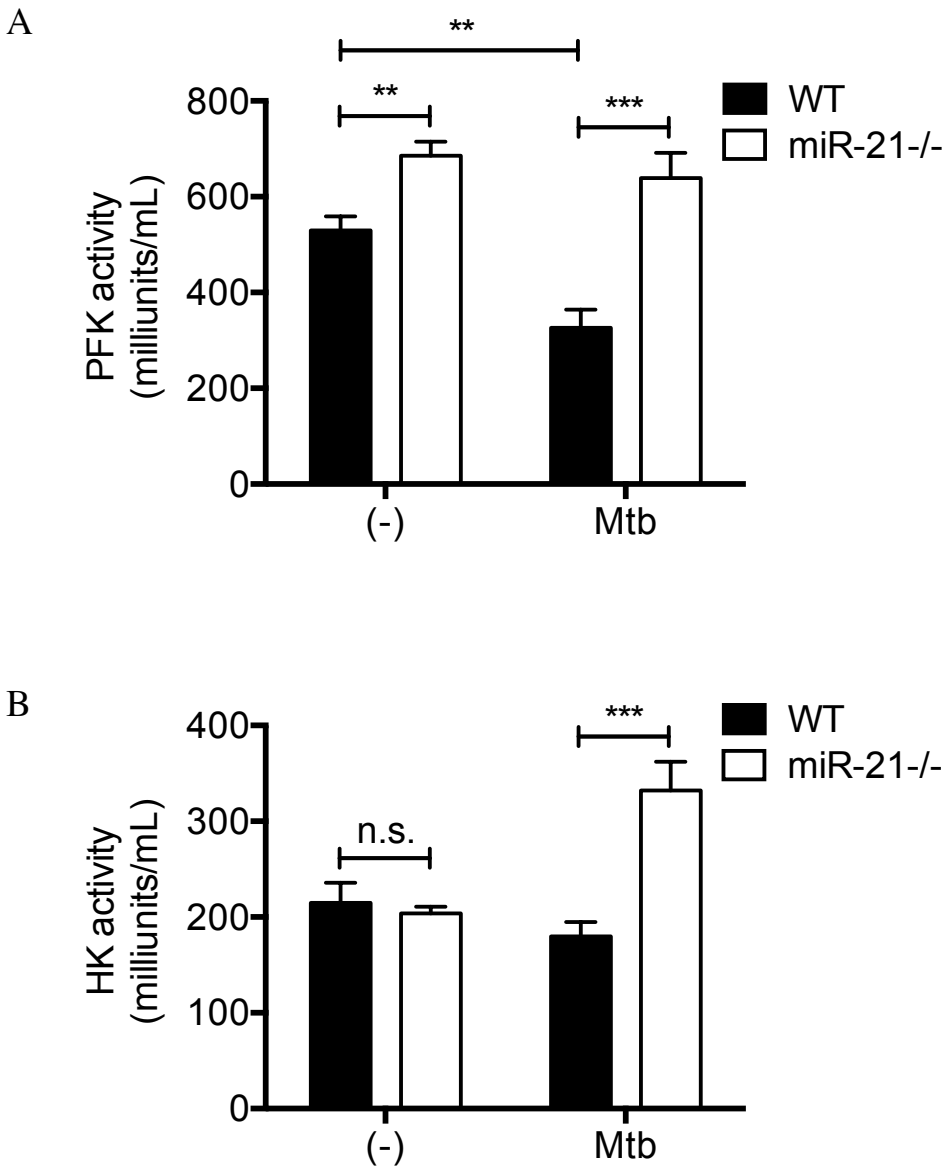

Figure 4.33 miR-21 deficient BMDM have higher basal phosphofructokinase activity than wild type BMDM. Wild-type and miR-21 knockout BMDM were infected with H37Ra at an MOI of 5 bacteria per cell for 24 hours. Cells were homogenised and colorimetric enzyme assays were used to measure (A) phosphofructokinase activity and (B) hexokinase activity. Statistical analysis was performed using a paired, two-tailed Student's t-test. *, ** and *** represent $p<0.05$, 0.01 and 0.001 respectively. Data shown as mean ± SEM, n = 6 and 5 mice per genotype spread over 3 independent experiments.

While macrophage PFK enzyme tetramers are heterotetramers of all 3 PFK isoforms, other tissues express one isoform more predominantly. Liver tissue PFK is composed of only PFK-L homotetramers, while heart tissue expresses a high proportion of PFK-M subunits. To confirm that miR-21 restricts PFK-M expression and activity in vivo, fresh liver and heart tissue was isolated from wild-type and miR-21 knockout mice and PFK activity measured. No difference in PFK enzyme activity was observed in the liver tissue between genotypes (**Figure 4.34A**) but strikingly, miR-21 knockout cardiac tissue had significantly higher PFK activity. As had been noted in macrophages, no significant difference in hexokinase activity was noted in either tissue (**Figure 4.34B**). Hexokinase enzyme activity was notably low in the liver tissue, where the predominant form of hexokinase, hexokinase IV, requires high glucose concentration for activity, not accounted for in this assay.

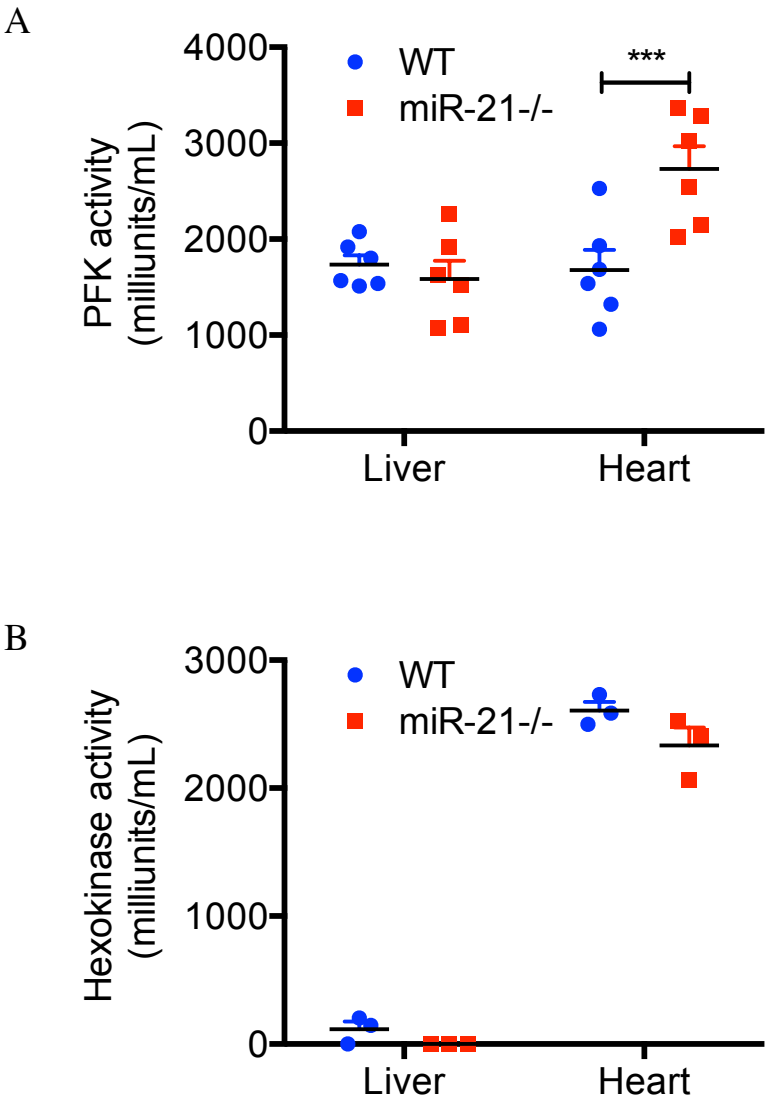

Figure 4.34 miR-21 deficient cardiac tissue has higher phosphofructokinase activity than wild-type. Equal weights of fresh liver and heart tissue from wild-type and miR-21 knockout mice were homogenised and colorimetric enzyme assays were used to measure (A) phosphofructokinase activity and (B) hexokinase activity. Statistical analysis was performed using a paired, two-tailed Student's t-test. *, ** and *** represent $p<0.05$, 0.01 and 0.001 respectively. Data shown as mean ± SEM, n = 3 mice per genotype in 2 independent experiments in (A) and n = 3 mice per genotype in one experiment in (B).

4.2.13 Blocking the interaction between miR-21 and PFK-M mRNA boosts PFK-M protein levels

Having demonstrated that PFK-M is a direct target of miR-21, to further confirm that this targeting affects macrophage responses to Mtb infection a target protection strategy was employed. Morpholino oligonucleotides are small, stable, modified oligonucleotides that block specific RNA interactions. A target-protecting morpholino was designed which binds to the predicted target site for miR-21 in the 3'UTR of PFK-M and blocks only this microRNA-mRNA interaction. This is far more specific than total blockade of miR-21 which would abolish other potential miR-21/mRNA interactions including PDCD4 and PTEN (**Figure 4.35**).

Firstly, the efficacy of the morpholino was verified. Wild-type BMDM were transfected with the target-protecting morpholino or a negative control morpholino and infected with Mtb. PFK-M protein was then measured by Western blot. The target protector enhanced PFK-M protein both basally and, more potently, following infection with Mtb (**Figure 4.36**).

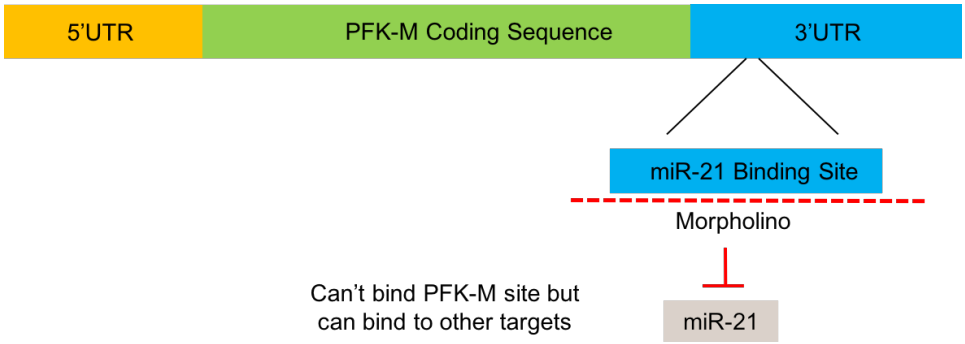

Figure 4.35 Mechanism of action of miR-21/PFK-M target protector. A target protecting morpholino specific for the miR-21 binding site in the 3'UTR of PFK-M is transfected into cells. The morpholino blocks miR-21 from binding to this target site however while allowing miR-21 to bind other targets.

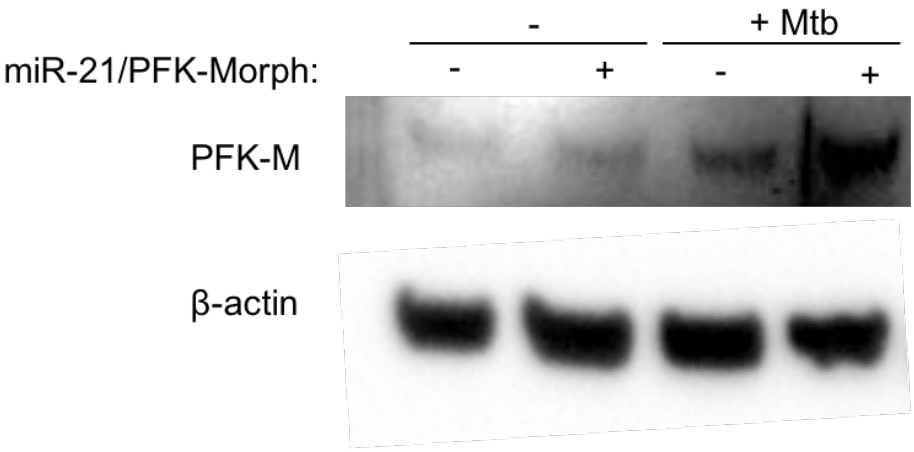

Figure 4.36 PFK-M protein is higher in BMDM treated with a miR-21/PFK-M target protector. Wild-type BMDM were transfected with 10 μM of a non-targeting morpholino or a PFK-M/miR-21 target protector morpholino. Cells were infected with H37Ra at an MOI of 5 bacteria per cell for 24 hours. Protein was isolated and western blot was performed. PFK-M and β-actin were detected with monoclonal antibodies.

4.2.14 Blocking miR-21 targeting of PFK-M boosts glycolysis and production of IL-1β

Having shown that the morpholino could enhance PFK-M protein expression, the functional outcome of this was assessed. Firstly, to test the efficacy of the morpholino, wild-type BMDM were transfected with two concentrations of target-protecting morpholino and infected with non-viable Mtb. Lactate was measured and found to be unchanged by transfection with the negative control morpholino, however the target-protecting morpholino significantly enhanced the production of lactate in response to iMtb infection, particularly at the 10 μM concentration (**Figure 4.37A**). IL-1β also showed a dose-dependent increase in expression in response to target-protecting morpholino treatment (**Figure 4.37B**). Hypothesis outlined in **figure 4.37C**.

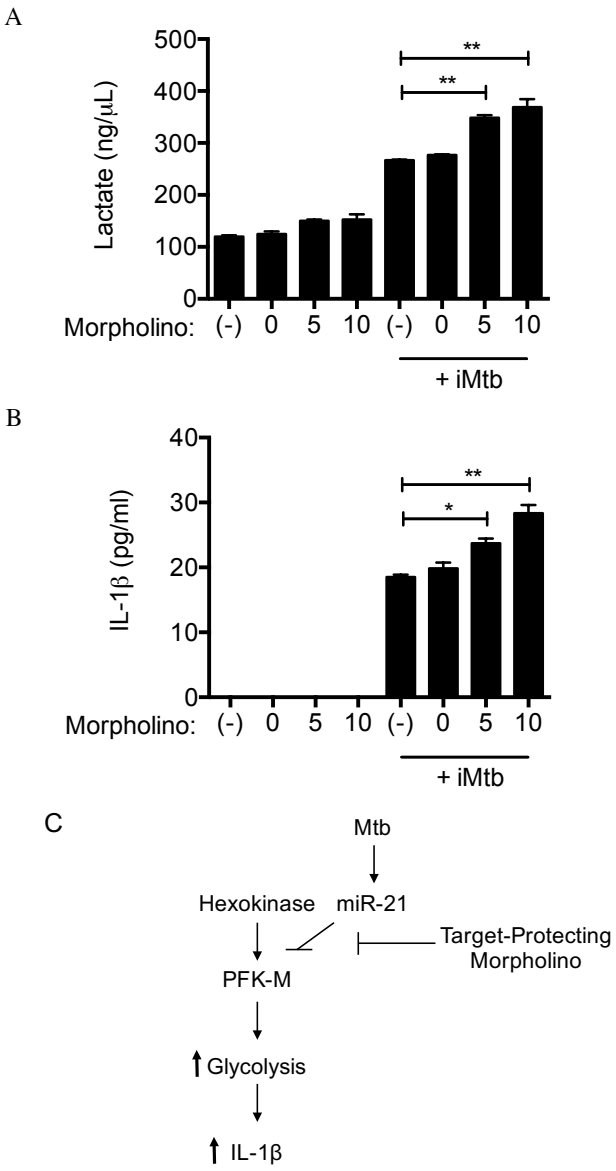

Figure 4.37 Protection of miR-21 target site in PFK-M 3'UTR enhances lactate production and IL-1β protein secretion in wild-type BMDM. Wild-type and miR-21 knockout BMDM were untransfected, transfected with 10 μM of a non-targeting morpholino or 5 and 10 μM of the PFK-M/miR-21 target protector morpholino. Cells were infected with non-viable iH37Rv at an MOI of 5 bacteria per cell for 24 hours. Supernatants were collected and lactate (A) and IL-1β protein measured (B). Hypothesis diagram shown in (C). Statistical analysis was performed using a paired, two-tailed Student's t-test. * and ** represent $p<0.05$ and 0.01 respectively. Data shown as mean ± SEM, n = 2 independent experiments.

10 μM of morpholino was found to significantly enhance lactate and IL-1β protein in response to non-viable Mtb infection. This concentration of morpholino was then used to investigate the effect of the target protection in live Mtb infection in both wild-type and miR-21 knockout BMDM. Macrophages were transfected with morpholino and infected with Mtb. Lactate was measured and found to be unchanged by transfection with the negative control morpholino, however the target-protecting morpholino significantly enhanced the production of lactate in response to Mtb infection in wild-type BMDM (**Figure 4.38A**). Importantly, the target-protecting morpholino had no effect on lactate production in miR-21-deficient BMDM (**Figure 4.38B**). Lactate production after Mtb infection was significantly higher in miR-21 knockout BMDM except when wild-type BMDM were treated with morpholino. Morpholino treatment boosted lactate production to a comparable level as that seen in miR-21-deficient macrophages.

Similarly, IL-1β protein was significantly higher in wild-type BMDM treated with target-protecting morpholino (**Figure 4.39A**) and boosted IL-1β protein in wild-type BMDM to a level not significantly different from miR-21 knockout BMDM (**Figure 4.39B**).

This boost in lactate production and IL-1β protein is indicative of enhanced glycolysis when miR-21 is prevented from degrading PFK-M after Mtb infection. Further evidence for the specificity of this effect was seen when TNF-α and IL-10 protein were examined after morpholino treatment. No significant difference was found for either of these cytokines after morpholino treatment, indicating that the earlier observed differences in these processes, which did not contribute to Mtb protection, were mediated by other miR-21 targets (**Figure 4.40**).

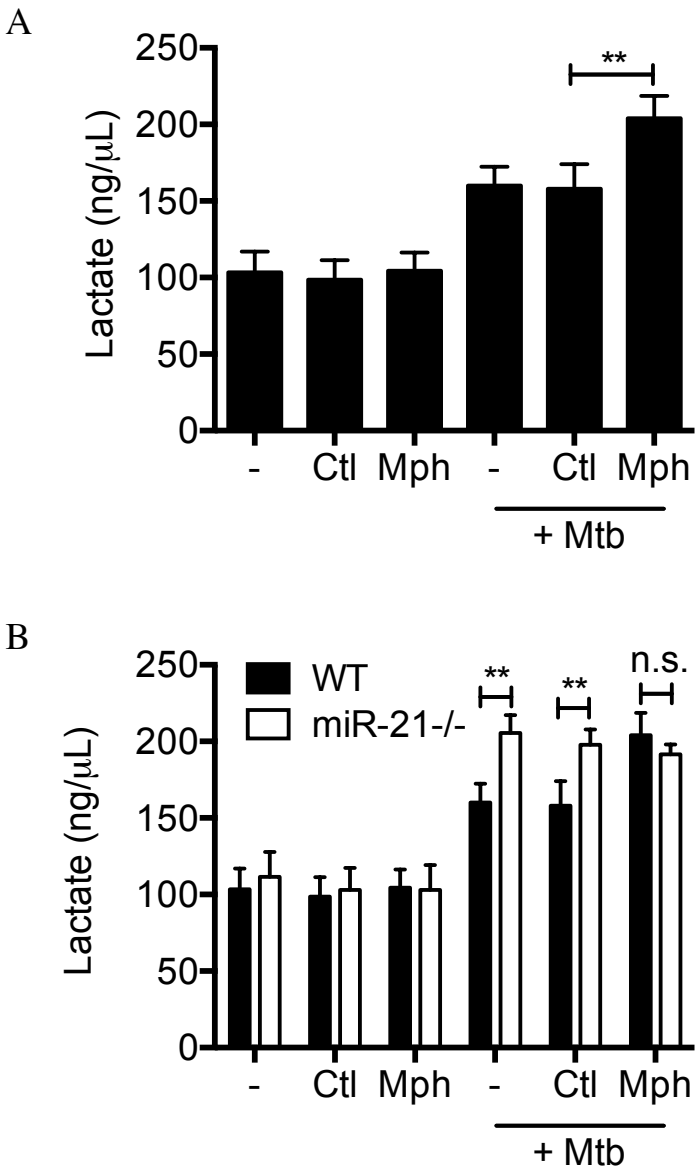

Figure 4.38 Protection of miR-21 target site in PFK-M 3'UTR enhances lactate production in wild-type BMDM. A) Wild-type and B) wild-type and miR-21 knockout BMDM were transfected with 10 μM of a non-targeting morpholino or a PFK-M/miR-21 target protector morpholino. Cells were infected with live H37Ra at an MOI of 5 bacteria per cell for 24 hours. Supernatants were collected and lactate measured by colorimetric assay. Statistical analysis was performed using a paired, two-tailed Student's t-test. *, ** and *** represent $p<0.05$, 0.01 and 0.001 respectively. Data shown as mean ± SEM, n = 6 independent experiments.

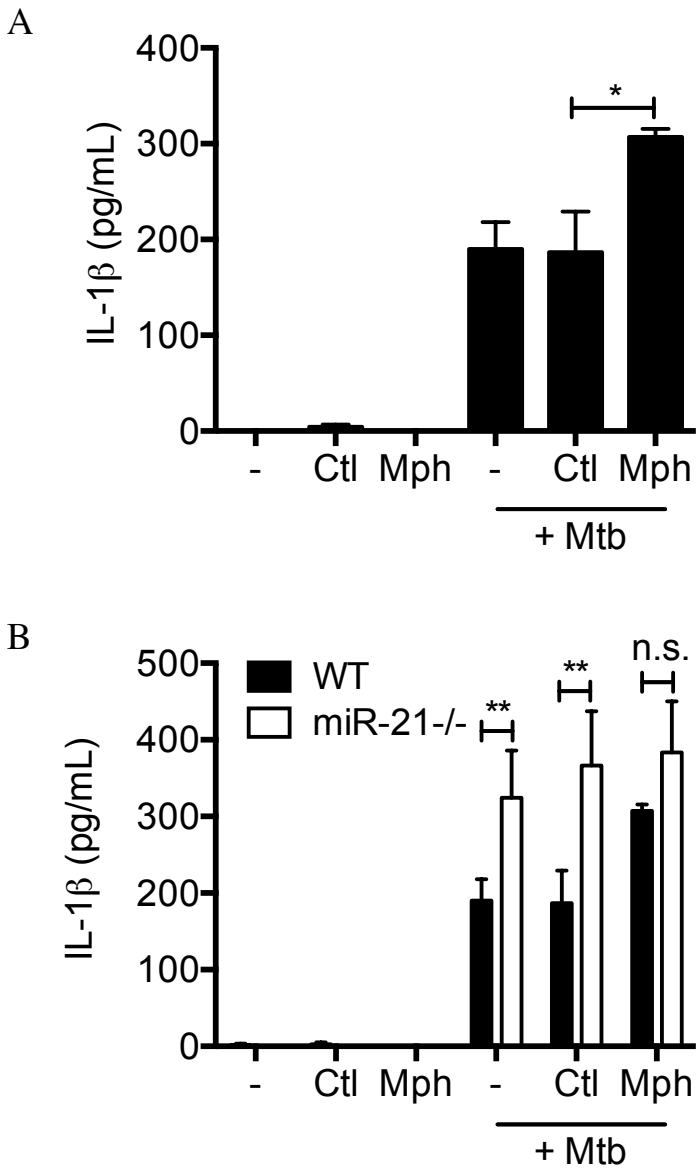

Figure 4.39 Protection of miR-21 target site in PFK-M 3'UTR enhances IL-1β production in wild-type BMDM. A) Wild-type and B) wild-type and miR-21 knockout BMDM were transfected with 10 μM of a non-targeting morpholino or a PFK-M/mR-21 target protector morpholino. Cells were infected with live H37Ra at an MOI of 5 bacteria per cell for 24 hours. Supernatants were collected and IL-1β protein measured by ELISA. Statistical analysis was performed using a paired, two-tailed Student's t-test. *, ** and *** represent $p<0.05$, 0.01 and 0.001 respectively. Data shown as mean ± SEM, n = 3 independent experiments.

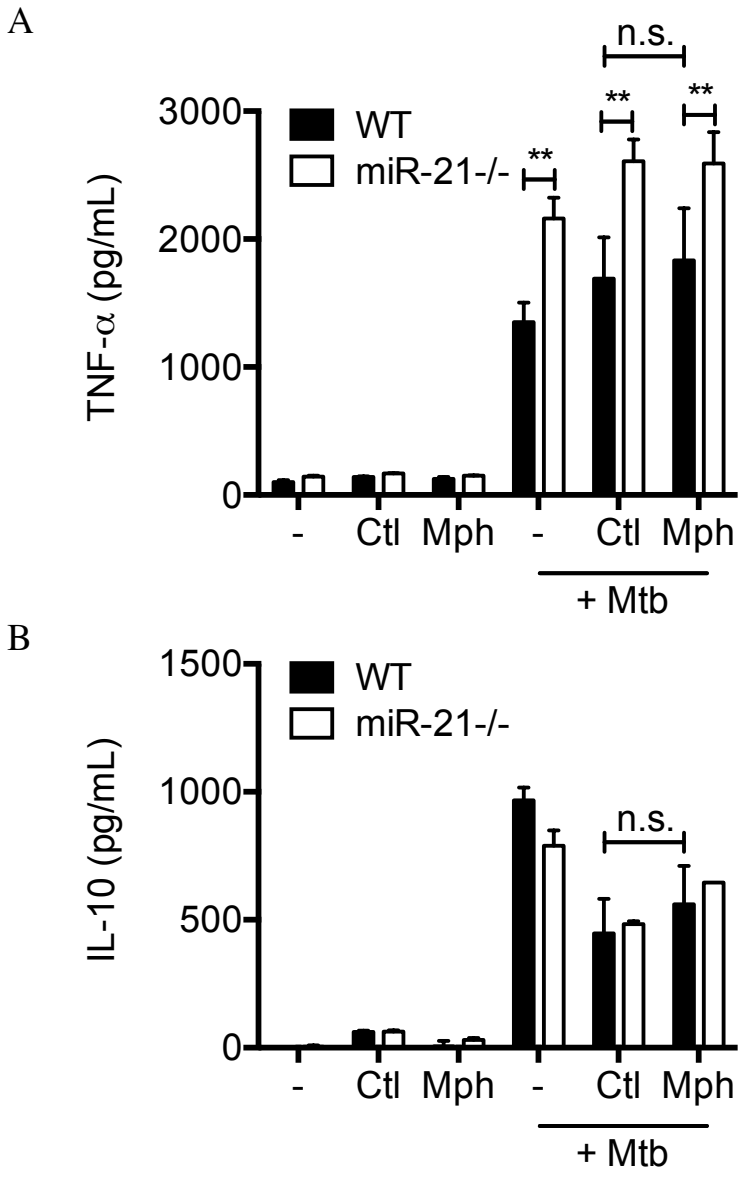

Figure 4.40 Protection of miR-21 target site in PFK-M 3'UTR does not alter TNF-α or IL-10 production. A) Wild-type and B) wild-type and miR-21 knockout BMDM were transfected with 10 μM of a non-targeting morpholino or a PFK-M/miR-21 target protector morpholino. Cells were infected with live H37Ra at an MOI of 5 bacteria per cell for 24 hours. Supernatants were collected and TNF-α (A) and IL-10 (B) protein measured by ELISA. Statistical analysis was performed using a paired, two-tailed Student's t-test. *, ** and *** represent $p<0.05$, 0.01 and 0.001 respectively. Data shown as mean ± SEM, n = 3 independent experiments.

4.2.15 Blocking miR-21 targeting of PFK-M enhances containment of Mtb growth

Finally, the consequence of blocking miR-21 from binding to PFK-M on the outcome of Mtb infection was assessed. BMDM were transfected with target-protecting or negative control morpholino and infected with live Mtb for 72 hours and bacterial growth observed.

Blocking miR-21 binding to PFK-M resulted in a significant reduction in Mtb growth in wild-type BMDM, bringing CFU counts to a level comparable to that of the miR-21 knockout BMDM (**Figure 4.41**).

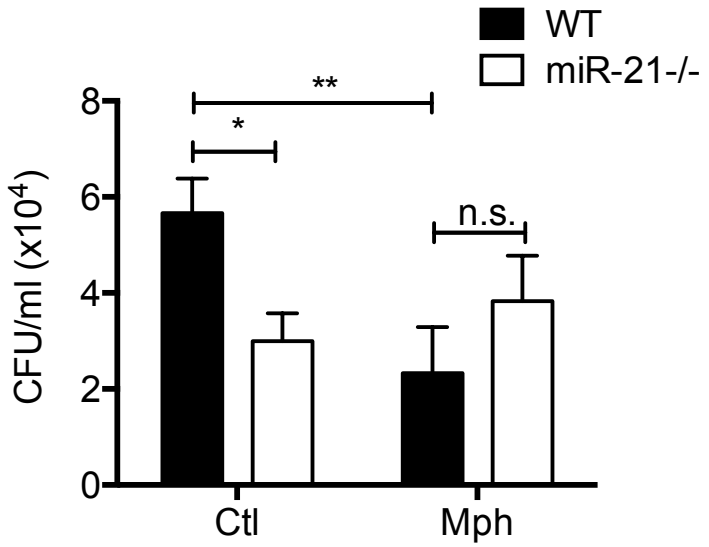

Figure 4.41 Protection of miR-21 target site in PFK-M 3'UTR enhances containment of Mtb growth in wild-type BMDM. Wild-type and miR-21 knockout BMDM were transfected with 10 μM of a non-targeting morpholino or a PFK-M/miR-21 target protector morpholino. Cells were infected with live H37Ra at an MOI of 5 bacteria per cell for 72 hours. Cells were lysed in 0.1% Triton X-100 and the lysates diluted in Middlebrook broth supplemented with ADC. Aliquots of the lysates were then streaked in triplicate on warm Middlebrook agar plates and incubated at 37°C for approximately 14 days. Colony forming units were counted. Statistical analysis was performed using a paired, two-tailed Student's t-test. *, ** and *** represent $p<0.05$, 0.01 and 0.001 respectively. Data shown as mean ± SEM, n = 3 mice per genotype.

4.3 Discussion

4.3.1 miR-21 is a regulator of macrophage glycolysis

The previous chapter found that miR-21 suppresses induction of IL-1β mRNA and protein and this facilitates Mtb growth within the macrophage. The mechanism by which miR-21 targets IL-1β was elucidated in this chapter.

Though Fabri et al showed that miR-21 could target the IL-1β 3'UTR, this was not confirmed in any functional studies blocking this interaction[163]. Actinomycin D experiments which reflect mRNA stability showed that IL-1β mRNA was more stable after Mtb infection in both wild-type and miR-21-deficient macrophages (**Figure 4.1**), indicating that though miR-21 may target IL-1β basally, Mtb-induced IL-1β mRNA is more stable and not subject to direct miR-21 regulation. MiR-21 may regulate IL-1β turnover or basal expression in some cells but may not be as important in macrophages. MiR-21-mediated repression of IL-1β may operate differently in activated cells where the expression of IL-1β is hugely increased and constantly triggered, and therefore less subject to direct regulation by miR-21. Furthermore, IL-1β had been found to be significantly higher in miR-21-depleted macrophages particularly at later time-points. Given that it is known that glycolytic reprogramming in activated macrophages has been shown to potentiate the later transcription of IL-1β through HIF-1α stabilisation[176, 239], this led to the hypothesis that miR-21 could be regulating the induction of glycolysis to control inflammation.

MiR-21-deficient macrophages (murine BMDM and AM and human MDM) were found to produce more lactate in response to pro-inflammatory stimuli including Mtb, indicative of increased glycolysis (**Figures 4.2-4.6**). Lactate accumulated to a higher

extent over the course of Mtb infection in miR-21-deficient macrophages suggesting a sustained induction of glycolysis in the absence of miR-21. Importantly, blocking IL-1β activity with a monoclonal antibody did not alter lactate production, indicating that increased lactate is promoting IL-1β production rather than a consequence of it (**Figure 4.7**). Blocking glycolysis did not alter miR-21 induction (**Figure 4.8**), however it was found to significantly inhibit bacterial containment in both wild-type and miR-21-deficient BMDM (**Figure 4.9**). Macrophages treated with 2-DG were unable to contain Mtb growth even in the early stages of infection. This finding is in line with similar reports in the literature[204]. Blocking glycolysis was found to partially reduce total TNF-α induction in response to Mtb, but miR-21-defiicent macrophages retained their phenotypic trait of higher induction (**Figure 4.10**). Contrastingly, IL-1β was more drastically stunted by 2-DG treatment and miR-21-deficient macrophages retained no advantage, highlighting the importance of glycolysis for IL-1β production and the dependence of the miR-21-deficient macrophage phenotype on glycolysis. Nitrite induction (**Figure 4.12**) in response to Mtb was also drastically stunted when glycolysis was impaired. MiR-21-deficient macrophages retained some enhanced nitrite production but the level was still dramatically lower than glycolytically-competent Mtb infected macrophages. This is reflective of the key role in glycolysis and the activation of HIF-1α[164] in driving the production of nitric oxide species. It should be noted that while lactate is a product of glycolysis, it can also be indicative of necrotic cell death which may improve bacterial containment in vitro by reducing the number of macrophages available for replication. The viability of macrophages of both genotypes after infection should be measured alongside lactate production to separate the contributions of glycolysis and necrotic cell death to the production of lactate and ultimately the containment of Mtb.

Extracellular flux analysis provided a more distinct profile of the metabolic profile of the activated macrophages. Consistent with the literature[176], LPS drove ECAR, representative of the induction of glycolysis, though no concomitant significant decrease in OCR was observed in this model. Irradiated Mtb was found to drive a similar induction of ECAR and significantly enhanced the ECAR:OCR ratio, indicative of glycolytic reprogramming (**Figure 4.14**). LPS is reported to block the TCA and consequently, there is a compensatory increase in glycolysis which is maintained. In this model of Mtb infection, there is no reduction in TCA cycle activity, while glycolysis is upregulated and this glycolytic induction in limited by Mtb via miR-21. Mtb infection has been shown to trigger fatty acid oxidation, the metabolites of which would feed the TCA cycle, and this may be why no downregulation is seen. Given this observation, the initial hypothesis that miR-21 acts a switch regulating the shift from oxidative phosphorylation to glycolysis can be revised. The results rather indicate that in Mtb infection, miR-21 limits glycolytic induction without affecting the rate of oxidative phosphorylation. As predicted by the lactate results, both iMtb and LPS induced significantly ECAR and the ECAR:OCR ratio significantly higher in miR-21-definicent macrophages. Though there was no difference in spare respiratory capacity between the genotypes, miR-21 knockout macrophages had a significantly higher glycolytic reserve even after infection, suggesting that miR-21-deficient cells had an increased potential to accelerate glycolysis when stressed (**Figure 4.18**). This phenotype was mirrored in human MDM in which miR-21 had been knocked down. Consistent with this phenotype higher induction of glycolytic genes including the glucose transporter Slc2a1, hexokinase 2 and lactate dehydrogenase A were significantly higher in miR-21-defiicent BMDM after Mtb infection or LPS stimulation (**Figure 4.22**). This enhanced glycolytic gene expression after iMtb infection was also seen in miR-21 deficient alveolar macrophages, though both Slc2a1 and HK2 were also more highly expressed basally in miR-

21 knockouts (**Figure 4.24**), consistent with some basal activation in these cells. Previous reports on how miR-21 limits innate immunity have focused on cytokine induction, however these results point at miR-21 as a key regulator of immunometabolism.

The unexpected finding that miR-21 knockout BMDM did not consume more glucose than wild-type BMDM after infection with Mtb (**Figure 4.26**) indicated that miR-21 could target a rate-limiting process in the glycolytic pathway, and perhaps the knockout phenotype (increased glycolytic rate, increased glycolytic reserve and increased bacterial containment) were as a result of a phenotype that allowed a burst of glycolysis, which could fuel pro-inflammatory processes at the critical stage of Mtb infection. This glucose assay is a crude measurement of the metabolic profile of the cell, and future studies tracking the fate of glucose in the miR-21-deficient macrophage would be of great interest.

In silico analysis identified the PFK-1 isoform PFK-M as a glycolytic enzyme with a highly conserved miR-21 binding site in its 3'UTR. Compared to the other isoforms of PFK-1, PFK-M mRNA has a long 3'UTR, indicative that it is subject to more transcriptional regulation (**Figure 4.27**). This miR-21 site is close to the open reading frame of PFK-M, another suggestion that it is of functional relevance. The PFK-M 3'UTR was cloned into a luciferase reporter and miR-21 levels were modulated. Suppression of luciferase activity with increasing concentrations of miR-21 mimic indicated that miR-21 could directly PFK-M (**Figure 4.28**). Importantly this suppression was lost when the predicted miR-21 binding site was mutated. The decrease in luciferase activity is modest but was highly consistent and dose-dependent and is in line with similar assays in the literature[367] and the concept that microRNAs are nuanced modulators of mRNA expression rather than potent inhibitors. This

result warranted further investigation of PFK-M in the miR-21-deficient model.

PFK-L and PFK-P were more represented than PFK-M, and expressed to as similar degree basally in wild-type macrophages, consistent with previous findings by Shi et al[231] (**Figure 4.29**). PFK-P was modestly boosted in response to Mtb infection, while PFK-L was significantly upregulated and was upregulated to a greater extent in miR-21 knockout macrophages (**Figure 4.30**). However, PFK-M demonstrated a differential expression pattern and was not upregulated in wild-type cells, as had been shown by Shi et al[231] by transcriptional profiling. Critically, miR-21-deficient macrophages were resistant to this Mtb suppression and levels were significantly higher and even modestly augmented, indicating that PFK-M is a target for miR-21. Interestingly, no induction of PFK-L or PFK-P was detected in murine alveolar macrophages following infection with Mtb, and no differences between genotypes were apparent, perhaps suggesting that the upregulation of PFKM is supporting increased glycolytic activation. PFK-M however was highly induced by Mtb infection in miR-21-deficient alveolar macrophages (**Figure 4.31**), again providing strong evidence that it is a miR-21 target of relevance in Mtb infection.

At the protein level, PFK-M was curiously modestly increased by Mtb infection in wild-type macrophages (**Figure 4.32**), despite not being significantly increased at the mRNA level. This may hint at post-transcriptional mechanisms by which PFK-M is stabilised after infection, not degraded, and is thus more easily detectable in the cytoplasmic pool. Of key importance, miR-21-deficient macrophages had significantly more PFK-M protein basally, and this was enhanced by Mtb infection, as was expected from the mRNA results. Furthermore, miR-21-deficient macrophages had

significantly greater PFK-1 enzyme activity than wild-type BMDM, and while Mtb infection reduced PFK-1 activity in wild-type cells, miR-21 knockout cells were resistant to this and retained their enzymatic capacity (**Figure 4.33**). Importantly, this effect was not observed in an earlier step in the glycolytic pathway, hexokinase activity was not down-regulated in wild-type cells in response to Mtb infection (**Figure 4.33**). These results support the idea that miR-21 negatively regulates PFK-M, targeting it for degradation after Mtb infection as a way to limit glycolysis. This is in line with the increased glycolytic activity in these cells, and reports that PFK-M is has a higher affinity for its substrate[363, 366], suggesting that PFK-1 tetramers in miR-21-deficient macrophages are comprised of a higher ratio of PFK-M subunits which allows them an increased propensity for enzymatic activity.

This idea that PFK-1 tetramer composition can be altered by the absence of miR-21 and affect the enzyme activity was further explored by examining PFK-1 activity in specific tissues in the murine model ex vivo. PFK-1 activity in liver tissue, which predominantly expresses the PFK-L isoform, was not significantly different (**Figure 4.34**), however cardiac tissue which expresses all three isoforms of PFK had significantly higher PFK-1 activity in miR-21 knockout animals, confirming that miR-21 can constrain glycolytic activity in vivo. As had been seen in the macrophage model, no difference in hexokinase activity was observed. Despite this, these mice have no gross phenotypical defects, and this key metabolic difference may only be revealed once the mice are challenged.

As further confirmation of direct miR-21 targeting of PFK-M to alter metabolic responses to Mtb infection, a target protection strategy was employed. A morpholino which specifically blocked the miR-

21/PFK-M interaction rather than total miR-21 activity was designed. Treatment of wild-type BMDM with the target-protecting morpholino boosted PFK-M protein both basally and to a greater extent after Mtb infection, i.e. treatment of wild-type macrophages with the miR-21/PFKM morpholino mimicked the miR-21-deficient phenotype (**Figure 4.36**). Consequently, morpolino-treated BMDM infected with iMtb also produced more lactate and IL-1β protein and this augmentation was dose-dependent (**Figure 4.37**). Similarly, when infected with live Mtb, wild-type BMDM treated with morpholino were able to boost lactate induction and IL-1β to the same extent as miR-21-deficient macrophages and no additional effect with morpholino treatment was observed in miR-21 knockout macrophages (**Figure 4.38 and 4.39**). Furthermore, TNF-α and IL-10 induction were not altered by morpholino treatment (**Figure 4.40**). Morpholino-treated wild-type macrophages were significantly better at containing Mtb growth, containing Mtb to a similar degree as miR-21 knockout cells. Together these results show that miR-21 directly targets PFK-M in the context of Mtb infection to limit its induction, and this results in less efficient constructs of the PFK-1 enzyme being formed, which in turn limit glycolysis, IL-1β and containment of Mtb.

4.4 Conclusion

Having observed increased levels of IL-1β production in miR-21 deficient cells, the role of miR-21 in glycolytic reprogramming was investigated. This chapter presents the novel finding that miR-21 negatively regulates glycolysis and that this renders the macrophages more permissive to Mtb infection. Furthermore, a new target for miR-21 has been identified – PFK-M. PFK-1 is a gatekeeper enzyme in the glycolytic pathway, however it has not been well studied in immunity. These results propose that PFK-M is differentially regulated to the other PFK-1 isoforms in Mtb infection, and that reduced PFK-M availability suppresses PFK-1 enzymatic activity and thus limits glycolysis and IL-1β. This supports the idea that miR-21 is a central regulator of immunometabolic responses in macrophages, but reveals a key role for PFK-1 activity in the control of metabolic reprogramming that is targeted by a successful human pathogen and therefore requires more investigation.

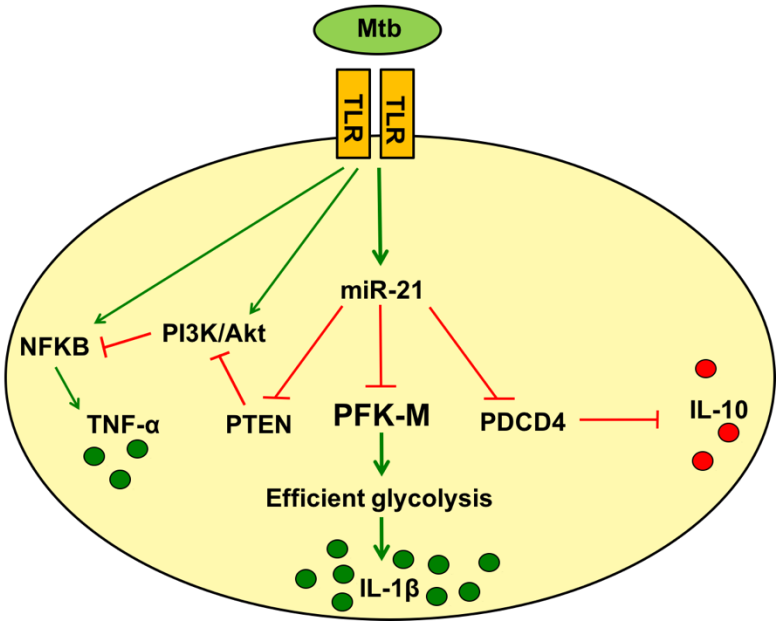

Figure 4.42. Diagram of the proposed model of key miR-21 targets in Mtb infection. MiR-21 expression is induced by Mtb infection in the macrophage downstream of TLR signalling. MiR-21 downregulates TNF-α expression by targeting PTEN. Targeting of the negative regulator of IL-10 expression, PDCD4, boosts IL-10 production. PFK-M is targeted by miR-21, resulting in lower PFK-1 enzyme activity, less efficient glycolytic activity and ultimately lower IL-1β production.

Chapter 5: Interferon-γ promotes macrophage glycolysis by targeting miR-21

5.1 Introduction

Macrophages are plastic and exist in a wide range of activation states[340]. After infection with Mtb, pro-inflammatory macrophage responses are induced, however these responses wane over time and are not always sufficient to contain Mtb growth[231]. Ways of augmenting anti-Mtb responses in macrophages are therefore of interest. IFN-γ is a central pro-inflammatory cytokine, known to coordinate macrophage activation and to be essential for anti-mycobacterial responses[82]. Clinical trials have indicated that IFN-γ, particularly when administered as an aerosol may be beneficial as an adjuvant therapy[166].

IFN-γ, mainly provided by T cells in the local environment, is a key mediator of macrophage activation and mycobacterial resistance. Patients suffering from Mendelian susceptibility to mycobacterial disease (MSMD) have a high susceptibility to clinical mycobacterial infections from weakly virulent mycobacteria including the BCG vaccine and non-tuberculous environmental bacteria as well as Mtb[153, 154, 155, 156, 157]. Furthermore, individuals who raise anti-IFN-γ autoantibodies are highly susceptible to both Mtb and opportunistic mycobacterial infections[158, 159, 160, 161]. Polymorphisms in the IFN-γ gene have been associated with Mtb susceptibility[368] and individuals with defects in the IFN-γ signalling pathway have increased risk of mycobacterial disease[369, 370].

Several key macrophage responses to Mtb are augmented by IFN-γ, mostly through triggering STAT1 homodimerisation and translocation to the nucleus[371]. IFN-γ also augments NFκB signalling[372], for example in response to TLR signalling during bacterial infection, IFN-γ can activate a unique initiation complex assembly with STAT1 and NFκB leading to higher NOS2

transcription than TLR signalling alone[373]. TLR-induced gene transcription is also promoted through the IFN regulatory factor (IRF) family of transcription factors, which license programs of gene transcription, boosting MyD88 signalling[374]. IFN-γ signalling through the TLR adaptor Mal which bridges MyD88 and TLR binding leads to phagosome maturation and Mtb killing[151]. A SNP in Mal which is protective in heterozygotes in several infectious diseases including Mtb was identified[375], and was found to affect Mal's affinity for the IFN-γ receptor and impair phagosome maturation, autophagy and bacterial killing[376].

IFN-γ also has a role in macrophage nitric oxide production[58]. Mice deficient in IFN-γ cannot produce reactive nitrogen species and as a result cannot contain Mtb growth[82]. IFN-γ induced nitric oxide can have direct killing effects but is also a key inducer of macrophage apoptosis and Mtb killing[377]. MHCII expression, essential for antigen presentation to induce an adaptive response is also augmented by IFN-γ[378].

IFN-γ has also recently been shown to induce a metabolic shift in macrophages through HIF-1α to induce aerobic glycolysis[164]. This enhanced glycolysis was found to be essential for the control of Mtb growth in macrophages and to form a positive feedback loop with HIF-1α to boost macrophage activation.

IFN-γ signals through the STAT family of signalling molecules[379] and induces expression of SMAD7, an inhibitory SMAD, through STAT1 activation to downregulate TGF-β signalling[380]. TGF-β has in turn been shown to promote an increase in mature miR-21 through a post-transcriptional mechanism which enhances the processing of pri-miR-21 into pre-miR-21 by DROSHA. SMAD

proteins interact with pri-miR-21 and are incorporated into the DROSHA complex, enhancing the stability of the interaction between pri-miR-21 and DROSHA[299]. There is some evidence for a role in IFN-γ-mediated downregulation of a microRNA to boost innate immune responses. IFN-γ-primed macrophages were demonstrated to downregulate miR-3473b which allowed accumulation of its target PTEN and suppression of IL-10 induction[260].

Given the crossover between the processes augmented by IFN-γ and the processes found to be negatively regulated by miR-21, summarized in **figure 5.0**, the interplay between miR-21 and IFN-γ in the context of Mtb infection was investigated.

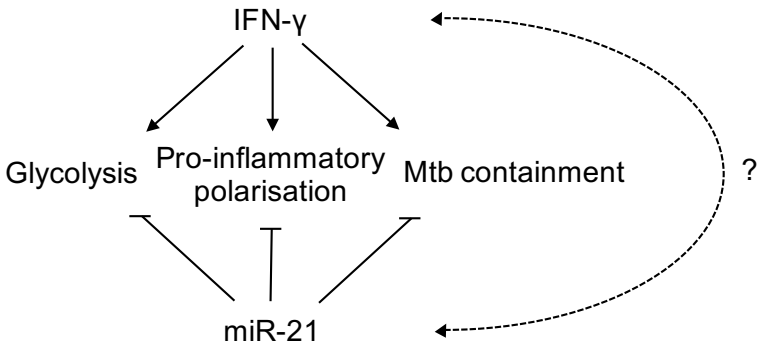

Figure 5.0 Chapter 5 Hypothesis. IFN-γ has been shown to promote pro-inflammatory macrophage activation including glycolytic induction, expression of pro-inflammatory polarisation genes such as iNOS and to promote Mtb containment. As miR-21 was shown to conversely limit these processes, it is hypothesised that there could be interplay between the IFN-γ and miR-21.

5.2 Results

5.2.1 IFN-γ boosts glycolytic reprogramming in response to inflammatory stimuli

miR-21 was found to be a negative regulator of immunometabolic programming in response to infection, negatively regulating PFK-M to limit glycolysis and thus IL-1β production. Given that this is a key point of regulation for macrophage function, other signals that could alter this pathway were investigated.

IFN-γ is known to coordinate macrophage activation and to be essential for anti-mycobacterial responses. This cytokine, mainly provided by NK and T cells in the local environment, has been shown to enhance macrophage nitric oxide and reactive oxygen species production, phagolysosomal maturation, glycolytic reprogramming and bacterial killing. Given the crossover between the processes augmented by IFN-γ and the processes found to be negatively regulated by miR-21, the interplay between miR-21 and IFN-γ was investigated.

The effect of IFN-γ on macrophage function was defined in the murine BMDM and human MDM models. Firstly, glycolytic reprogramming in response to pro-inflammatory stimuli was assessed. BMDM and human MDM were pre-treated for 30 minutes with IFN-γ and stimulated with LPS or Mtb and lactate production measured. Lactate production in response to stimulation was significantly enhanced by IFN-γ in both human and murine macrophages (**Figure 5.1**). Metabolic reprogramming was further probed by extracellular flux analysis in BMDM. IFN-γ was found to have no effect on OCR but significantly enhance ECAR in response to treatment with LPS (**Figure 5.2A and B**). The ratio of ECAR to

OCR was enhanced by IFN-γ however this did not reach significance (**Figure 5.2C**).

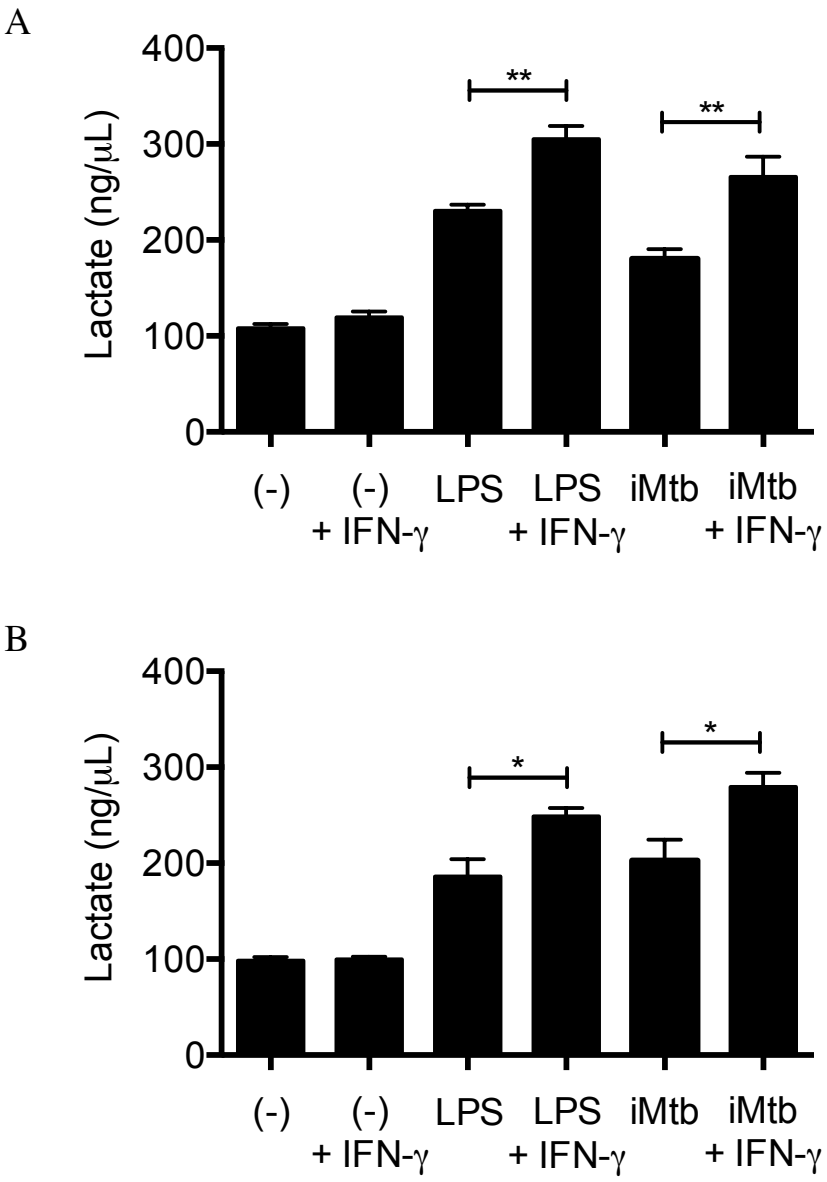

Figure 5.1 IFN-γ boosts lactate production in response to LPS and iMtb. Murine BMDM (A) and human MDM (B) were treated with 5 ng/mL of IFN-γ for 30 minutes and then stimulated with 100 ng/mL of LPS or infected with irradiated Mtb (strain H37Rv) (iMtb) at an MOI of 5 bacteria per cell for 24 hours. Supernatants were collected. Lactate was measured using a colorimetric lactate assay. Statistical analysis was performed using ordinary one-way ANOVA with Tukey's multiple comparisons test. *, ** and *** represent $p<0.05$, 0.01 and 0.001 respectively. Data shown as mean ± SEM, n = 4 and 3 independent experiments for (A) and (B) respectively.

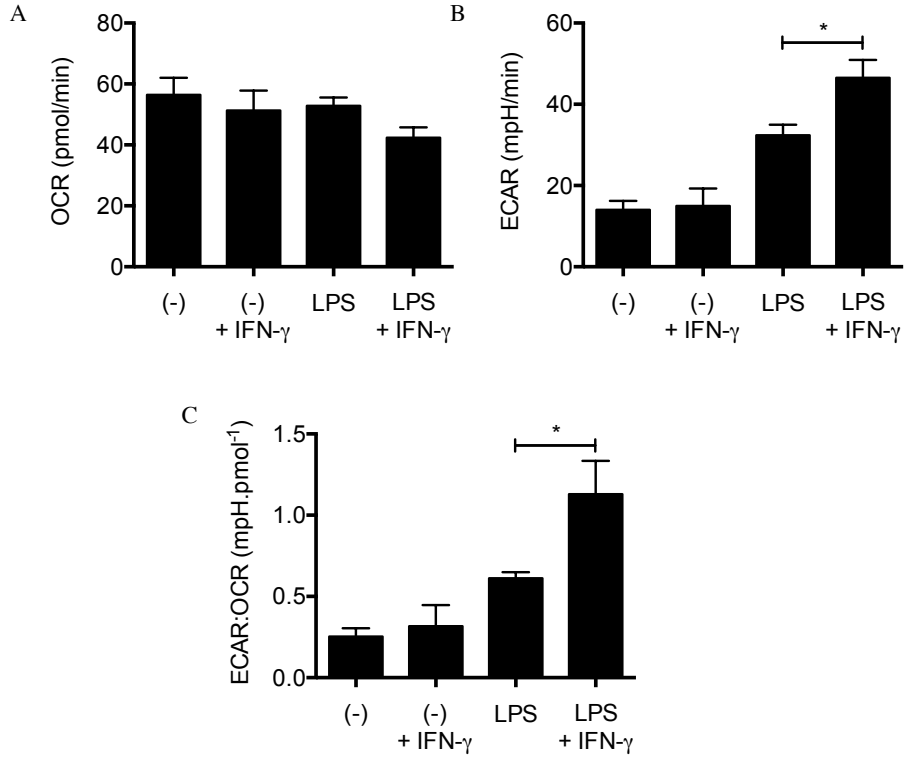

Figure 5.2 IFN-γ boosts glycolysis in response LPS. BMDM were stimulated 5 ng/mL IFN-γ and 100 ng/mL LPS for 24 hours. Extracellular flux analysis was performed and data normalised for cell number using a crystal violet assay. Corrected OCR (A), ECAR (B) and ECAR:OCR (C) were calculated. Statistical analysis was performed using ordinary one-way ANOVA with Tukey's multiple comparisons test. * represents $p<0.05$. Data shown as mean ± SEM, n = 3 independent experiments.

5.2.2 IFN-γ boosts IL-1β production and this is dependent on glycolysis

IFN-γ treatment resulted in higher lactate production and ECAR in activated macrophages, indicating that IFN-γ boosts the induction of glycolytic switching. Consequently, IFN-γ was also found to significantly augment IL-1β mRNA and protein in response to Mtb infection in both murine (**Figure 5.3**) and, particularly potently, in human macrophages (**Figure 5.4**). Moreover, this enhanced production of IL-1β was found to be dependent on glycolysis. MDM prevented from switching to glycolysis by being cultured in galactose-supplemented media cannot boost IL-1β production in response to Mtb infection (**Figure 5.5**).

5.2.3 IFN-γ augments induction of TNF-α and stunts induction of IL-10

The effect of IFN-γ on other cytokines was also examined. Induction of TNF-α was significantly enhanced by IFN-γ both in murine, and again particularly potently, in human macrophages (**Figure 5.6**). IL-10 production was suppressed by priming with IFN-γ, though this effect was more subtle (**Figure 5.7**).

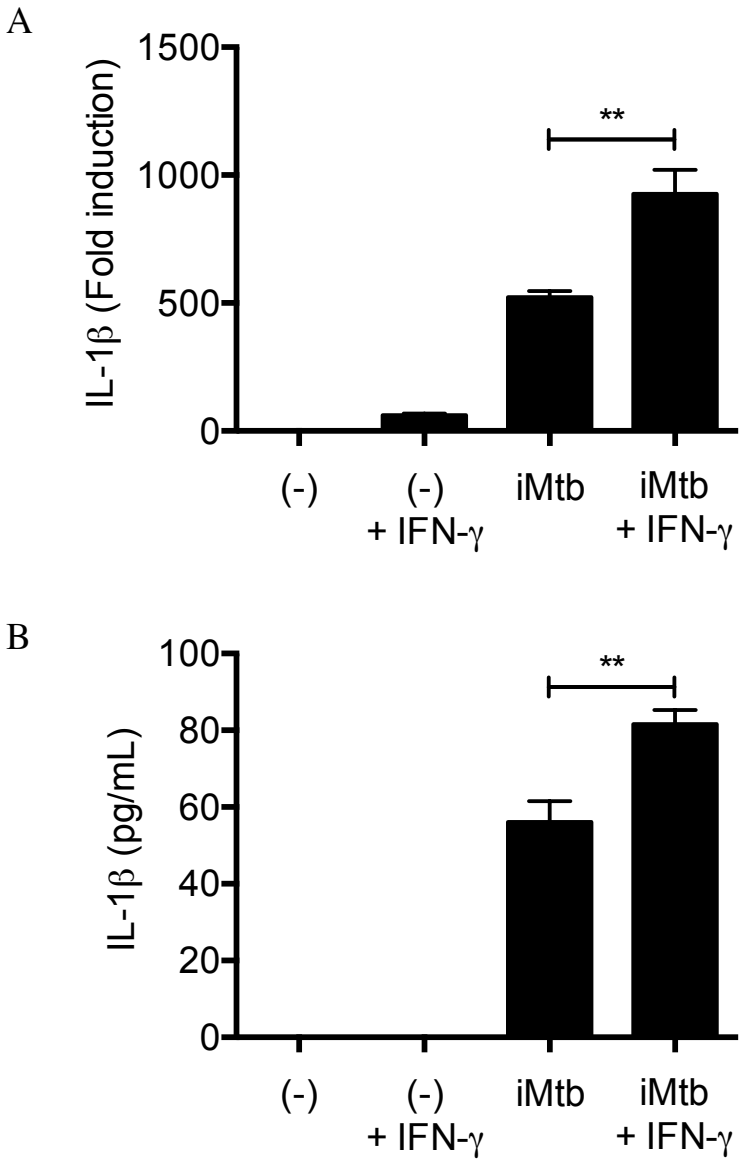

Figure 5.3 IFN-γ boosts IL-1β production in response to iMtb in murine BMDM. Murine BMDM were treated with 5 ng/mL of IFN-γ for 30 minutes and then infected with irradiated Mtb (strain H37Rv) (iMtb) at an MOI of 5 bacteria per cell for 24 hours. RNA and supernatants were collected. qPCR was performed and expression of IL-1β mRNA relative to the untreated control was calculated(A). Data were normalised to 18S. IL-1β protein was measured by ELISA (B). Statistical analysis was performed using ordinary one-way ANOVA with Tukey's multiple comparisons test. *, ** and *** represent $p<0.05$, 0.01 and 0.001 respectively. Data shown as mean ± SEM, n = 3 independent experiments.

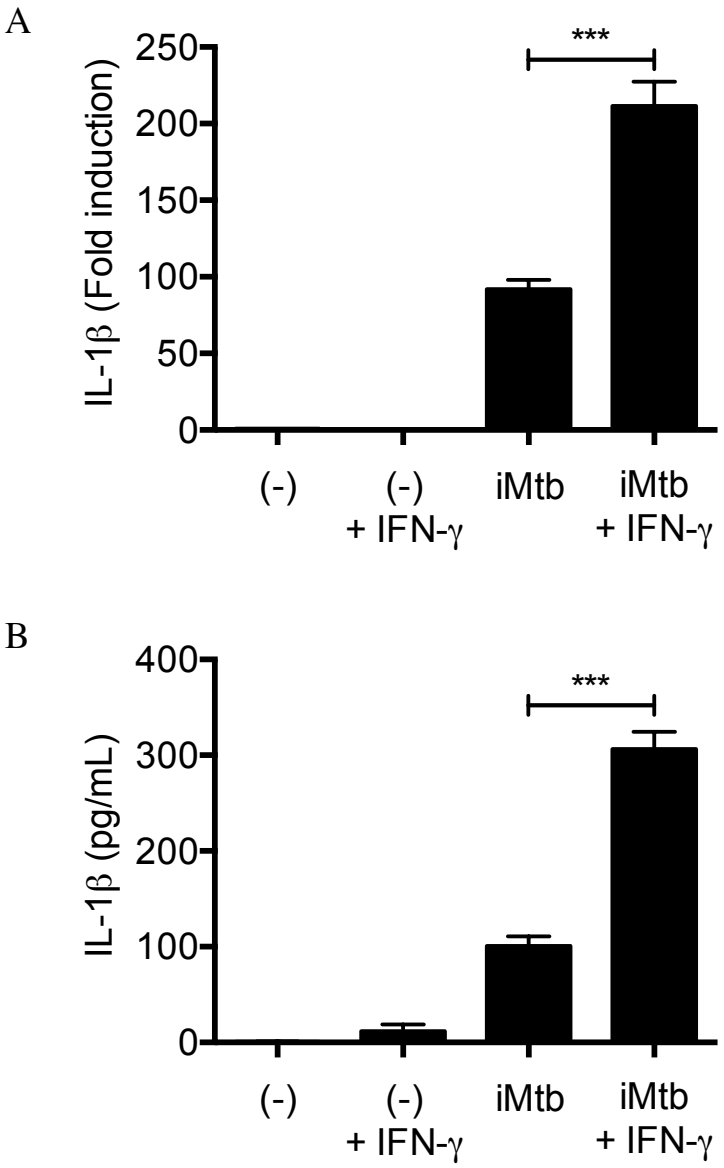

Figure 5.4 IFN-γ boosts IL-1β production in response to iMtb in human MDM. Human MDM were treated with 5 ng/mL of IFN-γ for 30 minutes and then infected with irradiated Mtb (strain H37Rv) (iMtb) at an MOI of 5 bacteria per cell for 24 hours. RNA and supernatants were collected. qPCR was performed and expression of IL-1β mRNA relative to the untreated control was calculated(A). Data were normalised to 18S. IL-1β protein was measured by ELISA (B). Statistical analysis was performed using ordinary one-way ANOVA with Tukey's multiple comparisons test. *, ** and *** represent $p<0.05$, 0.01 and 0.001 respectively. Data shown as mean ± SEM, n = 4 independent experiments.

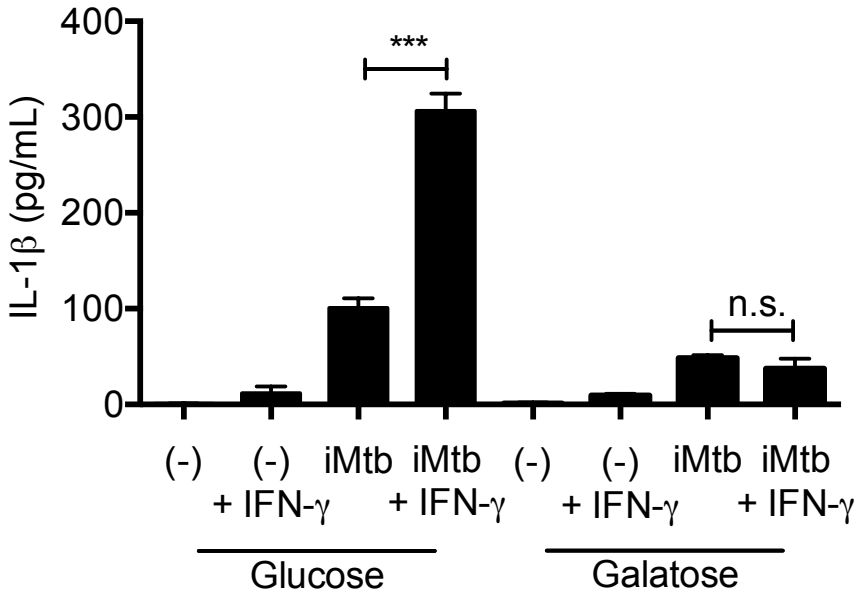

Figure 5.5 IFN-γ mediated augmentation of IL-1β production in response to iMtb is dependent on glycolysis. Human MDM were cultured in glucose- or galactose-supplement media and treated with 5 ng/mL of IFN-γ for 30 minutes and then infected with irradiated Mtb (strain H37Rv) (iMtb) at an MOI of 5 bacteria per cell for 24 hours. Supernatants were collected. IL-1β was measured by ELISA. Statistical analysis was performed using ordinary one-way ANOVA with Tukey's multiple comparisons test. *, ** and *** represent $p<0.05$, 0.01 and 0.001 respectively. Data shown as mean ± SEM, n = 3 independent experiments.

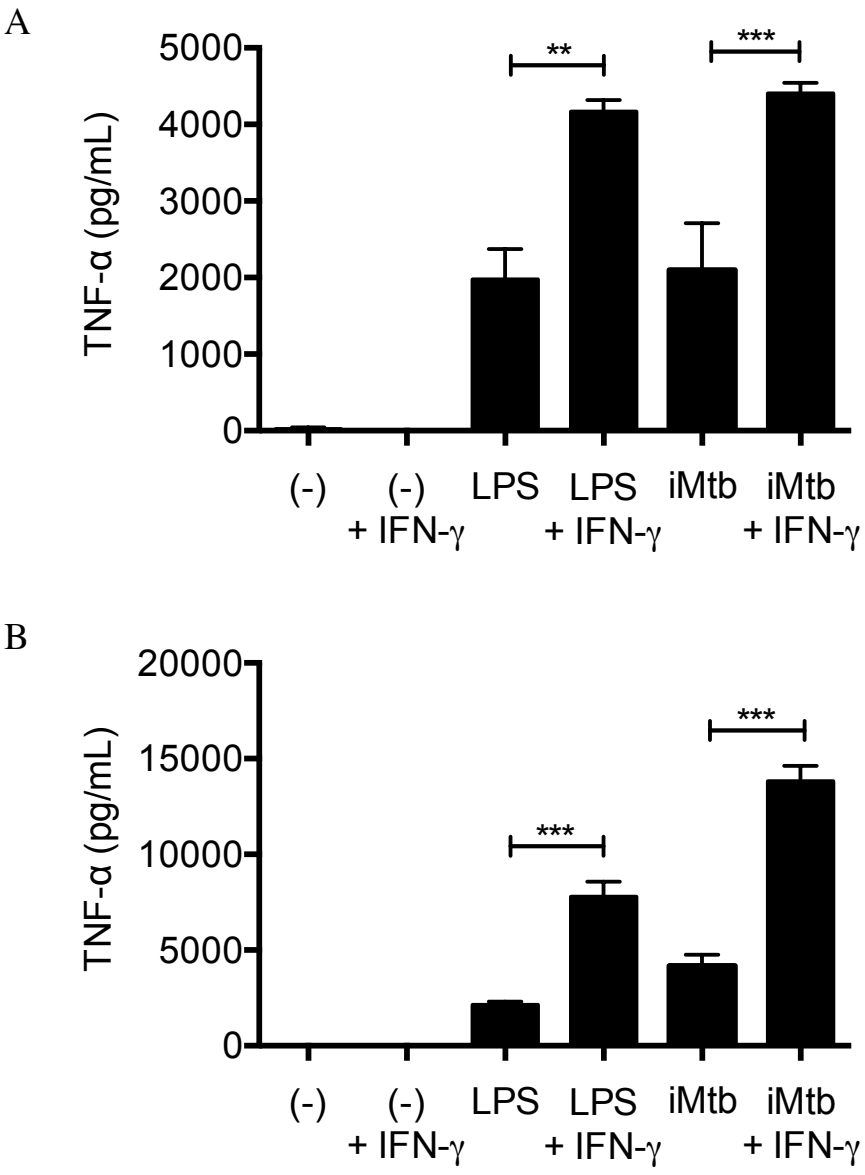

Figure 5.6 IFN-γ potentiates TNF-α production in response to LPS and iMtb. Murine BMDM (A) and human MDM (B) were treated with 5 ng/mL of IFN-γ for 30 minutes and then stimulated with 100 ng/mL of LPS or infected with irradiated Mtb (strain H37Rv) (iMtb) at an MOI of 5 bacteria per cell for 24 hours. Supernatants were collected and TNF-α protein quantified using an ELISA. Statistical analysis was performed using ordinary one-way ANOVA with Tukey's multiple comparisons test. *, ** and *** represent $p<0.05$, 0.01 and 0.001 respectively. Data shown as mean ± SEM, n = 3 and 5 independent experiments.

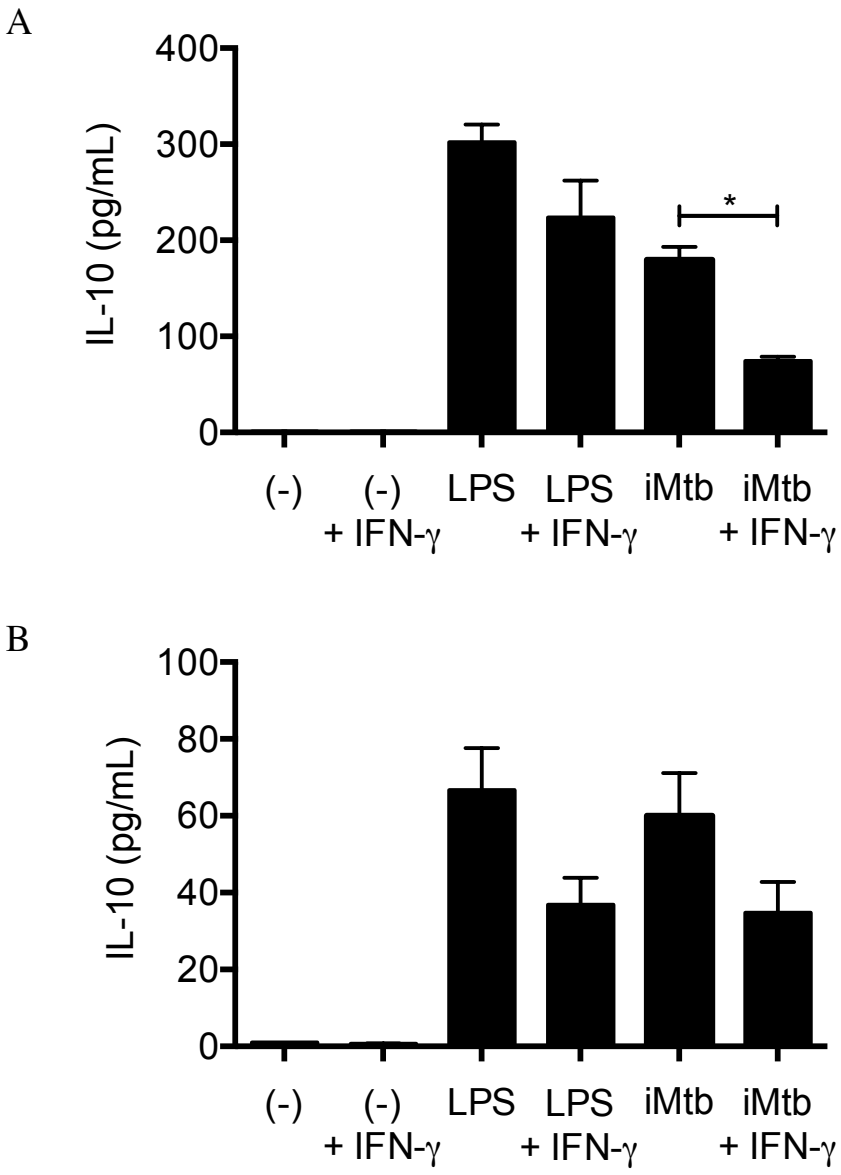

Figure 5.7 IFN-γ stunts IL-10 production in response to LPS and iMtb. Murine BMDM (A) and human MDM (B) were treated with 5 ng/mL of IFN-γ for 30 minutes and then stimulated with 100 ng/mL of LPS or infected with irradiated Mtb (strain H37Rv) (iMtb) at an MOI of 5 bacteria per cell for 24 hours. Supernatants were collected. IL-10 protein quantified using an ELISA (B). Statistical analysis was performed using ordinary one-way ANOVA with Tukey's multiple comparisons test. *, ** and *** represent $p<0.05$, 0.01 and 0.001 respectively. Data shown as mean ± SEM, n = 5 and 3 independent experiments.

5.2.4 IFN-γ enhances induction of reactive nitrogen and oxygen species

IFN-γ was found to boost the pro-inflammatory cytokine TNF-α and stunt the induction of the anti-inflammatory cytokine IL-10. Other macrophage polarisation markers were also examined. iNOS induction in response to LPS and iMtb was found to be significantly enhanced by IFN-γ, approximately double the induction with LPS or iMtb alone (**Figure 5.8A**). Conversely, arginase 1 induction in response to iMtb infection was significantly reduced by IFN-γ treatment (**Figure 5.8B**). IFN-γ also reduced arginase-1 induction in response to LPS stimulation though not significantly.

IFN-γ shifts the balance between iNOS and arginase-1 towards the use of arginine to produce nitric oxide species[381], thus it was not surprising to find that nitrite produced in response to LPS and iMtb was significantly higher after IFN-γ treatment (**Figure 5.9**). A pilot experiment (n=1) also indicated that IFN-γ was able boost ROS production in response to LPS and iMtb in human MDM.

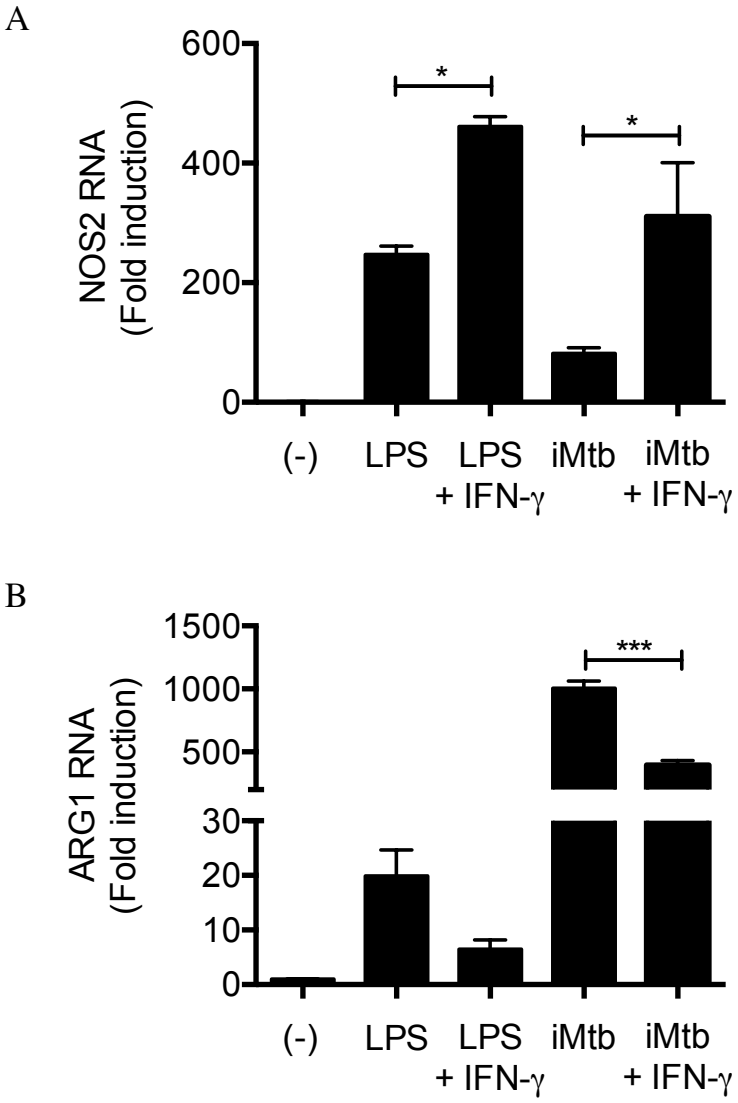

Figure 5.8 IFN-γ boosts iNOS induction and stunts Arg1 expression in response to LPS and iMtb. Murine BMDM were treated with 5 ng/mL of IFN-γ for 30 minutes and then stimulated with 100 ng/mL of LPS or infected with irradiated Mtb (strain H37Rv) (iMtb) at an MOI of 5 bacteria per cell for 24 hours. RNA and supernatants were collected. qPCR was performed and expression of NOS2 (A) and ARG1 (B) mRNA relative to the untreated control was calculated. Data were normalised to 18S. Statistical analysis was performed using ordinary one-way ANOVA with Tukey's multiple comparisons test. *, ** and *** represent $p<0.05$, 0.01 and 0.001 respectively. Data shown as mean ± SEM, n = 3 independent experiments.

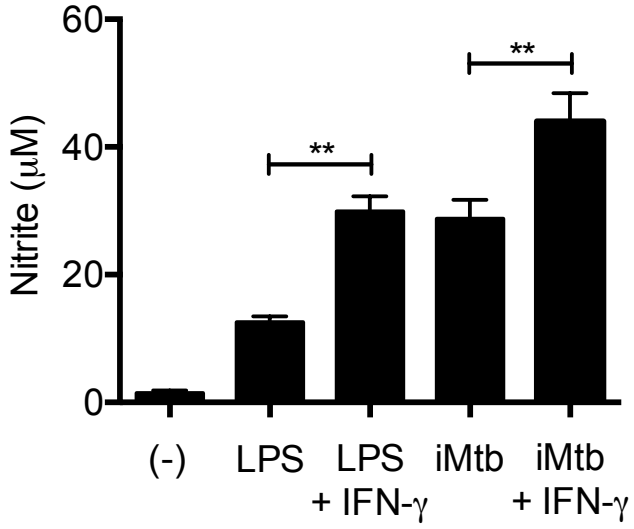

Figure 5.9 IFN-γ boosts nitrite production in response to LPS and iMtb. Murine BMDM were treated with 5 ng/mL of IFN-γ for 30 minutes and then stimulated with 100 ng/mL of LPS or infected with irradiated Mtb (strain H37Rv) (iMtb) at an MOI of 5 bacteria per cell for 24 hours. Supernatants were collected. Nitrite was measured using a colorimetric Griess assay. Statistical analysis was performed using ordinary one-way ANOVA with Tukey's multiple comparisons test. *, ** and *** represent $p<0.05$, 0.01 and 0.001 respectively. Data shown as mean ± SEM, n = 4 independent experiments.

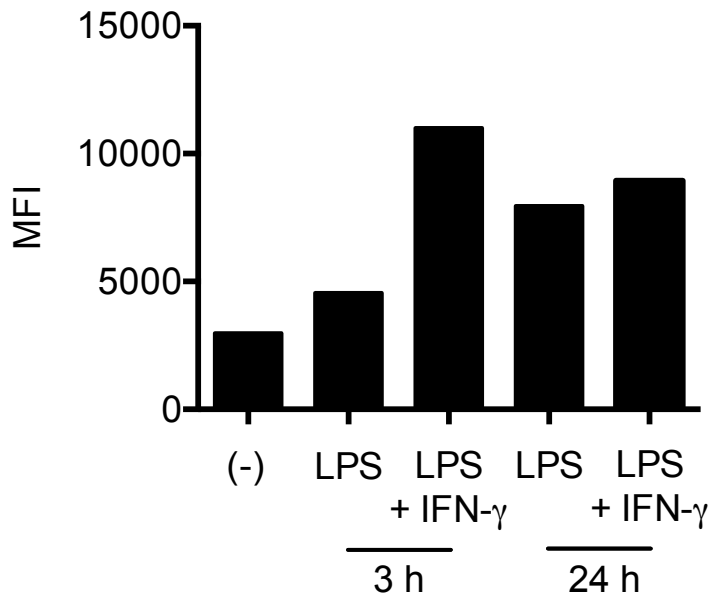

Figure 5.10 IFN-γ boosts ROS production in response to LPS and iMtb. Human MDM were treated with 5 ng/mL of IFN-γ for 30 minutes and then stimulated with 100 ng/mL of LPS for 3 and 24 hours. Cells were washed and stained with 20 μM DCFDA for 30 minutes at 37°C in the dark. Cells were scraped into a single-cell suspension and mean fluorescence intensity was measured by flow cytometry. n = 1.

5.2.5 IFN-γ enhances macrophage control of mycobacterial growth

Having found that IFN-γ boosts pro-inflammatory macrophage functions, including TNF-α production, IL-1β production, iNOS expression, nitrite production and ROS production, while limiting anti-inflammatory mediators such as IL-10 and arginase-1, the effect of IFN-γ on overall infection outcome was assessed. BMDM were pre-treated with IFN-γ and infected with live Mtb. IFN-γ pre-treatment was found to significantly enhance the ability of the macrophages to contain Mtb growth, reducing the number of bacterial colonies approximately 1.6-fold (**Figure 5.11**).

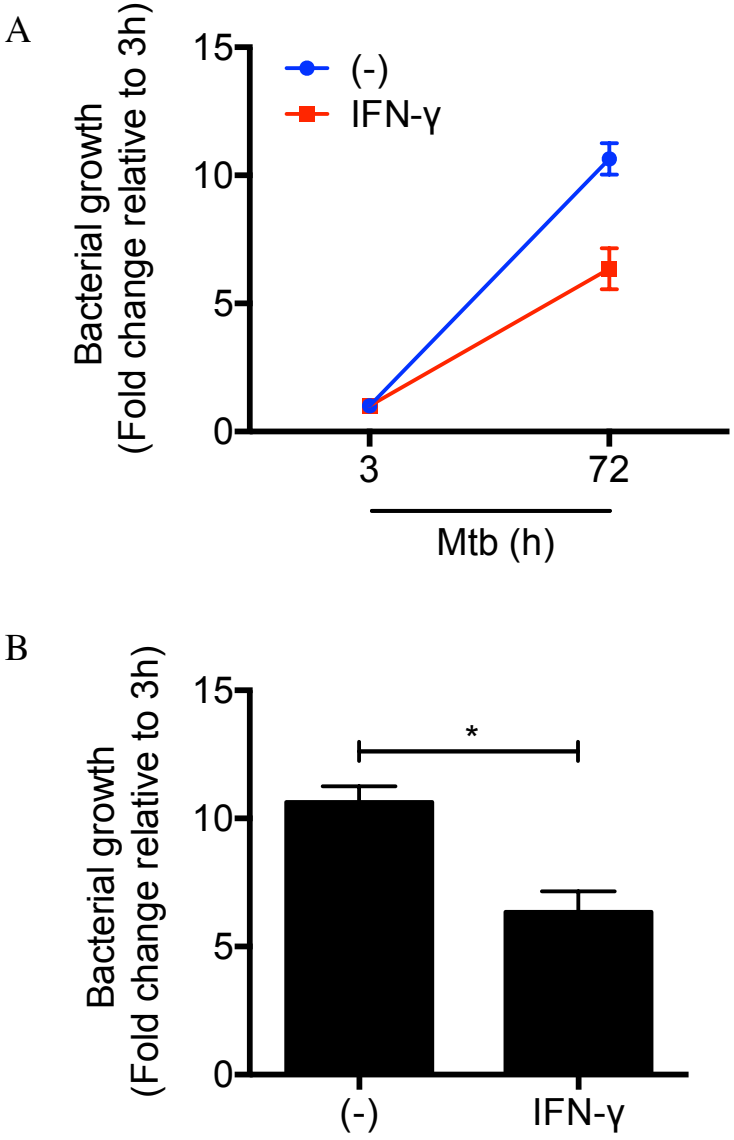

Figure 5.11 IFN-γ boosts the containment of Mtb growth. Murine BMDM were pre-treated with 5 ng/mL IFN-γ and infected with live Mtb (Strain H37Ra) at an MOI of 5 bacteria per cell for 72 hours. Cells were lysed in 0.1% Triton X-100 and the lysates diluted in Middlebrook broth supplemented with ADC. Aliquots of the lysates were then streaked in triplicate on warm Middlebrook agar plates and incubated at 37°C for approximately 14 days. Colony forming units were counted. Statistical analysis was performed using a paired, two-tailed Student's t-test. *, ** and *** represent $p<0.05$, 0.01 and 0.001 respectively. Data shown as mean ± SEM, n = 3 individual experiments.

5.2.6 IFN-γ reduces the levels mature miR-21 in response to infection

The effect of IFN-γ on macrophage responses was found to be similar to the effect of blocking miR-21 activity. For this reason, the effect of IFN-γ on miR-21 expression was examined. IFN-γ was found to significantly reduce the induction of miR-21 in response to LPS and iMtb, approximately 1.4- and 1.5-fold respectively (**Figure 5.12A**). IFN-γ treatment of unstimulated macrophages decreased levels of miR-21 though not significantly. When the primary transcript of miR-21 was measured however, there was no significant difference in induction after IFN-γ treatment (**Figure 5.12B**). This finding indicated that IFN-γ does not affect miR-21 induction, however it could affect the processing or accumulation of the primary transcript into the mature microRNA. This lead to the hypothesis that IFN-γ alters miR-21 processing to reduce its activity in order to potentiate pro-inflammatory responses.

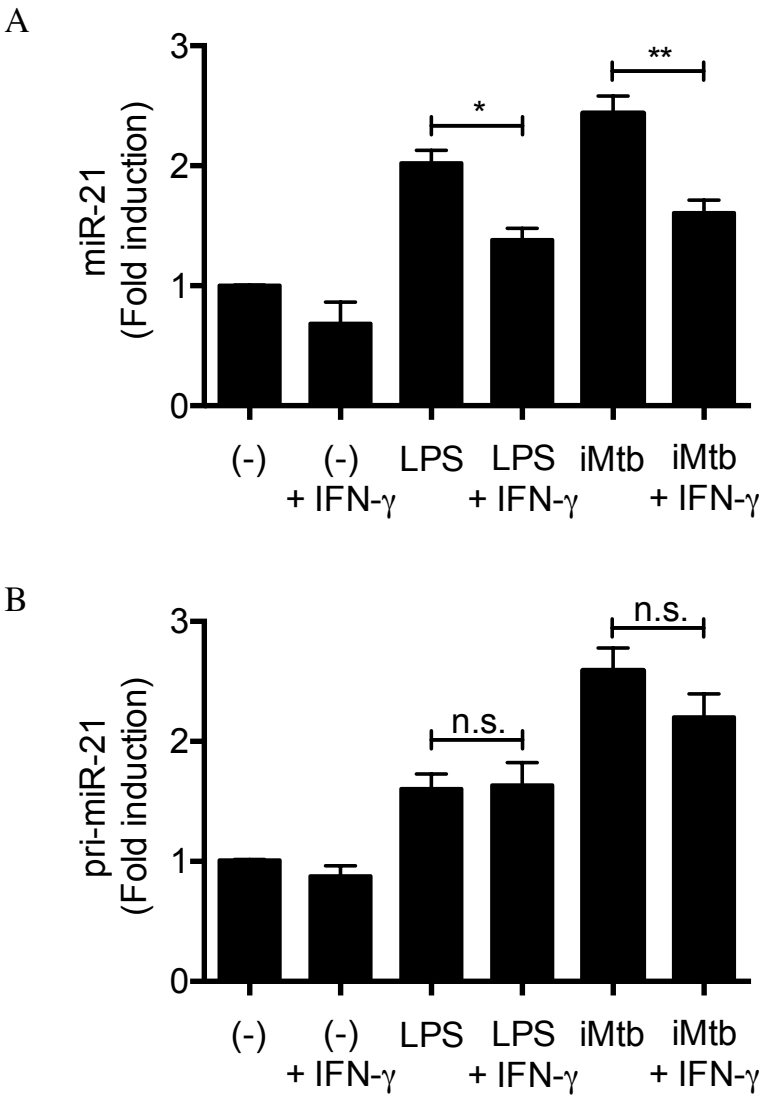

Figure 5.12 IFN-γ blocks the induction of mature miR-21 but not pri-miR-21 in response to LPS and iMtb. Murine BMDM were treated with 5 ng/mL of IFN-γ for 30 minutes and then stimulated with 100 ng/mL of LPS or infected with irradiated Mtb (strain H37Rv) (iMtb) at an MOI of 5 bacteria per cell for 24 hours. RNA and supernatants were collected. qPCR was performed and expression of miR-21 (A) and pri-miR-21 (B) mRNA relative to the untreated control was calculated. Data were normalised to RNU6B and 18S respectively. Statistical analysis was performed using ordinary one-way ANOVA with Tukey's multiple comparisons test. *, ** and *** represent $p<0.05$, 0.01 and 0.001 respectively. Data shown as mean ± SEM, n = 3 individual experiments.

5.2.7 miR-21-deficient macrophages are resistant to the glycolytic effects of IFN-γ

To assess the role of IFN-γ on miR-21 and augmented macrophage responses, the activity of IFN-γ on miR-21-deficient macrophages was investigated. Wild-type and miR-21 knockout murine macrophages and human MDM transfected with anti-miR control or anti-miR-21 were pre-treated with IFN-γ and stimulated with LPS or infected with Mtb. While lactate production in response to infection was significantly boosted in response to infection in wild-type macrophages, no boost in lactate production was associated with IFN-γ treatment in macrophages lacking miR-21 activity (**Figure 5.13**). Macrophages lacking miR-21 activity produced significantly more lactate in response to stimulation, however in the presence of IFN-γ, wild-type macrophage production of lactate was boosted to a similar level as that of the miR-21-deficient macrophage.

The lactate results indicated that while miR-21 knockout macrophages were better at inducing glycolytic reprogramming, IFN-γ could aid wild-type macrophages to achieve the level of reprogramming found in the knockout. IFN-γ had no potentiation effect in the absence of miR-21. This was further confirmed by extracellular flux analysis. While miR-21 knockout macrophages had significantly higher ECAR and ECAR:OCR in response to LPS, IFN-γ was found to have no additional effect on miR-21 knockout macrophages but to boost ECAR and ECAR:OCR in wild-type macrophages to knockout levels (**Figure 5.14**).

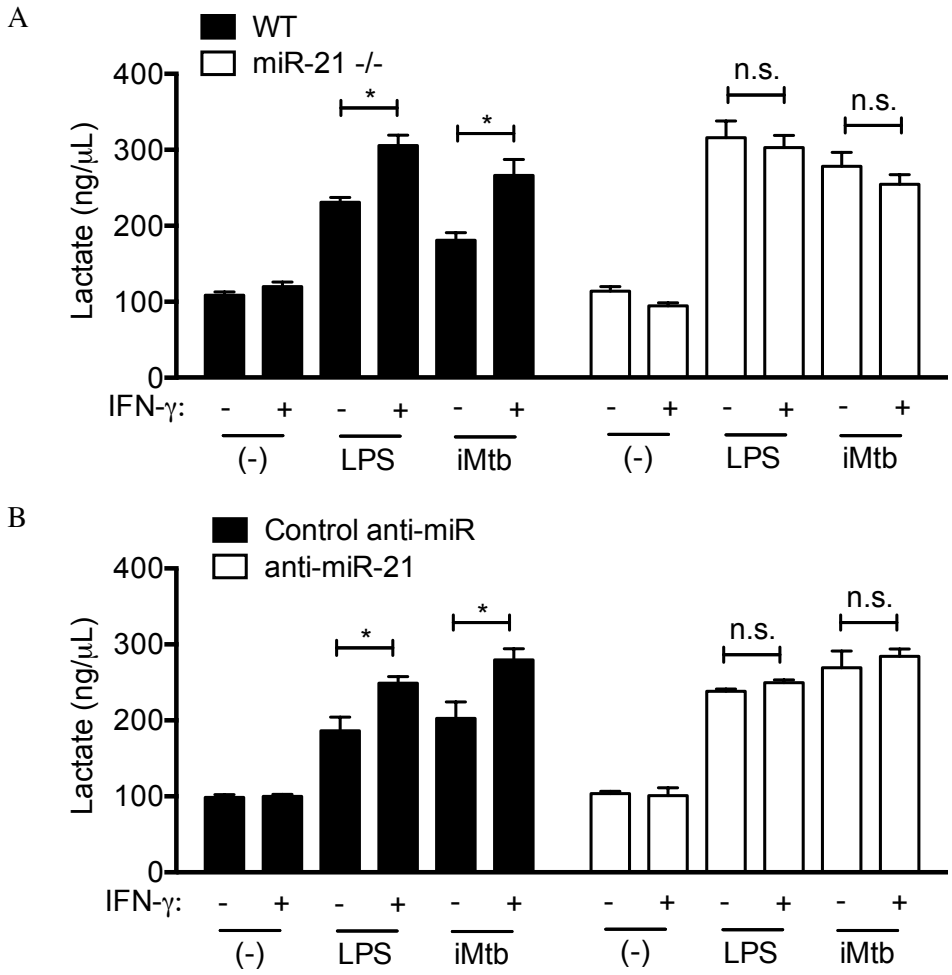

Figure 5.13 Loss of miR-21 blocks IFN-γ potentiation of lactate production in response to LPS and iMtb. Wild-type and miR-21 knockout murine BMDM (A) and human MDM transfected with control anti-miR or anti-miR-21 (B) were treated with 5 ng/mL of IFN-γ for 30 minutes and then stimulated with 100 ng/mL of LPS or infected with irradiated Mtb (strain H37Rv) (iMtb) at an MOI of 5 bacteria per cell for 24 hours. Supernatants were collected. Lactate was measured using a colorimetric lactate assay. Statistical analysis was performed using a paired, two-tailed Student's t-test. *, ** and *** represent $p<0.05$, 0.01 and 0.001 respectively. Data shown as mean ± SEM, n = 4 and 3 independent experiments.

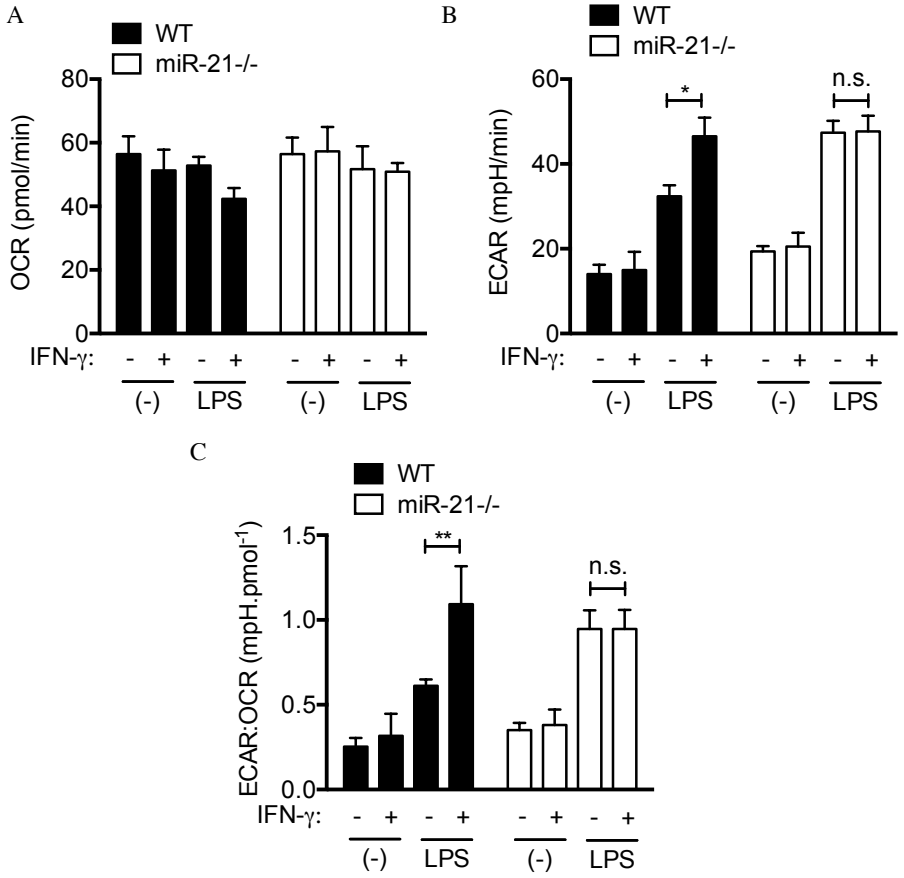

Figure 5.14 Loss of miR-21 blocks IFN-γ potentiation of glycolysis in response LPS. Wild-type and miR-21 knockout BMDM were stimulated 5 ng/mL IFN-γ and 100 ng/mL LPS for 24 hours. Extracellular flux analysis was performed and data normalised for cell number using a crystal violet assay. Statistical analysis was performed using a paired, two-tailed Student's t-test. *, ** and *** represent $p<0.05$, 0.01 and 0.001 respectively. Data shown as mean ± SEM, n = 3 independent experiments.

5.2.8 IFN-γ boosts wild-type IL-1β production in response to Mtb infection to levels observed in miR-21 knockout macrophages and this is dependent on glycolysis

Having found that IFN-γ boosts wild-type glycolytic reprogramming to levels similar to those observed in miR-21-deficient macrophages, the effect on IL-1β production was next examined. IFN-γ had no effect on IL-1β production in miR-21-deficient macrophages however it boosted IL-1β production by wild-type macrophages in response to Mtb to levels similar to miR-21 knockout macrophages (**Figure 5.15A**). This effect was also observed in human MDM. MDM treated with anti-miR control produced more IL-1β in response to Mtb in the presence of IFN-γ, while IL-1β produced by anti-miR-21 treated MDM did not change with IFN-γ treatment (**Figure 5.15B**). Furthermore, MDM cultured in galactose-supplemented media did not enhance IL-1β production in the presence of IFN-γ, indicating that the enhanced production of IL-1β in the presence of IFN-γ was dependent on glycolysis.

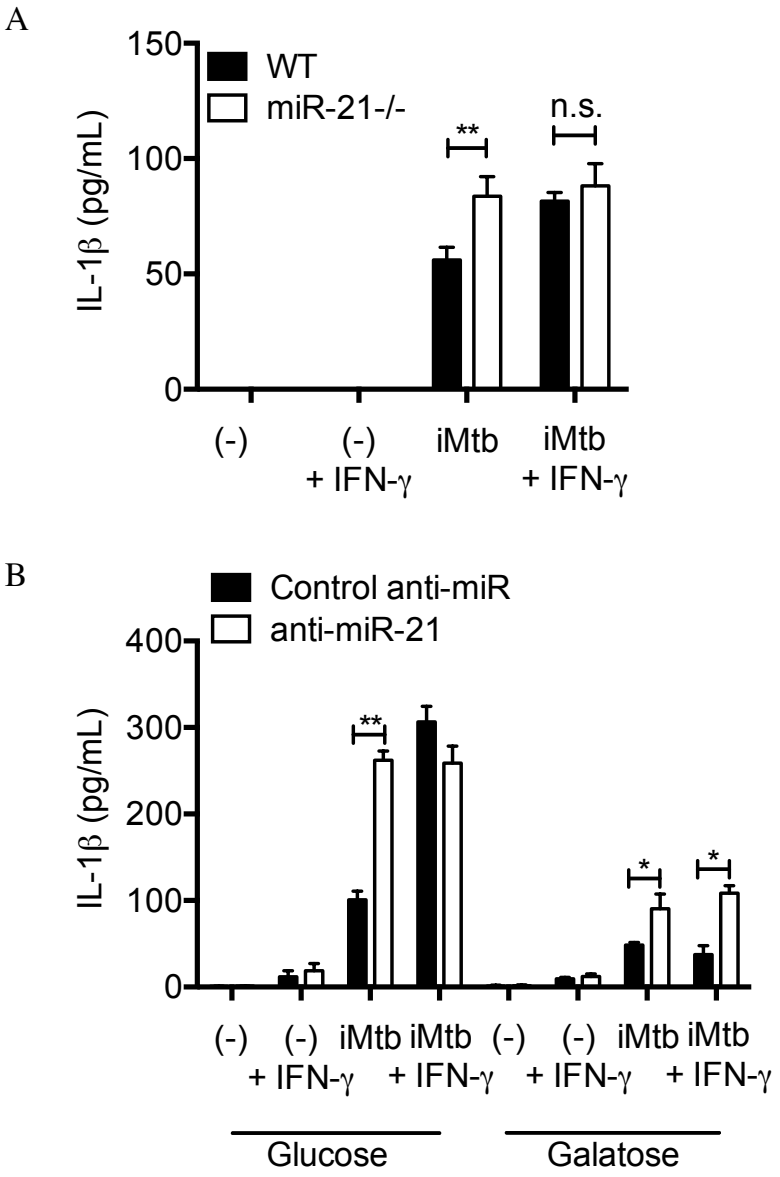

Figure 5.15 Loss of miR-21 blocks IFN-γ potentiation of IL-1β production in response to iMtb. Wild-type and miR-21 knockout murine BMDM (A) and human MDM transfected with control anti-miR or anti-miR-21 cultured in glucose- or galactose-supplemented media (B) were treated with 5 ng/mL of IFN-γ for 30 minutes and then infected with irradiated Mtb (strain H37Rv) (iMtb) at an MOI of 5 bacteria per cell for 24 hours. Supernatants were collected and IL-1β protein was measured by ELISA. Statistical analysis was performed using a paired, two-tailed Student's t-test. *, ** and *** represent $p<0.05$, 0.01 and 0.001 respectively. Data shown as mean ± SEM, n = 3 independent experiments.

5.2.9 IFN-γ does not alter TNF-α or IL-10 production in macrophages lacking miR-21 activity

Macrophages lacking miR-21 activity were found to be resistant to the potentiating effects of IFN-γ in the case of glycolytic reprogramming and IL-1β production. Other pro-inflammatory and anti-inflammatory macrophage mediators were also assessed. Similar trends were found as with IL-1β. Loss of miR-21 made macrophages resistant to IFN-γ-mediated potentiation of TNF-α at both the mRNA and protein level (**Figure 5.16**). IFN-γ boosted wild-type TNF-α to a level comparable to that of the knockout. Similarly, IFN-γ-mediated stunting of IL-10 production at the mRNA or protein level was not evident in miR-21 knockout macrophages (**Figure 5.17**).

5.2.10 IFN-γ does not alter iNOS or arginase 1 expression or nitrite production in macrophages lacking miR-21 activity

IFN-γ also failed to boost iNOS induction or stunt arginase 1 induction in response to Mtb in miR-21 knockout BMDM (**Figure 5.18**). Accordingly, miR-21-deficient macrophages were also resistant to IFN-γ-mediated boosting of nitrite species (**Figure 5.19**).

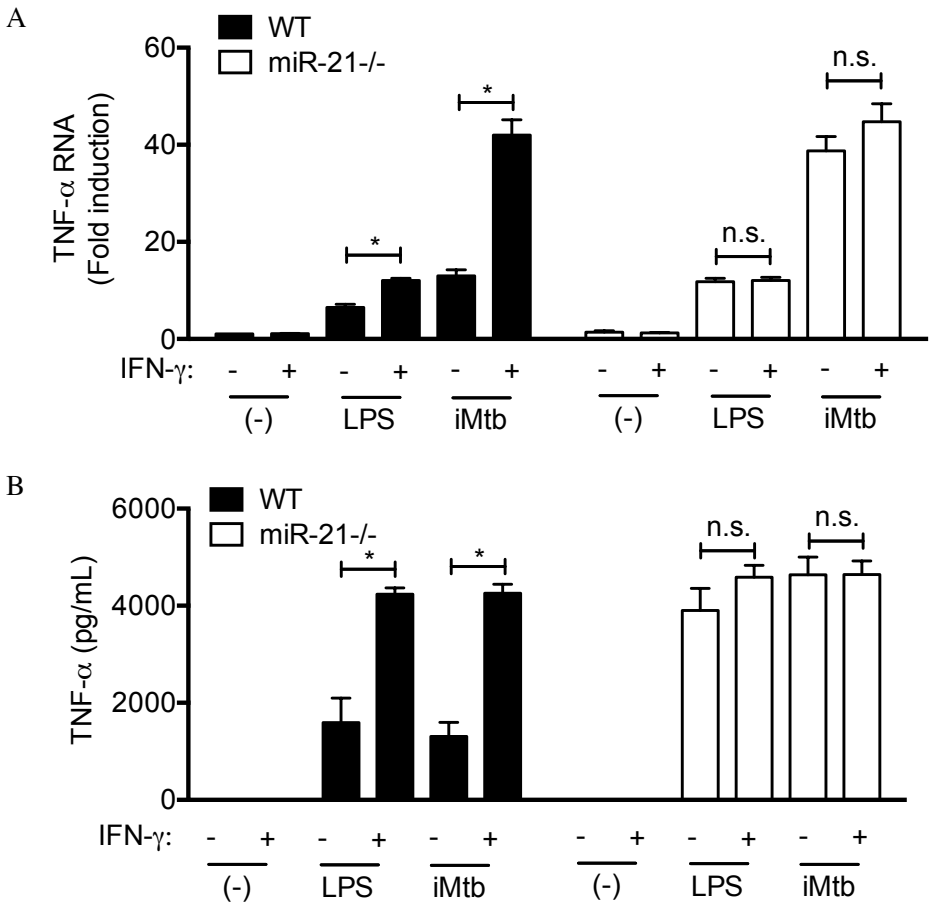

Figure 5.16 Loss of miR-21 blocks IFN-γ potentiation of TNF-α production response to LPS and iMtb in murine macrophages. Wild-type and miR-21 knockout murine BMDM were treated with 5 ng/mL of IFN-γ for 30 minutes and then stimulated with 100 ng/mL of LPS or infected with irradiated Mtb (strain H37Rv) (iMtb) at an MOI of 5 bacteria per cell for 24 hours. RNA and supernatants were collected. qPCR was performed and expression of TNF-α mRNA relative to the untreated control was calculated (A). Data were normalised to 18S. TNF-α protein quantified using an ELISA (B). Statistical analysis was performed using a paired, two-tailed Student's t-test. *, ** and *** represent $p<0.05$, 0.01 and 0.001 respectively. Data shown as mean ± SEM, n = 3 independent experiments.

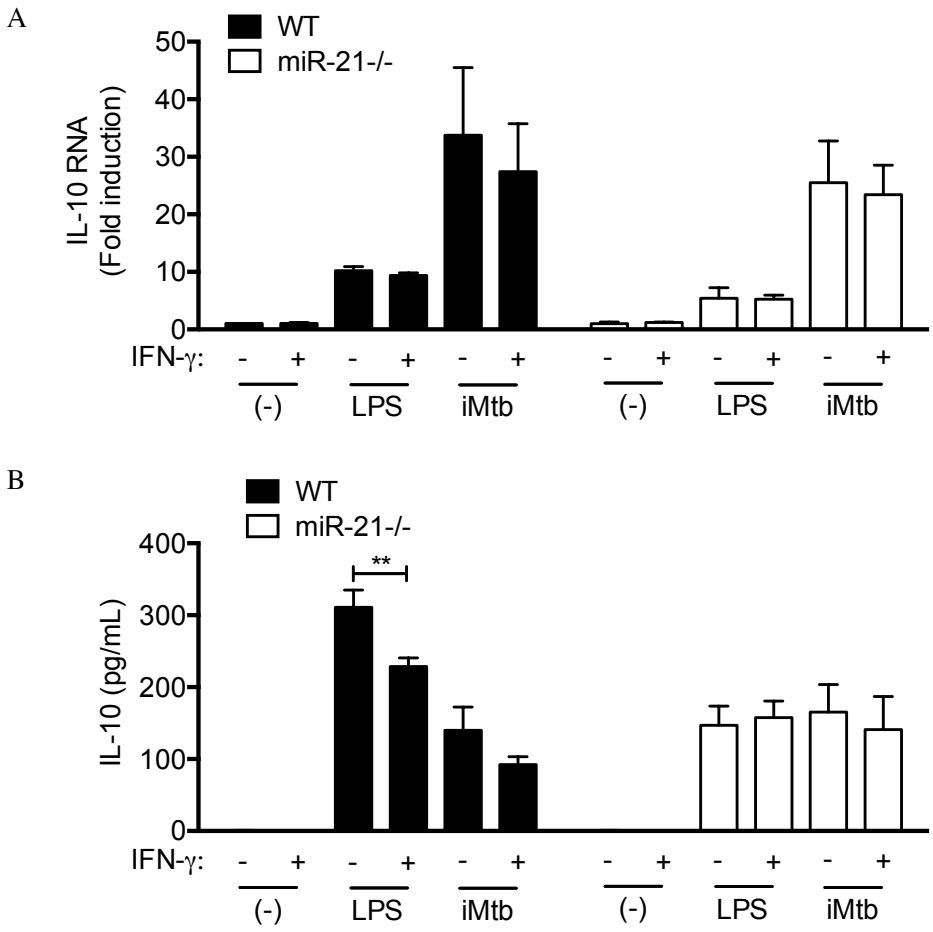

Figure 5.17 Loss of miR-21 blocks IFN-γ stunting of IL-10 production response to LPS and iMtb in murine macrophages. Wild-type and miR-21 knockout murine BMDM were treated with 5 ng/mL of IFN-γ for 30 minutes and then stimulated with 100 ng/mL of LPS or infected with irradiated Mtb (strain H37Rv) (iMtb) at an MOI of 5 bacteria per cell for 24 hours. RNA and supernatants were collected. qPCR was performed and expression of IL-10 mRNA relative to the untreated control was calculated (A). Data were normalised to 18S. IL-10 protein quantified using an ELISA (B). Statistical analysis was performed using a paired, two-tailed Student's t-test. *, ** and *** represent $p<0.05$, 0.01 and 0.001 respectively. Data shown as mean ± SEM, n = 3 independent experiments.

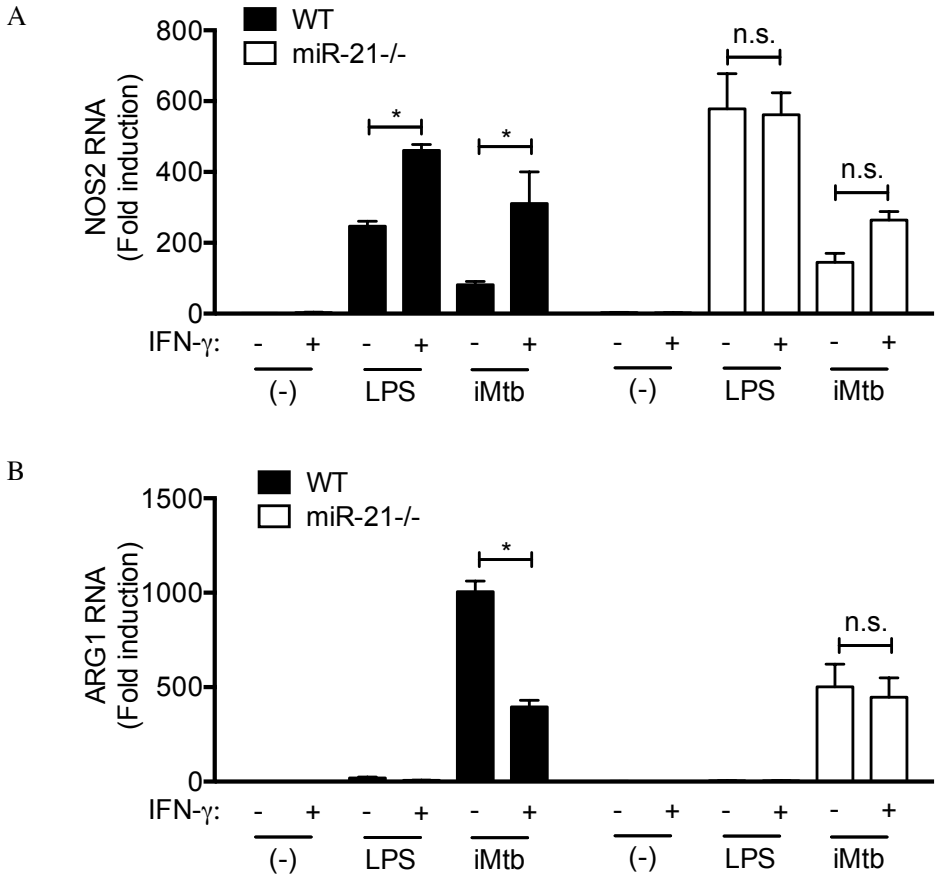

Figure 5.18 Loss of miR-21 blocks IFN-γ boosting iNOS induction and stunting Arg1 expression in response to LPS and iMtb. Wild-type and miR-21 knockout murine BMDM were treated with 5 ng/mL of IFN-γ for 30 minutes and then stimulated with 100 ng/mL of LPS or infected with irradiated Mtb (strain H37Rv) (iMtb) at an MOI of 5 bacteria per cell for 24 hours. RNA and supernatants were collected. qPCR was performed and expression of NOS2 (A) and ARG1 (B) mRNA relative to the untreated control was calculated. Data were normalised to 18S. Statistical analysis was performed using a paired, two-tailed Student's t-test. *, ** and *** represent $p<0.05$, 0.01 and 0.001 respectively. Data shown as mean ± SEM, n = 3 independent experiments.

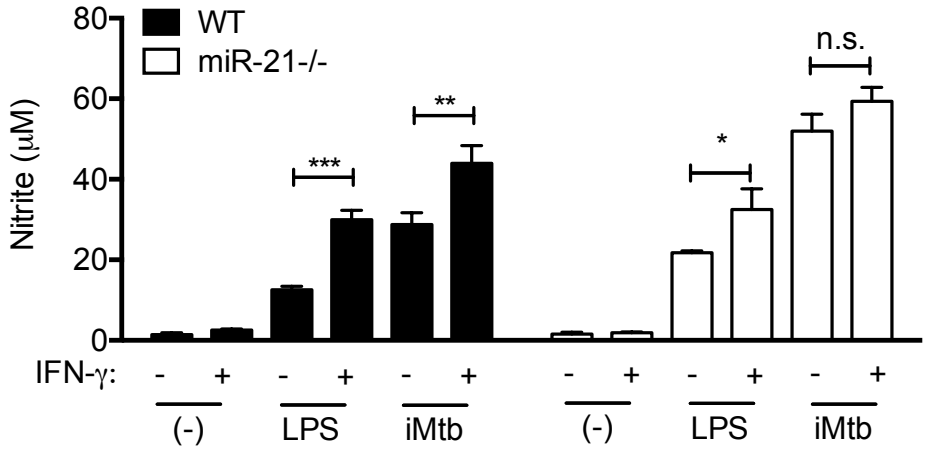

Figure 5.19 Loss of miR-21 blocks IFN-γ potentiation of nitrite production in response to LPS and iMtb. Wild-type and miR-21 knockout murine BMDM were treated with 5 ng/mL of IFN-γ for 30 minutes and then stimulated with 100 ng/mL of LPS or infected with irradiated Mtb (strain H37Rv) (iMtb) at an MOI of 5 bacteria per cell for 24 hours. Supernatants were collected. Nitrite was measured using a colorimetric Griess assay. Statistical analysis was performed using a paired, two-tailed Student's t-test. *, ** and *** represent $p<0.05$, 0.01 and 0.001 respectively. Data shown as mean ± SEM, n = 4 independent experiments.

5.2.11 IFN-γ does not enhance ROS production in macrophages lacking miR-21 activity

Murine macrophages lacking miR-21 were found to be resistant to the potentiating effect of IFN-γ on nitrite production. Similarly, a pilot experiment in human macrophages indicated that blocking miR-21 activity desensitised MDM to IFN-γ potentiation of ROS production after LPS stimulation (**Figure 5.20**).

5.2.12 IFN-γ has no additional effect on containment of Mtb growth in miR-21 deficient macrophages

Having found that miR-21-deficient macrophages were resistant to the polarising, pro-inflammatory effects of IFN-γ, the effect of IFN-γ on bacterial containment was assessed. Pre-treatment of wild-type BMDM with IFN-γ was shown to enhance containment of Mtb, however this effect was not observed in miR-21 knockout macrophages (**Figure 5.21**). IFN-γ reduced bacterial growth in wild-type BMDM, though it did not fully reach the level of containment achieved by miR-21 knockout BMDM. Wild-type macrophage bacterial growth was approximately double that in miR-21 knockout BMDM even in the presence of IFN-γ.

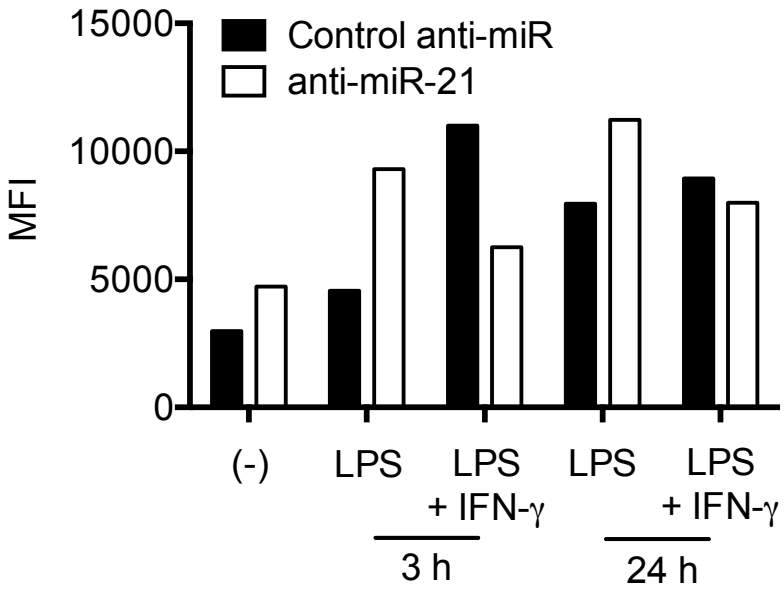

Figure 5.20 Loss of miR-21 blocks IFN-γ potentiation of ROS production in response to LPS and iMtb. Human MDM were transfected with anti-miR control or anti-miR-21 and treated with 5 ng/mL of IFN-γ for 30 minutes and then stimulated with 100 ng/mL of LPS for 3 and 24 hours. Cells were washed and stained with 20 μM DCFDA for 30 minutes at 37°C in the dark. Cells were scraped into a single-cell suspension and mean fluorescence intensity was measured by flow cytometry. n = 1.

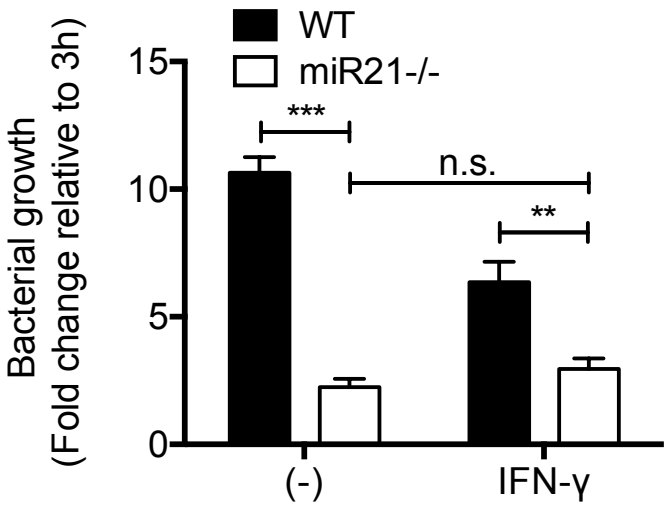

Figure 5.21 miR-21 deficient macrophages have no enhanced ability to contain Mtb growth when treated with IFN-γ. Wild-type and miR-21 knockout murine BMDM were pre-treated with 5 ng/mL IFN-γ and infected with live Mtb (strain H37Ra) at an MOI of 5 bacteria per cell for 3, 24 and 72 hours. Cells were lysed in 0.1% Triton X-100 at the indicated time points and the lysates diluted in Middlebrook broth supplemented with ADC. Aliquots of the lysates were then streaked in triplicate on warm Middlebrook agar plates and incubated at 37°C for approximately 14 days. Colony forming units were counted and the number of colonies relative to the 3-hour time point calculated. Statistical analysis was performed using a paired, two-tailed Student's t-test. *, ** and *** represent $p<0.05$, 0.01 and 0.001 respectively. Data shown as mean ± SEM, n = 3 independent experiments.

5.2.13 IFN-γ potentiates the expression of glycolytic genes in response to Mtb infection

miR-21 activity was found to be blocked by IFN-γ. In turn, IFN-γ potentiated the induction of pro-inflammatory responses and this potentiation was dependent on miR-21. This led to the hypothesis that IFN-γ targets miR-21 to block its negative regulation of glycolysis and pro-inflammatory mechanisms. The expression of several genes involved in the glycolytic pathway were examined in the context of IFN-γ treatment. IFN-γ significantly enhanced the expression of Slc2a1, hexokinase 2 and LdhA in response to Mtb infection to near miR-21 knockout levels (**Figure 5.22**). miR-21 knockout BMDM were resistant to the potentiation of gene expression by IFN-γ.

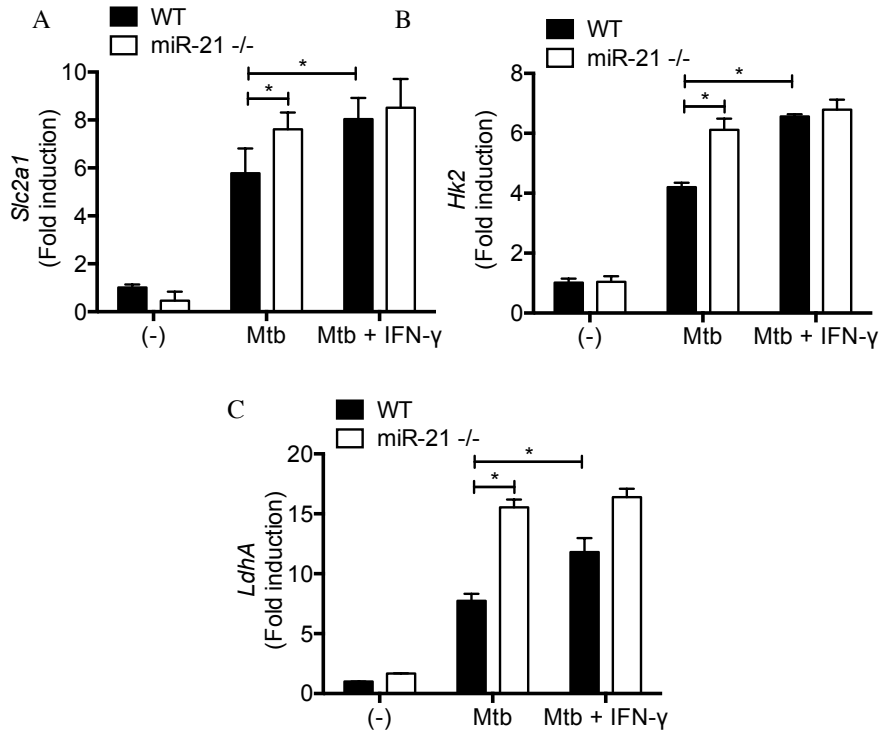

Figure 5.22 IFN-γ potentiates glycolytic genes in wild-type BMDM. BMDM were pre-treated with 5 ng/mL IFN-γ and infected with live Mtb (strain H37Ra) at an MOI of 5 bacteria per cell or 100 ng/mL LPS for 24 hours. qPCR was performed and expression of *Slc2a1* (A), *Hk2* (B) and *LdhA* (C) mRNA relative to the untreated control was calculated (A). Data were normalised to 18S. Statistical analysis was performed using a paired, two-tailed Student's t-test. *, ** and *** represent $p<0.05$, 0.01 and 0.001 respectively. Data shown as mean ± SEM, n = 3 independent experiments.

5.2.14 IFN-γ boosts PFK-M in Mtb-infected macrophages

miR-21 targets PFK-M to limit glycolysis, thus it was hypothesised that if IFN-γ blocks the activity of miR-21, PFK-M would have some protection from miR-21-mediated downregulation after Mtb infection.

Wild-type and miR-21 knockout BMDM were infected with LPS or Mtb and PFK-M mRNA was measured. Stimulation with LPS or Mtb suppressed induction of PFK-M, however IFN-γ treatment enhanced PFK-M expression above baseline (though not significantly) and protected its expression from degradation after stimulation with LPS or Mtb (**Figure 5.23A**). Though IFN-γ sustains wild-type PFK-M expression, miR-21 knockout BMDM still express higher levels of PFK-M mRNA in response to infection, increasing the levels above baseline (**Figure 5.23B**).

Though PFK-M mRNA was only modestly and not significantly higher in Mtb-infected macrophages pre-treated with IFN-γ compared to those untreated with IFN-γ, PFK-M protein was found to be enhanced by IFN-γ priming both basally and after Mtb infection (**Figure 5.24**).

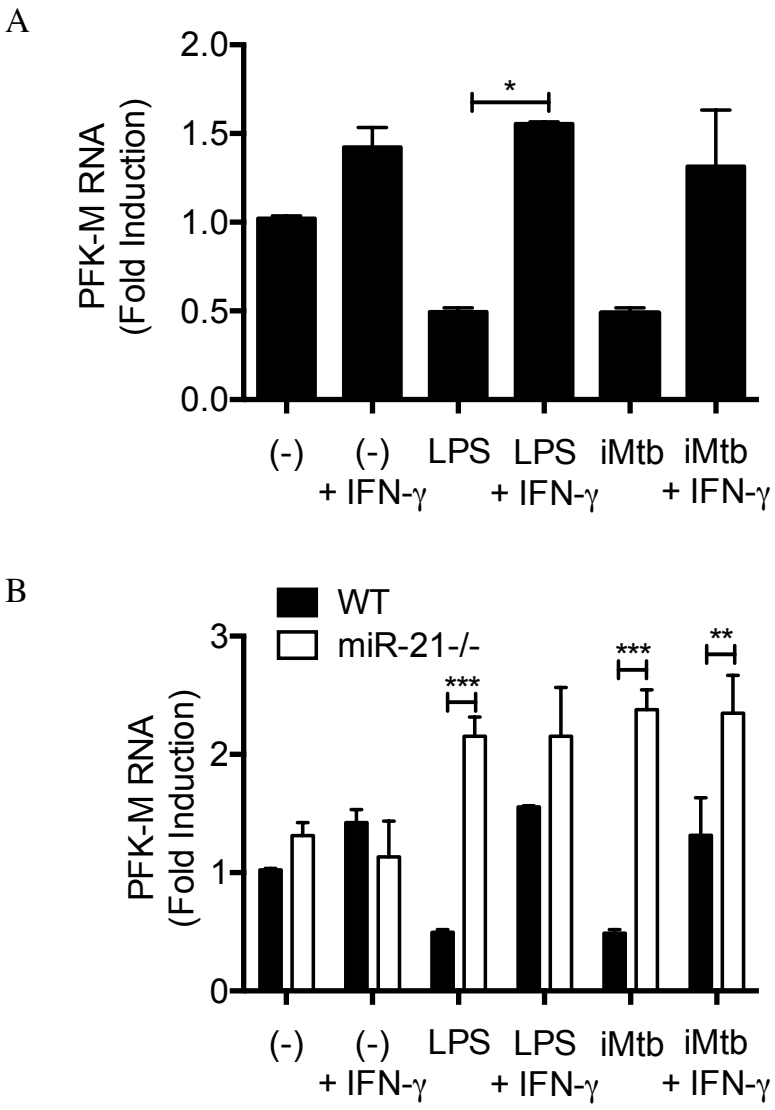

Figure 5.23 Expression of PFK-M is sustained after infection in the presence of IFN-γ. Wild-type and miR-21 knockout BMDM were pre-treated with 5 ng/mL IFN-γ and were stimulated with 100 ng/mL LPS or infected with irradiated Mtb (strain H37Rv) (iMtb) at an MOI of 5 bacteria per cell 24 hours. RNA was isolated and qPCR was performed. Expression of PFK-M mRNA relative to the untreated control was calculated. Data were normalised to 18S. Statistical analysis was performed using ordinary one-way ANOVA with Tukey's multiple comparisons test (A) and a paired, two-tailed Student's t-test (B). *, ** and *** represent $p<0.05$, 0.01 and 0.001 respectively. Data shown as mean ± SEM, n = 3 independent experiments.

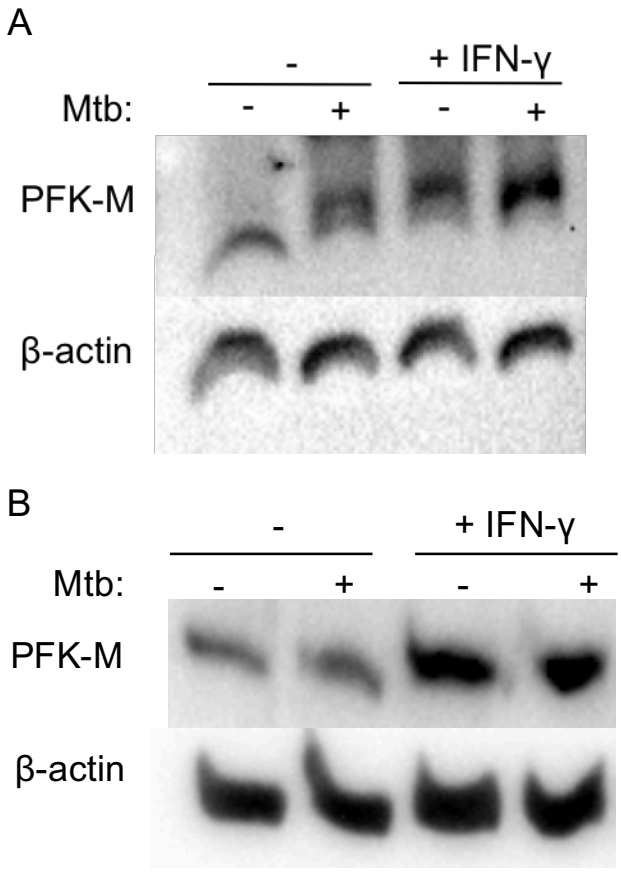

Figure 5.24 IFN-γ induces expression of PFK-M protein in BMDM. BMDM were pre-treated with 5 ng/mL IFN-γ and infected with H37Ra at an MOI of 5 bacteria per cell for 24 hours. Protein was isolated and western blot was performed. PFK-M and β-actin were detected with monoclonal antibodies. Two blots (A and B) were generated.

5.2.15 IFN-γ boosts PFK-1 activity in Mtb-infected macrophages

IFN-γ priming before Mtb infection was found to enhance PFK-M mRNA and protein levels. Total PFK-1 enzyme activity after IFN-γ pre-treatment was assessed. PFK-1 activity in wild-type BMDM was reduced by infection, and curiously by IFN-γ treatment alone (**Figure 5.24A**). A modest boost in PFK-1 activity in response to Mtb infection after IFN-γ priming was noted. This was more clearly identified when expressed as the relative fold change in activity relative to Mtb infection without IFN-γ priming (**Figure 5.24B**), in which case it is easier to identify approximately 25% protection of PFK-1 activity. This effect of IFN-γ priming on enzyme activity was shown to be specific to PFK-1. Hexokinase activity was measured concurrently and no significant difference between unprimed and IFN-γ-primed Mtb infected macrophages was found (**Figure 5.25**).

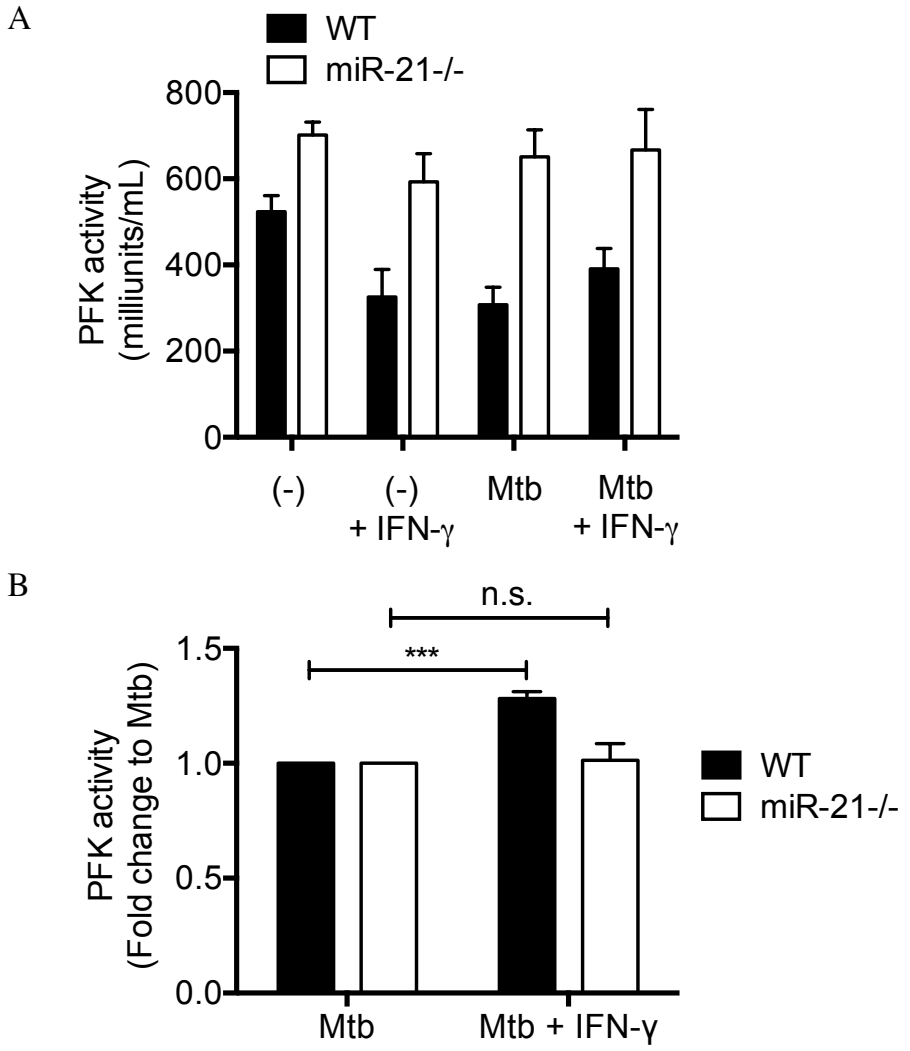

Figure 5.25 IFN-γ protects phosphofructokinase activity in wild type BMDM after Mtb infection. Wild-type and miR-21 knockout BMDM were pre-treated with 5 ng/mL IFN-γ and were infected with live Mtb (strain H37Ra) at an MOI of 5 bacteria per cell for 24 hours. Cells were homogenised and colorimetric enzyme assays were used to measure phosphofructokinase activity. Total PFK activity was calculated (A) and the relative fold change in PFK activity in Mtb-infected macrophages treated with IFN-γ compared to those infected with Mtb alone was determined (B). Statistical analysis was performed using a paired, two-tailed Student's t-test. *, ** and *** represent $p<0.05$, 0.01 and 0.001 respectively. Data shown as mean ± SEM, n = 5 independent experiments.

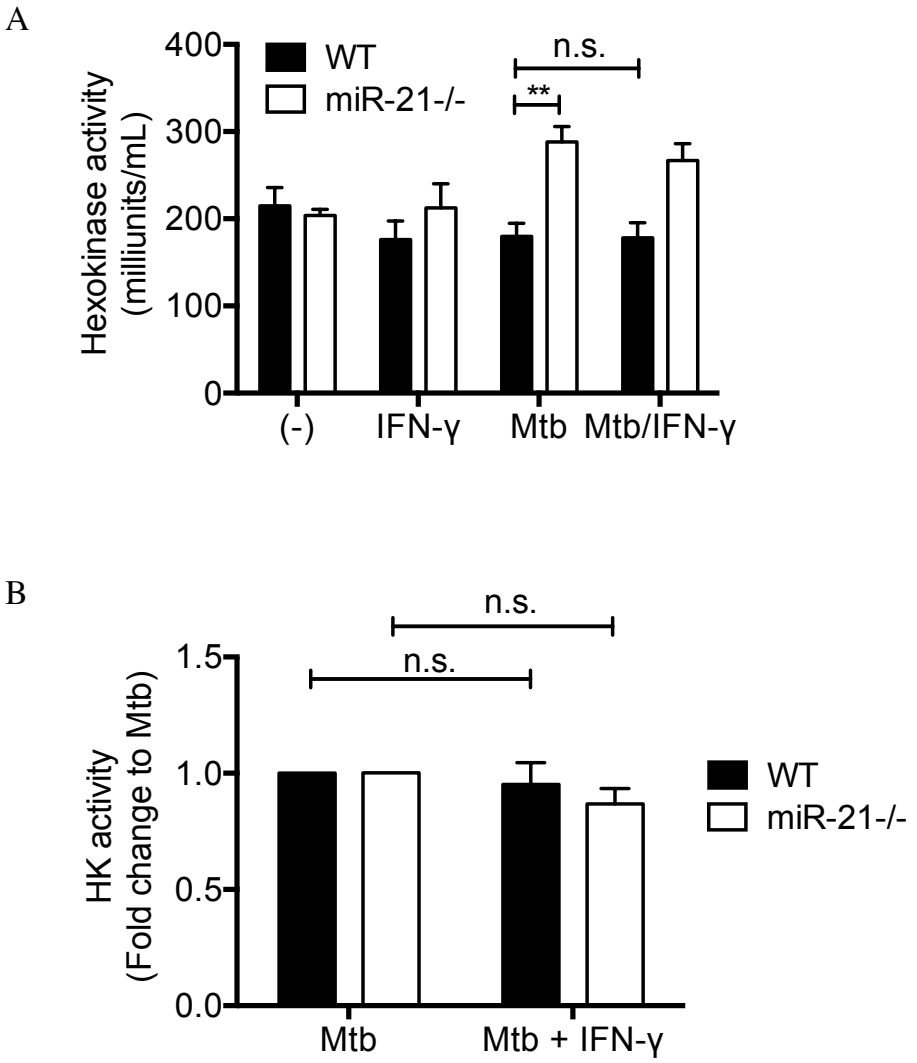

Figure 5.26 IFN-γ has no effect on hexokinase activity. Wild-type and miR-21 knockout BMDM were pre-treated with 5 ng/mL IFN-γ and were infected with live Mtb (strain H37Ra) at an MOI of 5 bacteria per cell for 24 hours. Cells were homogenised and colorimetric enzyme assays were used to measure phosphofructokinase activity. Total HK activity was calculated (A) and the relative fold change in HK activity in Mtb-infected macrophages treated with IFN-γ compared to those infected with Mtb alone was determined (B). Statistical analysis was performed using a paired, two-tailed Student's t-test. *, ** and *** represent $p<0.05$, 0.01 and 0.001 respectively. Data shown as mean ± SEM, n = 3 independent experiments.

5.2.16 IFN-γ improves containment of Mtb growth and this is dependent on glycolysis

IFN-γ is an important booster of macrophage responses to Mtb. It was found to boost macrophage anti-microbial effectors and glycolytic reprogramming, partly mediated through the miR-21-PFK-M axis, and to improve containment of Mtb growth, similar to the blockade of miR-21 activity. Glycolytic reprogramming was blocked by 2-DG treatment and the effect on bacterial containment examined. While IFN-γ significantly improved the ability of wild-type BMDM to improve bacterial containment, this effect was totally lost in the presence of 2-DG (**Figure 5.27**). No significant advantage in IFN-γ priming was found in either genotype when glycolytic reprogramming was blocked, underlining the importance of glycolysis in generating a miR-21 knockout phenocopy with IFN-γ priming.

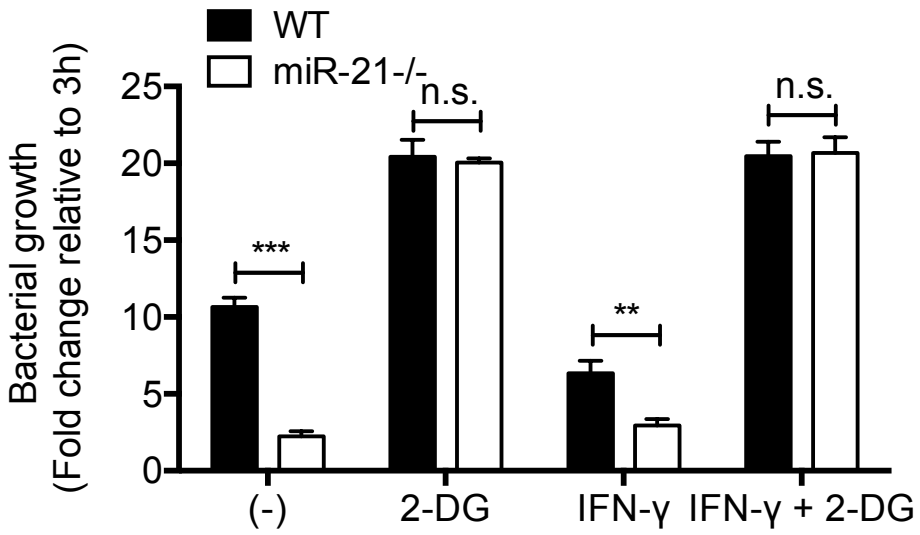

Figure 5.27 IFN-γ enhances containment of Mtb growth and this is dependent on glycolysis. Wild-type and miR-21 knockout murine BMDM were pre-treated with 5 ng/mL IFN-γ and 10 mM 2-DG for 30 minutes and infected with live Mtb (strain H37Ra) at an MOI of 5 bacteria per cell for 72 hours. Cells were lysed in 0.1% Triton X-100 and the lysates diluted in Middlebrook broth supplemented with ADC. Aliquots of the lysates were then streaked in triplicate on warm Middlebrook agar plates and incubated at 37°C for approximately 14 days. Colony forming units were counted. Statistical analysis was performed using a paired, two-tailed Student's t-test. *, ** and *** represent $p<0.05$, 0.01 and 0.001 respectively. Data shown as mean ± SEM, n = 3 individual experiments.

5.3 Discussion

Having defined a new target for miR-21 which is co-opted in Mtb infection to alter host immunometabolic response to infection, other signals altering this pathway were investigated.

IFN-γ has been shown to boost glycolytic responses to Mtb infection through HIF-1α[164] and is known to promote the induction of TLR-induced cytokines. The function of IFN-γ in Mtb infected macrophages was investigated. IFN-γ was shown to augment a range of pro-inflammatory responses in both murine and human macrophages in response to LPS and Mtb. Consistent with the findings of Braverman et al[164], IFN-γ significantly increased macrophage glycolytic rate as defined by increased lactate production and increased ECAR and ECAR to OCR ratio (**Figure 5.1 and 5.2**). This enhancement of glycolytic activity was associated with a boost in IL-1β production in both murine and human macrophages (**Figure 5.3 and 5.4**) and importantly the augmentation of IL-1β production was shown to be dependent on glycolysis. Human MDM grown in in the absence of glucose are unable to upregulate IL-1β production in response to IFN-γ priming (**Figure 5.5**).

As well as boosting glycolytic reprogramming and IL-1β production, IFN-γ boosted other cytokine responses, in line with literature indicating that IFN-γ signal-induced factors promote TLR signalling, for example enhancing NFκB signalling via STAT1 induction[372] and allowing more efficient function of MyD88 through IRF1[374]. TNF-α production was significantly enhanced, while IL-10 induction was supressed (**Figure 5.6 and 5.7**). IFN-γ is also known to be critical in the induction of NOS2 expression and absence of IFN-γ

signalling in a murine model of Mtb infection leads to uncontrolled Mtb growth due to insufficient production of nitrogen species[82]. This work demonstrates that IFN-γ treatment significantly enhanced NOS2 expression in response to LPS and particularly in response to Mtb infection, and this translated into increased production of nitrite (**Figure 5.8 and 5.9**). These improved responses effected better control of Mtb growth (**Figure 5.11**) emphasising the key role of IFN-γ in coordinating pro-inflammatory macrophage responses to promote bacterial containment. Furthermore, a key finding of these results has been to show that IFN-γ boosts macrophage metabolism and this metabolic boost is required for its pro-inflammatory and anti-microbial functions.

The similarity between the effect of IFN-γ treatment and the effect of blocking miR-21 on macrophage function (promotion of glycolysis, cytokine production, induction of NOS and improved bacterial containment) was recognised and this prompted investigation into the interplay between IFN-γ and miR-21. A decrease in the mature miR-21 transcript in response to LPS and iMtb treatment was observed with IFN-γ treatment (**Figure 5.12**). Interestingly, though IFN-γ was found to drive the transcription of cytokine, the primary miR-21 transcript was not altered by IFN-γ. MiR-21 is dysregulated in a broad range of diseases, with both insufficient and excess expression associated with disease pathology. Given the context of the findings of this chapter, this dysregulated miR-21 expression could be associated with IFN-γ status. Liu et al described two types of lesions in M. leprae disease – self-limiting and progressive[322], and each correlated with a distinct microRNA-21 high or low status respectively, and perhaps this subset of patients with high miR-21 status correlate with a low IFN-γ profile. This mechanism may also be applicable in cancer states, in which a dysregulated miR-21 profile is commonly

observed both in tumour cells and in the stromal cells including macrophages. This finding may open new therapeutic possibilities for correcting abrogated microRNA signalling.

This indicates that IFN-γ may have an additional means of altering macrophage function by way of altering miR-21 processing. Pri-miR-21 processing has been shown to be altered by TGF-β signalling through SMAD protein interactions which alter interactions of the primary transcript with the DROSHA processing machinery[380]. SMAD proteins are also targets of IFN-γ signalling[382], suggesting that this pathway may be involved in the post-transcriptional regulation of miR-21. There is some precedent for this notion of IFN-γ degrading microRNA as an additional immunomodulatory mechanism in immune cells. IFN-γ has been shown to downregulate miR-3473b in macrophages to promote PTEN accumulation and allow better induction of pro-inflammatory responses, though no molecular mechanism for this downregulation was elucidated[383]. The findings in this work would propose that this observation with miR-3473b may be due to IFN-γ-mediated downregulation of post-transcriptional processing of microRNA.

In line with the theory that IFN-γ downregulates mature miR-21 in Mtb infection, thus licensing the induction of a more pro-inflammatory phenotype capable of Mtb containment, miR-21-depleted macrophages were resistant to any additional boost in pro-inflammatory activation by IFN-γ. Lactate induction, ECAR and IL-1β production were all boosted to miR-21 knockout levels in wild-type macrophages, while no addition benefit to IFN-γ treatment was apparent in miR-21-deficient macrophages (**Figure 5.13-5.15**). Similarly TNF-α, iNOS and nitrite induction were boosted by IFN-γ to phenocopy miR-21 knockout macrophages (**Figure 5.16-5.19**),

but no additional boost was seen in knockout macrophages after IFN-γ treatment, and subsequently no additional ability to contain Mtb growth (**Figure 5.21**). This phenocopying would suggest that there are more specific ways of targeting key antimicrobial functions of IFN-γ, such as targeting miR-21 or a miR-21 target interaction, to make it a safer treatment.

These findings indicate that though miR-21 acts as a molecular brake on pro-inflammatory responses by limiting the induction of glycolysis, IFN-γ can lift this brake and allow glycolysis to proceed unimpeded and thus promote antimicrobial responses. Accordingly, IFN-γ was found to potentiate the induction of glycolytic genes in wild-type macrophages to miR-21 knockout levels (**Figure 5.22**). PFK-M was shown to be a direct target of miR-21, limiting the glycolytic rate. PFK-M mRNA was not boosted to the levels in miR-21-deficient macrophages, however PFK-M was resistant to transcription downregulation after treatment with LPS or iMtb (**Figure 5.23**) and this corresponded to an increase in protein levels after IFN-γ priming (**Figure 5.24**), and a subtle increase in PFK enzyme activity after Mtb infection (approximately 20%) (**Figure 5.25**). Thus IFN-γ relieves some of the miR-21-mediated suppression of PFK-M activity, allowing better glycolytic induction. The ability of IFN-γ to control Mtb infection was shown to be dependent on glycolysis. Blocking glycolysis with 2-DG resulted in a uncontrolled Mtb growth even in macrophages primed with IFN-γ (**Figure 5.27**). This work highlights the central regulation of glycolysis in immune cell reprogramming by PFK-M, placing it as a key hub in the metabolic network that can be targeted to modulate glycolytic rates.

5.4 Conclusion

This chapter has shown that IFN-γ is a potent driver of pro-inflammatory macrophage responses, boosting immunometabolic and antimicrobial functions in Mtb infected macrophages. IFN-γ-mediated augmentation of innate immunity has been shown to be instigated by the induction of molecules which boost TLR signalling. This work proposes an additional mechanism by which IFN-γ promotes anti-mycobacterial responses. Accumulation of mature miR-21, though not transcription of the miR-21 primary transcript was shown to be blocked by IFN-γ treatment of macrophages. Macrophages deficient in miR-21 were resistant to IFN-γ augmentation of pro-inflammatory and immunometabolic responses, providing further evidence that IFN-γ alters miR-21 expression to promote anti-microbial activity. The novel target for miR-21, PFK-M, was shown to be modulated by IFN-γ, with IFN-γ treatment relieving some of the degradation of its mRNA and suppression of enzymatic activity. These findings place miR-21 as a central signalling hub in the macrophage, integrating both activating and inhibitory signals to fine-tune immunometabolic and inflammatory responses, which has critical implications for cancer and inflammatory diseases.

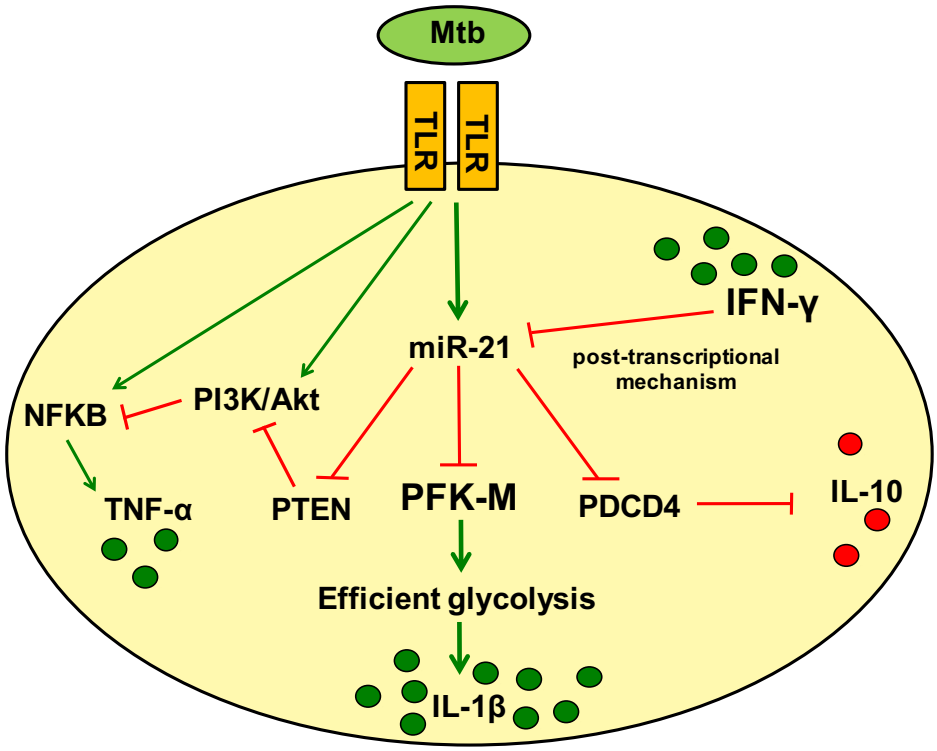

Figure 5.28 Diagram of the proposed model of key miR-21 targets in Mtb infection and how IFN-γ overrides miR-21 suppression. MiR-21 expression is induced by Mtb infection of the macrophage downstream of TLR signalling. MiR-21 downregulates TNF-α expression by targeting PTEN. Targeting of the negative regulator of IL-10 expression, PDCD4, boosts IL-10 production. PFK-M is targeted by miR-21, resulting in lower PFK-1 enzyme activity, less efficient glycolytic activity and ultimately lower IL-1β production. IFN-γ blocks miR-21 maturation and thus counteracts the inhibitory activities of miR-21 and promotes a pro-inflammatory macrophage response.

Chapter 6: Final Discussion

Metabolism has emerged as a new frontier in the field of immunology, providing a better insight into the processes governing immune cell responses and providing a wealth of new therapeutic targets. Mtb infection remains a global health pandemic and understanding the host immune response to this bacteria is of key importance for developing novel host-directed therapies. This work, in examining how Mtb manipulates the innate immune system, has identified a new central regulator of the immunometabolic response in macrophages, namely the control of PFK-M expression by miR-21 and consequently the activity of the key gatekeeper enzyme in glycolysis PFK-1.

This work has conclusively shown that miR-21 is upregulated in both human and murine macrophages in response to Mtb infection. Furthermore, this work has demonstrated that there is differential induction of miR-21 depending on the viability of the bacterium. Live Mtb was found to induce more miR-21 than dead Mtb of the same strain. This preferential induction of miR-21 by live bacteria presents itself as a mechanism by which viable Mtb can limit the antimicrobial effector mechanisms of the macrophage. Additionally, the induction of glycolysis and the resulting production of IL-1β, essential for bacterial containment, was not as substantial with live Mtb compared to dead. This suggests that live bacteria induce more miR-21 to limit the induction of glycolytic reprogramming. It could be postulated that different strains of Mtb have evolved to induce different degrees of miR-21 expression which impacts on the extent of glycolytic programming and thus on virulence. A recent publication by Howard et al reported that virulent Mtb have evolved mechanisms that bypass the induction of macrophage glycolysis by altering mycobacterial cell wall lipids[384] and prevent the induction of IL-1β. It could be hypothesised that this could be driven by induction of miR-21 by these lipids.

Previous work has shown miR-21 to negatively regulate innate immunity by modulating the expression of both pro-inflammatory and immunoregulatory cytokines, thus it was hypothesised that miR-21 would have a suppressive effect on immune responses to Mtb infection. This work showed that blocking miR-21 activity in the context of Mtb infection promoted bacterial containment. In beginning this work, it was thought that IL-10 would be the key process regulated by miR-21 during Mtb infection, given previous work showing that miR-21 promotes IL-10 production in response to LPS[296] and the key role for IL-10 in blocking phagosome maturation[117]. Surprisingly, although there was some decrease in IL-10 it wasn't always consistent and it wasn't the functional process regulating bacterial survival. This could be due to differential engagement of the mRNA target regulating IL-10, PDCD4, which was never drastically changed in this Mtb model. However, unlike LPS studies, a highly significant effect on IL-1β was found. This work places IL-1β as a key cytokine in the host response to Mtb which the bacterium has evolved to evade.

While the TLR activation of macrophages has been shown to suppress the TCA cycle and drive glycolysis through HIf-1α[176], how this is regulated over time in an infection setting is relatively unexplored. Glycolytic metabolism has recently been shown to be induced early in Mtb infection and is essential for the production of IL-1β and containment of mycobacterial growth[204]. Live Mtb bacteria were found to negatively regulate the induction of glycolysis in comparison to dead Mtb of the same strain, indicating that live bacteria were more potently inducing a limiting factor on host cell metabolism. This work describes the temporal regulation of glycolysis in Mtb infection and demonstrates how miR-21 induced by live bacteria negatively regulates this process. MiR-21 upregulation coincides with the shutting off of glycolytic metabolism and macrophages deficient in this microRNA have an increased

capacity for glycolysis and additionally can sustain this induction. Live bacteria have an inherent capacity to potentiate the induction of miR-21 later in infection and thus modulate the macrophage phenotype to render it permissive to bacterial survival and replication. This newly described role for miR-21 in immunometabolic reprogramming has implications beyond immunity. Dysregulated metabolism is a common signature in a range of disease states beyond infection including cancer and fibrosis, both of which miR-21 has been implicated in[295, 300, 301, 304, 306, 313, 383], thus targeting miR-21 to alter cellular metabolic functions may be applicable far beyond the scope of Mtb infection.

While NFκB is thought to be responsible for the early induction of IL-1β, HIF-1α can also induce IL-1β transcription, and is thought to be responsible for the sustained induction of IL-1β later in the course of inflammation[175, 176]. Expression of HIF-1α in turn is enhanced by increased glycolysis[239]. This work showed for the first time that Mtb-induced transcription of IL-1β was negatively regulated by miR-21, providing evidence for IL-1β as the key cytokine regulated by miR-21 in Mtb infection, in line with previous studies of *M. leprae*. Though there is some evidence that IL-1β may be directly targeted by miR-21, Mtb-induced IL-1β mRNA was less susceptible to actinomycin D degradation suggesting de novo transcribed IL-1β mRNA is more stable and is subject to indirect regulation through the metabolic environment.

Though studies with LPS have shown a concomitant suppression of TCA cycle activity when glycolysis is activated, no accompanying decrease in TCA cycle activity was observed in the miR-21-deficient macrophages when Mtb upregulated glycolysis. This is in line with reports that Mtb drives the accumulation of lipid droplets and promotes fatty acid oxidation in infected macrophages[385], the

metabolites of which would support the TCA cycle and oxidative phosphorylation alongside increased glycolysis. Here, a novel point of regulation in this process of glycolytic upregulation has been proposed. This work has found a previously unexplored target of miR-21, a subunit in the PFK-1 rate-limiting enzyme in glycolysis, is directly targeted by miR-21 to reduce PFK-1 activity and limit glycolysis. PFK-1 is the gatekeeper enzyme to glycolysis which determines whether glucose continues down the glycolytic pathway or is alternatively converted to glycogen or shunted down the PPP. Having found no significant difference in glucose consumption between wild-type and miR-21 knockout macrophages after infection despite significant differences in glycolytic activity, this suggests miR-21 regulates a more complex system of metabolic reprogramming than simply reduced oxidative phosphorylation and enhanced glycolysis. MiR-21 targeting of PFK-1 activity could be of benefit to Mtb by shunting glucose away from glycolysis towards other pathways such as the PPP and thus enhancing the production of beneficial metabolites such as nucleotide precursors and fatty acids which promote Mtb growth. This would also sustain the TCA cycle, avoiding pro-inflammatory, antimicrobial events associated with its downregulation such as succinate accumulation and subsequent IL-1β and ROS generation.

IFN-γ has been shown to override pathogen inhibitory activity on macrophages, such as by triggering the maturation of arrested phagosomes[386], and has been shown to upregulate glycolysis through HIF-1α to drive pro-inflammatory functions[164]. This work shows that the IFN-γ-driven antimicrobial functions and additional pro-inflammatory licensing given to macrophages is dependent on glycolysis. Furthermore, the modulation of miR-21 by IFN-γ to promote glycolysis by relieving suppression of PFK-M represents a novel supplementary mechanism by which IFN-γ regulates immunometabolism, and ultimately instructs the macrophage to

maintain a phenotype which favours bacterial containment. This finding is consistent with recent literature which has emphasised the essential role of IFN-γ in promoting macrophage glycolysis and the generation of nitric oxide species[58, 164], both of which were found to be enhanced in the Mtb-infected miR-21 knockout macrophage. Targeting of miR-21 by IFN-γ emphasises its key role as a central hub which fine-tunes the balance between pro-inflammatory and resolving immune processes.

Furthermore, this work has suggested a new mechanism by which IFN-γ promotes glycolysis and pro-inflammatory immune responses. The observation that IFN-γ post-transcriptionally represses mature miR-21 is novel. Post-transcriptional regulation of miR-21 has been described in response to TGF-β signalling[299]. TGF-β has been shown to promote an increase in mature miR-21 through a post-transcriptional mechanism which enhances the processing of pri-miR-21 into pre-miR-21 by DROSHA. SMAD1 and 5 proteins interact with pri-miR-21 and are incorporated into the DROSHA complex, enhancing the stability of the interaction between pri-miR-21 and DROSHA[299]. Conversely, IFN-γ activates the JAK/STAT signalling pathway, inducing the inhibitory SMAD7 through STAT1[380]. It could postulated that SMAD7 inhibits the pri-miR-21 interaction with DROSHA to limit miR-21 expression. In turn, miR-21 has recently been shown to target SMAD7[387], indicative of cross-talk between the IFN-γ/Jak/STAT and miR-21 pathways. There is some evidence for a role in IFN-γ-mediated downregulation of a microRNA to boost innate immune responses. IFN-γ-primed macrophages were demonstrated to downregulate miR-3473b which allowed accumulation of its target PTEN and suppression of IL-10 induction[260]. The findings here, in tandem with the limited existing literature, indicate that IFN-γ signalling may

post-transcriptionally regulate a panel of microRNA to alter macrophage phenotype.

Novel, inhaled IFN-γ treatments are being developed to treat Mtb infection. These findings propose that IFN-γ therapy may in part have efficacy by altering miRNA expression. Furthermore it warrants investigation into the delivery of inhalable miRNA therapeutics which could be delivered alongside or instead of IFN-γ to specifically block the activity of particular miRNA, either by miRNA silencing or more specifically using a target protection strategy. More broadly speaking, these findings may have implications for the understanding and treatment of other diseases of metabolic dysregulation including cancer, where silencing the exosomal microRNA secreted by tumour cells to modulate tumour-associated macrophages may tip the balance towards immune clearance of the tumour cells.

In summary, the findings of this thesis provide evidence for miR-21 as a key modulator of macrophage metabolism which is both exploited by Mtb to promote bacterial growth and curbed by IFN-γ to safeguard and promote a pro-inflammatory macrophage phenotype. The promising new field of immunometabolism is growing exponentially and the work presented here is one example of how a better understanding of the basic processes of the immune cell can provide new targets for therapeutic intervention. *Mycobacterium tuberculosis* is the world's biggest infectious killer and this work identifies miR-21 as a novel target which could be manipulated to improve host responses to eradicate this pathogen.

References

1. Organization, W.H. Global Tuberulosis Report. Geneva; 2017.

2. Paulson, T. Epidemiology: A mortal foe. *Nature* **502**, S2-3 (2013).

3. Lange, C. *et al.* Drug-resistant tuberculosis: An update on disease burden, diagnosis and treatment. *Respirology* **23**, 656-673 (2018).

4. Sharma, A. *et al.* Estimating the future burden of multidrug-resistant and extensively drug-resistant tuberculosis in India, the Philippines, Russia, and South Africa: a mathematical modelling study. *Lancet Infect Dis* **17**, 707-715 (2017).

5. Houben, R.M. & Dodd, P.J. The Global Burden of Latent Tuberculosis Infection: A Re-estimation Using Mathematical Modelling. *PLoS Med* **13**, e1002152 (2016).

6. Rodrigues, L.C., Diwan, V.K. & Wheeler, J.G. Protective effect of BCG against tuberculous meningitis and miliary tuberculosis: a meta-analysis. *Int J Epidemiol* **22**, 1154-1158 (1993).

7. Mangtani, P. *et al.* Protection by BCG vaccine against tuberculosis: a systematic review of randomized controlled trials. *Clin Infect Dis* **58**, 470-480 (2014).

8. Xue, X., Qiu, Y. & Yang, H.L. Immunoregulatory Role of MicroRNA-21 in Macrophages in Response to Bacillus Calmette-Guerin Infection Involves Modulation of the TLR4/MyD88 Signaling Pathway. *Cell Physiol Biochem* **42**, 91-102 (2017).

9. Delogu, G., Sali, M. & Fadda, G. The biology of mycobacterium tuberculosis infection. *Mediterr J Hematol Infect Dis* **5**, e2013070 (2013).

10. Banuls, A.L., Sanou, A., Anh, N.T. & Godreuil, S. Mycobacterium tuberculosis: ecology and evolution of a human bacterium. *J Med Microbiol* **64**, 1261-1269 (2015).

11. Gidel, R., Albert, J.P., Lefevre, M., Menard, M. & Retif, M. [Mycobacteria of animal origin isolated by the Muraz Center from 1965 to 1968: technics of isolation and identification; results]. *Rev Elev Med Vet Pays Trop* **22**, 495-508 (1969).

12. Brites, D. & Gagneux, S. Old and new selective pressures on Mycobacterium tuberculosis. *Infect Genet Evol* **12**, 678-685 (2012).

13. Blomgran, R., Desvignes, L., Briken, V. & Ernst, J.D. Mycobacterium tuberculosis Inhibits Neutrophil Apoptosis, Leading to Delayed Activation of Naive CD4 T cells. *Cell Host & Microbe* **11**, 81-90 (2012).

14. Comas, I. *et al.* Human T cell epitopes of Mycobacterium tuberculosis are evolutionarily hyperconserved. *Nat Genet* **42**, 498-503 (2010).

15. Coscolla, M. *et al.* M. tuberculosis T Cell Epitope Analysis Reveals Paucity of Antigenic Variation and Identifies Rare Variable TB Antigens. *Cell Host Microbe* **18**, 538-548 (2015).

16. Fonseca, K.L., Rodrigues, P.N.S., Olsson, I.A.S. & Saraiva, M. Experimental study of tuberculosis: From animal models to complex cell systems and organoids. *Plos Pathogens* **13** (2017).

17. Orme, I.M. The mouse as a useful model of tuberculosis. *Tuberculosis* **83**, 112-115 (2003).

18. Smith, C.M. *et al.* Tuberculosis Susceptibility and Vaccine Protection Are Independently Controlled by Host Genotype. *Mbio* **7** (2016).

19. Nadkarni, R.R., Abed, S. & Draper, J.S. Organoids as a model system for studying human lung development and disease. *Biochem Bioph Res Co* **473**, 675-682 (2016).

20. Fennelly, K.P. *et al.* Variability of infectious aerosols produced during coughing by patients with pulmonary tuberculosis. *Am J Respir Crit Care Med* **186**, 450-457 (2012).

21. Caws, M. *et al.* The influence of host and bacterial genotype on the development of disseminated disease with Mycobacterium tuberculosis. *PLoS Pathog* **4**, e1000034 (2008).

22. Ewer, K. *et al.* Dynamic antigen-specific T-cell responses after point-source exposure to Mycobacterium tuberculosis. *Am J Respir Crit Care Med* **174**, 831-839 (2006).

23. Cobat, A. *et al.* Two loci control tuberculin skin test reactivity in an area hyperendemic for tuberculosis. *J Exp Med* **206**, 2583-2591 (2009).

24. Morrison, J., Pai, M. & Hopewell, P.C. Tuberculosis and latent tuberculosis infection in close contacts of people with pulmonary tuberculosis in low-income and middle-income countries: a systematic review and meta-analysis. *Lancet Infect Dis* **8**, 359-368 (2008).

25. Andrews, J.R. *et al.* Risk of progression to active tuberculosis following reinfection with Mycobacterium tuberculosis. *Clin Infect Dis* **54**, 784-791 (2012).

26. Verver, S. *et al.* Rate of reinfection tuberculosis after successful treatment is higher than rate of new tuberculosis. *Am J Respir Crit Care Med* **171**, 1430-1435 (2005).

27. Julia, V. *et al.* A restricted subset of dendritic cells captures airborne antigens and remains able to activate specific T cells long after antigen exposure. *Immunity* **16**, 271-283 (2002).

28. Guilliams, M. *et al.* Alveolar macrophages develop from fetal monocytes that differentiate into long-lived cells in the first week of life via GM-CSF. *J Exp Med* **210**, 1977-1992 (2013).

29. Gibbings, S.L. *et al.* Three Unique Interstitial Macrophages in the Murine Lung at Steady State. *Am J Resp Cell Mol* **57**, 66-76 (2017).

30. Sabatel, C. *et al.* Exposure to Bacterial CpG DNA Protects from Airway Allergic Inflammation by Expanding Regulatory Lung Interstitial Macrophages. *Immunity* **46**, 457-473 (2017).

31. Liegeois, M., Legrand, C., Desmet, C.J., Marichal, T. & Bureau, F. The interstitial macrophage: A long-neglected piece in the puzzle of lung immunity. *Cell Immunol* **330**, 91-96 (2018).

32. Schlesinger, L.S. Entry of Mycobacterium tuberculosis into mononuclear phagocytes. *Tuberculosis* **215**, 71-96 (1996).

33. Kleinnijenhuis, J., Oosting, M., Joosten, L.A.B., Netea, M.G. & Van Crevel, R. Innate Immune Recognition of Mycobacterium tuberculosis. *Clin Dev Immunol* (2011).

34. Armstrong, J.A. & Hart, P.D. Response of cultured macrophages to Mycobacterium tuberculosis, with observations on fusion of lysosomes with phagosomes. *J Exp Med* **134**, 713-740 (1971).

35. Crowle, A.J., Dahl, R., Ross, E. & May, M.H. Evidence that vesicles containing living, virulent Mycobacterium tuberculosis or Mycobacterium avium in cultured human macrophages are not acidic. *Infect Immun* **59**, 1823-1831 (1991).

36. Malik, Z.A., Denning, G.M. & Kusner, D.J. Inhibition of Ca(2+) signaling by Mycobacterium tuberculosis is associated with reduced phagosome-lysosome fusion and increased survival within human macrophages. *J Exp Med* **191**, 287-302 (2000).

37. Beatty, W.L. *et al.* Trafficking and release of mycobacterial lipids from infected macrophages. *Traffic* **1**, 235-247 (2000).

38. Davis, J.M. & Ramakrishnan, L. The role of the granuloma in expansion and dissemination of early tuberculous infection. *Cell* **136**, 37-49 (2009).

39. Schaible, U.E., Sturgill-Koszycki, S., Schlesinger, P.H. & Russell, D.G. Cytokine activation leads to acidification and increases maturation of Mycobacterium avium-containing phagosomes in murine macrophages. *J Immunol* **160**, 1290-1296 (1998).

40. Cooper, A.M. Cell-mediated immune responses in tuberculosis. *Annu Rev Immunol* **27**, 393-422 (2009).

41. Means, T.K. *et al.* Differential effects of a Toll-like receptor antagonist on Mycobacterium tuberculosis-induced macrophage responses. *J Immunol* **166**, 4074-4082 (2001).

42. Stamm, C.E., Collins, A.C. & Shiloh, M.U. Sensing of Mycobacterium tuberculosis and consequences to both host and bacillus. *Immunological reviews* **264**, 204-219 (2015).

43. Underhill, D.M., Ozinsky, A., Smith, K.D. & Aderem, A. Toll-like receptor-2 mediates mycobacteria-induced proinflammatory signaling in macrophages. *Proc Natl Acad Sci U S A* **96**, 14459-14463 (1999).

44. Means, T.K. *et al.* The CD14 ligands lipoarabinomannan and lipopolysaccharide differ in their requirement for Toll-like receptors. *J Immunol* **163**, 6748-6755 (1999).

45. Sanchez, D. *et al.* Role of TLR2- and TLR4-mediated signaling in Mycobacterium tuberculosis-induced macrophage death. *Cell Immunol* **260**, 128-136 (2010).

46. Ozinsky, A. *et al.* The repertoire for pattern recognition of pathogens by the innate immune system is defined by cooperation between toll-like receptors. *Proc Natl Acad Sci U S A* **97**, 13766-13771 (2000).

47. Bulut, Y., Faure, E., Thomas, L., Equils, O. & Arditi, M. Cooperation of Toll-like receptor 2 and 6 for cellular activation by soluble tuberculosis factor and Borrelia burgdorferi outer surface protein A lipoprotein: role of Toll-interacting protein and IL-1 receptor signaling molecules in Toll-like receptor 2 signaling. *J Immunol* **167**, 987-994 (2001).

48. Hemmi, H. *et al.* A Toll-like receptor recognizes bacterial DNA. *Nature* **408**, 740-745 (2000).

49. Ke, Z.Q. *et al.* IL-10 Polymorphisms and Tuberculosis Susceptibility: An Updated Meta-Analysis. *Yonsei Med J* **56**, 1274-1287 (2015).

50. Holscher, C. *et al.* Containment of aerogenic Mycobacterium tuberculosis infection in mice does not require MyD88 adaptor function for TLR2, -4 and -9. *Eur J Immunol* **38**, 680-694 (2008).

51. Mayer-Barber, K.D. *et al.* Innate and Adaptive Interferons Suppress IL-1 alpha and IL-1 beta Production by Distinct Pulmonary Myeloid Subsets during Mycobacterium tuberculosis Infection. *Immunity* **35**, 1023-1034 (2011).

52. Slauch, J.M. How does the oxidative burst of macrophages kill bacteria? Still an open question. *Mol Microbiol* **80**, 580-583 (2011).

53. Cooper, A.M., Segal, B.H., Frank, A.A., Holland, S.M. & Orme, I.M. Transient loss of resistance to pulmonary tuberculosis in p47phox(-/-) mice. *Infect Immun* **68**, 1231-1234 (2000).

54. Esterly, J.R., Sturner, W.Q., Esterly, N.B. & Windhorst, D.B. Disseminated Bcg in Twin Boys with Presumed Chronic Granulomatous Disease of Childhood. *Pediatrics* **48**, 141-+ (1971).

55. Piddington, D.L. *et al.* Cu,Zn superoxide dismutase of Mycobacterium tuberculosis contributes to survival in activated macrophages that are generating an oxidative burst. *Infect Immun* **69**, 4980-4987 (2001).

56. Manca, C., Paul, S., Barry, C.E., Freedman, V.H. & Kaplan, G. Mycobacterium tuberculosis catalase and peroxidase activities and resistance to oxidative killing in human monocytes in vitro. *Infect Immun* **67**, 74-79 (1999).

57. Chan, J., Xing, Y., Magliozzo, R.S. & Bloom, B.R. Killing of Virulent Mycobacterium-Tuberculosis by Reactive Nitrogen Intermediates Produced by Activated Murine Macrophages. *J Exp Med* **175**, 1111-1122 (1992).

58. Braverman, J. & Stanley, S.A. Nitric Oxide Modulates Macrophage Responses to Mycobacterium tuberculosis Infection through Activation of HIF-1 alpha and Repression of NF-kappa B. *Journal of Immunology* **199**, 1805-1816 (2017).

59. Thomas, A.C. & Mattila, J.T. "Of mice and men": arginine metabolism in macrophages. *Front Immunol* **5**, 479 (2014).

60. Jung, J.Y. *et al.* The Intracellular Environment of Human Macrophages That Produce Nitric Oxide Promotes Growth of Mycobacteria. *Infect Immun* **81**, 3198-3209 (2013).

61. Rich, E.A. *et al.* Mycobacterium tuberculosis (MTB)-stimulated production of nitric oxide by human alveolar macrophages and relationship of nitric oxide production to growth inhibition of MTB. *Tubercle Lung Dis* **78**, 247-255 (1997).

62. Wang, C.H. *et al.* Increased exhaled nitric oxide in active pulmonary tuberculosis due to inducible NO synthase upregulation in alveolar macrophages. *Eur Respir J* **11**, 809-815 (1998).

63. Pym, A.S., Brodin, P., Brosch, R., Huerre, M. & Cole, S.T. Loss of RD1 contributed to the attenuation of the live tuberculosis vaccines Mycobacterium bovis BCG and Mycobacterium microti. *Mol Microbiol* **46**, 709-717 (2002).

64. Behar, S.M. *et al.* Apoptosis is an innate defense function of macrophages against Mycobacterium tuberculosis. *Mucosal Immunology* **4**, 279-287 (2011).

65. Kelly, D.M., ten Bokum, A.M.C., O'Leary, S.M., O'Sullivan, M.P. & Keane, J. Bystander macrophage apoptosis after Mycobacterium tuberculosis H37Ra infection. *Infect Immun* **76**, 351-360 (2008).

66. Velmurugan, K. *et al.* Mycobacterium tuberculosis nuoG is a virulence gene that inhibits apoptosis of infected host cells. *Plos Pathogens* **3**, 972-980 (2007).

67. Martin, C.J. *et al.* Efferocytosis Is an Innate Antibacterial Mechanism. *Cell Host & Microbe* **12**, 289-300 (2012).

68. Eruslanov, E.B. *et al.* Neutrophil responses to Mycobacterium tuberculosis infection in genetically susceptible and resistant mice. *Infect Immun* **73**, 1744-1753 (2005).

69. Eum, S.Y. *et al.* Neutrophils Are the Predominant Infected Phagocytic Cells in the Airways of Patients With Active Pulmonary TB. *Chest* **137**, 122-128 (2010).

70. Panteleev, A.V. *et al.* Severe Tuberculosis in Humans Correlates Best with Neutrophil Abundance and Lymphocyte Deficiency and Does Not Correlate with Antigen-Specific CD4 T-Cell Response. *Front Immunol* **8**, 963 (2017).

71. Mishra, B.B. *et al.* Nitric oxide prevents a pathogen-permissive granulocytic inflammation during tuberculosis. *Nat Microbiol* **2**, 17072 (2017).

72. Seiler, P. *et al.* Rapid neutrophil response controls fast-replicating intracellular bacteria but not slow-replicating Mycobacterium tuberculosis. *J Infect Dis* **181**, 671-680 (2000).

73. Braian, C., Hogea, V. & Stendahl, O. Mycobacterium tuberculosis-Induced Neutrophil Extracellular Traps Activate Human Macrophages. *J Innate Immun* **5**, 591-602 (2013).

74. Hedlund, S. *et al.* Dendritic cell activation by sensing Mycobacterium tuberculosis-induced apoptotic neutrophils via DC-SIGN. *Hum Immunol* **71**, 535-540 (2010).

75. Blomgran, R. & Ernst, J.D. Lung Neutrophils Facilitate Activation of Naive Antigen-Specific CD4(+) T Cells during Mycobacterium tuberculosis Infection. *Journal of Immunology* **186**, 7110-7119 (2011).

76. Steinman, R.M. Decisions About Dendritic Cells: Past, Present, and Future. *Annual Review of Immunology, Vol 30* **30**, 1-22 (2012).

77. Madan-Lala, R. *et al.* Mycobacterium tuberculosis Impairs Dendritic Cell Functions through the Serine Hydrolase Hip1. *Journal of Immunology* **192**, 4263-4272 (2014).

78. Marino, S. *et al.* Dendritic cell trafficking and antigen presentation in the human immune response to Mycobacterium tuberculosis. *J Immunol* **173**, 494-506 (2004).

79. Urdahl, K.B., Shafiani, S. & Ernst, J.D. Initiation and regulation of T-cell responses in tuberculosis. *Mucosal Immunol* **4**, 288-293 (2011).

80. Gallegos, A.M., Pamer, E.G. & Glickman, M.S. Delayed protection by ESAT-6-specific effector CD4+ T cells after airborne M. tuberculosis infection. *J Exp Med* **205**, 2359-2368 (2008).

81. Portevin, D., Via, L.E., Eum, S. & Young, D. Natural killer cells are recruited during pulmonary tuberculosis and their ex vivo responses to mycobacteria vary between healthy human donors in association with KIR haplotype. *Cell Microbiol* **14**, 1734-1744 (2012).

82. Flynn, J.L. *et al.* An Essential Role for Interferon-Gamma in Resistance to Mycobacterium-Tuberculosis Infection. *J Exp Med* **178**, 2249-2254 (1993).

83. Salie, M., Daya, M., Moller, M. & Hoal, E.G. Activating KIRs alter susceptibility to pulmonary tuberculosis in a South African population. *Tuberculosis* **95**, 817-821 (2015).

84. Mendez, A. *et al.* Study of KIR genes in tuberculosis patients. *Tissue Antigens* **68**, 386-389 (2006).

85. Feng, C.G. *et al.* NK cell-derived IFN-gamma differentially regulates innate resistance and neutrophil response in T cell-deficient hosts infected with Mycobacterium tuberculosis. *Journal of Immunology* **177**, 7086-7093 (2006).

86. Junqueira-Kipnis, A.P. *et al.* NK cells respond to pulmonary infection with Mycobacterium tuberculosis but play a minimal role in protection. *Faseb J* **17**, C153-C153 (2003).

87. Law, K. *et al.* Increased release of interleukin-1 beta, interleukin-6, and tumor necrosis factor-alpha by bronchoalveolar cells lavaged from involved sites in pulmonary tuberculosis. *Am J Respir Crit Care Med* **153**, 799-804 (1996).

88. Valone, S.E., Rich, E.A., Wallis, R.S. & Ellner, J.J. Expression of tumor necrosis factor in vitro by human mononuclear phagocytes stimulated with whole Mycobacterium bovis BCG and mycobacterial antigens. *Infect Immun* **56**, 3313-3315 (1988).

89. Henderson, R.A., Watkins, S.C. & Flynn, J.L. Activation of human dendritic cells following infection with Mycobacterium tuberculosis. *J Immunol* **159**, 635-643 (1997).

90. Harari, A. *et al.* Dominant TNF-alpha(+) Mycobacterium tuberculosis-specific CD4(+) T cell responses discriminate

between latent infection and active disease. *Nat Med* **17**, 372-U174 (2011).

91. Arora, P., Foster, E.L. & Porcelli, S.A. CD1d and Natural Killer T Cells in Immunity to Mycobacterium tuberculosis. *Adv Exp Med Biol* **783**, 199-223 (2013).

92. Lang, F. *et al.* Early activation of human V gamma 9V delta 2 T cell broad cytotoxicity and TNF production by nonpeptidic mycobacterial ligands. *J Immunol* **154**, 5986-5994 (1995).

93. Schuna, A.A. & Megeff, C. New drugs for the treatment of rheumatoid arthritis. *Am J Health-Syst Ph* **57**, 225-234 (2000).

94. Keane, J. *et al.* Tuberculosis associated with infliximab, a tumor necrosis factor (alpha)-neutralizing agent. *New Engl J Med* **345**, 1098-1104 (2001).

95. Nunez Martinez, O., Ripoll Noiseux, C., Carneros Martin, J.A., Gonzalez Lara, V. & Gregorio Maranon, H.G. Reactivation tuberculosis in a patient with anti-TNF-alpha treatment. *Am J Gastroenterol* **96**, 1665-1666 (2001).

96. Bean, A.G.D. *et al.* Structural deficiencies in granuloma formation in TNF gene-targeted mice underlie the heightened susceptibility to aerosol Mycobacterium tuberculosis infection, which is not compensated for by lymphotoxin. *Journal of Immunology* **162**, 3504-3511 (1999).

97. Keane, J. *et al.* Infection by Mycobacterium tuberculosis promotes human alveolar macrophage apoptosis. *Infect Immun* **65**, 298-304 (1997).

98. Flynn, J.L. *et al.* Tumor necrosis factor-alpha is required in the protective immune response against Mycobacterium tuberculosis in mice. *Immunity* **2**, 561-572 (1995).

99. Lin, P.L. *et al.* Tumor necrosis factor neutralization results in disseminated disease in acute and latent Mycobacterium tuberculosis infection with normal granuloma structure in a cynomolgus macaque model. *Arthritis Rheum* **62**, 340-350 (2010).

100. Harris, J. & Keane, J. How tumour necrosis factor blockers interfere with tuberculosis immunity. *Clin Exp Immunol* **161**, 1-9 (2010).

101. Bekker, L.G. *et al.* Immunopathologic effects of tumor necrosis factor alpha in murine mycobacterial infection are dose dependent. *Infect Immun* **68**, 6954-6961 (2000).

102. Roca, F.J. & Ramakrishnan, L. TNF Dually Mediates Resistance and Susceptibility to Mycobacteria via Mitochondrial Reactive Oxygen Species. *Cell* **153**, 521-534 (2013).

103. Saraiva, M. & O'Garra, A. The regulation of IL-10 production by immune cells. *Nature Reviews Immunology* **10**, 170-181 (2010).

104. Williams, L., Bradley, L., Smith, A. & Foxwell, B. Signal transducer and activator of transcription 3 is the dominant mediator of the anti-inflammatory effects of IL-10 in human macrophages. *Journal of Immunology* **172**, 567-576 (2004).

105. Malefyt, R.D., Abrams, J., Bennett, B., Figdor, C.G. & Devries, J.E. Interleukin-10(Il-10) Inhibits Cytokine Synthesis by Human Monocytes - an Autoregulatory Role of Il-10 Produced by Monocytes. *J Exp Med* **174**, 1209-1220 (1991).

106. Bogdan, C., Vodovotz, Y. & Nathan, C. Macrophage Deactivation by Interleukin-10. *J Exp Med* **174**, 1549-1555 (1991).

107. Koppelman, B., Neefjes, J.J., de Vries, J.E. & Malefyt, R.D. Interleukin-10 down-regulates MHC class II alpha beta peptide complexes at the plasma membrane of monocytes by affecting arrival and recycling. *Immunity* **7**, 861-871 (1997).

108. Almeida, A.S. *et al.* Tuberculosis Is Associated with a Down-Modulatory Lung Immune Response That Impairs Th1-Type Immunity. *Journal of Immunology* **183**, 718-731 (2009).

109. Barnett, R.E. *et al.* Anti-inflammatory effects of miR-21 in the macrophage response to peritonitis. *J Leukoc Biol* **99**, 361-371 (2016).

110. North, R.J. Mice incapable of making IL-4 or IL-10 display normal resistance to infection with Mycobacterium tuberculosis. *Clin Exp Immunol* **113**, 55-58 (1998).

111. Beamer, G.L. *et al.* Interleukin-10 promotes Mycobacterium tuberculosis disease progression in CBA/J mice. *J Immunol* **181**, 5545-5550 (2008).

112. Turner, J. *et al.* In vivo IL-10 production reactivates chronic pulmonary tuberculosis in C57BL/6 mice. *J Immunol* **169**, 6343-6351 (2002).

113. Wong, E.A., Kraus, C., Reimann, K.A. & Flynn, J.L. The role of IL-10 during early M. tuberculosis infection in a non-human primate model. *Journal of Immunology* **198** (2017).

114. Gong, J.H. *et al.* Interleukin-10 downregulates Mycobacterium tuberculosis-induced Th1 responses and CTLA-4 expression. *Infect Immun* **64**, 913-918 (1996).

115. Newton, S.M. *et al.* A deletion defining a common Asian lineage of Mycobacterium tuberculosis associates with immune subversion. *Proc Natl Acad Sci U S A* **103**, 15594-15598 (2006).

116. Manca, C. *et al.* Hypervirulent M. tuberculosis W/Beijing strains upregulate type I IFNs and increase expression of negative regulators of the Jak-Stat pathway. *J Interferon Cytokine Res* **25**, 694-701 (2005).

117. O'Leary, S., O'Sullivan, M.P. & Keane, J. IL-10 blocks phagosome maturation in mycobacterium tuberculosis-infected human macrophages. *Am J Respir Cell Mol Biol* **45**, 172-180 (2011).

118. Dutta, N.K. & Karakousis, P.C. Latent tuberculosis infection: myths, models, and molecular mechanisms. *Microbiol Mol Biol Rev* **78**, 343-371 (2014).

119. Saunders, B.M. & Cooper, A.M. Restraining mycobacteria: role of granulomas in mycobacterial infections. *Immunol Cell Biol* **78**, 334-341 (2000).

120. Ahsan, H. *et al.* A genome-wide association study of early-onset breast cancer identifies PFKM as a novel breast cancer gene and supports a common genetic spectrum for breast cancer at any age. *Cancer Epidemiol Biomarkers Prev* **23**, 658-669 (2014).

121. Ulrichs, T. *et al.* Differential organization of the local immune response in patients with active cavitary tuberculosis or with nonprogressive tuberculoma. *J Infect Dis* **192**, 89-97 (2005).

122. Dannenberg, A.M. & Sugimoto, M. Liquefaction of Caseous Foci in Tuberculosis. *Am Rev Respir Dis* **113**, 257-259 (1976).

123. Reiley, W.W. *et al.* ESAT-6-specific CD4 T cell responses to aerosol Mycobacterium tuberculosis infection are initiated in the mediastinal lymph nodes. *Proc Natl Acad Sci U S A* **105**, 10961-10966 (2008).

124. van Pinxteren, L.A., Cassidy, J.P., Smedegaard, B.H., Agger, E.M. & Andersen, P. Control of latent Mycobacterium tuberculosis infection is dependent on CD8 T cells. *Eur J Immunol* **30**, 3689-3698 (2000).

125. Bold, T.D. & Ernst, J.D. CD4+ T cell-dependent IFN-gamma production by CD8+ effector T cells in Mycobacterium tuberculosis infection. *J Immunol* **189**, 2530-2536 (2012).

126. Srivastava, S. & Ernst, J.D. Cutting edge: Direct recognition of infected cells by CD4 T cells is required for control of intracellular Mycobacterium tuberculosis in vivo. *J Immunol* **191**, 1016-1020 (2013).

127. Yang, J.D. *et al.* Mycobacterium tuberculosis-specific CD4+ and CD8+ T cells differ in their capacity to recognize infected macrophages. *PLoS Pathog* **14**, e1007060 (2018).

128. Gallegos, A.M. *et al.* A gamma interferon independent mechanism of CD4 T cell mediated control of M. tuberculosis infection in vivo. *PLoS Pathog* **7**, e1002052 (2011).

129. Saunders, B.M., Briscoe, H. & Britton, W.J. T cell-derived tumour necrosis factor is essential, but not sufficient, for protection against Mycobacterium tuberculosis infection. *Clin Exp Immunol* **137**, 279-287 (2004).

130. Kagina, B.M. *et al.* Specific T cell frequency and cytokine expression profile do not correlate with protection against tuberculosis after bacillus Calmette-Guerin vaccination of newborns. *Am J Respir Crit Care Med* **182**, 1073-1079 (2010).

131. Sutherland, J.S., Adetifa, I.M., Hill, P.C., Adegbola, R.A. & Ota, M.O. Pattern and diversity of cytokine production differentiates between Mycobacterium tuberculosis infection and disease. *Eur J Immunol* **39**, 723-729 (2009).

132. Glynn, J.R. *et al.* Effects of duration of HIV infection and secondary tuberculosis transmission on tuberculosis incidence in the South African gold mines. *AIDS* **22**, 1859-1867 (2008).

133. Sonnenberg, P. *et al.* HIV-1 and recurrence, relapse, and reinfection of tuberculosis after cure: a cohort study in South African mineworkers. *Lancet* **358**, 1687-1693 (2001).

134. Sonnenberg, P. *et al.* How soon after infection with HIV does the risk of tuberculosis start to increase? A retrospective cohort study in South African gold miners. *J Infect Dis* **191**, 150-158 (2005).

135. Whalen, C.C. *et al.* Impact of pulmonary tuberculosis on survival of HIV-infected adults: a prospective epidemiologic study in Uganda. *AIDS* **14**, 1219-1228 (2000).

136. Lawn, S.D., Myer, L., Edwards, D., Bekker, L.G. & Wood, R. Short-term and long-term risk of tuberculosis associated with CD4 cell recovery during antiretroviral therapy in South Africa. *AIDS* **23**, 1717-1725 (2009).

137. Kalsdorf, B. *et al.* HIV-1 infection impairs the bronchoalveolar T-cell response to mycobacteria. *Am J Respir Crit Care Med* **180**, 1262-1270 (2009).

138. Geldmacher, C. *et al.* Preferential infection and depletion of Mycobacterium tuberculosis-specific CD4 T cells after HIV-1 infection. *J Exp Med* **207**, 2869-2881 (2010).

139. Kuroda, M.J. *et al.* High Turnover of Tissue Macrophages Contributes to Tuberculosis Reactivation in Simian Immunodeficiency Virus-Infected Rhesus Macaques. *J Infect Dis* **217**, 1865-1874 (2018).

140. Barber, D.L., Mayer-Barber, K.D., Feng, C.G., Sharpe, A.H. & Sher, A. CD4 T cells promote rather than control tuberculosis in the absence of PD-1-mediated inhibition. *J Immunol* **186**, 1598-1607 (2011).

141. Tzelepis, F. *et al.* Mitochondrial cyclophilin D regulates T cell metabolic responses and disease tolerance to tuberculosis. *Sci Immunol* **3** (2018).

142. Lewinsohn, D.A., Lewinsohn, D.M. & Scriba, T.J. Polyfunctional CD4(+) T Cells As Targets for Tuberculosis Vaccination. *Front Immunol* **8**, 1262 (2017).

143. Ulrichs, T. *et al.* Human tuberculous granulomas induce peripheral lymphoid follicle-like structures to orchestrate local host defence in the lung. *J Pathol* **204**, 217-228 (2004).

144. Alkadi, A., Alduaiji, N. & Alrehaily, A. Risk of tuberculosis reactivation with rituximab therapy. *Int J Health Sci (Qassim)* **11**, 41-44 (2017).

145. Cantini, F. *et al.* Risk of Tuberculosis Reactivation in Patients with Rheumatoid Arthritis, Ankylosing Spondylitis, and Psoriatic Arthritis Receiving Non-Anti-TNF-Targeted Biologics. *Mediators Inflamm* **2017**, 8909834 (2017).

146. Kourbeti, I.S., Ziakas, P.D. & Mylonakis, E. Biologic therapies in rheumatoid arthritis and the risk of opportunistic infections: a meta-analysis. *Clin Infect Dis* **58**, 1649-1657 (2014).

147. Green, A.M., Difazio, R. & Flynn, J.L. IFN-gamma from CD4 T cells is essential for host survival and enhances CD8 T cell function during Mycobacterium tuberculosis infection. *J Immunol* **190**, 270-277 (2013).

148. Cooper, A.M., Magram, J., Ferrante, J. & Orme, I.M. Interleukin 12 (IL-12) is crucial to the development of protective immunity in mice intravenously infected with mycobacterium tuberculosis. *J Exp Med* **186**, 39-45 (1997).

149. Sullivan, B.M. *et al.* Increased susceptibility of mice lacking T-bet to infection with Mycobacterium tuberculosis correlates with increased IL-10 and decreased IFN-gamma production. *J Immunol* **175**, 4593-4602 (2005).

150. Khader, S.A. *et al.* Interleukin 12p40 is required for dendritic cell migration and T cell priming after Mycobacterium tuberculosis infection. *J Exp Med* **203**, 1805-1815 (2006).

151. Cooper, A.M. *et al.* Mice lacking bioactive IL-12 can generate protective, antigen-specific cellular responses to mycobacterial infection only if the IL-12 p40 subunit is present. *J Immunol* **168**, 1322-1327 (2002).

152. Cleary, A.M. *et al.* Impaired accumulation and function of memory CD4 T cells in human IL-12 receptor beta 1 deficiency. *J Immunol* **170**, 597-603 (2003).

153. Sicevic, S. Generalized BCG tuberculosis with fatal course in two sisters. *Acta Paediatr Scand* **61**, 178-184 (1972).

154. Heyne, K. [Generalized familial semibenign BCG infection, salmonella osteomyelitis and intestinal pseudotuberculosis--due to a familial defect of the macrophage system? (author's transl)]. *Eur J Pediatr* **121**, 179-189 (1976).

155. Engbaek, H.C. Three Cases in the Same Family of Fatal Infection with M. Avium. *Acta Tuberc Pneumol Scand* **45**, 105-117 (1964).

156. Al-Muhsen, S. & Casanova, J.L. The genetic heterogeneity of mendelian susceptibility to mycobacterial diseases. *J Allergy Clin Immunol* **122**, 1043-1051; quiz 1052-1043 (2008).

157. Tabarsi, P. *et al.* Lethal tuberculosis in a previously healthy adult with IL-12 receptor deficiency. *J Clin Immunol* **31**, 537-539 (2011).

158. Koya, T. *et al.* Anti-interferon-gamma autoantibody in a patient with disseminated Mycobacterium avium complex. *J Infect Chemother* **15**, 118-122 (2009).

159. Tanaka, Y. *et al.* Disseminated Mycobacterium avium complex infection in a patient with autoantibody to interferon-gamma. *Intern Med* **46**, 1005-1009 (2007).

160. Kampmann, B. *et al.* Acquired predisposition to mycobacterial disease due to autoantibodies to IFN-gamma. *J Clin Invest* **115**, 2480-2488 (2005).

161. Hoflich, C. *et al.* Naturally occurring anti-IFN-gamma autoantibody and severe infections with Mycobacterium cheloneae and Burkholderia cocovenenans. *Blood* **103**, 673-675 (2004).

162. Kim, M.J. *et al.* Caseation of human tuberculosis granulomas correlates with elevated host lipid metabolism. *EMBO Mol Med* **2**, 258-274 (2010).

163. Fabri, M. *et al.* Vitamin D Is Required for IFN-gamma-Mediated Antimicrobial Activity of Human Macrophages. *Sci Transl Med* **3** (2011).

164. Braverman, J., Sogi, K.M., Benjamin, D., Nomura, D.K. & Stanley, S.A. HIF-1alpha Is an Essential Mediator of IFN-gamma-Dependent Immunity to Mycobacterium tuberculosis. *J Immunol* **197**, 1287-1297 (2016).

165. Thillai, M., Pollock, K., Pareek, M. & Lalvani, A. Interferon-gamma release assays for tuberculosis: current and future applications. *Expert Rev Respir Med* **8**, 67-78 (2014).

166. Gao, X.F., Yang, Z.W. & Li, J. Adjunctive therapy with interferon-gamma for the treatment of pulmonary tuberculosis: a systematic review. *Int J Infect Dis* **15**, e594-600 (2011).

167. Rider, P. *et al.* IL-1alpha and IL-1beta recruit different myeloid cells and promote different stages of sterile inflammation. *J Immunol* **187**, 4835-4843 (2011).

168. Netea, M.G., van de Veerdonk, F.L., van der Meer, J.W.M., Dinarello, C.A. & Joosten, L.A.B. Inflammasome-Independent Regulation of IL-1-Family Cytokines. *Annual Review of Immunology Vol 33* **33**, 49-77 (2015).

169. Dinarello, C.A. Interleukin-1 in the pathogenesis and treatment of inflammatory diseases. *Blood* **117**, 3720-3732 (2011).

170. Lopez-Castejon, G. & Brough, D. Understanding the mechanism of IL-1beta secretion. *Cytokine Growth Factor Rev* **22**, 189-195 (2011).

171. Cogswell, J.P. *et al.* Nf-Kappa-B Regulates Il-1-Beta Transcription through a Consensus Nf-Kappa-B Binding-Site and a Nonconsensus Cre-Like Site. *Journal of Immunology* **153**, 712-723 (1994).

172. O'Neill, L.A.J. & Bowie, A.G. The family of five: TIR-domain-containing adaptors in Toll-like receptor signalling. *Nature Reviews Immunology* **7**, 353-364 (2007).

173. Hiscott, J. *et al.* Characterization of a Functional Nf-Kappa-B Site in the Human Interleukin-1-Beta Promoter - Evidence for a Positive Autoregulatory Loop. *Mol Cell Biol* **13**, 6231-6240 (1993).

174. Ojaniemi, M. *et al.* Phosphatidylinositol 3-kinase is involved in Toll-like receptor 4-mediated cytokine expression in mouse macrophages. *European Journal of Immunology* **33**, 597-605 (2003).

175. Fang, H.Y. *et al.* Hypoxia-inducible factors 1 and 2 are important transcriptional effectors in primary macrophages experiencing hypoxia. *Blood* **114**, 844-859 (2009).

176. Tannahill, G.M. *et al.* Succinate is an inflammatory signal that induces IL-1beta through HIF-1alpha. *Nature* **496**, 238-242 (2013).

177. Sorbara, M.T. & Girardin, S.E. Mitochondrial ROS fuel the inflammasome. *Cell Res* **21**, 558-560 (2011).

178. Bours, M.J., Dagnelie, P.C., Giuliani, A.L., Wesselius, A. & Di Virgilio, F. P2 receptors and extracellular ATP: a novel homeostatic pathway in inflammation. *Front Biosci (Schol Ed)* **3**, 1443-1456 (2011).

179. Dorhoi, A. *et al.* Activation of the NLRP3 inflammasome by Mycobacterium tuberculosis is uncoupled from susceptibility to active tuberculosis. *Eur J Immunol* **42**, 374-384 (2012).

180. Martinon, F., Agostini, L., Meylan, E. & Tschopp, J. Identification of bacterial muramyl dipeptide as activator of the NALP3/cryopyrin inflammasome. *Curr Biol* **14**, 1929-1934 (2004).

181. Saiga, H. *et al.* Critical role of AIM2 in Mycobacterium tuberculosis infection. *Int Immunol* **24**, 637-644 (2012).

182. Jo, E.K., Kim, J.K., Shin, D.M. & Sasakawa, C. Molecular mechanisms regulating NLRP3 inflammasome activation. *Cell Mol Immunol* **13**, 148-159 (2016).

183. Wang, B. & Yin, Q. AIM2 inflammasome activation and regulation: A structural perspective. *J Struct Biol* **200**, 279-282 (2017).

184. Latz, E., Xiao, T.S. & Stutz, A. Activation and regulation of the inflammasomes. *Nat Rev Immunol* **13**, 397-411 (2013).

185. Eklund, D. *et al.* Human gene variants linked to enhanced NLRP3 activity limit intramacrophage growth of Mycobacterium tuberculosis. *J Infect Dis* **209**, 749-753 (2014).

186. Mishra, B.B. *et al.* Nitric oxide controls the immunopathology of tuberculosis by inhibiting NLRP3 inflammasome-dependent processing of IL-1beta. *Nat Immunol* **14**, 52-60 (2013).

187. Mayer-Barber, K.D. *et al.* Cutting Edge: Caspase-1 Independent IL-1 beta Production Is Critical for Host Resistance to Mycobacterium tuberculosis and Does Not Require TLR Signaling In Vivo. *Journal of Immunology* **184**, 3326-3330 (2010).

188. Yamada, H., Mizumo, S., Horai, R., Iwakura, Y. & Sugawara, I. Protective role of interleukin-1 in mycobacterial infection in IL-1 alpha/beta double-knockout mice. *Lab Invest* **80**, 759-767 (2000).

189. Sugawara, I., Yamada, H., Hua, S. & Mizuno, S. Role of interleukin (IL)-1 type 1 receptor in mycobacterial infection. *Microbiol Immunol* **45**, 743-750 (2001).

190. Bourigault, M.L. *et al.* Relative contribution of IL-1alpha, IL-1beta and TNF to the host response to Mycobacterium tuberculosis and attenuated M. bovis BCG. *Immun Inflamm Dis* **1**, 47-62 (2013).

191. Cantarini, L. *et al.* Effectiveness and tuberculosis-related safety profile of interleukin-1 blocking agents in the management of Behcet's disease. *Autoimmun Rev* **14**, 1-9 (2015).

192. Settas, L.D., Tsimirikas, G., Vosvotekas, G., Triantafyllidou, E. & Nicolaides, P. Reactivation of pulmonary tuberculosis in a patient with rheumatoid arthritis during treatment with IL-1 receptor antagonists (anakinra). *J Clin Rheumatol* **13**, 219-220 (2007).

193. Nnoaham, K.E. & Clarke, A. Low serum vitamin D levels and tuberculosis: a systematic review and meta-analysis. *Int J Epidemiol* **37**, 113-119 (2008).

194. Verway, M. *et al.* Vitamin D induces interleukin-1beta expression: paracrine macrophage epithelial signaling controls M. tuberculosis infection. *PLoS Pathog* **9**, e1003407 (2013).

195. Gomez, L.M. *et al.* Analysis of IL1B, TAP1, TAP2 and IKBL polymorphisms on susceptibility to tuberculosis. *Tissue Antigens* **67**, 290-296 (2006).

196. Wilkinson, R.J. *et al.* Influence of polymorphism in the genes for the interleukin (IL)-1 receptor antagonist and IL-1beta on tuberculosis. *J Exp Med* **189**, 1863-1874 (1999).

197. Zhang, G. *et al.* Allele-specific induction of IL-1beta expression by C/EBPbeta and PU.1 contributes to increased tuberculosis susceptibility. *PLoS Pathog* **10**, e1004426 (2014).

198. Fremond, C.M. *et al.* IL-1 receptor-mediated signal is an essential component of MyD88-dependent innate response to Mycobacterium tuberculosis infection. *Journal of Immunology* **179**, 1178-1189 (2007).

199. Jayaraman, P. *et al.* IL-1beta promotes antimicrobial immunity in macrophages by regulating TNFR signaling and caspase-3 activation. *J Immunol* **190**, 4196-4204 (2013).

200. Mayer-Barber, K.D. *et al.* Host-directed therapy of tuberculosis based on interleukin-1 and type I interferon crosstalk. *Nature* **511**, 99-103 (2014).

201. Chen, M. *et al.* Lipid mediators in innate immunity against tuberculosis: opposing roles of PGE2 and LXA4 in the induction of macrophage death. *J Exp Med* **205**, 2791-2801 (2008).

202. Rodriguez-Prados, J.C. *et al.* Substrate fate in activated macrophages: a comparison between innate, classic, and alternative activation. *J Immunol* **185**, 605-614 (2010).

203. Krawczyk, C.M. *et al.* Toll-like receptor-induced changes in glycolytic metabolism regulate dendritic cell activation. *Blood* **115**, 4742-4749 (2010).

204. Gleeson, L.E. *et al.* Cutting Edge: Mycobacterium tuberculosis Induces Aerobic Glycolysis in Human Alveolar Macrophages That Is Required for Control of Intracellular Bacillary Replication. *J Immunol* **196**, 2444-2449 (2016).

205. Ginhoux, F. *et al.* Fate Mapping Analysis Reveals That Adult Microglia Derive from Primitive Macrophages. *Science* **330**, 841-845 (2010).

206. Schulz, C. *et al.* A Lineage of Myeloid Cells Independent of Myb and Hematopoietic Stem Cells. *Science* **336**, 86-90 (2012).

207. Epelman, S. *et al.* Embryonic and Adult-Derived Resident Cardiac Macrophages Are Maintained through Distinct Mechanisms at Steady State and during Inflammation. *Immunity* **40**, 91-104 (2014).

208. Nourshargh, S. & Alon, R. Leukocyte Migration into Inflamed Tissues. *Immunity* **41**, 694-707 (2014).

209. Yona, S. *et al.* Fate Mapping Reveals Origins and Dynamics of Monocytes and Tissue Macrophages under Homeostasis. *Immunity* **38**, 79-91 (2013).

210. Davies, L.C., Jenkins, S.J., Allen, J.E. & Taylor, P.R. Tissue-resident macrophages. *Nature Immunology* **14**, 986-995 (2013).

211. Hashimoto, D. *et al.* Tissue-Resident Macrophages Self-Maintain Locally throughout Adult Life with Minimal Contribution from Circulating Monocytes. *Immunity* **38**, 792-804 (2013).

212. Gautier, E.L. *et al.* Gene-expression profiles and transcriptional regulatory pathways that underlie the identity and diversity of mouse tissue macrophages. *Nature Immunology* **13**, 1118-1128 (2012).

213. Sica, A. & Mantovani, A. Macrophage plasticity and polarization: in vivo veritas. *Journal of Clinical Investigation* **122**, 787-795 (2012).

214. Sica, A. & Bronte, V. Altered macrophage differentiation and immune dysfunction in tumor development. *Journal of Clinical Investigation* **117**, 1155-1166 (2007).

215. Mosser, D.M. & Edwards, J.P. Exploring the full spectrum of macrophage activation. *Nature Reviews Immunology* **8**, 958-969 (2008).

216. Maus, U.A. *et al.* Resident alveolar macrophages are replaced by recruited monocytes in response to endotoxin-induced lung inflammation. *Am J Resp Cell Mol* **35**, 227-235 (2006).

217. Shaykhiev, R. *et al.* Smoking-Dependent Reprogramming of Alveolar Macrophage Polarization: Implication for Pathogenesis

of Chronic Obstructive Pulmonary Disease. *Journal of Immunology* **183**, 2867-2883 (2009).

218. Bazzan, E. *et al.* Dual polarization of human alveolar macrophages progressively increases with smoking and COPD severity. *Resp Res* **18** (2017).

219. Redente, E.F. *et al.* Differential polarization of alveolar macrophages and bone marrow-derived monocytes following chemically and pathogen-induced chronic lung inflammation. *J Leukocyte Biol* **88**, 159-168 (2010).

220. Ehrt, S. *et al.* Reprogramming of the macrophage transcriptome in response to interferon-gamma and Mycobacterium tuberculosis: Signaling roles of nitric oxide synthase-2 and phagocyte oxidase. *J Exp Med* **194**, 1123-1139 (2001).

221. Raju, B. *et al.* Gene expression profiles of bronchoalveolar cells in pulmonary TB. *Tuberculosis* **88**, 39-51 (2008).

222. Huang, Z.K. *et al.* Mycobacterium tuberculosis-Induced Polarization of Human Macrophage Orchestrates the Formation and Development of Tuberculous Granulomas In Vitro. *Plos One* **10** (2015).

223. O'Garra, A. *et al.* The immune response in tuberculosis. *Annu Rev Immunol* **31**, 475-527 (2013).

224. Palsson-McDermott, E.M. & O'Neill, L.A. The Warburg effect then and now: from cancer to inflammatory diseases. *Bioessays* **35**, 965-973 (2013).

225. Hard, G.C. Some biochemical aspects of the immune macrophage. *Br J Exp Pathol* **51**, 97-105 (1970).

226. Freemerman, A.J. *et al.* Metabolic reprogramming of macrophages: glucose transporter 1 (GLUT1)-mediated glucose metabolism drives a proinflammatory phenotype. *J Biol Chem* **289**, 7884-7896 (2014).

227. Wilson, J.E. Isozymes of mammalian hexokinase: structure, subcellular localization and metabolic function. *J Exp Biol* **206**, 2049-2057 (2003).

228. Qu, H.Q. *et al.* Host susceptibility to tuberculosis: insights from a longitudinal study of gene expression in diabetes. *Int J Tuberc Lung Dis* **16**, 370-372 (2012).

229. Pilkis, S.J., Weber, I.T., Harrison, R.W. & Bell, G.I. Glucokinase: structural analysis of a protein involved in susceptibility to diabetes. *J Biol Chem* **269**, 21925-21928 (1994).

230. Gottlieb, E. p53 guards the metabolic pathway less travelled. *Nat Cell Biol* **13**, 195-197 (2011).

231. Jha, A.K. *et al.* Network integration of parallel metabolic and transcriptional data reveals metabolic modules that regulate macrophage polarization. *Immunity* **42**, 419-430 (2015).

232. Haschemi, A. *et al.* The sedoheptulose kinase CARKL directs macrophage polarization through control of glucose metabolism. *Cell Metab* **15**, 813-826 (2012).

233. Hers, H.G. & Van Schaftingen, E. Fructose 2,6-bisphosphate 2 years after its discovery. *Biochem J* **206**, 1-12 (1982).

234. Jenkins, C.M., Yang, J., Sims, H.F. & Gross, R.W. Reversible high affinity inhibition of phosphofructokinase-1 by acyl-CoA: a mechanism integrating glycolytic flux with lipid metabolism. *J Biol Chem* **286**, 11937-11950 (2011).

235. Moreno-Sanchez, R., Rodriguez-Enriquez, S., Marin-Hernandez, A. & Saavedra, E. Energy metabolism in tumor cells. *FEBS J* **274**, 1393-1418 (2007).

236. Ruiz-Garcia, A. *et al.* Cooperation of adenosine with macrophage Toll-4 receptor agonists leads to increased glycolytic flux through the enhanced expression of PFKFB3 gene. *J Biol Chem* **286**, 19247-19258 (2011).

237. Sakakibara, R., Uemura, M., Hirata, T., Okamura, N. & Kato, M. Human placental fructose-6-phosphate,2-kinase/fructose-2,6-bisphosphatase: its isozymic form, expression and characterization. *Biosci Biotechnol Biochem* **61**, 1949-1952 (1997).

238. Mor, I., Cheung, E.C. & Vousden, K.H. Control of glycolysis through regulation of PFK1: old friends and recent additions. *Cold Spring Harb Symp Quant Biol* **76**, 211-216 (2011).

239. Palsson-McDermott, E.M. *et al.* Pyruvate kinase M2 regulates Hif-1alpha activity and IL-1beta induction and is a critical determinant of the warburg effect in LPS-activated macrophages. *Cell Metab* **21**, 65-80 (2015).

240. Kelly, B. & O'Neill, L.A. Metabolic reprogramming in macrophages and dendritic cells in innate immunity. *Cell Res* **25**, 771-784 (2015).

241. Rogatzki, M.J., Ferguson, B.S., Goodwin, M.L. & Gladden, L.B. Lactate is always the end product of glycolysis. *Front Neurosci* **9**, 22 (2015).

242. Haas, R. *et al.* Lactate Regulates Metabolic and Pro-inflammatory Circuits in Control of T Cell Migration and Effector Functions. *PLoS Biol* **13**, e1002202 (2015).

243. Colegio, O.R. *et al.* Functional polarization of tumour-associated macrophages by tumour-derived lactic acid. *Nature* **513**, 559-563 (2014).

244. Errea, A. *et al.* Lactate Inhibits the Pro-Inflammatory Response and Metabolic Reprogramming in Murine Macrophages in a GPR81-Independent Manner. *PLoS One* **11**, e0163694 (2016).

245. Nasi, A. *et al.* Dendritic cell reprogramming by endogenously produced lactic acid. *J Immunol* **191**, 3090-3099 (2013).

246. Billig, S. *et al.* Lactate oxidation facilitates growth of Mycobacterium tuberculosis in human macrophages. *Sci Rep* **7**, 6484 (2017).

247. Oren, R., Farnham, A.E., Saito, K., Milofsky, E. & Karnovsky, M.L. Metabolic patterns in three types of phagocytizing cells. *J Cell Biol* **17**, 487-501 (1963).

248. Sbarra, A.J. & Karnovsky, M.L. The biochemical basis of phagocytosis. I. Metabolic changes during the ingestion of particles by polymorphonuclear leukocytes. *J Biol Chem* **234**, 1355-1362 (1959).

249. Wang, T., Marquardt, C. & Foker, J. Aerobic glycolysis during lymphocyte proliferation. *Nature* **261**, 702-705 (1976).

250. Newsholme, P., Curi, R., Gordon, S. & Newsholme, E.A. Metabolism of glucose, glutamine, long-chain fatty acids and ketone bodies by murine macrophages. *Biochem J* **239**, 121-125 (1986).

251. Galvan-Pena, S. & O'Neill, L.A. Metabolic reprograming in macrophage polarization. *Front Immunol* **5**, 420 (2014).

252. Lachmandas, E. *et al.* Rewiring cellular metabolism via the AKT/mTOR pathway contributes to host defence against Mycobacterium tuberculosis in human and murine cells. *Eur J Immunol* **46**, 2574-2586 (2016).

253. Everts, B. *et al.* TLR-driven early glycolytic reprogramming via the kinases TBK1-IKKvarepsilon supports the anabolic demands of dendritic cell activation. *Nat Immunol* **15**, 323-332 (2014).

254. Teng, C.F. *et al.* Hepatitis B Virus Pre-S2 Mutant Induces Aerobic Glycolysis through Mammalian Target of Rapamycin Signal Cascade. *PLoS One* **10**, e0122373 (2015).

255. Peyssonnaux, C. *et al.* HIF-1alpha expression regulates the bactericidal capacity of phagocytes. *J Clin Invest* **115**, 1806-1815 (2005).

256. Byles, V. *et al.* The TSC-mTOR pathway regulates macrophage polarization. *Nat Commun* **4**, 2834 (2013).

257. Clementi, E., Brown, G.C., Feelisch, M. & Moncada, S. Persistent inhibition of cell respiration by nitric oxide: crucial role of S-nitrosylation of mitochondrial complex I and protective

action of glutathione. *Proc Natl Acad Sci U S A* **95**, 7631-7636 (1998).

258. Sag, D., Carling, D., Stout, R.D. & Suttles, J. Adenosine 5'-monophosphate-activated protein kinase promotes macrophage polarization to an anti-inflammatory functional phenotype. *J Immunol* **181**, 8633-8641 (2008).

259. Infantino, V. *et al.* The mitochondrial citrate carrier: a new player in inflammation. *Biochem J* **438**, 433-436 (2011).

260. Huang, J. *et al.* Pseudorabies viral replication is inhibited by a novel target of miR-21. *Virology* **456-457**, 319-328 (2014).

261. Wang, F. *et al.* Glycolytic Stimulation Is Not a Requirement for M2 Macrophage Differentiation. *Cell Metab* **28**, 463-475 e464 (2018).

262. Shin, J.H. *et al.* (1)H NMR-based metabolomic profiling in mice infected with Mycobacterium tuberculosis. *J Proteome Res* **10**, 2238-2247 (2011).

263. Coleman, M.T. *et al.* PET/CT imaging reveals a therapeutic response to oxazolidinones in macaques and humans with tuberculosis. *Sci Transl Med* **6**, 265ra167 (2014).

264. Ankrah, A.O. *et al.* PET/CT imaging of Mycobacterium tuberculosis infection. *Clin Transl Imaging* **4**, 131-144 (2016).

265. Jeon, C.Y. & Murray, M.B. Diabetes mellitus increases the risk of active tuberculosis: a systematic review of 13 observational studies. *PLoS Med* **5**, e152 (2008).

266. Gleeson, L.E. *et al.* Cigarette Smoking Impairs the Bioenergetic Immune Response to Mycobacterium Tuberculosis Infection. *Am J Respir Cell Mol Biol* (2018).

267. Lindsay, M.A. microRNAs and the immune response. *Trends Immunol* **29**, 343-351 (2008).

268. Baskerville, S. & Bartel, D.P. Microarray profiling of microRNAs reveals frequent coexpression with neighboring miRNAs and host genes. *RNA* **11**, 241-247 (2005).

269. Davis-Dusenbery, B.N. & Hata, A. Mechanisms of control of microRNA biogenesis. *J Biochem* **148**, 381-392 (2010).

270. Gregory, R.I., Chendrimada, T.P. & Shiekhattar, R. MicroRNA biogenesis: isolation and characterization of the microprocessor complex. *Methods Mol Biol* **342**, 33-47 (2006).

271. Bohnsack, M.T., Czaplinski, K. & Gorlich, D. Exportin 5 is a RanGTP-dependent dsRNA-binding protein that mediates nuclear export of pre-miRNAs. *RNA* **10**, 185-191 (2004).

272. Baek, D. *et al.* The impact of microRNAs on protein output. *Nature* **455**, 64-71 (2008).

273. Finnegan, E.F. & Pasquinelli, A.E. MicroRNA biogenesis: regulating the regulators. *Crit Rev Biochem Mol Biol* **48**, 51-68 (2013).

274. Graves, P. & Zeng, Y. Biogenesis of mammalian microRNAs: a global view. *Genomics Proteomics Bioinformatics* **10**, 239-245 (2012).

275. Cheng, C., Bhardwaj, N. & Gerstein, M. The relationship between the evolution of microRNA targets and the length of their UTRs. *BMC Genomics* **10**, 431 (2009).

276. Faraoni, I., Antonetti, F.R., Cardone, J. & Bonmassar, E. miR-155 gene: a typical multifunctional microRNA. *Biochim Biophys Acta* **1792**, 497-505 (2009).

277. Zhang, R. & Su, B. Small but influential: the role of microRNAs on gene regulatory network and 3'UTR evolution. *J Genet Genomics* **36**, 1-6 (2009).

278. Grimson, A. *et al.* MicroRNA targeting specificity in mammals: determinants beyond seed pairing. *Mol Cell* **27**, 91-105 (2007).

279. Krek, A. *et al.* Combinatorial microRNA target predictions. *Nat Genet* **37**, 495-500 (2005).

280. John, B. *et al.* Human MicroRNA targets. *PLoS Biol* **2**, e363 (2004).

281. Seitz, H. Redefining microRNA targets. *Curr Biol* **19**, 870-873 (2009).

282. Baccarini, A. *et al.* Kinetic analysis reveals the fate of a microRNA following target regulation in mammalian cells. *Curr Biol* **21**, 369-376 (2011).

283. Mohr, A.M. & Mott, J.L. Overview of microRNA biology. *Semin Liver Dis* **35**, 3-11 (2015).

284. Corcoran, D.L. *et al.* Features of mammalian microRNA promoters emerge from polymerase II chromatin immunoprecipitation data. *PLoS One* **4**, e5279 (2009).

285. Krol, J., Loedige, I. & Filipowicz, W. The widespread regulation of microRNA biogenesis, function and decay. *Nat Rev Genet* **11**, 597-610 (2010).

286. Bartel, D.P. MicroRNAs: genomics, biogenesis, mechanism, and function. *Cell* **116**, 281-297 (2004).

287. Rodriguez, A., Griffiths-Jones, S., Ashurst, J.L. & Bradley, A. Identification of mammalian microRNA host genes and transcription units. *Genome Res* **14**, 1902-1910 (2004).

288. Esteller, M. Non-coding RNAs in human disease. *Nat Rev Genet* **12**, 861-874 (2011).

289. van Rooij, E. & Kauppinen, S. Development of microRNA therapeutics is coming of age. *EMBO Mol Med* **6**, 851-864 (2014).

290. Rupaimoole, R. & Slack, F.J. MicroRNA therapeutics: towards a new era for the management of cancer and other diseases. *Nat Rev Drug Discov* **16**, 203-222 (2017).

291. Landgraf, P. *et al.* A mammalian microRNA expression atlas based on small RNA library sequencing. *Cell* **129**, 1401-1414 (2007).

292. Cai, X., Hagedorn, C.H. & Cullen, B.R. Human microRNAs are processed from capped, polyadenylated transcripts that can also function as mRNAs. *RNA* **10**, 1957-1966 (2004).

293. Loffler, D. *et al.* Interleukin-6 dependent survival of multiple myeloma cells involves the Stat3-mediated induction of microRNA-21 through a highly conserved enhancer. *Blood* **110**, 1330-1333 (2007).

294. Ozsolak, F. *et al.* Chromatin structure analyses identify miRNA promoters. *Genes Dev* **22**, 3172-3183 (2008).

295. Mudduluru, G. *et al.* Curcumin regulates miR-21 expression and inhibits invasion and metastasis in colorectal cancer. *Biosci Rep* **31**, 185-197 (2011).

296. Sheedy, F.J. *et al.* Negative regulation of TLR4 via targeting of the proinflammatory tumor suppressor PDCD4 by the microRNA miR-21. *Nat Immunol* **11**, 141-147 (2010).

297. Feng, J. *et al.* miR-21 attenuates lipopolysaccharide-induced lipid accumulation and inflammatory response: potential role in cerebrovascular disease. *Lipids Health Dis* **13**, 27 (2014).

298. Johnston, D.G.W. *et al.* MicroRNA-21 Limits Uptake of Listeria monocytogenes by Macrophages to Reduce the Intracellular Niche and Control Infection. *Front Cell Infect Microbiol* **7**, 201 (2017).

299. Davis, B.N., Hilyard, A.C., Lagna, G. & Hata, A. SMAD proteins control DROSHA-mediated microRNA maturation. *Nature* **454**, 56-61 (2008).

300. Loboda, A., Sobczak, M., Jozkowicz, A. & Dulak, J. TGF-beta1/Smads and miR-21 in Renal Fibrosis and Inflammation. *Mediators Inflamm* **2016**, 8319283 (2016).

301. Liu, G. *et al.* miR-21 mediates fibrogenic activation of pulmonary fibroblasts and lung fibrosis. *J Exp Med* **207**, 1589-1597 (2010).

302. Sheedy, F.J. Turning 21: Induction of miR-21 as a Key Switch in the Inflammatory Response. *Front Immunol* **6**, 19 (2015).

303. Hayashi, T., Koyama, N., Azuma, Y. & Kashimata, M. Mesenchymal miR-21 regulates branching morphogenesis in murine submandibular gland in vitro. *Dev Biol* **352**, 299-307 (2011).

304. Chan, J.A., Krichevsky, A.M. & Kosik, K.S. MicroRNA-21 is an antiapoptotic factor in human glioblastoma cells. *Cancer Res* **65**, 6029-6033 (2005).

305. Xu, L.F. *et al.* MicroRNA-21 (miR-21) regulates cellular proliferation, invasion, migration, and apoptosis by targeting PTEN, RECK and Bcl-2 in lung squamous carcinoma, Gejiu City, China. *PLoS One* **9**, e103698 (2014).

306. Volinia, S. *et al.* A microRNA expression signature of human solid tumors defines cancer gene targets. *Proc Natl Acad Sci U S A* **103**, 2257-2261 (2006).

307. Lu, J. *et al.* MicroRNA expression profiles classify human cancers. *Nature* **435**, 834-838 (2005).

308. Yu, L. *et al.* Early detection of lung adenocarcinoma in sputum by a panel of microRNA markers. *Int J Cancer* **127**, 2870-2878 (2010).

309. Link, A. *et al.* Fecal MicroRNAs as novel biomarkers for colon cancer screening. *Cancer Epidemiol Biomarkers Prev* **19**, 1766-1774 (2010).

310. Xu, J. *et al.* Circulating microRNAs, miR-21, miR-122, and miR-223, in patients with hepatocellular carcinoma or chronic hepatitis. *Mol Carcinog* **50**, 136-142 (2011).

311. Thum, T. *et al.* MicroRNA-21 contributes to myocardial disease by stimulating MAP kinase signalling in fibroblasts. *Nature* **456**, 980-984 (2008).

312. Simeoli, R. *et al.* Exosomal cargo including microRNA regulates sensory neuron to macrophage communication after nerve trauma. *Nat Commun* **8**, 1778 (2017).

313. Zheng, P. *et al.* Exosomal transfer of tumor-associated macrophage-derived miR-21 confers cisplatin resistance in gastric cancer cells. *J Exp Clin Cancer Res* **36**, 53 (2017).

314. Graff, J.W., Dickson, A.M., Clay, G., McCaffrey, A.P. & Wilson, M.E. Identifying functional microRNAs in macrophages with polarized phenotypes. *J Biol Chem* **287**, 21816-21825 (2012).

315. Meng, F. *et al.* MicroRNA-21 regulates expression of the PTEN tumor suppressor gene in human hepatocellular cancer. *Gastroenterology* **133**, 647-658 (2007).

316. Wang, Z. *et al.* MicroRNA 21 is a homeostatic regulator of macrophage polarization and prevents prostaglandin E2-mediated M2 generation. *PLoS One* **10**, e0115855 (2015).

317. Lu, T.X., Munitz, A. & Rothenberg, M.E. MicroRNA-21 is up-regulated in allergic airway inflammation and regulates IL-12p35 expression. *J Immunol* **182**, 4994-5002 (2009).

318. Pfeffer, S.R., Yang, C.H. & Pfeffer, L.M. The Role of miR-21 in Cancer. *Drug Dev Res* (2015).

319. Das, A., Ganesh, K., Khanna, S., Sen, C.K. & Roy, S. Engulfment of apoptotic cells by macrophages: a role of microRNA-21 in the resolution of wound inflammation. *J Immunol* **192**, 1120-1129 (2014).

320. Caescu, C.I. *et al.* Colony stimulating factor-1 receptor signaling networks inhibit mouse macrophage inflammatory responses by induction of microRNA-21. *Blood* **125**, e1-13 (2015).

321. Ernst, J.D. The immunological life cycle of tuberculosis. *Nat Rev Immunol* **12**, 581-591 (2012).

322. Liu, P.T. *et al.* MicroRNA-21 targets the vitamin D-dependent antimicrobial pathway in leprosy. *Nat Med* **18**, 267-273 (2012).

323. Bose, D. *et al.* The Tuberculosis Drug Streptomycin as a Potential Cancer Therapeutic: Inhibition of miR-21 Function by Directly Targeting Its Precursor. *Angewandte Chemie International Edition* **51**, 1019-1023 (2012).

324. Chen, S. *et al.* MiR-21-mediated Metabolic Alteration of Cancer-associated Fibroblasts and Its Effect on Pancreatic Cancer Cell Behavior. *Int J Biol Sci* **14**, 100-110 (2018).

325. Johnston, D.G.W. *et al.* Loss of MicroRNA-21 Influences the Gut Microbiota, Causing Reduced Susceptibility in a Murine Model of Colitis. *J Crohns Colitis* **12**, 835-848 (2018).

326. Weischenfeldt, J. & Porse, B. Bone Marrow-Derived Macrophages (BMM): Isolation and Applications. *CSH Protoc* **2008**, pdb prot5080 (2008).

327. O'Sullivan, M.P., O'Leary, S., Kelly, D.M. & Keane, J. A caspase-independent pathway mediates macrophage cell death in response to Mycobacterium tuberculosis infection. *Infect Immun* **75**, 1984-1993 (2007).

328. Biswas, S.K., Chittezhath, M., Shalova, I.N. & Lim, J.Y. Macrophage polarization and plasticity in health and disease. *Immunol Res* **53**, 11-24 (2012).

329. Martinez, F.O., Sica, A., Mantovani, A. & Locati, M. Macrophage activation and polarization. *Front Biosci* **13**, 453-461 (2008).

330. Skold, M. & Behar, S.M. Tuberculosis triggers a tissue-dependent program of differentiation and acquisition of effector functions by circulating monocytes. *J Immunol* **181**, 6349-6360 (2008).

331. van Crevel, R., Ottenhoff, T.H. & van der Meer, J.W. Innate immunity to Mycobacterium tuberculosis. *Clin Microbiol Rev* **15**, 294-309 (2002).

332. Ulrichs, T. & Kaufmann, S.H. New insights into the function of granulomas in human tuberculosis. *J Pathol* **208**, 261-269 (2006).

333. Mwandumba, H.C. *et al.* Mycobacterium tuberculosis resides in nonacidified vacuoles in endocytically competent alveolar macrophages from patients with tuberculosis and HIV infection. *J Immunol* **172**, 4592-4598 (2004).

334. Balcewicz-Sablinska, M.K., Gan, H. & Remold, H.G. Interleukin 10 produced by macrophages inoculated with Mycobacterium avium attenuates mycobacteria-induced apoptosis by reduction of TNF-alpha activity. *J Infect Dis* **180**, 1230-1237 (1999).

335. Patel, N.R., Swan, K., Li, X., Tachado, S.D. & Koziel, H. Impaired M. tuberculosis-mediated apoptosis in alveolar macrophages from HIV+ persons: potential role of IL-10 and BCL-3. *J Leukoc Biol* **86**, 53-60 (2009).

336. Byers, D.E. & Holtzman, M.J. Alternatively activated macrophages and airway disease. *Chest* **140**, 768-774 (2011).

337. Shearer, J.D., Richards, J.R., Mills, C.D. & Caldwell, M.D. Differential regulation of macrophage arginine metabolism: a proposed role in wound healing. *Am J Physiol* **272**, E181-190 (1997).

338. El Kasmi, K.C. *et al.* Toll-like receptor-induced arginase 1 in macrophages thwarts effective immunity against intracellular pathogens. *Nat Immunol* **9**, 1399-1406 (2008).

339. Mattila, J.T. *et al.* Microenvironments in tuberculous granulomas are delineated by distinct populations of macrophage subsets and expression of nitric oxide synthase and arginase isoforms. *J Immunol* **191**, 773-784 (2013).

340. Xue, J. *et al.* Transcriptome-based network analysis reveals a spectrum model of human macrophage activation. *Immunity* **40**, 274-288 (2014).

341. Ahluwalia, P.K., Pandey, R.K., Sehajpal, P.K. & Prajapati, V.K. Perturbed microRNA Expression by Mycobacterium tuberculosis Promotes Macrophage Polarization Leading to Pro-survival Foam Cell. *Front Immunol* **8**, 107 (2017).

342. Ruan, Q. *et al.* The microRNA-21-PDCD4 axis prevents type 1 diabetes by blocking pancreatic beta cell death. *Proc Natl Acad Sci U S A* **108**, 12030-12035 (2011).

343. Stagakis, E. *et al.* Identification of novel microRNA signatures linked to human lupus disease activity and pathogenesis: miR-21 regulates aberrant T cell responses through regulation of PDCD4 expression. *Ann Rheum Dis* **70**, 1496-1506 (2011).

344. Feng, C.G. *et al.* Transgenic Mice Expressing Human Interleukin-10 in the Antigen-Presenting Cell Compartment Show Increased Susceptibility to Infection with Mycobacterium avium Associated with Decreased Macrophage Effector Function and Apoptosis. *Infect Immun* **70**, 6672-6679 (2002).

345. Redford, P.S. *et al.* Enhanced protection to Mycobacterium tuberculosis infection in IL-10-deficient mice is accompanied by early and enhanced Th1 responses in the lung. *Eur J Immunol* **40**, 2200-2210 (2010).

346. Malardo, T. *et al.* MicroRNA expression signatures in lungs of mice infected with Mycobacterium tuberculosis. *Tuberculosis (Edinb)* **101**, 151-159 (2016).

347. Yang, Z. *et al.* Modulation of NF-kappaB/miR-21/PTEN pathway sensitizes non-small cell lung cancer to cisplatin. *PLoS One* **10**, e0121547 (2015).

348. Mills, C.D., Kincaid, K., Alt, J.M., Heilman, M.J. & Hill, A.M. M-1/M-2 macrophages and the Th1/Th2 paradigm. *J Immunol* **164**, 6166-6173 (2000).

349. Southan, G.J., Szabo, C. & Thiemermann, C. Inhibition of the induction of nitric oxide synthase by spermine is modulated by aldehyde dehydrogenase. *Biochem Biophys Res Commun* **203**, 1638-1644 (1994).

350. Redford, P.S., Murray, P.J. & O'Garra, A. The role of IL-10 in immune regulation during M. tuberculosis infection. *Mucosal Immunol* **4**, 261-270 (2011).

351. Dokka, S. *et al.* Interleukin-10-mediated inhibition of free radical generation in macrophages. *Am J Physiol Lung Cell Mol Physiol* **280**, L1196-1202 (2001).

352. Cunha, F.Q., Moncada, S. & Liew, F.Y. Interleukin-10 (IL-10) inhibits the induction of nitric oxide synthase by interferon-gamma in murine macrophages. *Biochem Biophys Res Commun* **182**, 1155-1159 (1992).

353. Chang, T.H. *et al.* Dectin-2 is a primary receptor for NLRP3 inflammasome activation in dendritic cell response to Histoplasma capsulatum. *PLoS Pathog* **13**, e1006485 (2017).

354. van den Bosch, M.W., Palsson-Mcdermott, E., Johnson, D.S. & O'Neill, L.A. LPS induces the degradation of programmed cell death protein 4 (PDCD4) to release Twist2, activating c-Maf transcription to promote interleukin-10 production. *J Biol Chem* **289**, 22980-22990 (2014).

355. Chang, J.H. *et al.* Crystal structure of the eIF4A-PDCD4 complex. *Proc Natl Acad Sci U S A* **106**, 3148-3153 (2009).

356. Pearce, E.L. & Pearce, E.J. Metabolic pathways in immune cell activation and quiescence. *Immunity* **38**, 633-643 (2013).

357. Liu, Y. *et al.* A feedback regulatory loop between HIF-1alpha and miR-21 in response to hypoxia in cardiomyocytes. *FEBS Lett* **588**, 3137-3146 (2014).

358. Danilova, N., Kumagai, A. & Lin, J. p53 Upregulation Is a Frequent Response to Deficiency of Cell-Essential Genes. *Plos One* **5** (2010).

359. Smerc, A., Sodja, E. & Legisa, M. Posttranslational Modification of 6-phosphofructo-1-kinase as an Important Feature of Cancer Metabolism. *Plos One* **6** (2011).

360. Tang, H. *et al.* Oxidative stress-responsive microRNA-320 regulates glycolysis in diverse biological systems. *Faseb J* **26**, 4710-4721 (2012).

361. Garcia, M. *et al.* Phosphofructo-1-kinase deficiency leads to a severe cardiac and hematological disorder in addition to skeletal muscle glycogenosis. *PLoS Genet* **5**, e1000615 (2009).

362. Nakajima, H., Raben, N., Hamaguchi, T. & Yamasaki, T. Phosphofructokinase deficiency; past, present and future. *Curr Mol Med* **2**, 197-212 (2002).

363. Dunaway, G.A. & Kasten, T.P. Nature of the subunits of the 6-phosphofructo-1-kinase isoenzymes from rat tissues. *Biochem J* **242**, 667-671 (1987).

364. Ben-Shlomo, I. *et al.* Interleukin (IL)-1beta increases glucose uptake and induces glycolysis in aerobically cultured rat ovarian cells: evidence that IL-1beta may mediate the gonadotropin-induced midcycle metabolic shift. *Endocrinology* **138**, 2680-2688 (1997).

365. Nam, J.W. *et al.* Global analyses of the effect of different cellular contexts on microRNA targeting. *Mol Cell* **53**, 1031-1043 (2014).

366. Dunaway, G.A., Kasten, T.P., Sebo, T. & Trapp, R. Analysis of the phosphofructokinase subunits and isoenzymes in human tissues. *Biochem J* **251**, 677-683 (1988).

367. Ito, Y. *et al.* Identification of targets of tumor suppressor microRNA-34a using a reporter library system. *Proc Natl Acad Sci U S A* **114**, 3927-3932 (2017).

368. Lai, C.C. *et al.* Statin treatment is associated with a decreased risk of active tuberculosis: an analysis of a nationally representative cohort. *Thorax* **71**, 646-651 (2016).

369. Bogunovic, D. *et al.* Mycobacterial disease and impaired IFN-gamma immunity in humans with inherited ISG15 deficiency. *Science* **337**, 1684-1688 (2012).

370. Filipe-Santos, O. *et al.* Inborn errors of IL-12/23- and IFN-gamma-mediated immunity: molecular, cellular, and clinical features. *Semin Immunol* **18**, 347-361 (2006).

371. Schroder, K., Hertzog, P.J., Ravasi, T. & Hume, D.A. Interferon-gamma: an overview of signals, mechanisms and functions. *J Leukoc Biol* **75**, 163-189 (2004).

372. Schroder, K., Sweet, M.J. & Hume, D.A. Signal integration between IFNgamma and TLR signalling pathways in macrophages. *Immunobiology* **211**, 511-524 (2006).

373. Farlik, M. *et al.* Nonconventional initiation complex assembly by STAT and NF-kappaB transcription factors regulates nitric oxide synthase expression. *Immunity* **33**, 25-34 (2010).

374. Negishi, H. *et al.* Evidence for licensing of IFN-gamma-induced IFN regulatory factor 1 transcription factor by MyD88 in Toll-like receptor-dependent gene induction program. *Proc Natl Acad Sci U S A* **103**, 15136-15141 (2006).

375. Khor, C.C. *et al.* A Mal functional variant is associated with protection against invasive pneumococcal disease, bacteremia, malaria and tuberculosis. *Nat Genet* **39**, 523-528 (2007).

376. Ni Cheallaigh, C. *et al.* A Common Variant in the Adaptor Mal Regulates Interferon Gamma Signaling. *Immunity* **44**, 368-379 (2016).

377. Herbst, S., Schaible, U.E. & Schneider, B.E. Interferon gamma activated macrophages kill mycobacteria by nitric oxide induced apoptosis. *PLoS One* **6**, e19105 (2011).

378. DiDonato, J.A., Hayakawa, M., Rothwarf, D.M., Zandi, E. & Karin, M. A cytokine-responsive IkappaB kinase that activates the transcription factor NF-kappaB. *Nature* **388**, 548-554 (1997).

379. Horvath, C.M. The Jak-STAT pathway stimulated by interferon gamma. *Sci STKE* **2004**, tr8 (2004).

380. Ulloa, L., Doody, J. & Massague, J. Inhibition of transforming growth factor-beta/SMAD signalling by the interferon-gamma/STAT pathway. *Nature* **397**, 710-713 (1999).

381. Rath, M., Muller, I., Kropf, P., Closs, E.I. & Munder, M. Metabolism via Arginase or Nitric Oxide Synthase: Two Competing Arginine Pathways in Macrophages. *Front Immunol* **5**, 532 (2014).

382. Ghosh, A.K., Yuan, W., Mori, Y., Chen, S. & Varga, J. Antagonistic regulation of type I collagen gene expression by interferon-gamma and transforming growth factor-beta. Integration at the level of p300/CBP transcriptional coactivators. *J Biol Chem* **276**, 11041-11048 (2001).

383. Wu, C. *et al.* IFN-gamma primes macrophage activation by increasing phosphatase and tensin homolog via downregulation of miR-3473b. *J Immunol* **193**, 3036-3044 (2014).

384. Howard, N.C. *et al.* Mycobacterium tuberculosis carrying a rifampicin drug resistance mutation reprograms macrophage metabolism through cell wall lipid changes. *Nat Microbiol* **3**, 1099-1108 (2018).

385. Knight, M., Braverman, J., Asfaha, K., Gronert, K. & Stanley, S. Lipid droplet formation in Mycobacterium tuberculosis infected macrophages requires IFN-gamma/HIF-1alpha signaling and supports host defense. *PLoS Pathog* **14**, e1006874 (2018).

386. Gutierrez, M.G. *et al.* Autophagy is a defense mechanism inhibiting BCG and Mycobacterium tuberculosis survival in infected macrophages. *Cell* **119**, 753-766 (2004).

387. Wang, W. *et al.* MicroRNA-21-5p mediates TGF-beta-regulated fibrogenic activation of spinal fibroblasts and the formation of fibrotic scars after spinal cord injury. *Int J Biol Sci* **14**, 178-188 (2018).